RECLAMATION

Managing Water in the West

Technical Memorandum No. 86-68210-2014-01

West-Wide Climate Risk Assessments: Irrigation Demand and Reservoir Evaporation Projections

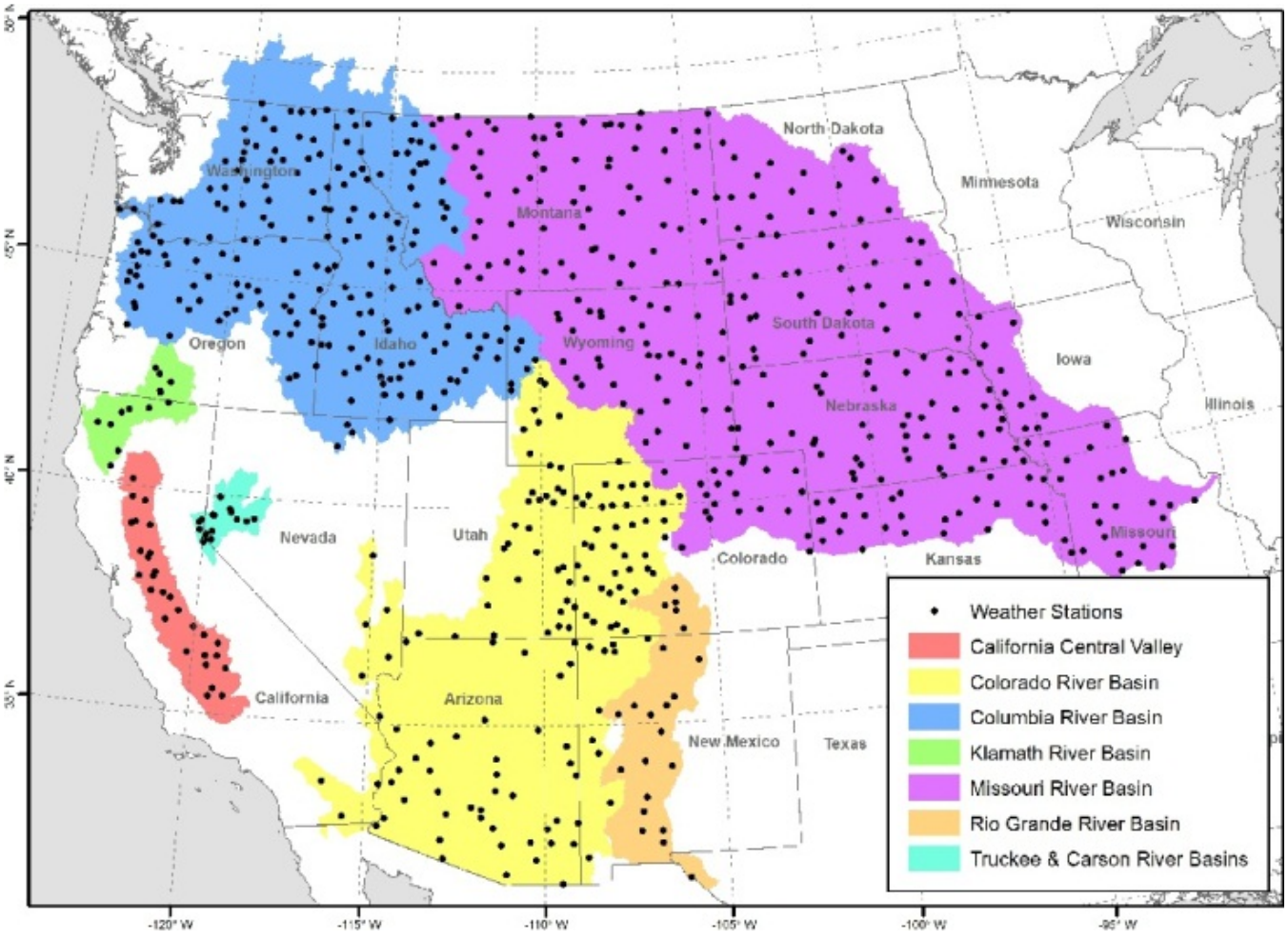

U.S. Department of the Interior
Bureau of Reclamation
Technical Service Center
Denver, Colorado

February 2015

MISSION STATEMENTS

The U.S. Department of the Interior protects America's natural resources and heritage, honors our cultures and tribal communities, and supplies the energy to power our future.

The mission of the Bureau of Reclamation is to manage, develop, and protect water and related resources in an environmentally and economically sound manner in the interest of the American public.

On the cover: Map of the western United States showing Cooperative Observer Program weather stations used for estimating crop evapotranspiration and the net irrigation water requirement.

Technical Memorandum No. 68-68210-2014-01

West-Wide Climate Risk Assessments: Irrigation Demand and Reservoir Evaporation Projections

Prepared by:

Bureau of Reclamation Technical Service Center, Water Resources Planning and Operations Support Group, Denver, Colorado
Desert Research Institute, Division of Hydrologic Sciences, Reno, Nevada

Justin Huntington, Desert Research Institute
Subhrendu Gangopadhyay, Bureau of Reclamation
Mark Spears, Bureau of Reclamation
Richard Allen, University of Idaho
David King, Bureau of Reclamation
Charles Morton, Desert Research Institute
Alan Harrison, Bureau of Reclamation
Daniel McEvoy, Desert Research Institute
Andy Joros, Desert Research Institute
Tom Pruitt, Bureau of Reclamation

Peer reviewed by:

Levi Brekke, Bureau of Reclamation
Richard Cuenca, Oregon State University

U.S. Department of the Interior
Bureau of Reclamation
Technical Service Center
Denver, Colorado

February 2015

ACRONYMS AND ABBREVIATIONS

ASC	antecedent soil-water conditions
ASCE	American Society of Civil Engineers
BCSD	bias correction and spatial disaggregation or bias-corrected and spatially downscaled as applied to weather data
CDF	cumulative distribution function
CDL	Cropland Data Layer (USDA-NASS 2010a)
CGDD	cumulative growing degree-days
CMIP	Coupled Model Intercomparison Project (CMIP1, CMIP2, CMIP3, and CMIP5 are CMIP phases 1, 2, 3, and 5, respectively)
CN	curve number method (USDA-SCS 1972)
CO_2	carbon dioxide
COOP	Cooperative Observer Program (NWS weather stations operated by volunteers)
CRB Study	*Colorado River Basin Water Supply and Demand Study* (Reclamation 2012a)
CRLE	Complementary Relationship Lake Evaporation model
CU&L	Reclamation's Consumptive Uses and Losses Reports
CVP IRP	*Central Valley Project Integrated Resource Plan* (Reclamation 2013a)
DRI	Desert Research Institute
ET	evapotranspiration
ET_c	crop ET
ET_0	reference ET based on the 0.12 m cool season, clipped grass reference
FAO-56	Food and Agriculture Organization of the United Nations, FAO Irrigation and Drainage Paper 56
GCM	general circulation model or global climate model
GDD	growing-degree-day
GHG	greenhouse gas
HD	hot-dry (climate change scenario)
HDe	ensemble-informed hybrid Delta (climate projection method)
HW	hot-wet (climate change scenario)
HUC8	Hydrologic Unit Code (eight digit) watershed boundaries
K_{cb}	basal crop coefficient
K_e	soil water evaporation coefficient
K_s	stress coefficient
LCCs	Landscape Conservation Cooperatives
MAD	maximum allowable depletion
NCGDD	normalized cumulative growing degree-day
NIWR	net irrigation water requirement
NOAA	National Oceanic and Atmospheric Administration
NRCS	Natural Resources Conservation Service
NWS	National Weather Service
PM	Penman-Monteith (method of calculating evapotranspiration)
PRISM	Precipitation-elevation Regressions on Independent Slopes Model (Daly et al. 1994; current data provided through the PRISM Climate Group at http://prism.nacse.org/)
P_{rz}	precipitation residing in the root zone
QAQC	quality assurance and quality control
RAWS	Remote Automatic Weather Station

RCP	representative concentration pathway
Reclamation	Bureau of Reclamation
R_s	solar radiation
SECURE	Science and Engineering to Comprehensively Understand and Responsibly Enhance (as defined in the SECURE Water Act, Public Law 111–11, Subtitle F)
STATSGO	State Soil Geographic Database (USDA-NRCS 1991)
TR	Thornton-Running equation
USDA	U.S. Department of Agriculture
VBA	Visual Basic for Applications
VIC	Variable Infiltration Capacity (hydrologic model)
WD	warm-dry (climate change scenario)
WEAP-CV	Water Evaluation and Planning Model of the Central Valley
WW	warm-wet (climate change scenario)
WWCRA	West-Wide Climate Risk Assessments
°	degree
°C	degrees Celsius
°F	degrees Fahrenheit
%	percent

CONTENTS

Tables

Page

Figures

Page

Appendices

Appendix

EXECUTIVE SUMMARY

Section 9503 of the SECURE Water Act, Subtitle F of Title IX of P.L. 111-11 (2009) (SECURE Water Act), authorizes the Bureau of Reclamation (Reclamation) to evaluate the risks and impacts of climate change in each of the eight major Reclamation river basins identified in the Act, and to work with stakeholders to identify climate adaptation strategies. Reclamation implements Section 9503 of the SWA through the Department of Interior's WaterSMART Program[1], which is working to achieve a sustainable water strategy to meet the Nation's water needs now and for the future. Through Basin Studies, part of WaterSMART, Reclamation works with State and local partners to evaluate the ability to meet future water demands within a river basin and to identify adaptation and mitigation strategies of the potential impacts of climate change. Through another activity, West-Wide Climate Risk Assessments (WWCRA), Reclamation is working to provide projections of future changes in water supplies, water demands, and river system operations that could result from changes in climate.

As part of WWCRA, Reclamation has conducted an analysis of the potential changes in crop irrigation demand in eight major river basins in the West and projections of evaporation for 12 reservoirs within those river basins when considering observed and projected impacts of climate change. This report contains the results of that analysis. The findings presented in this report are intended to be used for future basin-specific WWCRA impact assessments and Basin Studies conducted under WaterSMART if the teams conducting those studies elect to do so.

This technical assessment report provides: (1) an analysis of changes in irrigation demand, and (2) an analysis of changes in evaporation for selected reservoirs across the major Reclamation river basins with respect to presently observed and projected future impacts of global climate change. [2] The analysis involved developing irrigation demand and reservoir evaporation projections associated with World Climate Research Programme Coupled Model Intercomparison Project3 (WCRP CMIP3) climate projections that have been bias-corrected and spatially downscaled (BCSD) and served at the following Web site: http://gdo-dcp.ucllnl.org/downscaled_cmip_projections/dcpInterface.html. For the purposes of this study, CMIP3 climate projections were used because they represented the best available collection of climate projections at the onset of this effort (summer 2011 which was begun prior to the release of CMIP5). Although

[1] Descriptions of Reclamation WaterSMART activities are available at http://www.usbr.gov/WaterSMART/index.cfm.

[2] The major Reclamation river basins listed within the SECURE Water Act are the Colorado and Columbia River Basins and the Klamath, Missouri, Rio Grande, Sacramento and San Joaquin, and Truckee Basins. The Carson River Basin is operated jointly with the Truckee Basin by Reclamation, and results for the Carson River Basin have been included in the report.

the CMIP3 and CMIP5 projections are considered equally likely potential climate futures at this time, there is significant variability in the two sets of projections. This is especially true with regard to precipitation projections, and it is significant to note the potential impact of this variability on future irrigation demand and net evaporation estimates.

Changes to irrigation demand (model, described below) were analyzed for five climate change scenarios (warm-dry, warm-wet, hot-dry, hot-wet, and central tendency – ensemble median) that were informed by 112 BCSD-CMIP3 projections at three future periods: 2020s (years 2010-2039), 2050s (years 2040–2069), and 2080s (2070-2099) with 1950–1999 as the baseline period. The reservoir evaporation modeling (described below) was performed as transient simulations using the individual 112 BCSD-CMIP3 projections. Both the irrigation demands modeling and the reservoir evaporation modeling used observed data from weather stations representative of irrigated land areas and reservoir sites in a secondary bias correction step to account for local scale climate conditions in the climate change scenarios.

Although it would be ideal to calculate future irrigation demands for all 112 projections using the transient method as was done for the future reservoir evaporation estimates, such calculations were not feasible given the multiple crops and numerous locations modeled.

Irrigation Demands

The future irrigation demand estimates presented in this report are meant to provide a potential starting point for ongoing and future WaterSMART Basin Studies, impact assessments and other planning efforts. The estimates do not account for changing crop patterns and other socio-economic considerations that are best handled with stakeholder input. Hence, it is important that care be taken when comparing the irrigation demand estimates from this report to those of previous basin studies and impact assessments.

The evapotranspiration (ET) and irrigation demands model (also referred to as the ET Demands model) was developed at the spatial resolution (average size of 700 square miles) of hydrologic unit code eight (HUC8), as defined by the USGS in its watershed cataloging system, with weather data provided at individual points within the watershed, and HUC8 spatial scale information of soil type and crop acreage. The irrigation demands modeling was based on (1) widely accepted approaches for estimation of crop evapotranspiration (ET_c) and net irrigation water requirement (NIWR), (2) successful and accepted applications of methods used in the Western United States, (3) robust model results with limited projected climate variables of daily maximum and minimum temperature and daily precipitation used to estimate solar radiation and humidity, and (4) providing

more accurate future irrigation water demands by considering non-growing season soil moisture accumulation and variable growing season lengths.

The ET Demands model is based on common reference ET crop coefficient approach, where the reference ET (ET_o) is multiplied by time-varying crop coefficients to estimate the actual ET of a vegetated area. ET_o refers to ET for the cool season clipped grass reference crop that is actively growing, not limited by soil moisture, and is continuously maintained at full cover and peak height. The professional and scientific communities generally recognize the FAO-56 (Allen et al., 1998) and ASCE-EWRI (2005) standardized PM method (ASCE-PM) as the most appropriate and recommended ET_o method for estimating crop ET. In this study, the FAO-56 method was applied with the dual crop coefficient approach for estimating the NIWR. The dual crop coefficient approach is much preferred with regard to estimating effective precipitation, relative to the use of empirical methods as is done with the single coefficient approach. The dual crop coefficient approach allows for separate accounting of transpiration and evaporation to better quantify evaporation from variable precipitation and simulated irrigation events, and in turn allows for accounting of winter time soil moisture gains. Accounting for winter soil moisture gains and losses is essential for accurate estimation of NIWR. The NIWR is defined as the annual ET_c less the effective precipitation entering the root zone that is available for evaporation or transpiration.

The ET demands model was developed and calibrated for multiple crop types (e.g., pasture grass, alfalfa, grains, etc.) in each of the HUC8s where irrigated agriculture was present for all the major Reclamation river basins over the 1950-1999 baseline period. The calibrated ET Demands model was run using precipitation and temperature time-series representative of the five climate change scenarios for the three future periods 2020s, 2050s, and 2080s. Subsequently, changes to reference ET, crop ET and NIWR were calculated for the three future periods from the baseline period. At the same time, an analysis of the hydroclimate variables, precipitation and temperature, was carried out to document changes between a future period and the baseline (1950–1999).

Reservoir Evaporation

The open water evaporation model was developed and applied to 12 reservoirs located in the major Reclamation river basins. The reservoirs at which evaporation was estimated include: Lake Powell (Colorado River), Lake Mead (Colorado River), American Falls (Columbia, Snake River tributary), Grand Coulee (Columbia), Upper Klamath Lake (Klamath River), Canyon Ferry Lake (Missouri River), Boysen Reservoir (Missouri River), Elephant Butte Reservoir (Rio Grande) , Lake Shasta (Sacramento River), Millerton Lake (San Joaquin River), Lake Tahoe (Truckee River), and Lahontan Reservoir (Carson River).

Open water evaporation from lakes and reservoirs is an important water budget component to consider for water planning, modeling of hydrologic systems, and projections of future water demands and supply. Evaporation pans are typically used to estimate lake and reservoir evaporation, however the timing and magnitude of pan evaporation is not necessarily representative of actual evaporation from a lake or reservoir for numerous reasons, including significant time lags between peak pan evaporation and peak reservoir evaporation during a year, and has been shown to be highly uncertain (Hounam, 1973; Morton, 1979). Open water evaporation in this study was estimated using an energy balance model referred to as the Complementary Relationship of Lake Evaporation (CRLE), which has been widely applied for estimating operational reservoir and lake evaporation with limited climatic and heat storage information.

The CRLE model was calibrated and applied to all 12 reservoirs and was forced with secondary bias-corrected daily precipitation and temperature derived from the 112 BCSD-CMIP3 climate projections. Changes in reservoir evaporation were estimated using the transient or time-evolving projections. The reporting periods were the same as those used in the BCSD Irrigation Demands analysis (i.e., over the three future period 2020s, 2050s and 2080s with 1950–1999 as the baseline period).

Results and Findings

In the context of assessing future irrigation demand and reservoir evaporation impacts using the BCSD-CMIP3 climate projections, the findings from the assessment are:

- Precipitation projections are highly variable and basin dependent, with the central tendency scenario showing general basin-wide tendencies towards either slight increases or slight decreases for most basins by the 2050s. Slight decreases are shown for the Colorado, Rio Grande, Sacramento and San Joaquin, and Truckee basins and slight increases are shown in the Columbia and Missouri basins. The Klamath River Basin is the exception with slight decreases shown in the central and southwest portion of the basin and slight increases in the northeast portion.

- Temperature has an increasing trend from the baseline level for all river basins.

- Reference ET is projected to increase in all basins due to increasing temperatures. The central tendency scenario shows annual ET_o increases of up to approximately 12 percent by the 2080s. Central tendency scenario ET_o increases by 2080 range from a low of 1.1 percent in portions of the Columbia River Basin to 12.3 percent in portions of the Rio Grande Basin.

- Annual crop ET is projected to increase for perennial crops, with smaller increases, and sometimes slight decreases, for annual crops. Perennial crop ET increases are due to longer growing seasons and increases in ET_o. While annual crops also experience increased ET rates, earlier potential planting dates and reduced growing season due to increased temperatures and crop development sometimes result in decreased annual crop ET.

- The net irrigation water requirement (NIWR) incorporates growing season and non-growing season soil moisture gains and losses from precipitation, bare soil evaporation, and crop ET. Therefore, projections of NIWR are subject to uncertainties in each of these components, and primarily the precipitation scenario considered.

- The ensemble median of annual reservoir evaporation and net evaporation (evaporation minus precipitation) is projected to increase in all basins. Projected annual evaporation increases are typically around 2 to 6 inches by 2080 at most reservoirs modeled. However, the increase in annual net evaporation is relatively small at some reservoirs due to increased precipitation, and nearly equal to or slightly greater than historical evaporation at others due to decreased precipitation.

Uncertainties in the results are associated with the climate projections and the methods used for assessing irrigation demand and reservoir evaporation. While this report summarizes potential future climate impacts on irrigation demand and reservoir evaporation across the western United States using best available datasets and methodologies, there are a number of uncertainties not reflected in this report's characterization of potential future changes. Uncertainties associated with the climate impact assessments include characterization of future global climate forcings, global climate response to these forcings, correcting global climate model outputs for biases, and spatially downscaling global climate model outputs to basin-relevant resolution. The primary factors associated with climate projection uncertainties are the significant variability in the climate models and the emission scenarios that force the models, as well as the bias corrections and spatial downscaling of the climate model output. Chapter 6 discusses uncertainties in the data and methods used, including discussions on the magnitudes and quantification of uncertainties where appropriate.

Calculation of ET_o rates used for future irrigation demand estimates required estimation of solar radiation and humidity based on daily projected maximum and minimum temperatures. In addition, historical monthly average windspeed values were used for calculating future ET_o estimates. The levels of uncertainty associated with the solar radiation and humidity approximation methods are assumed to be small since the ET_o estimates for historical periods using these methods compare favorably to ET_o estimated from agricultural weather stations. The levels of uncertainty associated with the assumptions on future wind speed and minimum air temperature (T_{min}) – dewpoint temperature (T_{dew}) differences, referred to as dewpoint depression, are likely more significant, since these

parameters may change under future drier or wetter climates. Warmer climates are known to produce higher wind speeds and drier climates produce larger dewpoint depressions.

The largest uncertainty in the procedures used to calculate future irrigation demands may come from the absence of incorporation of potential impacts of elevated carbon dioxide (CO_2) levels on crop ET. The impact of increased CO_2 on reduced crop transpiration and increased water use efficiency and yield is a much debated topic and several studies have described how elevated CO_2 concentrations may reduce stomatal aperture, transpiration, and crop production processes (Rosenberg 1981; Kimball and Idso, 1983; Manabe and Wetherald, 1987; Kruijt et al. 2008; Islam et al. 2012; Ko et al. 2010). These reductions may moderate projected increases in ET. The wide ranges of potential impacts of CO_2 on ET, and suggestions for both increasing and decreasing trends of ET, prevented the inclusion of CO_2 impacts in this study on future irrigation demands.

Other areas of uncertainty associated with future irrigation demand estimates include assumptions of temperature dependent planting and harvest dates, or in some cases, static planting and harvest dates, for future periods. Likewise, the use of generalized winter ground cover classes that control evaporation rates during the dormant season, and the assumption that precipitation gains in winter to soil are immediate, rather than delayed following melting of snow, introduce some uncertainties into timing of evaporation losses from barren surfaces during dormant seasons. A snow accumulation and melt model was beyond the scope of this study.

Uncertainties in future estimated reservoir evaporation calculations are centered on CRLE energy balance related estimations. Heat storage was estimated using an average depth value rather than employing a more precise quantification of reservoir geometry. In addition, the lack of historical reservoir inflow and outflow volumes and respective water temperature information prevented the estimation of advected energy into and out of reservoirs. In spite of these limitations the CRLE method provides realistic seasonal patterns of evaporation for many lakes and reservoirs and tends to account well for effects of depth and associated heat storage on the timing and magnitude of lake evaporation (Morton, 1986).

It is important to note that this is not a comprehensive demand assessment, but a focused examination of primary climate impacts on plant water needs and reservoir evaporation. Beyond climate related considerations, a number of additional factors may influence irrigation demands in the future such as changing cropping patterns driven by market prices, changes in irrigation practices and soil-evaporation components, changes in crop varieties and phenologies and total acres kept in production. A completely comprehensive future irrigation demand

assessment would require consideration of all factors and strong stakeholder involvement.

CHAPTER 1 — INTRODUCTION

Section 9503 of the SECURE Water Act, Subtitle F of Title IX of P.L. 111-11 (2009) (SECURE Water Act), authorizes the Bureau of Reclamation (Reclamation) to evaluate the risks and impacts of climate change in each of the eight major Reclamation river basins identified in the Act, and to work with stakeholders to identify climate adaptation strategies. 3 Reclamation implements Section 9503 of the SWA through the Department of Interior's WaterSMART Program, which is working to achieve a sustainable water strategy to meet the Nation's water needs now and for the future.

Within WaterSMART, Reclamation is carrying out Basin Study Program, including West-Wide Climate Risk Assessments, Basin Studies, and Landscape Conservation Cooperatives (LCCs).[4] These activities are complementary and represent a three-part approach to the assessment of climate change risks and impacts for water and environmental resources and development of strategies to mitigate or adapt to such impacts.

- Through the Basin Studies, Reclamation works with State and local partners in a cooperative manner to evaluate the ability to meet future water demands within a river basin and to identify adaptation and mitigation strategies of the potential impacts of climate change.
- Through its participation within the LCCs, Reclamation is partnering with Federal, State, and local governments as well as conservation groups and nongovernmental organizations.
- The West-Wide Climate Risk Assessments (WWCRA) are meant to complement these two activities. The WWCRAs will provide projections of future changes in water supplies, water demands, and river system operations that could result from changes in climate. The assessments are being conducted in a consistent manner within the eight major Reclamation river basins listed within the SECURE Water Act.

Since 2011, as part of WWCRA, Reclamation has been working to develop future estimates of crop irrigation water requirements and reservoir evaporation in

[3] The major Reclamation river basins listed within the SECURE Water Act are the Colorado, Columbia, Klamath, Missouri, Rio Grande, Sacramento–San Joaquin, and Truckee River Basins. Furthermore, though the Carson River Basin is not explicitly mentioned in the Act as a major Reclamation river basin, it is included in the Truckee River Basin analysis for this report due to the diversions that occur between the Truckee and Carson basins.

[4] http://www.usbr.gov/WaterSMART/.

Reclamation's eight major river basins. These estimates are intended to provide risk assessment information for metrics described in the SECURE Water Act Section 9503(b)(2), including climate change risks associated with increasing agricultural water demands and reservoir evaporation rates. Although WaterSMART Basin Study Program activities will over time address additional demand assessment metrics under Section 9503(b)(2), the water demand projections in this report are intended to inform assessment of impacts related to crop evapotranspiration, net irrigation water requirements, and open-water evaporation.

The focus of this report is the development of generalized crop irrigation and reservoir evaporation water demand projections, and a summary evaluation of climate change implications associated with water demands in the eight major Reclamation river basins listed in the SECURE Water Act. The evaluation includes assessment of future climate conditions over each basin (i.e., precipitation and temperature) as well as irrigation water demand responses (i.e., growing season, crop evapotranspiration, and net irrigation water requirement response) and changes in reservoir evaporation and net evaporation (i.e., evaporation minus precipitation).

The information presented in this report does not provide a complete picture of future projected irrigation demands. The impact of climate change on agricultural irrigation demands is just one element of many that may influence the future of demands. To get a complete picture of future agricultural irrigation demands, other socioeconomic factors must be considered. These include changes in future irrigated acreage, improved conveyance and application efficiencies, changes in farming practices, changes in crop patterns driven by market conditions, etc. This more comprehensive picture of projected agricultural demands is determined under a Basin Study process in collaboration with basin stakeholders, as discussed in chapter 2.

The report is organized as follows:

- Chapter 2, Background, provides background information and a summary of the methods used to estimate future crop evapotranspiration, net irrigation water requirements, and reservoir evaporation under multiple climate change scenarios.
- Chapter 3, Climate Projections, describes the future climate projections used for developing the crop irrigation and reservoir evaporation water demand projections, including how the climate projections were bias-corrected and spatially downscaled for use in this activity.
- Chapter 4, Developing Irrigation Water Demand And Open-Water Evaporation Projections From Climate Projections, presents the methodology used for developing the crop irrigation and reservoir evaporation water demands for baseline and future projections.

- Chapter 5, Baseline And Projected Demands Results For Major Reclamation River Basins, presents an overview of baseline and projected crop irrigation water requirements in the eight major Reclamation river basins listed above, as well as the reservoir evaporation modeling results. The overview focuses on the baseline period and three future periods.
- Chapter 6, Uncertainties, presents a summary discussion of the uncertainties associated with the analyses of crop irrigation and reservoir evaporation water demands projections presented in this report. These uncertainties have components related to the climate projections and to the modeling approach used to assess the impacts.

CHAPTER 2 — BACKGROUND

This chapter provides technical and programmatic background information relevant to the water demands assessment. The technical background section includes brief summaries of the methods used for incorporating climate projections and to estimate future irrigation water requirements and reservoir evaporation.

2.1 Technical Approach

Evapotranspiration (ET) is the driving component for irrigation water requirements of agricultural crops, and is a primary component of hydrologic systems and water balances. Quantifying ET and the net irrigation water requirement (NIWR) for specific crops and regions is required for design of irrigation systems, basin water balance estimates, irrigation water management, review and litigation of water right applications and disputes, and climate impact assessments. The NIWR is defined as the annual crop ET less the effective precipitation entering the root zone that is available for evaporation or transpiration. NIWR is that portion of the total irrigation demand that is consumed during crop production and impacts the overall water supply system.

Reclamation and other water resource management agencies regularly conduct assessments of water resources management and reservoir systems operations. Such assessments might focus on current system conditions or analysis of proposed changes in operations and/or infrastructure conditions intended to provide service through an identified future time period. For discussion purposes here, assessments that consider operations over a future time period greater than 10 to 20 years in duration are referred to as long-term assessments, and require making assumptions about possible future water supplies, demands, and operational constraints that would affect system operations.

Recent information suggests that future envelopes of climate variability may differ from historical climate variability, particularly in terms of temperature for all regions and precipitation for many regions (IPCC 2007; USGCRP 2009). As a result, there is an increasing need to blend future climate projections with historical information when defining planning assumptions about future water supplies, demands, and operational constraints. Such blending often involves combining historical variability information (e.g., sequencing information, such as the alternation of wet and dry spells or warm and hot spells) with information suggested by climate projections (e.g., projected means and extremes). The process of incorporating climate projection information into longer-term water resources assessments leads to several method choices and related questions on the survey of available climate projections, such as decisions about which climate

projections are credible for assessment purposes and about how to use credible projections for assessment purposes. A detailed discussion of these questions is given in Reclamation (2011).

Two general approaches are used for relating climate projection information to water resources planning:

- Period change methods extend from transient methods and involve (a) identifying a climate change scenario within a projection context, and (b) generating weather inputs for impacts modeling that reflects historical observed weather adjusted by the scenario's climate change to produce weather representative of the future period. A change scenario may be informed by one or more climate projections; when multiple projections are used, the result is called an ensemble-informed scenario. The climate change definition itself is also a choice; commonly used definitions are change in monthly means or monthly distributions for precipitation and temperature. Some of the common methods under this approach are outlined below.
    - Scenarios informed by single projections using either the Delta method (e.g., Hamlet and Lettenmaier 1999; Lettenmaier and Gan 1990; Lettenmaier et al. 1999; Miller et al. 2003) or a hybrid Delta method (e.g., McGuire and Hamlet 2010)
    - Ensemble-informed versions of both the Delta method (Vano et al. 2010) and ensemble informed hybrid Delta (HDe) methods (Reclamation 2010)
- Time-evolving projection, or transient, methods involve translating time-series climate projections into time-series projections of weather inputs for impacts modeling (e.g., for hydrology, irrigation demands, open-water evaporation, etc.). There have been numerous applications of this approach for hydrology impacts assessment (e.g., Wood et al. 2004; Payne et al. 2004; Christensen et al. 2004; Van Rheenen et al. 2004; Christensen and Lettenmaier 2007; Maurer 2007; Reclamation 2011; Reclamation 2012a). This approach often involves having to reconcile time resolutions when translating from climate projections to weather input projections (e.g., for Reclamation 2011 and 2012a, monthly BCSD climate projections had to be time-disaggregated to the daily timestep of hydrology analysis.)

Chapter 3 of this report provides information on the decisions made as a part of the study related to selecting specific climate projections and how the projections were used to develop climate change scenarios. Chapter 4 provides information on the decisions made as part of the study related to irrigation and reservoir evaporation demands model selection, background, and application.

The following sections summarize methods that are described in detail in chapter 3 (Climate Projections) and chapter 4 (Irrigation and Evaporation Demands).

2.1.1 Climate Projections and Scenarios

Contemporary climate model projections were used to develop ET and NIWR demands for agricultural crops and open-water evaporation demands in this report. However, it is important to note that climate model projections cannot be directly used in such impact assessments given the coarse time and spatial resolutions of climate models. This step of translating projections from the climate model scale (coarse spatial resolution, ~100–250 km) to the impacts assessment scale (finer spatial resolution, ~10 km) is referred to as downscaling. It is important to note that climate models produce a large number of climate variables used to formulate projections. However, the projected climate variables used in this impact assessment include only precipitation and air temperature, which are widely considered to be the primary drivers of changing demands for irrigation water. Their use in climate change impact studies is routine.

Climate projections of precipitation and temperature from the CMIP3 (Coupled Model Intercomparison Project Phase 3) archive were downscaled using a statistical algorithm referred to as bias correction and spatial disaggregation (BCSD). Reclamation in collaboration with other Federal and non-Federal partners has developed archives of downscaled climate projections from the CMIP3 climate model experiments. The monthly BCSD climate projections archive consists of 112 individual projections of monthly total precipitation and monthly average temperature downscaled to 1/8° latitude by 1/8° longitude grid squares (approximately 12 kilometers on each side) using 16 different CMIP3 climate models simulating three different future emissions paths (B1 – low, A1B – middle, and A2 – high).[5]

The next step in the process is to drive the impacts assessment models using the projections of precipitation and temperature. Ideally, one would like to run each of the more than 100 climate projections through the impacts models. In this case, for the ET Demands model runs, this was not practical given the diversity of crops and agricultural practices across the major Reclamation river basins, and therefore the enormous computational and data handling requirements. A choice was made by the WWCRA team to perform the analysis where the 112 climate projections were used to inform a set of five climate-change scenarios using precipitation and temperature changes defined for conditions – (1) warm-dry (WD); (2) warm-wet (WW); (3) hot-dry (HD); (4) hot-wet (HW); and (5) central tendency. For each of the five climate change scenarios, assessments of changes to irrigation demands were determined at three future periods labeled 2020s (for years covering the period 2010–2039), 2050s (2040–2069), and 2080s (2070–2099) from the baseline period, 1950–1999. This approach of selecting a set of

[5] From the *Special Report on Emission Scenarios* (IPCC 2000); in which the A1 scenarios are of a more integrated world, the A2 scenarios are of a more divided world, the B1 scenarios are of a world more integrated and more ecologically friendly, and the B2 scenarios are of a world more divided but more ecologically friendly.

future periods and analyzing change from a baseline period is referred to as period change, as discussed above.

For the assessment of changes to reservoir evaporation, however, all 112 BCSD projections were used in a transient analysis with evaporation results aggregated to the same three future periods, i.e., 2020s, 2050s, and 2080s. Details on the development of climate projections and weather data to run the impacts models are provided in chapter 3 of the report.

2.1.2 Irrigation Demands

The overall process described below for developing future irrigation demand estimates using the ET Demands model is illustrated in the flow chart shown on figure 1.

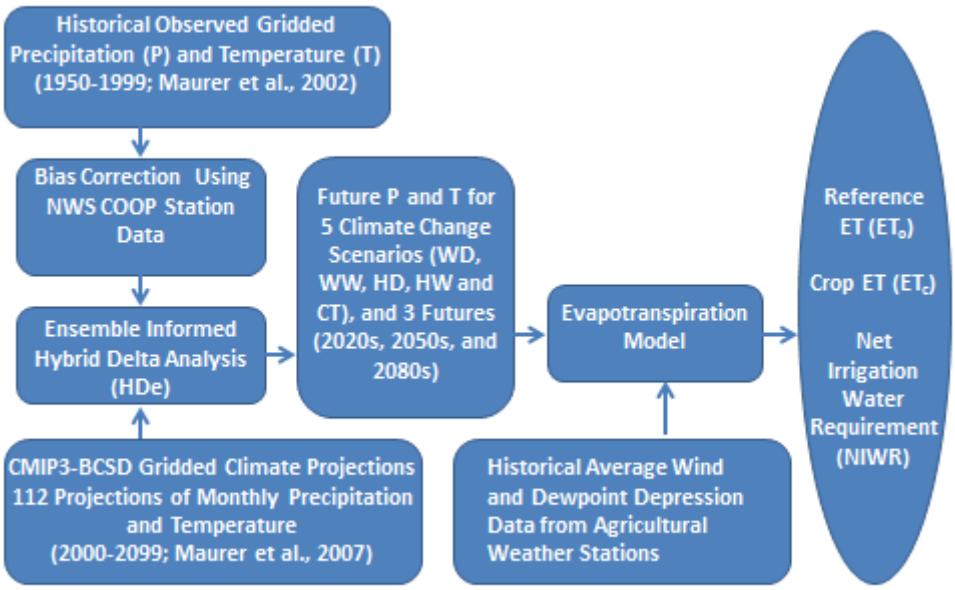

Figure 1.—Flow chart illustrating the general process used for estimating future irrigation demands.

The current or baseline irrigation demand estimates developed for this study are based on the most recent available crop data and climate conditions occurring during the period 1950 through 1999. With a few exceptions, crop types and quantities were derived from data collected by the U.S. Department of Agriculture (USDA) National Agricultural Statistics Service and reported for 2010 (USDA-NASS 2010a). The 1950 through 1999 climate data used are from the published data set by Maurer et al. (2002).

Baseline NIWR estimates were calculated for each river basin's HUC8 subbasins. The baseline NIWR estimates were developed using the ET Demands model

originally developed collaboratively by the University of Idaho, Idaho Department of Water Resources, Nevada Division of Water Resources, and Desert Research Institute (DRI) (Allen and Robison 2007; Huntington and Allen 2010). More recent modifications to the model were made through a collaborative effort by Reclamation, DRI, and the University of Idaho to facilitate its application to this study.

The ET Demands model utilizes a combination of the Penman-Monteith (PM) reference ET method and a dual crop coefficient method, as described in the Food and Agriculture Organization of the United Nations, FAO Irrigation and Drainage Paper 56 (FAO-56) (Allen et al. 1998). The American Society of Civil Engineers (ASCE) has adopted the FAO-56 PM equation as the standardized equation for calculating the cool season, clipped grass reference ET (ET_0) (ASCE-EWRI 2005). The short grass reference defined by the PM equation is consistent with previous Reclamation work.

The PM–dual crop coefficient approach was chosen over the traditionally used single crop coefficient approach. Transpiration and evaporation are accounted for separately in the PM–dual crop coefficient approach, which is able to better quantify variation in evaporation stemming from variable precipitation and simulated irrigation events. This separation of transpiration and evaporation also helps account for the effects of winter soil moisture conditions on evaporation from dormant soil surfaces, which can be a significant factor when estimating early irrigation season NIWR. The dual crop coefficient approach provides a more physically based method for estimating NIWR based on continuous accounting of soil moisture balance (Allen et al. 2005b).

The ET Demands model first calculates daily reference ET (ET_0) at assigned weather station nodes for each HUC8 subbasin as a function of maximum and minimum temperature (T_{max} and T_{min}) from the 1950–1999 climate data set mentioned above. The variables vapor pressure, solar radiation, and windspeed required by the PM equation are empirically estimated as recommended by ASCE-EWRI (2005) and as described in chapter 4.

Spatially averaged soil parameters for irrigated lands in each HUC8 were input to the ET Demands model. The soils information is based on data from the Natural Resources Conservation Service (NRCS) State Soil Geographic (STATSGO) database (USDA-NRCS 1991). The soil parameters, consisting primarily of upper and lower limits of soil water holding capacities, layering, and infiltration rates, affect the estimation of irrigation schedules, evaporation losses from soil, deep percolation from root zones, antecedent soil moisture conditions, and runoff from precipitation.

Daily crop ET (ET_c) is calculated in the ET Demands model as a function of the two primary crop coefficients K_{cb} and K_e, and a crop stress coefficient K_s for all crop types within a given HUC8 as follows:

$$ET_c = (K_s K_{cb} + K_e) ET_0$$

where ET_0 is the ASCE-PM grass reference ET, K_{cb} is the basal crop coefficient, K_e is the soil water evaporation coefficient and K_s is a stress coefficient invoked when soil water is not sufficient to sustain full ET. K_{cb} and K_e are dimensionless and range from 0 to 1.4. Daily K_{cb} values over a season, commonly referred to as the crop coefficient curve, represent impacts on crop ET from changes in vegetation cover, leaf area, and vegetation height due to changes in crop phenology. These properties vary during the growing season and can vary from year to year depending on the start, duration, and termination of the growing season, all of which are dependent on temperature. K_s ranges from 0 to 1, where 1 represents a condition of no water stress. K_s is also dimensionless. A daily soil water balance of the simulated effective root zone is a key component of the ET Demands model to calculate K_s. In most cases, the ET Demands model was operated assuming full water supplies when computing ET_c and NIWR, so that K_s was generally 1.0. However, K_s can be less than 1 during the dormant season (winter) if precipitation is low.

Values for K_{cb} for a given crop generally vary seasonally and annually according to simulated plant phenology. Plant phenology is, in turn, impacted by solar radiation, temperature, precipitation, and agricultural practices. The ability to simulate year-to-year variation in the timing of green-up or planting, and timing of effective full cover, harvest, and termination, is necessary for integrating the effects of temperature on growing-season length and crop growth and development, especially under changing climate scenarios. Seasonal and year-to-year changes in vegetation cover and maturation are simulated in ET Demands for each crop K_{cb} as a crop-specific function of air temperature, based on cumulative growing degree days (GDD). After planting of annuals or the emergence of perennials, the value of K_{cb} tends to gradually increase with increasing temperature until the crop reaches full cover. Once this happens and throughout the middle stage of the growing season, the K_{cb} value is generally constant, or is reduced to simulate cuttings and harvest. From the middle stage to the end of the growing season the K_{cb} value reduces to simulate senescence. A full description on how GDD is calculated in ET Demands is provided in chapter 4.

The NIWR rate or depth is calculated in ET Demands as ET_c minus effective precipitation residing in the root zone (P_{rz}), and represents the amount of additional water that the crop would evapotranspire in excess of precipitation residing in the root zone. The NIWR is synonymous with the terms irrigation demand, net consumptive use, and precipitation deficit. P_{rz} is calculated as a function of daily precipitation (from the climate data set), antecedent soil moisture prior to a precipitation event, deep percolation of precipitation, and precipitation runoff. Soil moisture is a function of the moisture-holding capacity of the weighted average soil type input to the model for agricultural areas within each

HUC8 subbasin. Precipitation runoff is calculated based on daily precipitation using the NRCS curve number method (USDA-SCS 1972).

Irrigation is simulated in the ET Demands model when the crop root zone moisture content drops to the crop-specific maximum allowable depletion threshold. Irrigation depths are specified to fill the root zone by the difference between field capacity[6] and the cumulative soil moisture depletion depth amount.

The NIWR and ET_c rates for each crop within a given HUC8 subbasin are multiplied by the ratio of the acres of the crop to total irrigated acres within the HUC8 subbasin, and all crop values are summed to calculate weighted average HUC8 subbasin NIWR and ET_c rates as:

$$HUC8\ subbasin\ rate\ = \sum_{i=1}^{i=n} crop\ ratio\ i * crop\ rate\ i$$

The historical baseline results presented in chapter 5 include mean annual precipitation, temperature, windspeed and dewpoint depression (a humidity indicator), ET_0, ET_c, and NIWR.

Future irrigation water demand estimates were also calculated using the ET Demands model and the temperature and precipitation estimates for the future scenarios discussed above and in chapter 3. Changes in future farming practices for annual crops, such as the potential for earlier planting, development, and harvest under warming climates, are highly uncertain due to human behavior and economic drivers of crop production. These potential changes will likely be highly dependent on future crop cultivars, water availability, economics, and market forces. For these reasons, two scenarios were considered. One scenario assumes static phenology K_{cb} curves for which historical baseline temperatures are used in simulating planting, crop development, and harvest dates using the GDD approach. These K_{cb} curves vary year to year, but involve no increasing or decreasing trends in the future. The second scenario assumes non-static phenology K_{cb} curves, for which estimated future temperatures were used for simulating planting, crop development, and harvest dates using the GDD approach. A detailed discussion on this approach is included in chapter 4.

The future irrigation demands results presented in chapter 5 cover mean annual precipitation, temperature, ET_0, ET_c, and NIWR. Mean monthly values of perennial crop ET_c for future time periods and scenarios are also presented to highlight potential changes in seasonal ET_c.

[6] Field capacity is the amount of water that a well-drained soil can hold against gravitational forces, or the amount of water remaining when downward drainage has markedly decreased (Allen et al. 1998).

2.1.3 Reservoir Evaporation Demands

Estimated historical and future evaporation rates for 12 representative and significant Reclamation reservoirs in the eight major Reclamation river basins were calculated using the Complementary Relationship Lake Evaporation (CRLE) model. CRLE is an open-water evaporation model that estimates monthly evaporation as a function of solar radiation, humidity, air temperature, water temperature, albedo, emissivity, and depth-controlled heat storage. Reclamation collaborated with DRI in the development and application of the model for this study. A detailed description of the CRLE model and its application is provided in chapter 4.

The CRLE model was used to calculate estimated evaporation for the period 1950–2099 in a transient mode, as opposed to the period change mode used in the irrigation demands analysis. Average annual historical reservoir depth was computed based on storage volume and surface area using historical data and was assumed to be constant for the analysis period. For the 1950–1999 portion of the analysis, a weather-station-based bias correction was used for the Maurer et al. (2002) data set introduced previously. All 112 BCSD projections (see the previous HDe discussion) were bias corrected to nearby weather stations and used for the 2000–2099 portion of the analysis. Since the CRLE model requires solar radiation and humidity inputs, these parameters were estimated using temperature-based relationships, as was done for the ET Demands model. The CRLE model results presented in chapter 5 include mean monthly evaporation and net evaporation (evaporation minus precipitation) rates for each of 12 reservoirs modeled.

2.2 Programmatic Background

Reclamation's Basin Study Program includes implementation of Basin Studies, WWCRAs, and participation in Landscape Conservation Cooperatives (LCCs). These activities are complementary and represent a three-part approach to the assessment of climate change risks to water supplies and associated resources as well as impacts to operations and the identification of adaptation strategies.

The WWCRAs provide important baseline projections of risks to water supplies and potential operational impacts. WWCRAs completed to date include the *Bias-Corrected and Spatially Downscaled Surface Water Projections* (Reclamation 2011), the *Upper Rio Grande Impact Assessment* (Llewellyn and Vaddey 2013) and *Sacramento – San Joaquin Basins Impact Assessment* (Reclamation 2014). The demand assessment presented in this report, a WWCRA product, strives to apply well-accepted methods for a west-wide assessment across multiple river basins.

The LCCs are partnerships of governmental (Federal, State, tribal, and local) and nongovernmental entities. The primary goal of the LCCs is to bring together science and resource management to inform climate adaptation strategies to address climate change and other stressors within an ecological region or "landscape." The LCCs function in specific geographic areas forming a national network.

Through the Basin Studies, Reclamation works with States, Indian tribes, local partners, and other stakeholders in a cooperative manner to evaluate the ability to meet future water demands within a river basin and to identify adaptation and mitigation strategies of the potential impacts of climate change. Basin Studies are typically performed at a regional scale and may adopt different methods than those presented in this report if other methods are found to better suit local responses for a specific river basin. Basin Studies have been completed for the Colorado River, Lower Rio Grande, Santa Anna Watershed, St. Mary and Milk Rivers, and Yakima River. There are currently 22 other ongoing Basin Studies.

The major river basins evaluated in this work are illustrated on figure 2 and are:

- Colorado River Basin and the Imperial Valley (section 5.2)
- Columbia River Basin (section 5.3)
- Klamath River Basin (section 5.4)
- Missouri River Basin (section 5.5)
- Rio Grande Basin (section 5.6)
- Sacramento and San Joaquin River Basins (grouped as Central Valley, section 5.7)
- Truckee and Carson River Basins (section 5.8)

2.2.1 Considering Previously Completed Basin Studies and WWCRA Impact Assessments

It is significant to note that a Basin Study has been completed for the Colorado River Basin and an impact assessment and integrated resource plan have been completed for the California Central Valley. These studies and their relevance to this effort are discussed below.

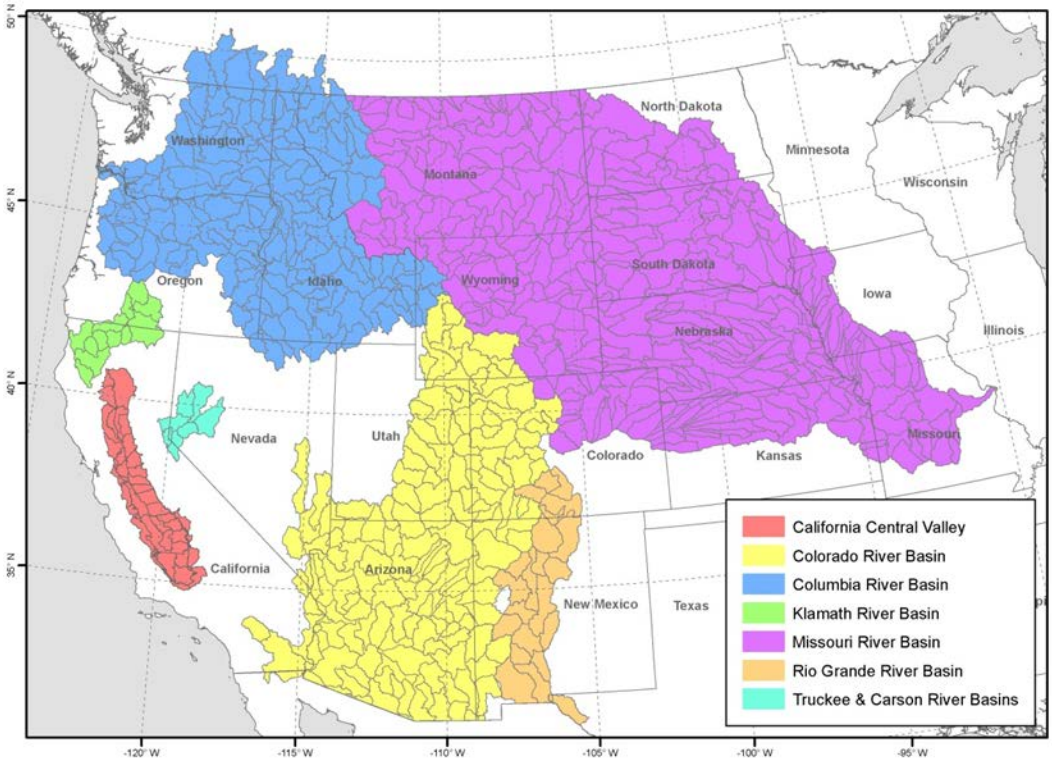

Figure 2.—Study region and eight-digit hydrologic unit code (HUC8) boundaries used for aggregating results of irrigation water demands.

In December 2012, Reclamation's Upper and Lower Colorado Regions and agencies representing the seven Colorado River Basin States completed the *Colorado River Basin Water Supply and Demand Study* (CRB Study; Reclamation 2012a). Conducted with participation and input from a broad range of stakeholders throughout the basin, the purpose of the CRB Study was to define future imbalances in water supply and demand in the basin through the year 2060, and to develop and analyze options and strategies to resolve those imbalances.

The CRB Study analyzed future water supply and demand scenarios based on factors such as projected changes in climate and varying levels of growth in communities, agriculture, and business in the seven basin States of Arizona, California, Colorado, New Mexico, Nevada, Utah, and Wyoming.

The demand assessment component of the study quantified the impacts of climate change on demands, relying on different methods than presented in this report. The CRB Study's Technical Report C Appendix C15, Section 3, titled "Selection of PET Method for Application to Basin Demands," discusses methods used to quantify the impact of climate change on demands and explains the reasoning behind the study's choice of methods. In summary, the CRB Study sought to sustain consistency between the calculations used to estimate supply and demand changes under future climate conditions, using the Variable Infiltration Capacity (VIC) hydrologic model, which employs the Penman-Monteith method. The PM

method was proposed for estimating potential change in demands due to climate change. However, it was not used because it was observed to potentially underestimate the response of warming to ET change at high demands for those areas. Though the CRB Study used a different methodology than this report, the results presented here for the Colorado River Basin are generally consistent with the findings from the CRB Study. However, the magnitudes of baseline conditions and the projected percent change in agricultural demands do vary somewhat from the CRB Study. These differences result primarily from differences in data sources and in the methods used. These differences include but are not limited to, the decision to use the VIC model PM algorithm for agricultural areas below 1,800 m. Furthermore the VIC algorithm relies on four inputs: precipitation, maximum and minimum temperature, and windspeed. The other variables required for standard PM are estimated internally within the VIC algorithm. Data sources for windspeed and the estimates of maximum and minimum temperature differ from sources used for this report.

The CRB Study relied on the change in evaporation computed based on the VIC PM algorithm. Using this algorithm resulted in significantly lower estimates of changes in reservoir evaporation as a result of climate change projections. Further analysis of these differences is warranted to determine if the methodology chosen in this report is an improved representation of change in evaporation rate at major reservoirs, and if it should be included in future studies of the Colorado River Basin.

Lastly, the CRB Study differed from this report in that it included critical input from basin stakeholders to capture additional change in projected demands that are not directly attributed to a changing climate, such as changes in irrigated acreage and per acre water delivery efficiencies under each scenario. The baseline demand scenario developed for this study assumed historical acreage and delivery efficiency will remain unchanged throughout the future projection time frames.

In October 2013, Reclamation's Mid-Pacific Region completed the *Central Valley Project Integrated Resource Plan* (CVP IRP) study (Reclamation 2013a). The purposes of the CVP IRP were (1) to assess the impacts of future socioeconomic and climatic uncertainties on the Central Valley Project water supplies, agricultural and urban demands and on other performance characteristics and (2) to explore the effectiveness of potential adaptation strategies for addressing future imbalances between supplies and demands. Differences between the CVP IRP study and this study exist for a variety of reasons. First, this study includes the entire Central Valley area, whereas the CVP IRP study reported results for only the portion of the Central Valley where Reclamation provides water supplies. Second, this study evaluates NIWR based on crop groups and acreages identified using the USDA's Cropland Data Layer information (USDA-NASS 2010a), whereas the CVP IRP study used crop groups and acreages developed for the California Water Plan Update 2013 (Department of Water Resources 2013). In

this regard it is important to note that, because the CVP IRP and the California Water Plan use a transient socioeconomic-climate scenario based approach, assumptions about the influences of population growth and land use changes result in changing crop acreages over time, which have a significant effect on agricultural water demands. Finally with regard to ET_c, the CVP IRP used the Water Evaluation and Planning Model of the Central Valley (WEAP-CV) to compute ET_c. WEAP-CV computes ET_c based on directly linking the full PM ET equation with a plant growth model instead of using crop coefficients. However, it should be noted that the WEAP-CV plant growth model was calibrated to previous PM-dual crop coefficient simulations performed across California (Burt et al. 2002). In addition to the meteorological inputs used in this study, the WEAP-CV plant growth model simulates the effects of carbon dioxide (CO_2) on ET_c.

Through the WWCRA program, the *Sacramento and San Joaquin Basins Climate Impact Assessment* study has recently been completed (Reclamation 2014). Reasons for differences between that study and the present work are similar to those described in the preceding paragraph for the CVP IRP study, except that the Sacramento/San Joaquin study includes all the irrigated lands in the Central Valley.

CHAPTER 3 — CLIMATE PROJECTIONS AND SCENARIOS

3.1 Global Climate Models and Climate Projections

This chapter provides descriptions of the future climate projections used and methods employed for developing climate change scenarios from these projections, as well as the rational for the methods used.

Projections of future precipitation and temperatures, among other climate variables, to describe impacts of changing atmosphere, land, and ocean conditions, are developed by simulating global climate conditions from the late 19th century (from about 1860) through the end of the 21st century using general circulation models (GCMs, also referred to as global climate models). These coupled atmosphere-ocean GCMs model physical processes using a three-dimensional grid over the globe. Given their global resolution, they provide climate-variable projections on relatively coarse grid cells measuring around 100 to 250 km on a side. For the period from about 1860 through 1999, GCMs are constrained by estimated historical atmospheric composition, including historical atmospheric concentrations of greenhouse gases (GHGs) and aerosols that affect the atmospheric radiation and energy budgets. However, it is difficult to project future atmospheric and ocean conditions and anthropogenic factors — the drivers that influence climate. Thus, various assumptions are used to produce a range of possible climate system drivers or forcings over the period 2000–2099. Specifically, GCMs simulate the potential global climate system response to several trajectories of climate system drivers, such as GHG emissions. The Coupled Model Intercomparison Project Phase-3 (CMIP3) climate experiments (IPCC 2000) refer to the GHG emissions drivers as emissions scenarios, and the Coupled Model Intercomparison Project Phase-5 (CMIP5) climate experiments (Taylor et al. 2012) refer to the emission trajectories as representative concentration pathways (RCPs).[7]

The CMIP3 climate projections are based on three primary GHG emissions scenarios:

- "High" emissions scenario: A2.

[7] RCPs are four greenhouse gas concentration (not emissions) trajectories selected and defined in IPCC (2013) by their total radiative forcing (cumulative measure of human emissions of GHGs from all sources expressed in watts per square meter) pathway and level by 2100.

- "Middle" emissions scenario: A1B.
- "Low" emissions scenario: B1.

The CMIP5 climate projections are based on four RCPs:

- "Business-as-usual" pathway: RCP8.5. This is considered the high radiative forcing pathway.
- "Middle" pathways: RCP4.5 and RCP6.0. These pathways lie between the RCP8.5 and RCP2.6.
- "High mitigation" pathway: RCP2.6. This is considered the low emissions pathway.

For the purposes of this study, CMIP3 climate projections were used because they represented the best available collection of climate projection at the onset of this effort (summer 2011). A comparison between the three CMIP3 emissions scenario and the four CMIP5 RCPs is available from Knutti and Sedláček (2013) and Reclamation (2013b). As an overall comparison at global and regional scales, although there are minor differences, the climate model outputs from CMIP3 and CMIP5 show generally consistent spatial patterns of temperature and precipitation change. Furthermore, it is anticipated that given the continued authorizations, the demands analysis presented within this report will be updated as new information becomes available in conjunction with the SECURE Water Act.

3.2 Downscaled Climate Projections

The outputs from GCMs are at relatively coarse spatial scales (100 to 250 km on each side of a grid) and, therefore, cannot be directly used in impacts assessments such as the crop irrigation and reservoir evaporation demands assessments presented in this report. This issue is independent of the climate forcings and is tied to space-time resolutions in climate models that balance physical process representations with available computing resources. The development of climate projections at a higher spatial resolution from these coarse global climate model outputs is commonly referred to as downscaling. Two methodology classes are available to downscale GCM outputs:

- Dynamical – in which a fine-scale regional climate model, using a better representation of local terrain than was available for the GCM, simulates climate processes over the region of interest.
- Statistical – in which large-scale climate features from the coarse-grid GCMs are statistically related to the fine-scale climate data available for the region.

Reviews of downscaling methodological choices, method strengths, and weaknesses include those by Hewitson and Crane (1996), Wilby and Wigley (1997), Murphy (1999), Wigley (2004), and Brekke et al. (2009a).

Reclamation, in collaboration with other Federal and non-Federal partners, has developed archives of downscaled climate projections from the CMIP3 (Maurer et al. 2007) and CMIP5 (Maurer et al. 2013) climate projections. These downscaled climate projections were developed using the statistical downscaling approach referred to as the bias correction and spatial disaggregation (BCSD) method (Wood et al. 2002). This technique was used to generate downscaled translations of 112 CMIP3 projections, which are available online at the "Downscaled CMIP3 and CMIP5 Climate and Hydrology Projections" archive[8] (BCSD climate projections, referring to the methodology described above). The BCSD climate projections ensemble was produced collectively by 16 different CMIP3 models simulating 3 different emissions paths (B1, A1B and A2).

The BCSD method has been shown to provide downscaling skill comparable to other statistical and dynamical methods in the context of hydrologic impacts (Wood et al. 2004). A potential limitation of BCSD, like any statistical downscaling method, is the assumption of some statistical stationarity (i.e., statistical properties such as mean, variance, autocorrelation, etc., are all constant over time) in the relationship between GCM and finer scale precipitation and temperature data not only over a common observation period, but also for future periods.

Another BCSD limitation is variability within the BCSD cells. Even at the downscaled cell size of 1/8° latitude by 1/8° longitude or approximately 12 kilometers square, there are local climate effects that must be considered. The BCSD cell average temperature and precipitation values may not be representative of the irrigated lands within the cell if there are large elevation gradients within the BCSD cell. This issue was addressed through a secondary bias correction to observed weather station values typically in the same HUC8 basin where a grid cell is located over a common time period. Specifically, a temperature offset and precipitation multiplier were calculated for each cell using the historical baseline data (Maurer et al. 2002)[9] and observed weather station data. In a few isolated cases the weather stations were located in a HUC8 basin adjacent to that encompassing the grid cell.

In summary:

Why did Reclamation use BCSD projections?

- The BCSD methodology is:

[8] Available from http://gdo-dcp.ucllnl.org/downscaled_cmip_projections/dcpInterface.html. Accessed January 2014.

[9] Maurer et al. (2002) modeled minimum and maximum air temperature, precipitation, and windspeed for a 1/8-degree latitude/longitude grid covering the U.S. for the period 1950-2000. The model interpolates data from NWS Cooperative Observer Program (COOP) weather stations and adjusts for altitude effects.

- Well tested and documented, especially for applications in the United States.
- Efficient enough to permit the downscaling of many 21st century climate projections, thereby supporting a comprehensive assessment of regional to local climate projection uncertainty.
- Able to produce output that statistically reproduces a range of characteristics, including spatial and temporal patterns of historical observations when driven by climate simulations for retrospective periods.
- Capable of producing spatially continuous, fine-scale fields of precipitation and temperature suitable for water resources and other watershed-scale impacts analysis.

What are some interpretation issues that users should be aware of when using monthly BCSD climate projections?

- Residual biases remain in historical climate conditions at sub-monthly time scales.
- When bias-correcting 21st century projections, the trend for temperature projections was constrained to remain the same as that of raw GCM output, but the trend for precipitation projections was permitted to vary.[10]
- Both bias correction and spatial disaggregation affect locally portrayed climate change in BCSD projections.

Downscaled and bias-corrected CMIP3 projections form the basis for developing climate scenarios and are used to drive climate impacts assessment models in this report. The development of climate change scenarios from downscaled CMIP3 climate projections is described in the following section.

3.3 Developing Climate Change Scenarios from Downscaled Climate Projections

Climate change scenarios used in impact studies make use of downscaled climate projections. The downscaled projections are generally used in two ways:

- *Transient or Time Evolving* – Downscaled climate projections of precipitation and temperature are largely used as direct inputs to the impacts models. (Depending on the application, secondary bias correction could be needed, as was done in this study.) In essence, the temporal persistence from GCMs is conserved in driving the impacts assessment, and the impacts

[10] See http://gdo-dcp.ucllnl.org/downscaled_cmip_projections/dcpInterface.html#About) website, http://gdo-dcp.ucllnl.org/downscaled_cmip_projections/techmemo/downscaled_climate.pdf.

models are run to simulate impacts that evolve through time (i.e., transient or time evolving simulations).

- *Period Change* – Downscaled climate projections are used to inform a finite set of climate change scenarios (typically around five) by analyzing changes in precipitation and temperature between a prescribed set of future periods (e.g., three discrete future periods defined by 2010–2039, 2040–2069, and 2070–2099) compared to a reference base period (e.g., 1950–1999). Variables other than temperature and precipitation, like windspeed, can also be included.

In this report, two sets of impacts assessments were performed to meet the SECURE Water Act reporting requirements of section 9503(b)(2)(D) for any increase in (1) the demand for water as a result of increasing temperatures and changes in precipitation or (2) the rate of reservoir evaporation due to increasing temperatures and changes in precipitation. In this report, the analysis of changing demand as a result of increasing temperatures and changes in precipitation is focused on studying crop water requirements under a changing climate in the eight major Reclamation river basins. Changes to reservoir evaporation rates were analyzed for 12 reservoirs, generally one large reservoir in each of the eight major Reclamation river basins.

The BCSD projections were used to develop period change scenarios for future irrigation demand estimates, and transient scenarios for future reservoir evaporation estimates. A transient analysis would have been preferred for irrigation demands, but this was not practical given the diversity of crops and agricultural practices across the eight major Reclamation river basins, and the resulting enormous computational and data handling requirements. However, for the reservoir evaporation analysis, the modeling was simpler since there were only 12 locations and one resultant. However, to be consistent with irrigation demands climate change periods and evaluations, reservoir evaporation estimates are summarized for the periods of the 2020s, 2050s, and 2080s.

Before developing the change scenario and transient analyses, a secondary bias correction was applied to the 12 km by 12 km grid cell historical and CMIP3 BCSD projections using local weather station data. This was done because the historical and BCSD grid cell average temperature and precipitation values may not be representative of the irrigated lands within the cell if there is a large elevation gradient or difference across the cell. In addition, there are inherent model biases in estimated temperature and precipitation due to interpolation techniques, assumed lapse rates, local conditioning of near-surface temperature due to irrigation, etc. This issue was addressed through bias correction of single grid cell historical and BCSD projections to coincident observed weather station measurements of temperature and precipitation over a common time period. Specifically, a temperature offset and a precipitation multiplier were calculated

for each grid cell using the historical baseline data (Maurer et al. 2002)[11] and coincident observed weather station data. These adjustments, in essence, represent lapse rate corrections (or other bias corrections) for temperature and precipitation. In a few isolated cases, no weather station was located in a particular HUC8 basin, and so data from an adjacent basin were used. Weather-station-based bias corrections for coincident and non-coincident grid cells were applied to the full set of historical baseline data (Maurer et al. 2002). Since the period change approach used to model irrigation demands scales weather-station-based bias-corrected historical baseline time series to represent future scenarios, bias correction of future BCSD projections was not needed. This is discussed in more detail in the following paragraph.

Running a large number of downscaled climate projections through a complex impacts model such as the ET Demands model (model description is given in chapter 4) is data intensive and computationally prohibitive. Also, managing the model outputs, including interpretation of model results for effective communication, is challenging. An approach that lends itself to keeping this task manageable is to define a finite number of climate change scenarios that are used as inputs to the crop demands model. To analyze crop irrigation water requirements, a set of five climate change scenarios were developed using the method referred to as the ensemble informed hybrid delta (HDe) (Hamlet et al. 2013; Reclamation 2011). This method requires identifying a baseline period of climate and a future period of climate to estimate changes in precipitation and temperature between the base period and a future period. The baseline period used in this study is 1950–1999. Three future periods were also defined: (1) 2010–2039; (2) 2040–2069; and (3) 2070–2099. In this report, these three future periods are labeled the 2020s, 2050s, and 2080s respectively.

Changes in precipitation and temperature are first calculated for each of the 112 CMIP3 projections between the baseline period and a given future period. These precipitation and temperature changes are then mapped in two dimensions to inform climate change scenarios. Such a mapping is referred to as the projection membership diagram and is shown schematically in figure 3.

In the projection membership diagram, the point (P50, T50) represents the median (50^{th} percentile) change in precipitation and temperature between the base period (1950–1999) and a future period (e.g., 2010–2039; 2040–2069; and 2070–2099), estimated from the annual values of total precipitation and average temperature for each of the 112 downscaled CMIP3 projections. The point (P50, T50) is used as the intersection point of the change in precipitation axis and change in temperature axis. The resulting quadrants are then used to assign projections.

[11] Maurer et al. (2002) modeled minimum and maximum air temperature, precipitation, and windspeed for a 1/8 degree latitude/longitude grid covering the U.S. for the period 1950–2000. The model interpolates NWS COOP weather station observed data and adjusts for altitude effects.

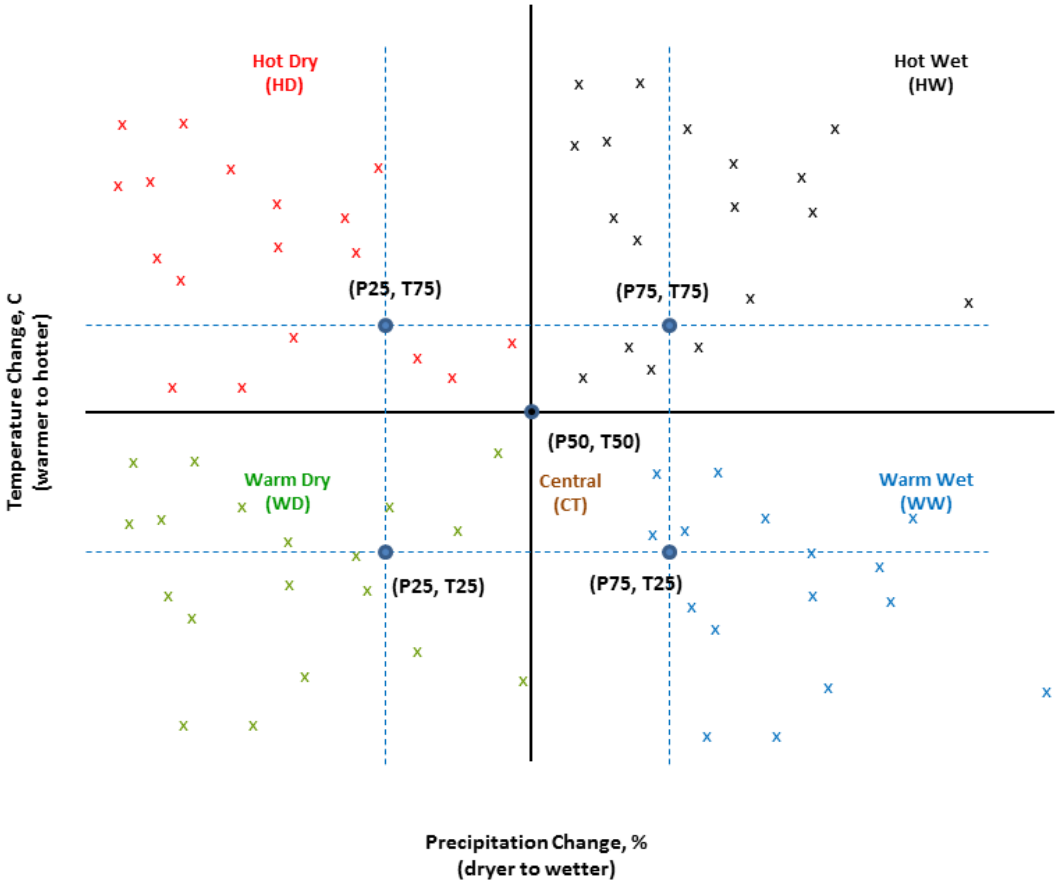

Figure 3.—Projection membership diagram to define climate change scenarios.

Changes in precipitation values along the precipitation axis range from dryer to wetter, and temperature changes along the temperature axis range from warmer to hotter. Each group of projections within a quadrant is used to inform a specific climate change scenario. A total of four climate change scenarios are defined in this manner. The fifth climate change scenario is defined by projections that fall within the box defined by the points (P75, T75), (P25, T75), (P25, T25), and (P75, T25). In summary the five climate change scenarios used in the estimation of crop water demand are:

- Scenario 1 – Warm Dry (WD) – Climate change scenario is informed by projections that show precipitation change less than P50 and temperature change less than T50.
- Scenario 2 – Warm Wet (WW) – Climate change scenario is informed by projections that show precipitation change greater than or equal to P50 and temperature change less than T50.
- Scenario 3 – Hot Dry (HD) – Climate change scenario is informed by projections that show precipitation change less than P50 and temperature change greater than or equal to T50.

- Scenario 4 – Hot and Wet (HW) – Climate change scenario is informed by projections that show precipitation change greater than or equal to P50 and temperature change greater than equal to T50.
- Scenario 5 – Central Tendency – Climate change scenario is informed by projections defined by the boundaries (P75, T75), (P25, T75), (P25, T25), and (P75, T25).

In the HDe approach (Hamlet et al. 2013), all projections corresponding to a given climate change scenario are pooled to develop two average sets of cumulative distribution functions (CDFs) for each month over the projected period. The first set is the simulated base period CDF, and the second set is the simulated future period CDF. For example, if the hot wet (HW) scenario for the future period 2010–2039 (record length, 30 years) is informed by 30 projections, the base period is 1950–1999 (record length, 50 years), and the chosen month is January, then there are 1,500 January values of precipitation (or temperature) that will be used to develop the January CDF for the simulated base period and simulated future period. The CDF of the base period (e.g., developed from a point weather station's historical observations) precipitation and temperature will, however, consist of only 30 January values. These two CDFs (simulated base period and simulated future period) are then used to develop percentile-specific monthly change factors. These change factors were used to adjust daily 12 km by 12 km spatial resolution baseline period precipitation and temperature data from Maurer et al. (2002). Unique climate change factors were developed for each of the HUC8 sub-basins with irrigated lands within the major Reclamation river basins, and for each of the three future periods: 2010–2039, 2040–2069, and 2070–2099.

The 12 km by 12 km grid cells (BCSD and historical baseline) used in the irrigation demands analysis were selected for each ET cell (HUC8 subbasin) to match the locations of the Met Node (National Weather Service Cooperative Observer Program weather station) that corresponds to the ET cell. Specifically, the temperature and precipitation data for the grid cell that typically overlies the Met Node were used to calculate irrigations demands for all irrigated lands within the associated ET cell.

For the open-water evaporation analysis, time-evolving (or transient) climate data from the 112 BCSD CMIP3 projections were used. Details of developing daily weather data from the monthly BCSD climate projections are described in the supply report (Reclamation 2011). As previously discussed, a secondary bias correction to a National Weather Service (NWS) Cooperative Observer Program (COOP) weather station near the water body of interest was applied to the projections used in this analysis.

The 12 km by 12 km grid cells (BCSD and historical baseline) used in the reservoir evaporation demands analysis were selected for each reservoir to match the location of a nearby NWS COOP weather station. Specifically, the bias-corrected temperature and precipitation data for the grid cell overlying a nearby weather station were used to calculate evaporation estimates.

CHAPTER 4 — DEVELOPING IRRIGATION WATER DEMAND AND OPEN-WATER EVAPORATION PROJECTIONS FROM CLIMATE PROJECTIONS

This chapter provides descriptions of the methods used to estimate future crop irrigation and reservoir evaporation demands, as well as the rationale for selecting the particular methods.

Irrigation water demands and evaporation models are commonly used to study historical and future irrigation water demands of crops and open-water evaporation. Several different models have been applied in Western United States basins; some examples of irrigation water demand models are:

- Land Atmosphere Water Simulator (LAWS) in the Central Valley (Tansey et al. 2011)
- ET Toolbox in the Rio Grande Basin (Brower 2008)
- Blaney-Criddle Model in Colorado River Consumptive Uses and Losses Accounting Reports (Reclamation 2013c)
- Lower Colorado River Accounting System (LCRAS) for the Lower Colorado region (Jensen 1998)
- ET Demands Model in Nevada and Idaho (Huntington and Allen 2010, Allen and Robison 2007)

A number of factors affect the selection of an irrigation demands model. Application of an irrigation water demand model to a study basin generally involves the following types of considerations (not an exhaustive list) to determine the most feasible approach:

- Spatial structure and resolution at which water balance variables will be calculated (i.e., gridded area elements such as those associated with regional and global climate models versus point locations represented by weather stations)
- Spatial scales and diversity of soil classes and characteristics that govern infiltration, soil water-holding capacity, etc.
- Dynamic responsiveness of crop characteristics that affect rooting depth , access to soil moisture, and other ET-related properties
- Sensitivity to and requirements for meteorological variables forcing the simulation such as precipitation, temperature, solar radiation, humidity, and windspeed

- Ability to compute potential and/or reference evapotranspiration using temperature only versus requiring a full suite of measured and/or simulated meteorological variables
- The complexity and accuracy of model structure and physics, such as simulation of the energy balance, soil water balance, non-growing-season evapotranspiration and precipitation accumulation, seasonal crop development and harvest for different crop types, and variable growing-season lengths
- Time steps used in simulating the soil water balance, crop phenology, open-water evaporation, and crop ET (i.e., daily or monthly)
- Calibration objectives defining which model variables are to be compared, such as simulated versus measured greenup and harvest dates, killing frost temperatures, or crop evapotranspiration

This chapter summarizes various aspects involved in developing projections of irrigation water demands and open-water evaporation, including:

- Considerations in irrigation water demands and open-water evaporation model selection to give the reader perspective on why the models were selected for this effort
- Descriptions of the irrigation water demands and open-water evaporation models selected and discussions of previous applications
- Descriptions of how meteorological data were prepared and estimated, and how these weather data were used to develop irrigation water demand estimates, including simulation setup and generation of daily weather data consistent with monthly HDe climate projections
- Discussions of model parameterization and calibration
- Discussions of simulated components for the irrigation water demands and open-water evaporation models, to help the reader better understand model results

4.1 Considerations in Selection of Irrigation Water Demands and Open-Water Evaporation Models

Considerations in selecting the irrigation water demands and open-water evaporation models are presented here to give the reader perspectives on why the particular models were selected.

4.1.1 Irrigation Water Demands

Considerations for irrigation water demands model selection focused on (1) using a widely accepted approach for estimation of crop ET (ET_c) and net irrigation water requirements (NIWR), (2) a record of successful and accepted application in the Western United States, and (3) potential for robust model application with limited projected climate variables of daily maximum and minimum temperature and daily precipitation. Among available models, there were two model types that generally satisfied these criteria:

- Models that utilize reference ET, dual crop coefficients, a daily soil water balance, and crop ET as outlined by the American Society of Civil Engineers (ASCE) and the Food and Agriculture Organization of the United Nations, FAO Irrigation and Drainage Paper 56 (Allen et al. 1998; ASCE-EWRI 2005)
- Full crop simulation and crop growth models that consider the water, nitrogen, and carbon balances, such as the Decision Support System for Agrotechnology Transfer (DSSAT) (Jones et al. 2003), Land Atmosphere Water Simulator (LAWS) (Tansey et al. 2011), and Cupid soil-plant-atmosphere model (Norman 1979)

While full crop simulation and growth models have many research advantages, and are largely biologically and physically based, the ASCE and FAO-56 irrigation water demand methodology is well suited for robust application under historical and future climate at the regional scale. This methodology has a good physics basis through the use of the reference ET (ET_{ref}) concept, and has wide acceptance among the ASCE and international agricultural engineering communities. The methodology is currently used in Arizona, California, Colorado, Idaho, Kansas, Nebraska, Nevada, and New Mexico, and is used by Reclamation for the Lower Colorado River Accounting System (LCRAS) and ET Toolbox models (Jensen 1998; Brower 2008). The University of Idaho, Nevada Division of Water Resources, and Desert Research Institute recently developed relatively robust computer code that implements the ASCE and FAO-56 reference ET and dual crop coefficient approaches, and they have made statewide applications of the model, which were referred to as ETIdaho and ETNevada models when applied in those two States (Allen 1998; Allen et al. 2005a; Allen and Robison 2009; Huntington and Allen 2010). Reclamation's west-wide application is referred to here as the ET Demands model. Results from ET Demands applications are currently used by the States of Idaho and Nevada for water rights transfers and for supporting modeling and water budget studies.[12]

[12] ET Demands model background and state applications described at "ET Idaho" http://www.kimberly.uidaho.edu/ETIdaho/online.php and at "ET Nevada" http://water.nv.gov/mapping/et/et_general.cfm documented in Allen and Robison, 2009, and Huntington and Allen, 2010, respectively.

The primary factors used in selecting the ET Demands model for this study included the following:

- Model heritage traceable to the widely accepted FAO-56 reference ET equation and dual crop coefficient approach
- Widespread general application of the K_c ET_{ref} approach across major Western United States river basins
- Flexibility for simulating future irrigation water demands by considering non-growing-season soil moisture accumulation and variable growing-season lengths

Later sections of this chapter outline general details of the ET Demands model; however, readers are referred to the above-mentioned references for more detailed explanations.

4.1.2 Reservoir Evaporation Demands

Common theoretical approaches for estimating open-water evaporation include aerodynamic mass transfer methods, the radiation-based Priestley-Taylor (1972) method, the Penman (1948) or Penman-Monteith (Monteith 1965) combination energy-mass transfer methods (Harbeck 1962; Kohler and Parmele 1967; Brutsaert and Yeh 1976), and the Bowen ratio energy balance-based method. Successful application of these methods is dependent on the quality and accuracy of the required variables, such as measured net radiation, over-water air temperature, vapor pressure, windspeed, water-surface "skin" temperature, vapor and temperature gradients, and water temperature profiles. In the case of the Priestley-Taylor, combination, and Bowen ratio methods, the generally large magnitude and significant uncertainty of heat flux into the water (G) makes the application of these methods uncertain. For operational purposes where daily, weekly, and monthly estimates are needed, the aerodynamic mass transfer approach is likely the most robust (Harbeck 1962; Allen and Tasumi 2005) since available energy (i.e., net radiation – stored heat flux) is not required, and the method has the fewest inputs. However, accurate over-the-water weather data sets (for example, collected from floating weather stations) of air and water surface temperature, vapor pressure, and windspeed are required for the most accurate application of aerodynamic mass transfer approaches, making the approach challenging to apply for operational purposes where only land-based weather data are available.

Recognizing these limitations, a simplified approach was developed by Morton (1983a) for practical and operational purposes that is based on combined energy and aerodynamic equations and that uses a simple heat storage accounting procedure. The approach, termed the Complementary Relationship Lake Evaporation (CRLE) model (Morton 1983a, Morton et al. 1985; Morton 1986), requires monthly estimates of solar radiation (R_s), air temperature (T_a), and dewpoint temperature (T_{dew}). The model, in turn, estimates water surface

temperature, albedo, emissivity, and heat storage impacts. The CRLE model is largely based on the Priestly-Taylor available energy approach in which windspeed and dewpoint are not used directly. The CRLE model is fairly insensitive to biases in T_a and T_{dew} caused by using land based weather data. The CRLE model has been fairly well tested and extensively applied in operations and modeling of open-water evaporation (Morton 1986; DosReis and Dias 1998; Sadek et al. 1997; Jones et al. 2001; Vallet-Coulomb et al. 2001; Huntington and McEvoy 2011). It overcomes many limitations of the more data-intensive mass transfer and combination approaches, thereby allowing for robust application for regional and long-range applications having limited weather data. Given these attributes and the previous successful applications of CRLE over Reclamation reservoirs (Huntington and McEvoy 2011), the CRLE model was chosen for estimating WWCRA regional baseline and projected open-water evaporation.

4.2 ET Demands and Open-Water Evaporation Model Background and Applications

4.2.1 ET Demands Model Description and Parameterization

The ET Demands model is based on the common reference ET-crop coefficient approach, in which the reference ET (ET_0), representing climatic demand for water and based on physical relationships, is multiplied by a crop coefficient (K_c) to estimate the crop ET (ET_c) of a vegetated area. ET_0 refers to ET from a reference surface that is actively growing, not limited by soil moisture, and is at full cover and peak height. There are many methods available for estimating ET_0. While many of these methods are simple temperature-based techniques, others are more data intensive, physically based models such as the Penman-Monteith (PM) method. Estimates of ET_0 vary widely among the methods, and until the last decade there was considerable debate as to the more correct and appropriate method. The professional and scientific communities now generally recognize the FAO-56 (Allen et al. 1998) and ASCE-EWRI (2005) standardized PM method (ASCE-PM) as the most appropriate and recommended ET_0 method for computing crop ET and NIWR. This was a primary consideration and reason that it was incorporated into the ET Demands model.

Measurements of solar radiation, air humidity, and windspeed are often limited, but are required for the ASCE-PM method. Limited measurements of solar radiation, humidity, and windspeed needed for the physically based ET_0 methods have, in the past, led to the use of simpler and limited temperature-based methods to assess historical and future crop ET. To facilitate use of the more accepted and accurate ASCE-PM ET_0 method in this work, the approach used here merges empirical techniques and interpolation of agricultural weather station information.

The result is the production of robust and climatically sensitive data sets of crop ET and NIWR estimates that are based on a widely accepted approach.

The ratio of ET_c to ET_0 is known as the crop coefficient (K_c). K_c curves are developed to represent specific crop phenological development and are used to scale ET_0 to produce the ET_c of a particular crop or surface. Many commonly utilized K_c curves were derived from research weighing lysimeter measurements of ET_c from stress-free crops and using ET_0 calculated from data collected near the lysimeter site. The two primary ET research sites in the 1960s to the 1980s were at the University of California-Davis and the USDA's Agricultural Research Service laboratory in Kimberly, Idaho (Doorenbos and Pruitt 1977; Wright 1981, 1982).

This work uses a dual crop coefficient and daily soil water approach to compute ET_c. In this approach, the K_c value is separated into a "basal" crop coefficient, K_{cb}, and a soil evaporation coefficient, K_e (Allen et al. 1998; Allen et al. 2005a). The advantage of using a dual crop coefficient over a "mean" or single crop coefficient approach is that it allows for separate accounting of transpiration and evaporation to better quantify evaporation from specific precipitation and modeled irrigation events. That separation allows for accounting of wintertime soil moisture gains, which is essential for accurately computing the NIWR. The NIWR is defined as the annual crop ET less the effective precipitation entering the root zone that is available for evaporation or transpiration. NIWR is synonymous with the terms *irrigation demand*, *net consumptive use*, and *precipitation deficit* (Allen and Wright 2009; Huntington and Allen 2010).

The heritage of many K_{cb} values utilized in this study can be traced to Wright (1982), the Reclamation AgriMet program (http://www.usbr.gov/pn/agrimet/), and FAO-56 (Allen et al. 1998). The following sections describe the development of weather variables, crop coefficients, soil variables, and cropping information required for computing ET_0, ET_{cc}, and NIWR in the ET Demands Model.

4.2.1.1 Reference ET Estimation

Reference ET is estimated in ET Demands using the standardized reference ET equation for an extensive surface of short (0.12 m tall) grass as a reference (ASCE-EWRI 2005). The standardized reference ET equation for short grass is

$$ET_o = \frac{0.408\Delta(R_n - G) + \gamma \frac{C_n}{T + 273} u_2 (e_s - e_a)}{\Delta + \gamma(1 + C_d u_2)}$$

where:

ET_0 = Standardized reference crop evapotranspiration for short grass [mm d^{-1}]

R_n = Calculated net radiation for the standardized grass reference surface [MJ m^{-2} d^{-1}] and is a function of daily average solar radiation, maximum and minimum temperature, average vapor pressure, and elevation

G = Soil heat flux density at the soil surface [MJ m^{-2} d^{-1}] and is assumed to be 0 over a day

T = Mean daily air temperature at the 1.5 to 2.5 m height [°C]

u_2 = Mean daily windspeed at 2 m height [m s^{-1}]

e_s = Saturation vapor pressure at 1.5 to 2.5 m height [kPa], calculated for daily time steps as the average of saturation vapor pressure at maximum and minimum air temperatures

e_a = Mean actual vapor pressure at 1.5 to 2.5 m height [kPa]

Δ = Slope of the saturation vapor pressure-temperature curve [kPa $°C^{-1}$]

γ = Psychrometric constant [kPa $°C^{-1}$]

C_n = Numerator constant of 900

C_d = Denominator constant of 0.34

The short grass standardized reference ET, as opposed to the taller alfalfa standardized reference ET, was chosen due to previous usage across several major Reclamation projects. BCSD historical and future climate projections utilized in this study are restricted to daily maximum and minimum air temperature and precipitation, similar to most historical NWS climate records. This did facilitate comparison to large numbers of selected NWS COOP stations (table 1 and appendix 2) but required the estimation of daily dewpoint temperature, solar radiation, and windspeed to compute ET_0. The estimation of these parameters followed recommendations of ASCE-EWRI (2005) and the approach outlined by Allen and Robison (2009) and Huntington and Allen (2010). The following three sections describe the background and approaches used for quality assurance and quality control (QAQC) of measured weather station data, and procedures used to estimate mean daily actual vapor pressure, solar radiation, and windspeed.

Measured agricultural weather station data were downloaded from 564 weather stations (appendix 2) and from 14 different agricultural and research weather networks (see table 1). Measured weather data sets containing daily maximum and minimum temperature (T_{max} and T_{min}), daily average dewpoint temperature (T_{dew}), daily average solar radiation (R_s), and daily average windspeed (u_2) were assembled for the periods of record for each station and were then closely checked for QAQC following guidelines and recommendations by ASCE-EWRI (2005), Allen (2008), and Allen (1996). Custom Matlab scripts were written to display data, provide QAQC options, and correct or omit questionable data for each station.

The most common variable needing correction at stations was measured R_s. Measured R_s at 43 agricultural weather stations was used for calibrating a general empirical formulation for estimating R_s following the approach of Thornton and Running (1999), which is more fully described in the following paragraphs. R_s is commonly under- or over-measured due to debris on the pyranometer window, a non-level base plate, sensor miscalibration or drift, or obstructions. Errors also

result from faulty recording of time. Corrections to measured R_s were made using the theoretical clear sky solar radiation, R_{so_b} (ASCE-EWRI 2005), where daily ratios of R_s/R_{so_b} for specified time windows (usually 30–90 days duration) were ranked, and the top 10 percentile were computed. The average ratio for the top 10 percentile was used to scale the respective measured R_s for all days within the specified time window. The scaling generally corrected for faulty calibration, nonlevelness, or a soiled instrument. These correction procedures were applied as needed to user-specified periods based on visual inspection of R_s and R_{so_b}. For examples and illustrations of this correction procedure see ASCE-EWRI (2005), Allen (2008), and Allen (1996).

Dewpoint temperature (T_{dew}) is defined as the temperature to which a parcel of air must be cooled to become saturated with water vapor. In an irrigated setting, daily minimum temperature (T_{min}) often approaches T_{dew}, due to conditioning of the near-surface boundary layer, especially during early morning if the wind is calm and soil moisture is high. In this study, the daily average T_{dew} for baseline and projected climate was estimated as $T_{dew} = T_{min} - K_{o(i)}$, where T_{min} is the daily minimum air temperature (°C) and $K_{o(i)}$ is an offset coefficient (°C) for each month *i*. K_o is the dewpoint depression. This approach has been used in large regional studies by Thornton et al. (1997) and in gridded weather data sets such as PRISM (Daly et al. 1994) to produce estimates of humidity.

It is common in arid and semiarid regions to have a T_{dew} of 2 to 8°C below T_{min} under well watered conditions (Allen 1996; ASCE-EWRI 2005; Huntington and Allen 2010). In this work, mean monthly K_o was estimated for each month over each basin by utilizing available agricultural station network weather data, computing mean monthly K_o values for each station (appendix 2), and spatially interpolating mean monthly K_o values for station locations. Figure 4 illustrates mean monthly K_o for four agricultural weather stations spanning a range of climatic zones (Klamath Falls, OR, Twin Falls, ID, Fallon, NV, and Aguila, AZ), where it is evident that regional and local humidity levels greatly impact the seasonal value of K_o in irrigated environments. Mean monthly, spatially interpolated K_o results were averaged over unique HUC8 drainage areas. The HUC8 mean monthly K_o values were then assigned to respective HUC8 Met Nodes. Spatial distributions of mean annual K_o for each basin are illustrated in basin-specific results sections (chapter 5).

Table 1.—West-Wide Climate Risk Assessment Basin Information

Basin	Number of HUC8s	Number of study Met Nodes	Type of historical Met Nodes	Agricultural dewpoint depression and wind stations	Number of dewpoint depression and wind stations	Number of ET cells	Type of ET cells	Source of crop mix	Irrigated acres
Central Valley	29 ([2])	26	COOP	CIMIS	49	38	Planning Model	USDA Cropland Data Layer (CDL)	6,277,365
Columbia	164	192	COOP	Reclamation AgriMet	67	209	Portions of HUC8s based on distribution of CDL data to Met Nodes[3]	CDL	11,812,144
Imperial	2	2	COOP	CIMIS	7	2	HUC8	CDL	449,411
Lower Colorado	57	55	COOP	AZMET, CIMIS, NICE Net, AgWxNet	50	76	Union of counties and HUC8s[4]	Consumptive Uses and Losses (CU&L) Report and CDL	995,618
Upper Colorado	57	85	COOP	HPRCC-AWDN, AgWxNet, CoAgMet, DRI-WRCC, NRCS-SCAN	47	193	Union of counties and HUC8s[4]	CU&L Report	1,533,713
Klamath	12	13	COOP	CIMIS and Reclamation AgriMet	9	13	All HUC8s except Klamath Project lands, which were computed by CA and OR area offices	All CDL except Klamath Project lands, which were provided by area office by CA and OR	363,475
Missouri[5]	310	310	COOP	HPRCC-AWDN, CoAgMet, Reclamation AgriMet, MSU, NOAA	307	310	HUC8	Great Plains Region access database	14,818,198
Rio Grande	22	22	COOP	CoAgMet, NMSU Agrimet	24	22	HUC8	CDL	756,419
Truckee	12	22	COOP	Reclamation AgriMet, USGS Bowen and eddy stations	7	22	Portions of HUC8s based on distribution of CDL data to Met Nodes[3]	CDL	234,016

[1] Crop types and acres are summarized for each basin and all HUC8 areas in Appendix 11.
[2] Planning Areas provided by Reclamation Mid-Pacific Region Office were used instead of HUC8s.
[3] Proportions are determined by number of Met Nodes in HUC. Two Met Nodes (0.5), Three Met Nodes (0.3333), etc.
[4] Planning model nodes, aka Units, that are the geographic union of a county and HUC8.
[5] Great Plains region Access database has 258 Met nodes. Some are shared between HUCs. For WWCRA, a unique Met node was identified for each HUC.

Weather Station Acronym Descriptions:

AgWxNet – Utah Agricultural Weather Network – http://climate.usurf.usu.edu/agweather.php
AZMET – The Arizona Meteorological Network – http://ag.arizona.edu/azmet/
CIMIS – California Irrigation Management Information System – http://wwwcimis.water.ca.gov/cimis/
COOP – NOAA Cooperative Observer Program – http://www.nws.noaa.gov/om/coop/
CoAgMet – Colorado Agricultural Meteorological Network – http://ccc.atmos.colostate.edu/~coagmet/
DRI-WRCC – Desert Research Institute – Western Regional Climate Center – Uinta Ag. Stations – http://www.wrcc.dri.edu/uintabasin/
HPRCC-AWDN – High Plains Regional Climate Center – Automated Weather Data Network – http://www.hprcc.unl.edu/awdn/
MSU – Montana State University Southern Agricultural Research Center – http://www.sarc.montana.edu/php/
NICE Net –Nevada Integrated Climate and Evapotranspiration Network – http://nicenet.dri.edu/
NMSU Agrimet – New Mexico State University Middle Rio Grande Agricultural Weather Data – http://weather.nmsu.edu/
NOAA – National Oceanic and Atmospheric Administration – NCDC – http://www.ncdc.noaa.gov/http://www.ncdc.noaa.gov/
NRCS-SCAN – Natural Resource Conservation Service Soil Climate Analysis Network – http://www.wcc.nrcs.usda.gov/scan/
Reclamation AgriMet – http://www.usbr.gov/pn/agrimet/agrimetmap/agrimap.html
USGS – U.S. Geological Survey Nevada Water Science Center ET Studies – http://nevada.usgs.gov/water/et/

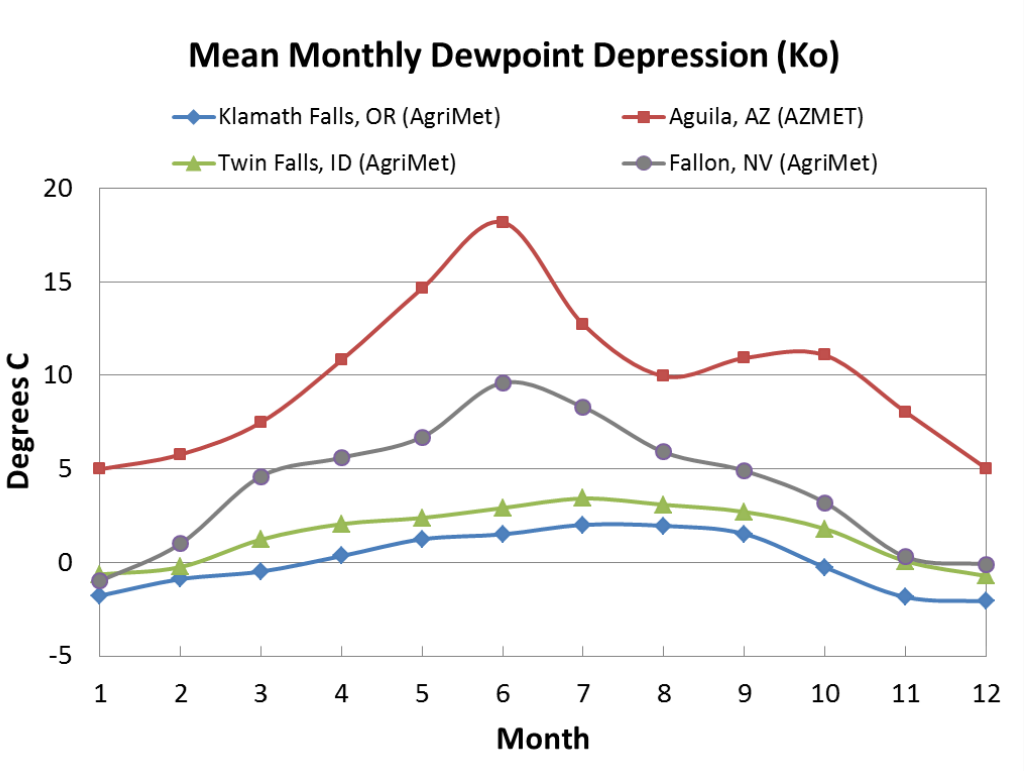

Figure 4.—Mean monthly $T_{min} - T_{dew}$, termed dewpoint depression (K_o), for agricultural weather stations in the Klamath (Klamath Falls, OR), Columbia (Twin Falls, ID), Lower Colorado (Aguila, AZ), and Truckee (Fallon, NV) River Basins.

In general, the spatial distributions of mean monthly and mean annual K_o co-vary with precipitation distribution and amount. K_o is lower where available water is regionally more abundant and higher where available water is regionally limited (i.e., where the air is more or less humid, respectively) (see chapter 5 figures). The production of spatial distributions of K_o derived from agricultural weather stations is advantageous because it produces a simple approximation of the humidity of the lower air mass that is consistent and representative of agricultural areas, while preserving regional and local advection and aridity effects. Additionally, several recent studies have shown good skill in estimating actual ET and ET_0 when utilizing mean monthly K_o and T_{min} to estimate humidity (Crago et al. 2010; Huntington and Allen 2010). Crago et al. (2010) showed that the use of K_o and daily T_{min} estimated humidity to within 5 and 7 percent of measured humidity. Historical and projected daily average vapor pressure, e_a, needed in the ASCE-PM equation, was computed from daily average estimated T_{dew} following Murray (1967) as

$$e_a = 0.6108 \exp\left[\frac{17.27 T_{dew}}{T_{dew} + 237.3}\right]$$

Where T_{dew} is in °C and e_a is in kPa. Saturated vapor pressure, e_s, was computed using the same equation, but with T_{max} and T_{min}, and then averaged to estimate daily average e_s.

A general empirical formulation of Thornton and Running (1999) was used to estimate daily average R_s for baseline and future climate projections. The formulation utilizes the difference between daily maximum and minimum air temperature and an estimate of the daily average clear sky solar radiation for a specific elevation and latitude. The Thornton and Running (1999) method estimates R_s as

$$R_s = R_{so\_b}\left[1 - 0.9\exp\left(-B\left(T_{\max} - T_{\min}\right)\right)^{1.5}\right]$$

and

$$B = b_0 + b_1 \exp\left(b_2 \Delta T_{month}\right)$$

where

R_{so_b} is the theoretical clear sky solar radiation (MJ m^{-2} d^{-1}), which accounts for variations in e_a following ASCE-EWRI (2005),

T_{max} is the daily maximum air temperature (°C),

T_{min} is the daily minimum air temperature (°C),

B is an empirical fitting function, with coefficients, b_0, b_1, and b_2, being 0.023, 0.1, and –0.2, respectively and

ΔT_{month} (°C) is the difference in long-term values for T_{max} and T_{min} on a monthly basis.

The general premise of the method is based on cloud cover reducing daily T_{max} and increasing daily T_{min} due to reduced R_s during the day and increased downward emission of long wave radiation by clouds during the night (Allen 1997). A modified version of the Thornton and Running (1999) approach was recently developed by adjusting fitting function coefficients specific to the region of interest, and has been applied with good results by Allen and Robison (2009) and Huntington and Allen (2010) in Idaho and Nevada for estimating R_s from T_{max} and T_{min} at NWS and agricultural weather stations. A similar approach was used here where basin-specific fitting function coefficients were optimized by uniform random search Monte Carlo sampling (15,000 iterations per station), and by finding station-specific coefficient sets (i.e., b_0, b_1, and b_2) that produced the least average difference between predicted and measured R_s for historical periods at 43 agricultural weather stations across the study area (appendix 3). Equal weighting for growing-season and non-growing-season periods was assumed when finding the optimal coefficient sets for each station. Optimal coefficient sets for each station were then averaged across multiple stations in each of the seven study area river basins (table 1) to develop basin average specific coefficient sets (i.e., one set of b_0, b_1, and b_2 for each basin). Location-specific R_s was then estimated using the respective basin average calibrated Thornton-Running (TR) equation, and compared to respective agricultural weather station R_s measurements (appendix 4).

An example illustrating the comparison of measured and estimated R_s using the standard and basin average calibrated TR equation is shown in figure 5 for the Colorado State University Fruita CoAgMet station located in the Upper Colorado basin. The basin-derived values for b_0, b_1, and b_2 were 0.018, 0.20 and –0.25, respectively, which compare to standard coefficients of 0.023, 0.10, and –0.20. Estimation of R_s was improved using the optimized coefficients due to the tendency of the optimized coefficients to reduce the number of overestimated values for R_s, even though the modal values for estimated R_s were, on average, less than measured modal values.

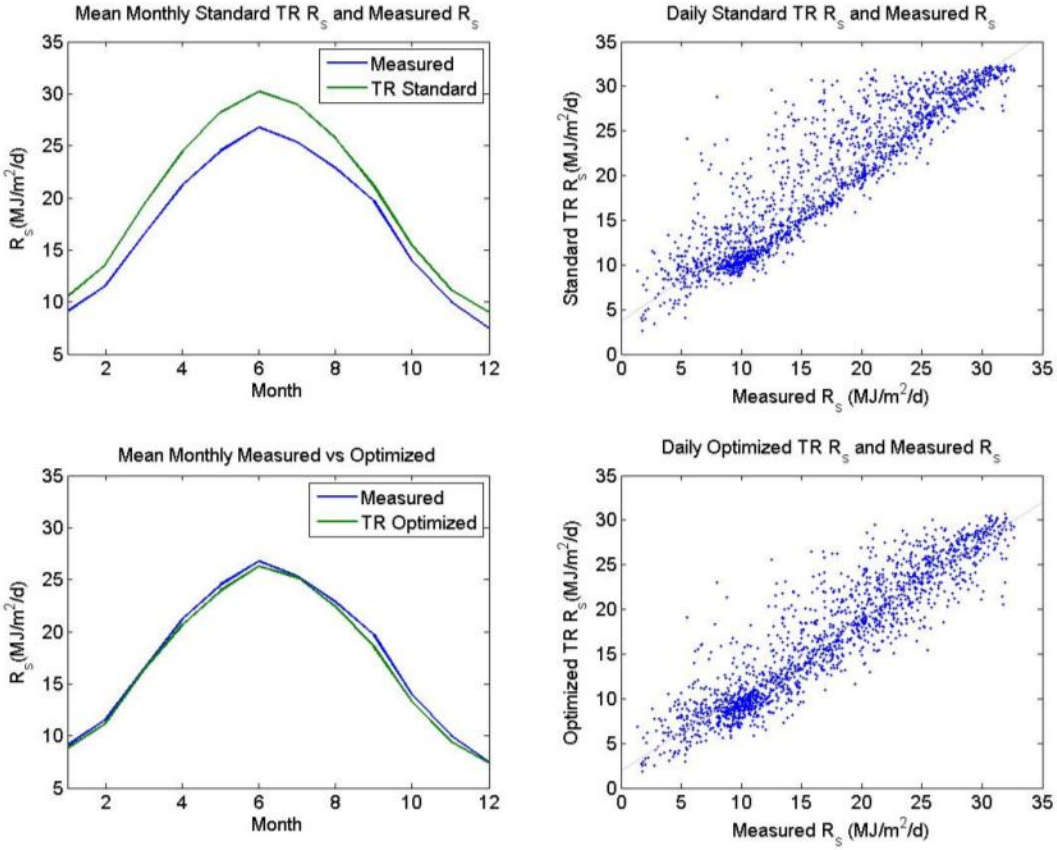

Figure 5.—Comparison of measured and estimated incoming shortwave solar radiation (Rs) using the standard TR equation (top), and basin-specific optimized TR equation coefficients (bottom) for the Colorado State University Fruita CoAgMet station located in the Upper Colorado basin.

The average monthly ratios of estimated optimized R_s to measured R_s for each basin ranged from 0.98 to 1.03, with a study-wide average of 1.00 and a standard deviation of 1.07. The basin average root mean squared error for daily estimated R_s ranged from 2.25 MJ/m^2/d to 3.55 MJ/m^2/d, with a study-wide average of 2.84 MJ/m^2/d (appendix 4). In general the TR equation using basin averaged optimized coefficients was judged to provide reasonable estimates for R_s over ranges measured and during all months of the year.

Quality assured and controlled historical measured windspeeds at 564 agricultural weather stations across the study area were used to estimate the 2-meter height equivalent daily windspeed for baseline and future projected climate at each Met Node. The QAQC of wind data was conducted using visual assessments of day-to-day variation in windspeed, visual inspection of low and high ranges, and comparison of windspeed data among regional stations.

Given that future projections of windspeed are largely uncertain, especially at local scales of many irrigated areas in the western U.S., it is difficult to make projections of change in windspeed from historical conditions. As a result, future windspeed is estimated using historical mean monthly observations that are currently representative of impacts of the local terrain and impacts of surface energy balance conditions that exist in the areas of interest. This usage is likely to minimize significant error in baseline and future projections of ET_0. As a result, and similar to estimating K_o information for unique HUC8s and respective Met Nodes, mean monthly windspeed was summarized from historical agricultural station data, spatially interpolated, and spatially averaged to HUC8 boundaries for each primary river basin. Mean monthly spatially averaged windspeed values were then paired to baseline and projected climate data sets for respective Met Nodes. Daily windspeed estimates were paired with daily historical and projected climate for each Met Node as

$$u_2 = u_{2\ mean\ monthly\ (i)}$$

where u_2 is the estimated daily average 2 meter height windspeed, and $u_{2\ mean\ monthly\ (i)}$ is the respective HUC8 and Met Node 2 meter height windspeed assigned for month *i*.

4.2.1.2 Crop ET Estimation

ASCE-PM-based grass reference ET_0 was computed for baseline and projected climate data sets at each Met Node using baseline and projected T_{max} and T_{min} paired with estimated R_s, $T_{dew,}$ and u_2 based on historical agricultural weather station data. Actual ET for a range of crop types was estimated at each Met Node using the FAO-56 dual crop coefficient approach having the form:

$$ET_c = (K_s K_{cb} + K_e) ET_0$$

where ET_0 is ASCE-PM grass reference ET, K_{cb} is the basal crop coefficient, and K_e is a coefficient representing evaporation from the soil surface. K_{cb} and K_e are dimensionless and range from 0 to 1.4 when used with ASCE-PM grass reference ET. Daily K_{cb} values over a season, commonly referred to as the crop coefficient curve, represent impacts of changes in vegetation phenology on crop ET, which can vary from year to year depending on the start, duration, and termination of the growing season, all of which are dependent on temperature conditions during spring, summer, and fall periods. The stress coefficient (K_s) ranges from 0 to 1, where 1 equates to no water stress, which is generally the case for fully irrigated crops during the irrigation season as opposed to rain fed crops or native vegetation, which commonly experience some soil water-induced stress. A daily

soil water balance for the simulated effective root zone is required to calculate K_s and is computed in ET Demands. K_s is generally 1 when computing ET_c and NIWR for irrigated crops, but can become less than 1 during winter when precipitation is low. ET Demands estimates of K_s during winter, for dormant covers of mulch and grass, can go below 1 since there is no irrigation specified for dormant periods. A second daily soil water balance for the upper 0.1 m of soil is used in ET Demands to estimate K_e. The upper 0.1 m zone is assumed to be the only layer supplying water for direct evaporation from the soil surface.

The NIWR is estimated as the ET_c minus precipitation residing in the root zone, P_{rz}. Precipitation residing in the root zone is the amount of gross reported precipitation that infiltrates into the soil and that remains in the root zone for consumption by evaporation or transpiration. Although P_{rz} includes precipitation that is later evaporated and possibly not transpired by the crop, ET_c includes evaporation of precipitation, therefore ET_c minus P_{rz} represents the net irrigation water requirement, and not ET_c minus the P_{rz} portion that is effective toward transpiration only. P_{rz} is computed as P – Runoff – $DPerc_p$ where P is gross reported precipitation, Runoff is estimated surface runoff, and $DPerc_p$ is deep percolation of any precipitation below the maximum root zone for the crop or land-use condition.

The daily soil and root zone water balances in ET Demands are based on a two-stage drying procedure following the work of Allen et al. (1998) and Allen et al. (2005a). Recent research has shown that the relatively simple two-stage drying soil water balance model adopted for ET Demands is robust in simulating bare soil evaporation when compared to the more physically based model HYDRUS-1D (Allen 2011). Soil attributes needed for ET Demands parameterization were obtained from the NRCS State Soil Geographic (STATSGO) database (USDA-NRCS 1991). STATSGO is a spatial soils GIS database and contains attributes of the physical character of soils needed to estimate soil water holding and infiltration parameters in the ET Demands model's dual soil and root zone water balance and runoff modules. Specifically, STATSGO attributes of available water capacity, and sand, silt, and clay fractions were used to estimate the spatial distribution of total evaporable water and readily evaporable water used in the surface soil layer water balance, and total available water and readily available water were used in the root zone water balance. A schematic of the FAO-56 root zone water balance adopted for ET Demands is shown on figure 6. These parameters affect the estimation of irrigation scheduling, evaporation losses from soil, deep percolation from root zones, antecedent soil moisture condition, and runoff from precipitation. Gridded soil attributes for available water capacity and sand, silt, and clay fractions were averaged over 60-inch (150-cm) depths and were then intersected with irrigated crop land areas and spatially averaged within each HUC8. This limited the soil parameterization to cropland areas only. Except for portions of the Colorado and Klamath River Basins, croplands were identified from the 2010 Cropland Data Layer (CDL) (USDA-NASS 2010a). 2009 cropland data for Reclamation's Klamath Project portion of the Klamath

River Basin were provided by Reclamation's Klamath Basin Area Office. In the Colorado Basin, the primary source of cropping data came from Reclamation's Consumptive Uses and Losses (CU&L) Reports. 2005 CU&L data were used for the lower basin (Reclamation 2012b), and 2008 CU&L data were used for the upper basin (Reclamation 2013c). Supplemental cropping data for the Imperial and Decree accounting areas of the lower basin (for which CU&L data were not produced) was taken from the 2007 CDL since that data was the closest to the 2005 CU&L data. Spatially averaged cropland HUC8 soil attributes were intersected with coincident HUC8 Met Nodes for parameter input into the ET Demands model.

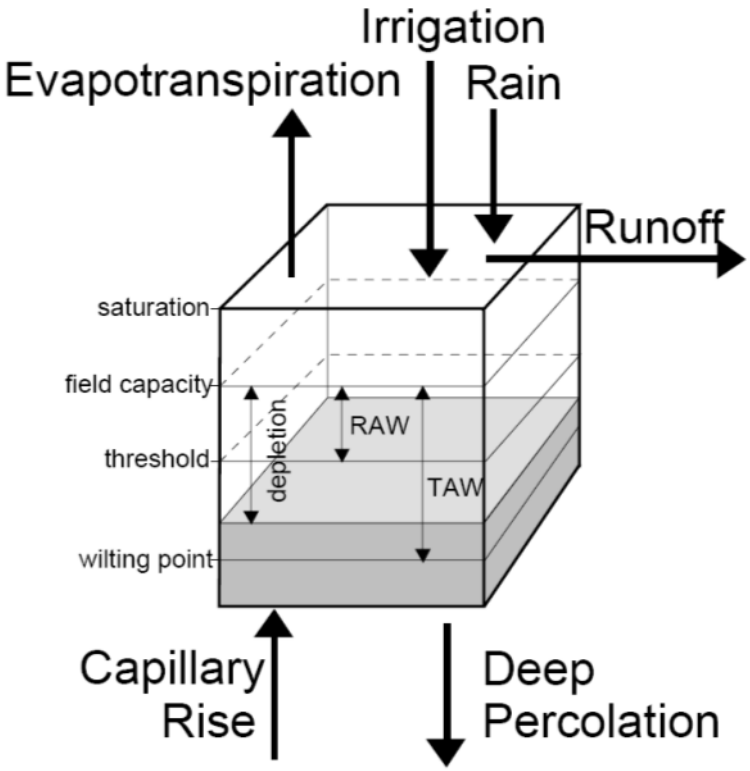

Figure 6.—Schematic of the FAO-56 soil and root zone water balance adopted in the ET Demands Model. Capillary rise in this study was assumed to be negligible. Modified from Allen et al. (1998).

Root growth is simulated in ET Demands for each crop as a function of time and is used to calculate the root zone volume for soil water balance calculations. Root growth is assumed to begin from a specified initial depth at the simulated time of planting or greenup and to attain maximum effective root depth after a specified time. The Borg and Grimes (1986) root growth function is used to estimate a sinusoidal root depth rate as a function of time. For a full description on the background of soil and root zone water balance parameters, readers are referred to Allen et al. (1998, 2005a) and Bos et al. (2008). For examples of estimation and

application of parameters, readers are referred to Allen and Robison (2009) and Huntington and Allen (2010).

Although most agricultural areas are relatively flat, runoff from those areas can be significant during large precipitation events, and are accounted for in estimating the NIWR. The magnitude and duration of runoff is influenced by soil texture, soil structure, sealing of the soil surface, slope, local land management such as tillage and furrowing, antecedent moisture, and precipitation intensity and duration. Because of the difficulties and uncertainties in estimating sealing, tillage, intensity and duration parameters, runoff was not estimated using the more data intensive and physically based models. Instead, the fairly simple and widely accepted USDA-NRCS curve number (CN) approach (USDA-SCS 1972) is used in ET Demands. Required data for the CN method are soil texture-based properties, crop type, and daily precipitation depth. A daily soil water balance is used to estimate antecedent soil-water conditions (ASC). Curve number hydrologic soil groupings were determined from spatially averaged percent sand, silt, and clay fractions over agricultural areas within each HUC8 in the study area. Curve number hydrologic groupings of A, B, and C were estimated using the following logic: if sand is greater than 50 percent then the type is A; if clay is greater than 40 percent then the type is C; otherwise the type is B. Antecedent soil water content impacts the CN value due to the dependency of soil water content on unsaturated hydraulic conductivity. To approximate this effect, ET Demands adjusts the CN value according to the estimated soil water content prior to any precipitation. Adjustment of CN values is based on the approach of USDA-SCS (1972) and Allen (1988) for dry (ASC I) and wet (ASC III) conditions. Expressions by Hawkins et al. (1985) are utilized in ET Demands to scale CN values in between dry and wet conditions according to antecedent soil water contents.

Simulation of irrigation events by ET Demands occurs when the root zone dries to the crop-specific maximum allowable depletion (MAD) threshold, where stress is specified to occur. For most irrigated crops in ET Demands, an unlimited water supply is assumed and irrigations are scheduled at the onset of MAD. Irrigations are specified to fill the root zone according to the cumulative depletion amount. Parameterization of crop-specific initial and growing-season MAD values were adopted from Allen et al. (1998) and Allen and Robison (2009) and were modified for some crops to better simulate typical frequencies of observed irrigations. Deep percolation past the root zone is assumed to occur when the soil water content exceeds the field capacity due to precipitation. Deep percolation from irrigations is simulated as 10 percent of the simulated irrigation depth on the day of the simulated irrigation (Allen and Robison 2009). Deep percolation due to irrigation is typical in practice to allow roots to develop and grow into moist soil throughout the season. Deep percolation of irrigation in ET Demands does not increase the NIWR but is only estimated for hydrologic purposes.

4.2.1.3 Crop Coefficients

Vegetation phenology is impacted by seasonal and annual changes in solar radiation, temperature, precipitation, and agricultural practices. Seasonal changes in vegetation cover and maturation are simulated in ET Demands using crop coefficient curves. Figure 7 illustrates the seasonal progression of a typical K_{cb} curve for different crop stages using the widely used linear, time-based FAO-56 curve construction.

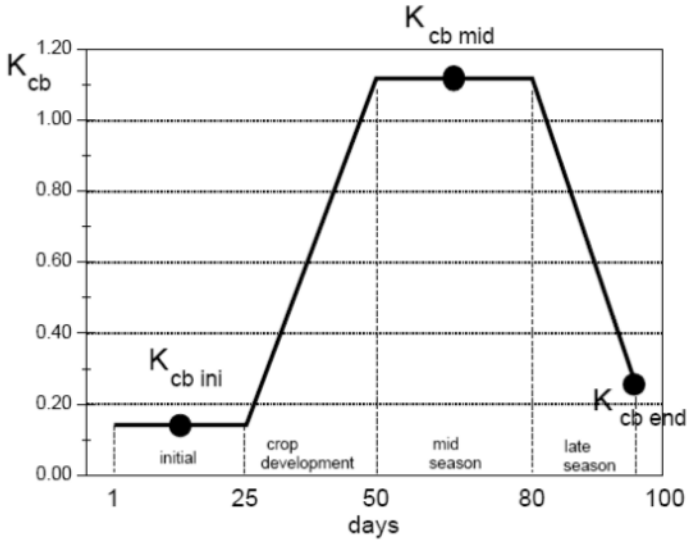

Figure 7.—Schematic showing the typical shape of the FAO-56 K_{cb} curve with four different crop stages. Modified from Allen et al. (1998).

Shortly after planting of annuals or the emergence of perennials, the value of K_{cb} gradually increases from an initial value of ~0.1 to 0.2, and, as the vegetation develops and leaf area increases during the growing season, the K_{cb} curve increases until the vegetation reaches full cover or some maximum cover. During the middle stage of the growing season, the K_{cb} curve is generally constant or is reduced due to simulated cuttings and harvest. From the middle stage to the end of the growing season the K_{cb} curve is reduced over time to simulate aging and drying of leaves.

For this work, basal crop coefficient (K_{cb}) curves from Allen and Robison (2009) were adopted for the application of ET Demands. The Allen-Robison curves are largely traceable to lysimeter-based K_{cb} curves of Wright (1982, 2001) and are based on the taller alfalfa reference ET (ET_r). Additional K_{cb} curves were added to the ET Demands model based on FAO-56 values, making a total of 49 crop-specific K_{cb} curves. Details of K_{cb} curve source, values, and figures for each crop are provided in appendix 5. Because the relatively more widely utilized ASCE standardized Penman-Monteith short reference (ET_0) method was used in the application of ET Demands, K_{cb} curves derived from Wright (2001) by Allen and Robison (2009) were converted from an ET_r to an ET_0 basis by multiplying the

K_{cb} curve values by 1.20, which is a standardized ratio of tall to short reference ET for a standard subhumid climate condition proposed by FAO-56, in which the mean 2-m-height windspeed averages 2 m/s and mean daily minimum relative humidity is 45 percent. Following the conversion of K_{cb} to the standard climate, the ET Demands model simulates the impacts of aridity and advective conditions on the K_{cb} value following procedures outlined in FAO-56 and Bos et al. (2008), which increase the daily K_{cb} based on the estimated daily relative humidity, windspeed, and simulated crop height.

Air and soil temperatures regulate nearly all plant functions; therefore, vegetation phenology is closely related to thermal heat units rather than calendar dates. For this reason, the cumulative growing degree-days (CGDD) concept has gained widespread use and is used as a primary method in ET Demands. Rather than using the popular linear interpolation, time-based approach for constructing the K_{cb} between specified time intervals and growth points (i.e., as shown on figure 7), ET Demands uses three complementary methods based on thermal heat units and normalized time. The thermal heat unit method is the primary method used to simulate the effects of air and soil temperature on vegetation development and on the start, duration, and termination of annual growing-season and non-growing-season periods. The three methods define the advancement of the K_{cb} curve based on (1) normalized cumulative growing-degree-days from planting or greenup to effective full cover, with this ratio extended until termination of the cropping period; (2) percent time from planting to effective full cover, with this ratio extended until termination; and (3) percent time from planting to effective full cover and then number of days after full cover to termination. These K_{cb} development approaches allow for time interpolation and shape of crop-specific K_{cb} curves to be a function of cumulative growing degree days and temperature-dependent planting or greenup estimates rather than specified and constant calendar dates. Figures of K_{cb} curves for the three different time interpolation methods are shown in appendix 5. CGDD has previously been used for defining planting and greenup times, crop coefficient development, scaling of development periods, and transferring K_{cb} curves among regions in a wide range of studies (Sammis et al. 1985; Slack et al. 1996; Howell et al. 1997; Snyder et al. 1999; Wright 2001; deTar 2004; Marek et al. 2006; Allen and Robison 2009). The growing-degree-day (GDD) value is estimated in ET Demands following Mitchell (1997) and Wright (2001) as

$$GDD = \max\left(\frac{T_{\max} + T_{\min}}{2} - T_{base}, 0\right)$$

where T_{max} and T_{min} (°C) are the daily maximum and minimum air temperatures, respectively, and T_{base} is the crop-specific base temperature. If T_{min} is far enough below T_{base} (°C) to cause the average daily temperature to be below T_{base}, then GDD is zero. The formulation above is suggested by Wright (2001) for areas where cold nighttime temperatures can limit growth and is realistic for many

crops in semi-arid climates. A common formulation of the GDD equation, known as the standard corn GDD equation, is used in ET Demands for corn where

$$GDD_{corn} = \left(\frac{\max\left(\min\left(T_{\max},30\right),10\right) + \max\left(\min\left(T_{\min},30\right),10\right)}{2} \right) - 10$$

This formulation assumes no growth for portions of a day having air temperatures above 30°C and no negative adjustment to the GDD value if the minimum temperature goes below 10°C. The normalized cumulative growing-degree-day (NCGDD) is adopted in ET Demands following Wright (2001); it is

$$NCGDD = \frac{CGDD_i}{CGDD_{EFForTERM}}$$

where $CGDD_i$ is the cumulative growing-degree-day total for the i^{th} day of the crop's growing period, and $CGDD_{EFF\ or\ TERM}$ is the specified crop-dependent value for CGDD from the time of planting or greenup to the attainment of effective full cover. Values for NCGDD range from 0 to 1 for the period from planting or greenup to effective full cover, and NCGDD usually ranges from 1 to 2 for the period extending from time of effective full cover until harvest or killing frost. The NCGDD, as computed, is used as the basis for defining K_{cb} values over time. This is generally done by specifying values for K_c for each 10-percent increase in the value for NCGDD. Formulation of percent-time-based curves is similar to that for NCGDD, but is time based. Crops were assigned NCGDD or time-based parameters, based on previous applications of Allen and Robison (2009). The majority of crops were NCGDD based as summarized in appendix 5. Basal K_{cb} crop coefficient curves are computed daily in ET Demands by interpolating between K_{cb} values according to the NCGDD or according to the percent of time. Harvests or termination of crops are estimated in ET Demands by evaluating when crop-specific CGDD values are reached, or based on a specified percent of time since planting or greenup. In some cases, termination is based on days after effective full cover. For most crops, the season is terminated when a killing frost occurs. Killing frost temperature varies with crop type. The starting date for accumulation of GDD begins on January 1 in ET Demands and is used to estimate greenup for some crops such as alfalfa. CGDD generally begins at greenup or planting for all crops except for winter wheat, for which the beginning date is specified as October 1 of the previous year.

Timing of greenup and planting is strongly dependent on soil temperature at the root depth or seedbed. Because air temperature and soil temperature are highly correlated at weekly to monthly timescales, two approaches that rely on air temperature are used in ET Demands to estimate greenup or planting dates for each crop. The first approach is to use a moving average of daily average temperature for the previous 30 days (i.e., a 30-day average ending on the 30^{th} day), referred to as T_{30}. The second approach is CGDD from January 1. Initial

T_{30} and CGDD values were adopted from Allen and Robison (2009) and Huntington and Allen (2010) and later adjusted during the calibration process to fit local observations from the literature or from personal communications and observations. Having the ability to simulate year-to-year variations in the timing of greenup or planting, timing of effective full cover, harvest, and termination, is necessary for integrating the effects of temperature into growing-season initiation and length and into crop growth and development, especially under a changing climate. The T_{30} approach for defining greenup and planting dates has been previously applied in Washington (James et al. 1982), Idaho (Allen and Brockway 1983; Allen and Robison 2009), and Nevada (Huntington and Allen 2010). The CGDD approach has been recently applied in Idaho (Wright 2001; Allen and Robison 2007), Texas (Marek et al. 2006), Oregon (Mitchell 1997), and Nevada (Huntington and Allen 2010). Actual farm and field practices can differ significantly from simulated greenup, planting, time to effective full cover, harvest, and termination dates, due to random human behavior and market factors. Therefore dates simulated by ET Demands for defining different crop stages should be considered realistic, but approximate.

Calibration of crop stage parameters that determine planting, greenup, effective full cover, and harvest times was accomplished by driving (forcing) the ET Demands model using historical BCSD air temperature at each Met Node, and determining optimal values for T_{30}, time, and $CGDD_{EFF\ or\ TERM}$ for each crop to fit observed planting, greenup, and development dates. Optimal values were concluded when simulated crop stages compared well with documented dates for major agricultural areas in each basin. Values for T_{30}, time, and $CGDD_{EFF\ or\ TERM}$ were initially adopted from Allen and Robison (2009) and Huntington and Allen (2010) and modified accordingly during the calibration process for each basin and crop. For forage crops of alfalfa and grass hay, simulated in-season harvest times were calibrated by adjusting the $CGDD_{TERM}$ parameter so that cutting dates simulated documented typical cutting dates in each basin. Due to the size and spatially variable climatology, Colorado and Missouri basin ET Demands models were split into multiple submodels for the Lower and Upper Colorado and for the Western, Northern, and Southeastern Missouri subbasins, so that crop stage timing was better simulated across each subbasin. Documented crop stage dates for respective areas were derived from published data, as well as from verbal and written communications. Primary sources are listed in table 2. Simulated greenup, planting, and cutting and harvest dates were assumed to represent average conditions, recognizing the large variations in actual populations of cutting, harvest, and termination dates that occur due to random farming practices and rotations of cuttings. Calibration results suggest that historical mean annual greenup, planting, cutting, and harvest can be relatively well simulated considering the large spatial variation in air temperature within each basin and sub-basin. Simulated crop stages were typically within ±15 days of the documented stages for each crop and basin.

Because planting and harvest dates for annual crops are temperature dependent, and are simulated using the T_{30} and the GDD approach, shifts in planting, development, and harvest dates for future time periods occur in simulations, especially towards the 2080 time period. Projections of changes in future farming practices for annual crops, such as potential earlier plantings and more rapid development and harvest, are uncertain under warming climatic conditions. These potential changes will likely be highly dependent on future crop cultivars, water availability, and economics. For these reasons, in addition to simulation of thermally based K_{cb} curves for future time periods, "static phenology" K_{cb} curves were also simulated for future periods, using baseline temperatures to simulate planting, crop development, and harvest dates in accord with the T_{30} and GDD approaches as previously described. The use of the two sets of K_{cb} curves provides an estimate of the influence of changing temperature on growing-season lengths and resulting ET. Including the "static phenology" approach for annual crops allowed for the accommodation of a range of crop changes — bracketed by no change and by thermal unit-based change — in simulating crop planting, development, and harvest dates under future conditions. In effect, under the static phenology K_{cb} approach, all scenarios and time periods have identical baseline crop-dependent seasonal K_{cb} shapes that vary from year to year according to baseline temperatures, and only exhibit differences in daily ET_c magnitudes due to daily ET_0 and precipitation differences.

Table 2.—Primary Sources Used for Calibration of ET Demands Simulated Greenup, Planting, Harvest, and Termination Dates for Each Basin

Basin	Simulated crop greenup, planting, harvest, and termination calibration source
Central Valley	USDA-NASS (2010b), Allen et al. (2005b), Burt et al. (2002), Howitt et al. (1999)
Colorado (Lower)	Hill et al. (2011), USDA-NASS (2010b), Allen et al. (2005), Jensen (1998), Hill (1994), AZMET (http://ag.arizona.edu/azmet/)
Colorado (Upper)	USDA-NASS (2010b), Pochop et al. (1992), Hill et al. (2011), Hill (1994)
Columbia	Allen and Robison (2009), Peters (2012), and AgriMet cooperators greenup, planting, and harvest, notes and electronic communication from Jama Hamel at Reclamation (2012)
Klamath	AgriMet cooperators documented greenup, planting, and harvest, notes and electronic communication from Jama Hamel at Reclamation (2012)
Missouri (Northern)	USDA-NASS (2010b), USDA-SCS (1974)
Missouri (Southeastern)	USDA-NASS (2010b)
Missouri (Western)	USDA-NASS (2010b), Pochop et al. (1992), USDA-SCS (1974)
Rio Grande	Sammis et al. (1979), Sammis et al. (1985), Brower (2008), USDA-NASS (2010b), and electronic communication from Reclamation (2012)
Truckee and Carson	Huntington and Allen (2010), Maurer et al. (2006), Rashedi (1983), Rush (1976), Sakamoto and Gifford (1970), and verbal communication from Latin Farms (2008)

It is important to once again note the assumption of adequate irrigation water supplies to fulfill crop water needs when estimating ET demands and NIWR, especially with regard to growing-season length impacts on total crop water consumption. This analysis illustrates that as climate warms, with the assumption that there are no constraints on crop cycles due to water scarcity, then ET_c rates will increase, plant phenologies may shift, and the growing season could shorten, expand, or stay static depending on crop type.

The non-growing-season period is represented in ET Demands as the period starting at the end of the growing cycle K_{cb} curve, or the occurrence of a killing frost. The non-growing-season period terminates at the onset of planting or greenup for the same crop. The same crop is used to promote consistency in simulations in spite of uncertainty and wide ranges in farmer behavior on selecting crop rotations. Non-growing-season ET is important for estimating effective precipitation and the net irrigation water requirement for annual periods. Wintertime soil moisture accounting through simulation of ET and soil and root zone water balance is necessary for estimating the accumulation of non-growing-season precipitation that is available to the plant at the beginning of the growing season. Non-growing-season ET is highly variable, depending on available energy, soil moisture, frozen soil, snow cover, and condition and amount of dormant vegetation. Few studies have measured non-growing-season ET from dormant agricultural vegetation; however, those studies offer baseline information needed for approximating non-growing-season ET in ET Demands. Wright (1991, 1993) conducted a series of non-growing-season measurements of ET in Kimberly, Idaho, using dual precision weighing lysimeter systems with clipped fescue grass and bare soil conditions of disked alfalfa, disked wheat stubble, disked soil, dormant alfalfa, and dormant alfalfa and winter wheat. He concluded that the non-growing-season K_c (i.e., $K_{cb} + K_e$) rarely approached ~1.2 for a grass reference basis, even for periods of ample soil moisture supply. Allen (1996) measured non-growing-season ET from dormant fescue grass using two paired weighing lysimeters near Logan, Utah, and concluded that an average K_c of ~ 0.5 for the winter period provided acceptable results when daily estimates of ET were to be summed over weeks to months. Sammis et al. (1979) reported non-growing-season ET using lysimeter measurements in New Mexico and found that the K_c ranged from 0.05 to 0.5 for dormant alfalfa using the Penman ET equation (Penman 1948). Guitjens and Goodrich (1994) compiled numerous water balance lysimeter measurement datasets during the non-growing season for dormant alfalfa in Fallon, Nevada, and found that the average annual K_c for non-growing-season dormant alfalfa was around 0.35 and that the K_c of bare soil was around 0.15. Southern New Mexico and northern Nevada experience less precipitation than do northern Utah and southern Idaho in the winter, which accounts for the lower values found for K_c.

Based on the previous findings on non-growing-season agricultural ET in the Western U.S., a non-growing-season K_{cb} of 0.12 was assigned in ET Demands for bare soil conditions, surfaces covered with some amount of mulch, and for dormant grass. The assumed K_{cb} of 0.12 for non-growing-season periods

represents conditions under which bare soil, mulch, and dormant grass have a dry surface but also have available moisture at depth to supply some diffusive evaporation. The K_{cb} is reduced according to the stress coefficient (K_s) during calculations if the soil moisture becomes dry during extended periods of no precipitation. The total K_c is increased beyond K_{cb} by simulating the evaporation component, K_e, using a daily soil water balance, in which $K_{c\ max}$ (i.e., $K_{cb} + K_e$ under ample water supply) during the non-growing season is limited to 1.1, 1.0, and 0.96 for bare soil, mulch, and dormant grass, respectively. The lower value for grass is assumed to account for the higher albedo and insulation effects of dormant grass. Mulch is assumed to represent surfaces that are partway between bare and grassy conditions. The effective fraction of cover assumed in ET Demands for estimation of exposed soil surface area and K_e was specified as 0 for bare soil, 0.4 for mulch, and 0.7 for dormant grass. Previous application of this approach over regional scales has yielded satisfactory results when comparing average simulated non-growing-season K_c and ET_c estimates to lysimeter measurements (Allen and Robison 2009; Allen and Wright 2009; Huntington and Allen 2010). Allen and Wright (2009) outline a simple approach for considering snow accumulation and melt when daily snow accumulation is reported; however, in this work snow accumulation and melt were not considered due to the lack of snow accumulation information. Future enhancements to ET Demands will include a simple snow accumulation and melt module based on precipitation and temperature to provide a better representation of non-growing-season ET and accumulation of soil moisture. Further details on the background and application of the general ET Demands approach used for estimating non-growing-season ET can be found in Allen and Robison (2009) and Allen and Wright (2009).

4.2.2 Open-Water Evaporation Model

Open-water evaporation from lakes and reservoirs is an important water budget component for water planning, modeling of hydrologic systems, and projection of future water demands and supply. Evaporation from open water is a function of net radiation, air temperature, water surface temperature, humidity, windspeed, stability of the atmosphere, temperature and quantities of water flowing in and out of the water body, and heat storage of the water body of interest. Evaporation pans are commonly used to estimate lake and reservoir evaporation; however, the timing and magnitude of pan evaporation is not necessarily representative of actual evaporation from a lakes or reservoirs for a variety of reasons, and estimates based on pan evaporation have been shown to be highly uncertain (Hounam 1973; Morton 1979). Freezing conditions also limit the use of pans for estimating evaporation in winter months. The amount and timing of changes in heat storage in the water body as compared to a shallow evaporation pan is a main component of this uncertainty. Heat storage impacts both the rate and timing of evaporation and is dependent on the volume, depth, geometry, clarity, and surrounding environment of the water body. Shallow water bodies have smaller amounts of heat storage, whereas deep water bodies can have significant heat storage, creating seasonal shifts in monthly evaporation that can span many

months. For example, Trask (2007) concluded that peak evaporation from Lake Tahoe occurs from September to November rather than during summer months as the measured pan evaporation located in Tahoe City indicates. Similar results were found for Walker Lake, Nevada, a deep lake where energy balance estimates of evaporation peaked during the fall months and had a significant seasonal shift when compared to ET_0 (Allander et al. 2009; Huntington and Allen 2010).

The CRLE model was selected for this study for reasons outlined in section 4.1.2. The CRLE relies on a numerical energy-aerodynamic approach by iteratively solving energy balance and vapor transfer equations to estimate the ambient potential evaporation (E_p). The ambient potential evaporation is used to obtain an estimate of the equilibrium wet environment surface temperature. This temperature is in turn used to estimate the slope of the saturation vapor pressure curve (Δ) and Priestley-Taylor potential evaporation for a spatially extensive wet surface (E_w). The relationship between E_p and E is generally complementary, hence the model is termed the Complementary Relationship Lake Evaporation model. The modified Priestley-Taylor equation (Morton 1983a) used in the CRLE is defined as

$$E = b_1 + b_2 \frac{\Delta_w (R_w - G)}{(\Delta_w + \gamma)}$$

where R_w is the net radiation for a water surface, calibration constants b_1 and b_2 suggested by Morton (1983a) are 13 W/m^2 and 1.12, respectively, and Δ_w is the wet-environment slope of the saturation vapor pressure curve (kPa °C^{-1}) computed with the wet-environment surface temperature obtained from an iterative solution, and γ is the psychrometric constant (kPa °C^{-1}). Constants b_1 and b_2 and the net radiation constants required to estimate R_w were calibrated by Morton (1983a) using water-budget estimates of lake evaporation from Dauphin Lake in Manitoba, Pyramid and Winnemucca Lakes in Nevada, the Salton Sea and Silver Lake in California, Lake Victoria in Newfoundland, Lake Ontario on the border of New York and Ontario, Lake Hefner in Oklahoma, and Last Mountain Lake in Saskatchewan. The heat storage term (G) is solved using an approach outlined by Morton (1983a,1986), in which absorbed shortwave solar radiation is lagged by t months as a fraction, where t is a function of salinity and average water body depth. CRLE simulates the hypothetical, linear heat storage to lag behind absorbed shortwave solar radiation, similar to Muskingum's routing method used to route floods through reservoirs (DosReis and Dias 1998). The functions and constants for t and storage constant k, outlined by Morton (1986), were developed by calibration based on monthly water-balance estimates of evaporation from previous studies of U.S. and Canadian lakes. For more information regarding the background and development of CRLE see Morton (1983a, 1986) and for recent applications see Jones et al. (2001), Vallet-Coulomb et al. (2001), and Huntington and McEvoy (2011).

4.3 Use of ET Demands and CRLE Model Applications to Develop Irrigation Water Demand and Open-Water Evaporation Estimates

The common requirements among ET Demands and CRLE applications are daily historical baseline and BCSD projections of T_{max}, T_{min}, and precipitation. As discussed in chapter 3 (section 3.3) , 12 km by 12 km grid cells were selected based on the location of NWS COOP weather stations (i.e., Met Nodes) used to represent larger HUC8 areas, and specific water bodies of interest (figures 8 and 9). Appendix 2 lists the Met Nodes used for application of the ET Demands and CRLE models.

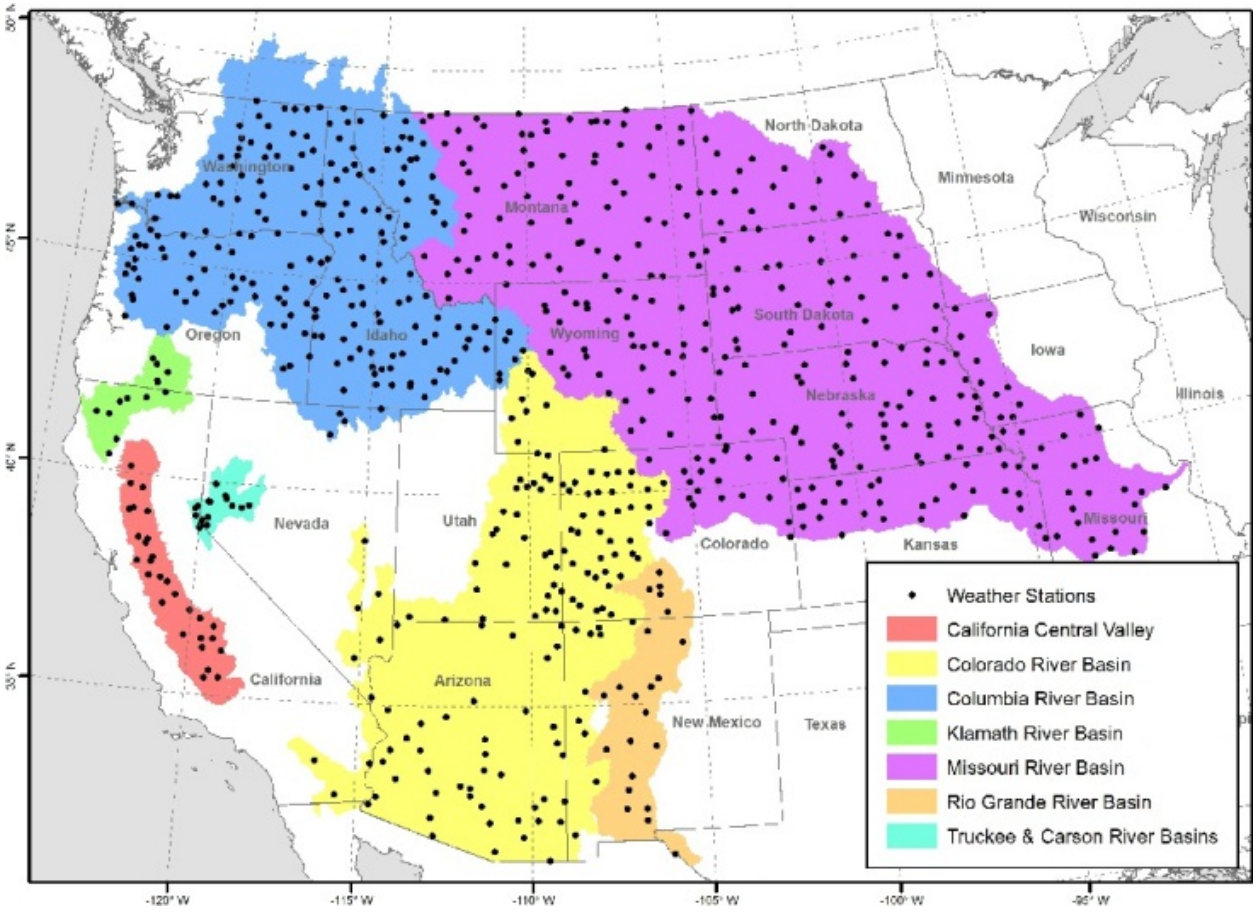

Figure 8.—Met Node NWS COOP weather stations used during application of the ET Demands Model for estimating crop ET (ET_c) and the net irrigation water requirement (NIWR).

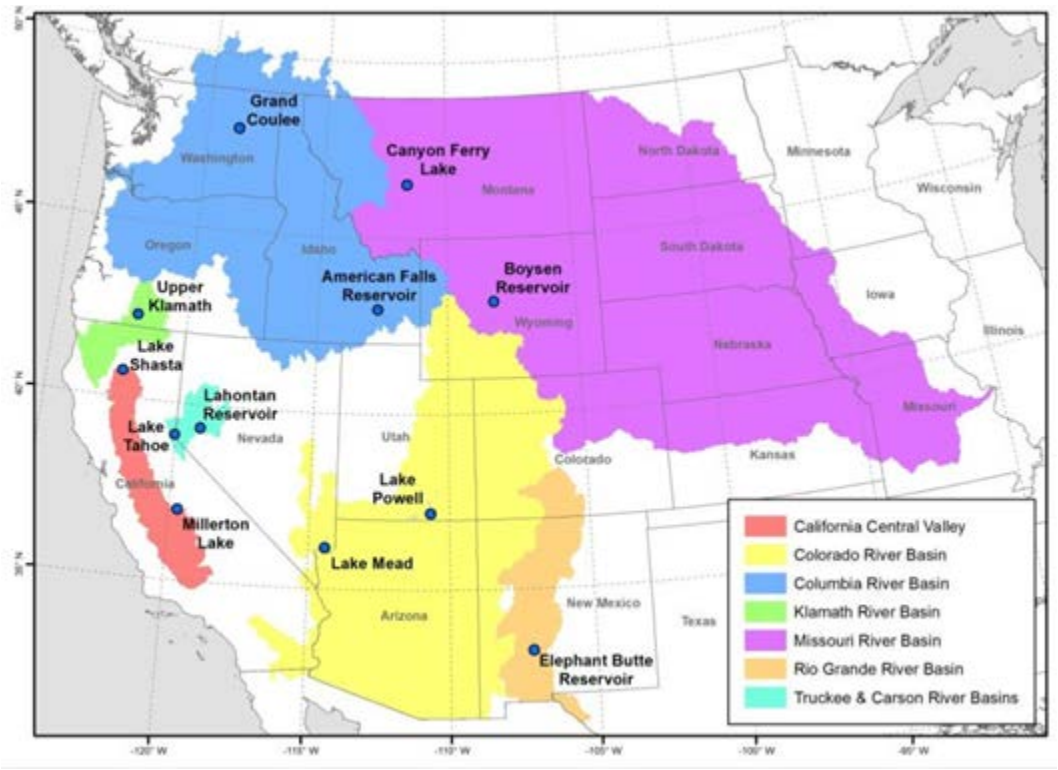

Figure 9.—Reservoirs and lakes where the CRLE model was applied at Met Node NWS COOP weather stations locations near the water bodies.

4.3.1 ET Demands Application

The ET Demands model was applied to derive baseline and projected climate for each basin using data managers[13] developed using Visual Basic for Applications (VBA) in Excel. The data managers apply the bias correction to historical values of T_{max}, T_{min}, and precipitation from NWS COOP weather stations, and perform the HDe calculations described in chapter 3. Once the historical baseline data are bias corrected and the HDe scenarios' data are organized and formatted, the ET Demands VBA manager[14] executes the ET Demands VB.net program to read input baseline and projected climate (T_{max}, T_{min} and precipitation) for estimating required input fields of R_s, T_{dew}, and windspeed. The model then simulates ET_0, growing-season and non-growing-season soil and root zone water balance components (K_{cb}, K_s, K_e), irrigations, and ET_c and NIWR, all at daily time-steps. ET_0 is computed at each Met Node, while all subsequent values are computed for each ET cell and crop type specified. ET cells incorporate spatial information such as soil type and crop type and acreages, which are used with Met Node

[13] West Wide Climate Risk Assessment – Data and Model Managers Manual, Bureau of Reclamation, Technical Service Center, December 2013.

[14] ET Demands Manager – User Manual, Bureau of Reclamation, Technical Service Center, November 2013.

estimated ET_0 to estimate ET_c and NIWR for each ET cell. In all basins, ET cells are equivalent to HUC8 areas, with the exception of the Central Valley, where specified Planning Areas are used. Crop types and acres are summarized for each basin and all HUC8 areas in Appendix 11.

Daily NIWR rates for each ET cell were computed using unique irrigated crop types and associated areas[15] (i.e., crop mix). Irrigated crop mix sources varied among the basins depending on availability of detailed Reclamation operations model support data. In basins where detailed irrigated crop mix information was not available, USDA Cropland Data Layer (CDL) data for 2010 (USDA-NASS 2010a) were used to estimate the crop mix in each ET cell (see table 1). In areas where non-irrigated CDL crops were identified, such as the Columbia River basin where substantial rain-fed agriculture exists in eastern Washington and western Idaho, non-irrigated crop mix areas were removed from ET cell total crop mix areas.

Area weighted daily ET_c and NIWR rates ($ET_c - P_e$) for each ET cell were computed as

$$ET\ cell\ rate = \sum_{i=1}^{i=n} crop\ proportion\ i * crop\ rate\ i$$

where ET cell rate is the crop mix area weighted ET_c or NIWR rate, *n* is the number of crops in the crop mixture for an ET cell, crop proportion *i* is the proportion of crop *i* total acreage for the ET cell, and crop rate *i* is the ET_c or NIWR rate for crop *i*. Typically, the use of ET cell data by planning and operations models is on a daily basis. For the WWCRA, data were temporally aggregated to ET cell annual rates and volumes using the Data Utilities Toolkit[16]. In some basins, ET cells were spatially aggregated across multiple HUC8s and planning areas to larger WWCRA reporting units using another VBA application (CCTimeSeriesDataWeightingManager[17]). The computations for aggregating to larger WWCRA reporting units were

$$unit\ rate = \sum_{i}^{n} ET\ Cell\ proportion\ i * ET\ Cell\ rate\ i$$

and

$$unit\ volume = \sum_{i}^{n} ET\ Cell\ volume\ i$$

[15] ET Demands Manager user can optionally enter areas or fractions. Internal computations use fractions.

[16] Data Utilities Toolkit, Excel Add-in User Manual, Bureau of Reclamation, Technical Service Center, December 2011.

[17] ET Demands Manager – User Manual, Bureau of Reclamation, Technical Service Center, November 2013.

where the *unit rate* is the area weighted ET or NIWR rate (depth) for the reporting unit, *n* is the number of ET cells for the unit, *ET cell proportion i* is the proportion of *ET cell i* crop acreage to the total unit crop acreage, and *ET cell rate i* is the crop area weighted ET_c or NIWR rate for *ET cell i*. Average annual rates and volumes were computed in the ET Demands Manager.

4.3.2 CRLE Application

Several steps were required for application of the CRLE model, including software conversion and modification, bias correction of BCSD baseline and projected climate of T_a and precipitation (P), and T_{dew} and R_s estimation. The original CRLE model software is fully documented in "Operational Estimates of Areal Evapotranspiration and Lake Evaporation - Program WREVAP" (Morton et al. 1985), which describes a series of programs, one of which is the CRLE model and software. A copy of the original WREVAP program was obtained from Dr. J. Szilagyi, University of Nebraska, Lincoln, and was reprogramed from Fortran to Python by the Desert Research Institute to allow for batch processing of multiple stations and multiple climate projections, estimation of daily R_s and T_{dew} from daily T_{max} and T_{min}, averaging of R_s, T_{dew}, and T_a from daily to monthly time steps, and post-processing and aggregation from monthly to annual evaporation totals, all within the Python program framework. Similar to estimating R_s and T_{dew} for the ET Demands Model, daily R_s was estimated using the Thornton and Running (1999) equation with basin-specific optimized coefficients, and daily T_{dew} was estimated using daily T_{min} and mean monthly K_o (i.e., T_{min}–T_{dew}) values computed from agricultural weather stations located near reservoirs of interest. Table 3 lists the Met Nodes (i.e., NWS COOP weather stations) used for bias correction of 0.125 degree BCSD data of T_{max}, T_{min}, and precipitation; paired agricultural weather stations used to compute mean monthly K_o for estimation of T_{dew}; and main CRLE input parameters for each reservoir. The CRLE Python program was run in batch mode for each reservoir Met Node to estimate monthly evaporation using all 112 BCSD transient climate forcings spanning from 1950 to 2100. Results of CRLE estimated monthly evaporation for each Met Node and BCSD climate forcings were then aggregated and summed to annual totals for period change and statistical analyses of monthly and annual results (discussed in section 5).

4.4 Assessment of ET Demands and CRLE Model Applications for Baseline Period

Before proceeding to estimate irrigation water demands and open-water evaporation projections, ET Demands and CRLE model performance was evaluated based on how well the models simulated historical ET_0 and open-water evaporation with estimated forcings when compared to ET_0 and open-water evaporation computed using measured forcings of T_a, T_{dew}, R_s, and U_2. NWS Met Node and agricultural weather stations were paired based on proximity to one another and similar elevation. Met Nodes and agricultural weather station sites

used for comparison of computed ET_0 with estimated forcings and measured forcings for respective time periods are listed in appendix 6 and in table 3 for comparison of CRLE open-water evaporation. Bias corrected Maurer et al. (2002) baseline 1950–1999 variables of T_{max}, T_{min}, and P at each Met Node were used to estimate required forcings of ET Demands and CRLE models, and ET_0 and open-water evaporation were estimated with respective models. If there were no overlapping time periods between the estimated and measured data periods, mean annual values of ET_0 and open-water evaporation were respectively compared. Results of the comparison indicate that ET_0 and open-water evaporation are well simulated using empirically derived weather forcings. Ratios of the mean annual estimated ET_0 to the measured ET_0 (i.e., using measured forcings) from 50 paired Met Node and agricultural stations were found to range from 0.86 to1.15, with an average of 1.03, standard deviation of 0.06, and average root mean squared error for annual estimated ET_0 of 3.7 in/yr (94 mm/yr) (appendix 6, table 6-1). The ratio of CRLE mean annual estimated to computed evaporation ranged from 0.87 to 1.06, with an average of 0.99, and a standard deviation of 0.05 (appendix 6, table 6-2). These results (as well as monthly and daily ratios shown in appendix 6, table 6-1) were considered good given the fact that ET Demands and CRLE estimates of ET_0 and evaporation are dependent on estimated R_s from optimized TR equations, spatially distributed mean monthly K_o, and U_2. There were no significant trends identified relative to river basin, elevation, or other basin-related variables.

The following section gives a summary of comparisons between ET Demands and CRLE estimates of ET_c and open-water evaporation and measurements derived from lysimeters, Bowen ratio energy balance, and eddy flux stations.

4.4.1 ET Demands Performance Assessment

Previous comparisons have been made between ET Demands and FAO-56 dual crop coefficient predictions of ET_c and research estimates in the Truckee and Carson River Basin of California and Nevada and in the Imperial Valley, and Central Valley of California. Huntington and Allen (2010) compared ET Demands model NWS COOP station estimated growing-season and non-growing-season alfalfa and pasture grass ET_c to previous research measurements of ET_c for respective crop types and time periods in the Truckee and Carson River Basins, and found that the average ratio of estimated to measured ET_c was 1.04, with a standard deviation of the ratio of 0.12. Measurements of alfalfa and pasture grass ET_c were derived from nine studies in the Truckee-Carson that ranged from 2 to 12 years in length and relied on water balance lysimeters, soil moisture depletion, Bowen ratio energy balance, and eddy flux stations (Huntington and Allen 2010).

Table 3.—List of Reservoirs, Met Nodes, Weather Stations, and Parameters Used for CRLE Application and Comparison Using Both Measured and Projected Weather Data

Reservoir / Lake	State	Met Node / NWS COOP name	COOP ID	Latitude	Longitude	Elevation (ft)	Solar radiation station (R_s)	Dewpoint station (T_{dew})	Period for validation simulation	Mean water depth (m)	Total dissolved solids (mg/L)
American Falls	ID	Aberdeen Exp Stn	100010	42.95	–112.83	4405	Aberdeen (AgriMet)	Aberdeen (AgriMet)	4/1/1991 – 4/30/2012	7	266 ([2])
Boysen Reservoir	WY	Boysen Dam	481000	43.41	–108.16	4810	Split Rock Creek (RAWS)	Riverton AP (GSOD)/ PRISM	9/1/1998 – 12/31/2010	11	300 ([3])
Upper Klamath Lake	OR	Klamath Falls Ag Stn	354511	42.16	–121.76	4092	Klamath Falls (AgriMet)	Klamath (AgriMet)	4/1/1998 – 5/31/2012	1	150 ([4])
Lake Mead	NV	Overton	265846	36.55	–114.46	1250	Overton (CEMP)	Moapa (NICE Net)	12/1/2000 – 12/31/2010	53	600 ([5])
Canyon Ferry Lake	MT	Canyon Ferry Dam	241470	46.65	–111.73	3672	Helena Valley (AgriMet)	Helena Valley (AgriMet)	1/1/1997 – 4/30/2012	16	300 ([3])
Elephant Butte	NM	Elephant Butte Dam	292848	33.15	–107.18	4576	Bosque (RAWS)	South Bosque (NMSU)/ PRISM	2/1/2001 – 10/31/2010	14	300 ([6])
Lake Shasta	CA	Shasta Dam	48135	40.71	–122.42	1075	Oakbottom (RAWS)	Oakbottom (RAWS)/ PRISM	8/1/2001 – 6/30/2010	46	300 ([3])
Millerton Lake	CA	Friant Government Camp	43261	37.00	–119.71	410	Fresno State (CIMIS)	Fresno State (CIMIS)/ PRISM	10/1/1988 – 12/31/2010	26	50 ([7])
Lake Powell	AZ	Wahweap	29114	37.00	–111.49	3730	Telegraph Flat (RAWS)	Page AP (AWOS)/ PRISM	2/1/1998 – 10/31/2009	46	500 ([8])
Grand Coulee	WA	Coulee Dam 1 Sw	451767	47.95	–119.00	1719	Grand Coulee Dam (AgriMet)	Grand Coulee Dam (AgriMet)	5/1/2002 – 2/28/2013	34	300 ([3])
Lahontan Reservoir	NV	Lahontan Dam	264349	39.47	–119.06	4167	Fallon (AgriMet)	Fallon (AgriMet)	1/1/2000 – 12/31/2009	7	300 ([3])

Reservoir / Lake	State	Met Node / NWS COOP name	COOP ID	Latitude	Longitude	Elevation (ft)	Solar radiation station (R_s)	Dewpoint station (T_{dew})	Period for validation simulation	Mean water depth (m)	Total dissolved solids (mg/L)
Lake Tahoe	CA	Tahoe City	48758	39.17	–120.14	6230	Stampede (RAWS; 2000–2003)/ Lake Tahoe UC Davis Coast Guard pier (2004–2009)	Truckee AP (GSOD; 2000–2003)/ Lake Tahoe UC Davis Coast Guard pier (2004–2009)	1/1/2000 – 12/31/2009	60 ([1])	60 ([9])

[1] Represents average thermocline depth.
[2] Smith, R. 1991. Hatchery Trout Evaluations: American Falls Reservoir Fishery Evaluations. Idaho Fish and Game. Volume 086, Article 09.
[3] Estimated.
[4] Obtained from Natural Resource Conservation Service.
[5] Estimated from http://ndep.nv.gov/forum/docs/LakeLV_Fact_Sheet_2.pdf
[6] Estimated from http://www.scerp.org/pubs/m2c2.pdf
[7] Obtained from Reclamation.
[8] Estimated from http://www.waterquality.utah.gov/watersheds/lakes/LAKEPOWL.pdf
[9] Estimated from Huntington and McEvoy (2011).

Allen et al. (2005b) used water-balance estimates of project-wide ET_c in the Imperial Valley and compared these estimates to FAO-56 ET_0 dual crop coefficient estimates of ET_c for 30 crops. The FAO-56 soil and root zone water balance approach and algorithms used by Allen et al. (2005) to estimate ET_c are effectively the same as those being applied in this work through the use of the ET Demands model. Allen et al. (2005b) estimated that the accuracy of estimated water balance annual ET_c was ±6 percent at the 95-percent confidence level, and that ET_0 dual crop coefficient estimates of ET_c exceeded water balance estimates by 8 percent (i.e., ratio of 1.08 estimated to measured) on an annual basis over a 7-year period). The authors attributed this overestimation to the fact that not all crops in the project area had the benefit of ample water availability, lack of stress, proactive management, etc. Similar conclusions could be made regarding previous research estimates of ET_c in the Truckee and Carson River Basins.

Similar to applications made by Allen et al. (2005b), Burt et al. (2002) applied a precursor of the ET Demands model in the Central Valley and conducted a detailed uncertainty analysis of different FAO-56 model components of ET_0, dual crop coefficient and soil and root zone water balance parameters, irrigation system type, and crop area. They concluded that the 95-percent confidence level for project-wide ET_c estimates made in the Central Valley was ± 14 percent. Burt et al. (2005) and Mutziger et al. (2005) compared FAO-56 water-balance model estimates of bare soil evaporation to research estimates of evaporation derived from lysimeters in Bushland and Temple, TX (Howell et al. 1995; Ritchie 1972), Davis, CA (Parlange and Katul. 1992) and in Kimberly, ID (Wright 1982). They also studied Bowen ratio energy balance estimates in Fort Collins, CO (Farahani and Bausch 1995). Burt et al. (2005) concluded that the ratio of average mean daily FAO-56 modeled evaporation to mean daily "measured" evaporation was 0.98, with an average percent difference in cumulative study period totals of 4.7 percent (absolute value).

More recently, Allen (2011) compared FAO-56 daily soil water balance model estimates of bare soil evaporation to lysimeter measurements of bare soil evaporation in Kimberly, ID, and bare soil evaporation simulated by Hydrus-1D, which is based on the Richards unsaturated flow equation. He found that the original FAO-56 bare soil evaporation model was fairly robust, with results within 15 percent of those from Hydrus-1D and Kimberly lysimeter measurements.

4.4.2 CRLE Performance Assessment

Several studies have evaluated CRLE evaporation estimates using research estimates of evaporation derived from water budget, mass transfer, Bowen ratio energy balance, bulk aerodynamic-mass transfer, and a combination of these estimation techniques (Morton 1986; DosReis and Dias 1998; Sadek et al. 1997; Jones et al. 2001; Vallet-Coulomb et al. 2001). Huntington and McEvoy (2011) summarized previous studies and made additional comparisons of CRLE predicted evaporation to 18 research evaporation estimates over Western U.S.

reservoirs and lakes in Nevada, Utah, California, and Arizona. Findings from this evaluation, with the addition of a recent study at Lake Mead (Moreo and Swancar 2013), show that CRLE-predicted evaporation is largely within 10 percent of 19 research estimates analyzed at annual time-steps (appendix 7). The ratio of CRLE estimates to research estimates ranged from 0.9 to 1.20, with an average annual ratio of 1.02 and a standard deviation of 0.09.

Stannard et al. (2013) recently conducted an open-water and wetland evaporation study for Upper Klamath Lake, OR. They used the Bowen ratio energy balance to estimate open-water evaporation during the summer and fall of 2008 and the growing seasons of 2009 and 2010. To evaluate the skill of the CRLE application in the Klamath River Basin, the CRLE model was forced with measured R_s, T_a, and T_{dew} obtained from the Klamath Falls Agrimet station for the 2008–2010 study period of Stannard et al. (2013). Results of the seasonal comparison are shown in appendix 8, where it is evident that the CRLE model simulates seasonal evaporation from Upper Klamath Lake fairly well when compared to Bowen ratio energy balance estimates reported by Stannard et al. (2013). Monthly CRLE evaporation rates were linearly interpolated to daily time-steps for comparison to reported energy budget period rates (appendix 8, figure 8-1). The ratio of CRLE to Bowen ratio energy balance estimated evaporation for 40 energy budget periods, spanning 14 days each for two sites (Stannard et al. open-water sites MDL and MDN), ranged from 0.83 to 1.10, with an average energy budget period ratio of 0.98 and a standard deviation of 0.06 (appendix 8, table 8-1).

4.4.3 Performance Assessments Summary

Favorable ET Demands and CRLE skill for simulating previous research estimates support the application of these models across WWCRA study areas. Further validation of the ET Demands and CRLE model components for different crops, areas, and open-water bodies is a research area needing future attention. Additional detailed model evaluations, other than those reported in this section, will require a large effort to compile high-quality historical crop ET and evaporation estimates, to do adequate QAQC on the forcing data and results, and to produce simulated ET Demands and CRLE estimates using both dependent and independent forcing data. These research efforts are currently the focus of ongoing and future work related to estimating irrigation and open-water demands by Reclamation.

CHAPTER 5 — BASELINE AND PROJECTED DEMANDS RESULTS FOR MAJOR RECLAMATION RIVER BASINS

This chapter presents an overview of historical baseline conditions and estimates of future crop irrigation water requirements in the eight major Reclamation river basins, as well as the reservoir evaporation modeling results. The evaluation approach and results format is presented first, and then each set of results is presented for each of the eight basins.

5.1 Evaluation Approach

In this chapter, baseline and projected irrigation water demands and open-water evaporation estimates are presented for WWCRA study areas. Results include spatial distributions of baseline and future period estimates of mean annual precipitation, temperature, reference evapotranspiration (ET_0), crop evapotranspiration (ET_c), and net irrigation water requirement (NIWR). Mean monthly values of ET_c for baseline and future time periods and scenarios are also presented to highlight potential changes in seasonal ET_c. Open-water evaporation results for BCSD transient projections are presented as annual totals and as annual and monthly averages for a range of time periods, with associated statistics for each. An overview of the results and figures is presented for each major Reclamation river basin. The overview locations in each of the eight[18] major Reclamation river basins, and the sections below that describe them, are:

- Colorado River Basin – Colorado River and Imperial Valley (section 5.2)
- Columbia River Basin (section 5.3)
- Klamath River Basin – Klamath River near Klamath (section 5.4)
- Missouri River Basin (section 5.5)
- Rio Grande Basin (section 5.6)
- Sacramento and San Joaquin River Basins – Central Valley (section 5.7)
- Truckee and Carson River Basins (section 5.8)

[18] The Sacramento, San Joaquin, and Tulare Lake basins are considered together as part of Reclamation's Central Valley Project operations, and the Truckee and Carson River basins are also combined.

In each basin-specific section, three plot types are presented: (1) spatial plots of baseline mean annual values and projected absolute and percent change from baseline conditions, (2) seasonal time series plots of mean daily ET_c for selected crops and mean monthly open-water evaporation for different future time periods, and (3) transient projections of annual evaporation and net evaporation (evaporation minus precipitation).

5.1.1 Spatial Plots and Tables of Baseline and Projected Climate, Crop ET, and Irrigation Water Requirement Results

The first set of plots for each basin section includes spatial plots of mean annual baseline (1950–1999) precipitation and temperature. They also include agricultural weather station based spatial distributions of mean annual dewpoint depression and windspeed, where daily data derived for these variables were used for estimating baseline daily and mean annual ET_0, ET_c, and NIWR. The second set of plots includes estimated spatial distribution of baseline mean annual ET_0, ET_c, NIWR, and associated irrigated crop acreage. All spatial plots are presented at the HUC8 level, even though the simulations are point-based (i.e., Met Nodes). The third set of plots include projected changes in temperature, precipitation, ET_0, ET_c, and NIWR for different climate scenarios and time periods. Projected changes are presented as differences from baseline averages for temperature, and percent change from baseline averages for all other variables. As discussed in chapter 4, the assumption of water availability with regard to extended growing periods is an important one. Projected changes in ET_0, ET_c, and NIWR mean annual rates for different scenarios and time periods are presented in appendix 1.

As previously described in section 3.3, climate scenarios represent climate projection conditions relative to the central tendency (S5); specifically, they are warmer and drier (S1), warmer and wetter (S2), hotter and drier (S3), and hotter and wetter (S4), while the ensemble median (i.e., central tendency) is S5 given the 112 BCSD projections. Different time periods of the 2020s, 2050s, and 2080s were chosen for evaluating projected changes in mean annual conditions for each variable under different scenarios of S1–S5. Averaging windows for the 2020, 2050, and 2080 time periods were 2010–2039, 2040–2069, and 2070–2099, respectively. Tables of basin-specific HUC8 level baseline and projected rate and percent changes for each scenario and time period can be found in appendix 1.

5.1.2 Time-Series Plots and Tables of Baseline and Projected Crop ET and Open-Water Evaporation

Seasonal time-series plots include mean daily time series of baseline and projected ET_c for selected crops in each basin to illustrate the potential shift in planting or greenup, crop development, and harvest times. Mean daily time series of ET_c for selected crops are shown for baseline and future time periods of 2020, 2050, and 2080. Specifically, mean daily ET_c computed over the calendar year

are shown for the historical baseline and each of the three future periods under the five climate change scenarios.

Seasonal time series of annual open-water evaporation and net evaporation (i.e., evaporation minus precipitation) were computed for all 112 BCSD transient projections, and the results are presented to reflect ensemble central tendency and ensemble spread. The central tendency is measured using the ensemble median and the 5th and 95th percentile bounds from the 112 projections providing the lower and upper bounds in the envelope of evaporation and net evaporation possibility through time. Mean monthly evaporation and net evaporation is also presented showing mean monthly ensemble median and 5th and 95th percentiles.

5.2 Colorado River Basin

5.2.1 Baseline and Projected Irrigation Water Demands

Figure 10 illustrates COOP station based Met Nodes that were used to estimate irrigation water demands, as well as HUC8 boundaries used to upscale Met Node estimates in the Colorado River Basin and the Imperial Valley (technically outside of the basin). Figure 11 illustrates the spatial distribution of baseline (1950–1999) mean annual temperature (top left) and mean annual precipitation (top right) derived from BCSD data (discussed in section 3.3), mean annual dewpoint depression (bottom left) and mean annual windspeed (bottom right) estimated from historical agricultural weather data (discussed in section 4.2.1). Gray-hatched HUC8 polygons illustrated on figure 11 (and other results figures) represent areas where no significant crop acreage was present, so baseline and projected climate and irrigation water demands were not simulated for those areas. Figure 11 illustrates conditions ranging from cooler and wetter in the north to warmer and drier in the south. The mean annual dewpoint depression (i.e., $T_{min} - T_{dew}$) is used here as a simple approximation of the humidity of the lower air mass that is consistent and representative of agricultural areas while preserving regional and local advection effects. Its spatial distribution clearly shows southern areas are more arid and northern areas are more humid.[19] Figure 11 also shows mean annual windspeed is generally lower in the north and south-central areas and higher in the western and northern portions of the basin. Figure 12 illustrates reference ET (ET_0) (top left), crop evapotranspiration (ET_c) (top right), net irrigation water requirement (NIWR) (bottom left), and total crop acreage within each HUC8 boundary (bottom right). ET_0, ET_c, and NIWR are all higher in the southern portion of the basin, where air temperature, solar radiation, and dewpoint depression are significantly larger than in the north. The projected

[19] As discussed in chapter 4, dewpoint depression ($T_{min} - T_{dew}$) is an indicator of humidity in which smaller values indicate higher humidity.

values range from around 40 to 80 in/yr for ET_0, 20 to 62 in/yr for ET_c, and 10 to 54 in/yr for NIWR.

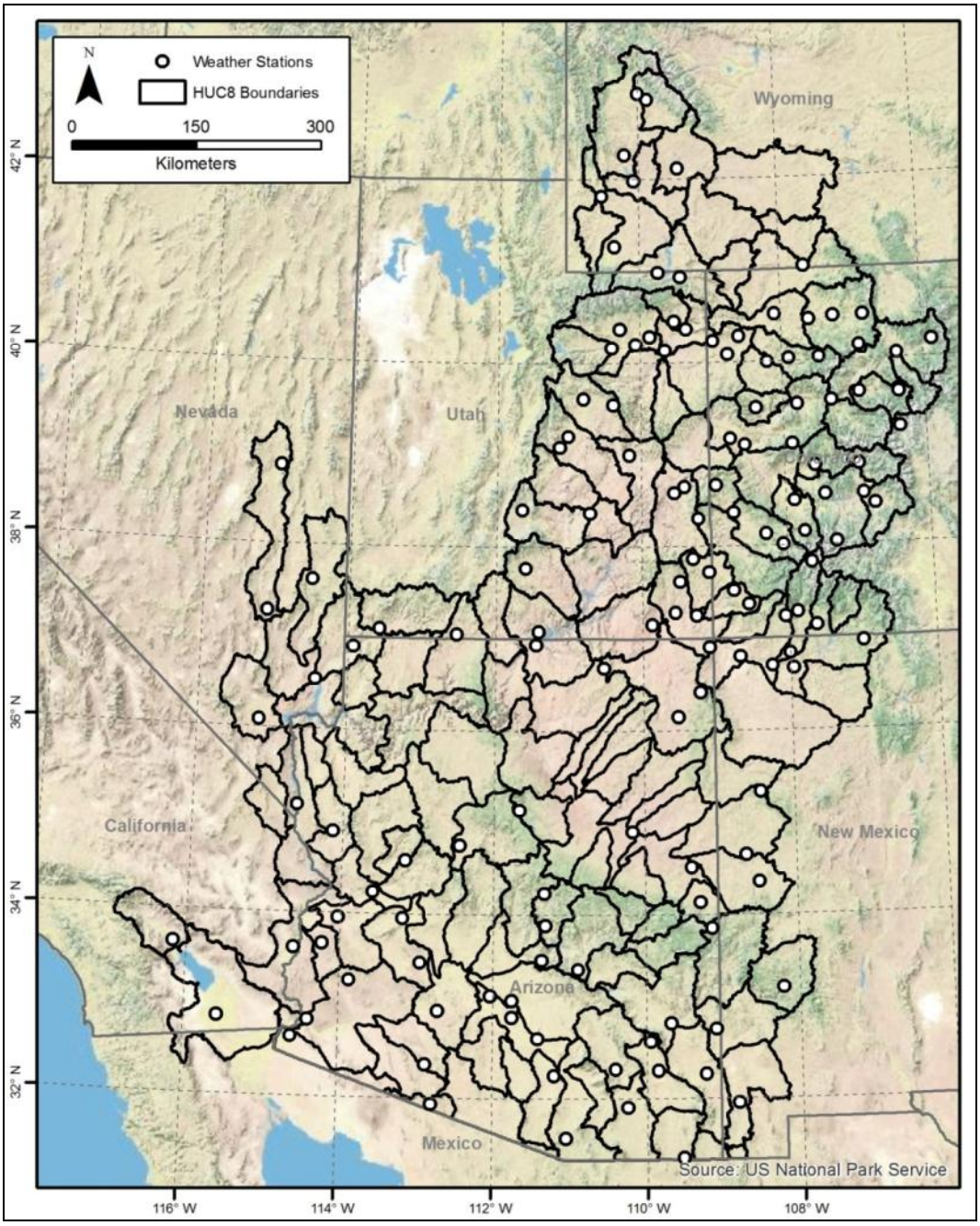

Figure 10.—Colorado River Basin (including Imperial Valley) – COOP stations used to simulate baseline and projected irrigation demands.

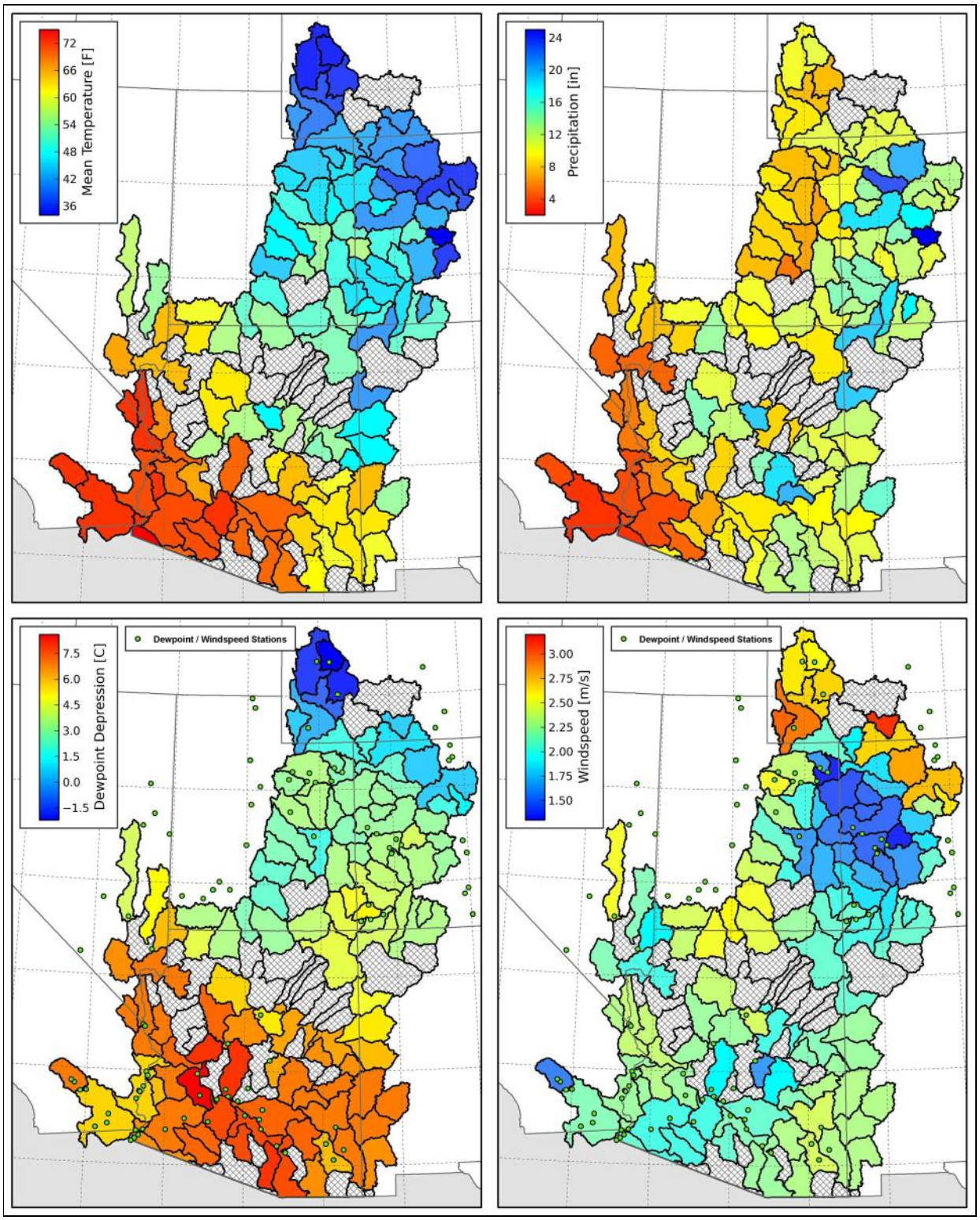

Figure 11.—Colorado River Basin – Spatial distribution of baseline temperature, precipitation, dewpoint depression, and windspeed. Gray hatch areas represent HUCs with no crop acreage.

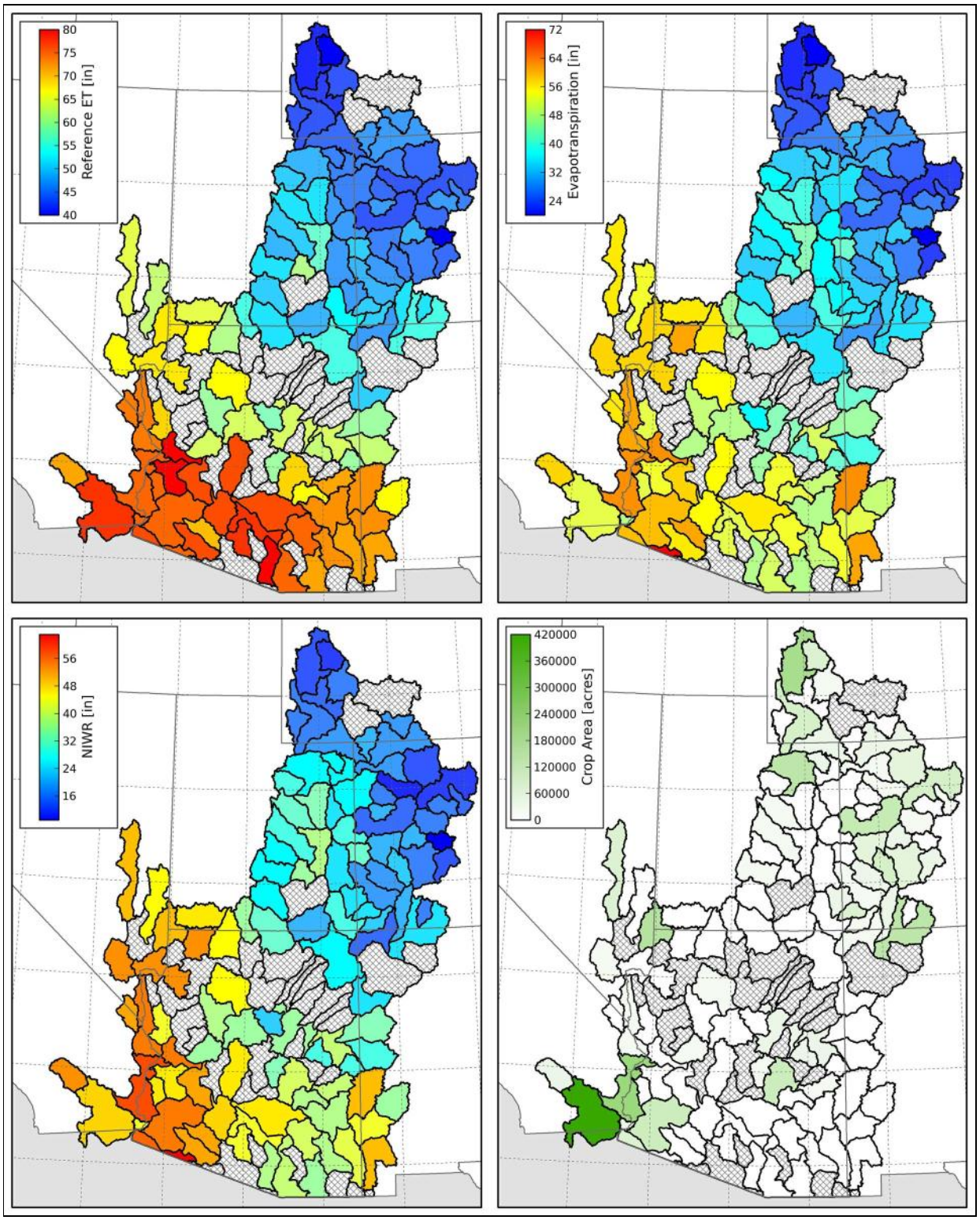

Figure 12.—Colorado River Basin – Spatial distribution of baseline reference evapotranspiration, crop evapotranspiration, net irrigation water requirements (NIWR), and crop acreage.

Figure 13 shows the spatial distribution of projected mean temperature change for different climate scenarios and time periods, and it is evident that the changes shown there are generally spatially uniform for all scenarios, with scenario S3 (hot-dry) having the largest change. Figure 14 illustrates the spatial distribution of projected precipitation percent change for different scenarios and time periods. Depending on the scenario, precipitation percent changes range from –20 to 50 percent for the 2080 time period, with the ensemble median scenario (S5) generally showing a slight decrease in the southern portions of the basin, and a slight increase in the northern portions.

Figure 15 shows the spatial distribution of projected ET_0 percent change for different climate scenarios and time periods. Similar to temperature, the projected percent change in ET_0 is generally spatially uniform for all scenarios, with scenario S3 having the largest change. The northern portions of the basin exhibit the largest percent change due to the fact that the difference between the projected and baseline ET_0 is relatively large compared to the relatively low baseline estimate of ET_0. Figure 16 illustrates the spatial distribution of projected ET_c percent change for different climate scenarios and time periods assuming non-static crop phenology for annual crops, where projected future temperatures were used for simulating projected planting, crop coefficient development, and termination as described in section 4.2.1. Spatial differences in the distribution of projected percent change in ET_c are largely due to differences in crop type and baseline ET_c. The northern portion of the basin is projected to experience the largest percent change for all projected time periods, largely due to the fact that the difference between the projected and baseline ET_c is fairly large relative to the baseline estimate of ET_c (see figure 12). ET_c in the southern portion of the basin is projected to slightly decrease, or increase, depending on the scenario. This is largely because significantly more annual variety crops are grown in the south, and are projected to have fairly static or reduced growing-season lengths due to increased temperatures, and therefore the dates of planting, crop coefficient development, and harvest may be advanced. Perennial forage crops are primarily grown in the north, and are projected to have earlier greenup, longer harvest periods (i.e., more cuttings), and later killing frosts, leading to longer growing seasons and large percentage increases relative to baseline ET_c. Figure 17 shows the spatial distribution of projected ET_c percent change for different climate scenarios and time periods assuming static crop phenology for annual crops, where baseline temperatures were used for simulating projected planting, crop coefficient development, and termination for all future time periods and scenarios as described in section 4.2.1. All HUCs show increasing or static ET_c, with the exception of five HUCs in the lower basin that exhibit slight decreases in ET_c by 2080 due to the fact that perennial grass hay is the primary crop, and mid-season harvests are predicted to occur earlier in the season from increased temperatures, thereby reducing K_{cb} values during peak ET_0. For both static and non-static phenology scenarios, the modeled increase in ET_c is significantly greater than for ET_0 due to the increases in the length of growing seasons.

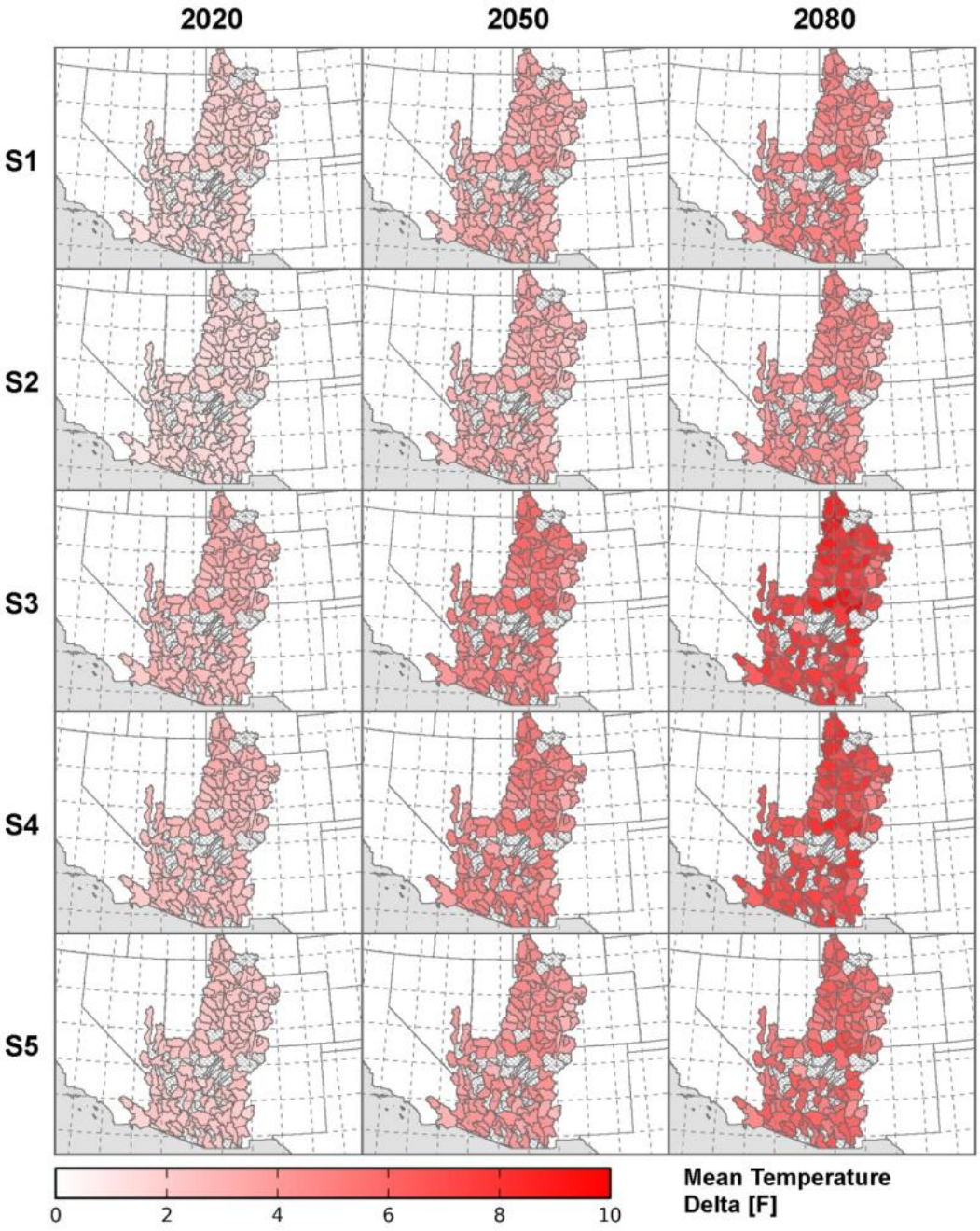

Figure 13.—Colorado River Basin – Spatial distribution of temperature change for different climate scenarios and time periods (S1 = WD, S2 = WW, S3 = HD, S4 = HW, S5 = Central).

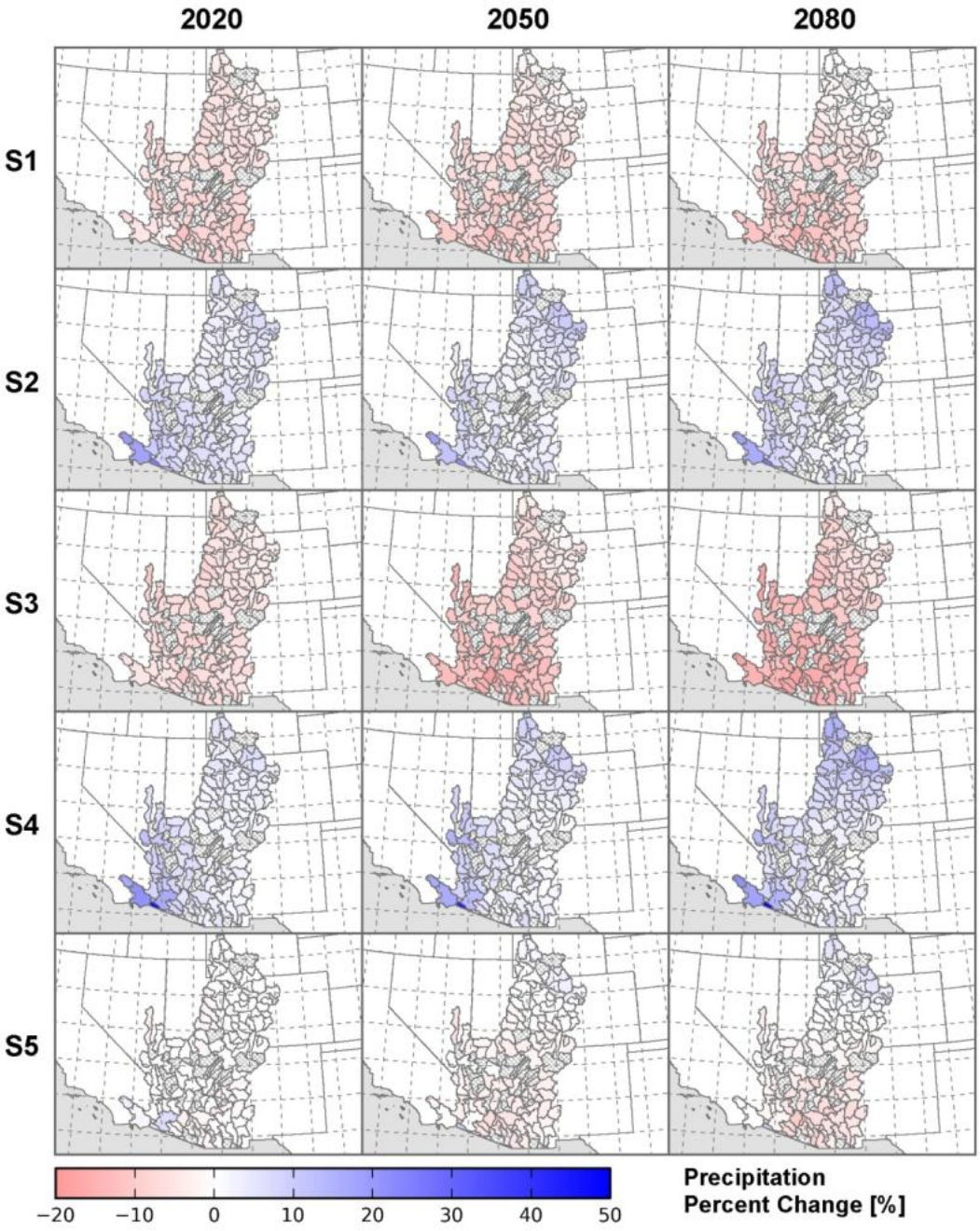

Figure 14.—Colorado River Basin – Spatial distribution of projected precipitation percent change for different climate scenarios and time periods (S1 = WD, S2 = WW, S3 = HD, S4 = HW, S5 = Central).

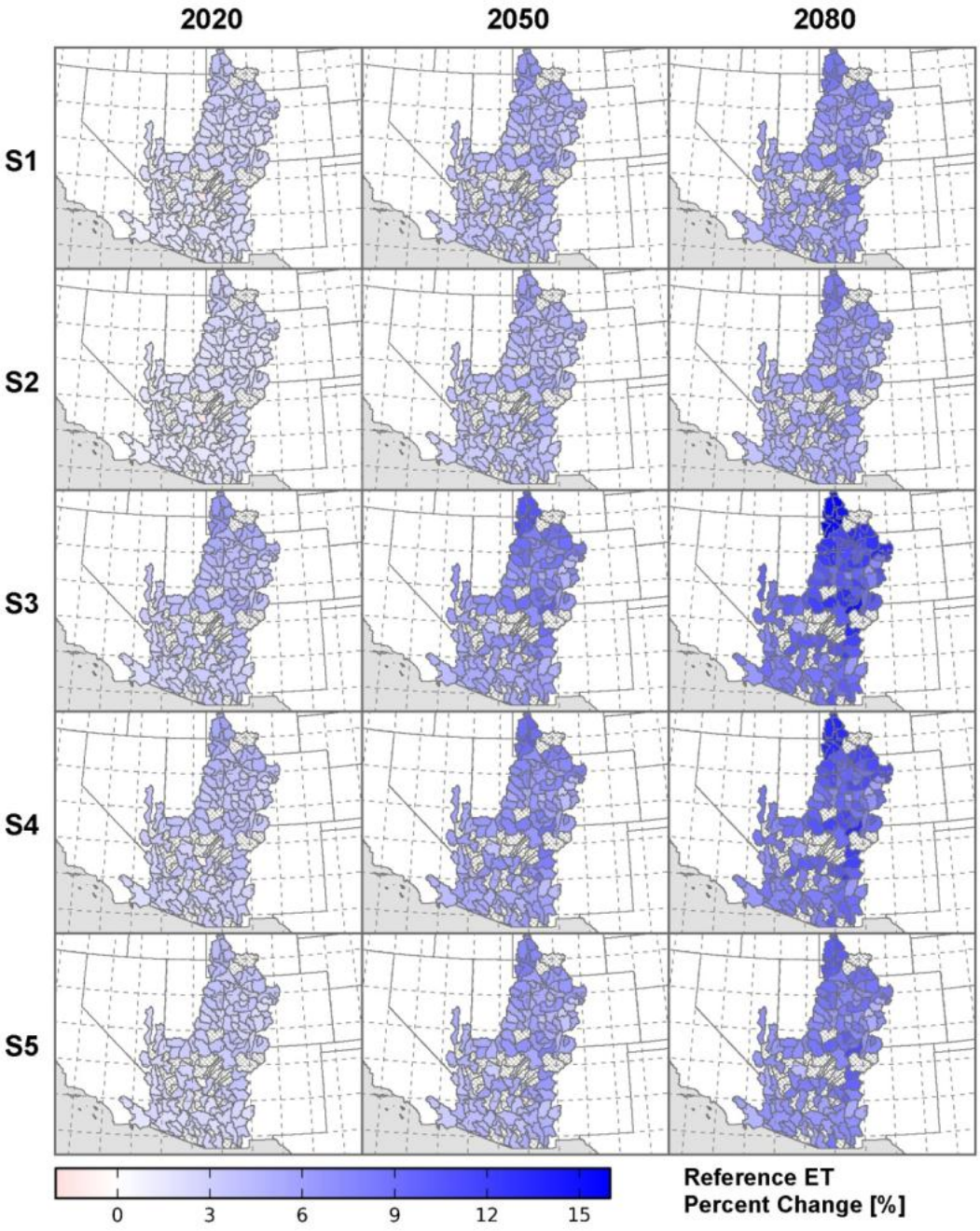

Figure 15.—Colorado River Basin – Spatial distribution of projected reference evapotranspiration percent change for different climate scenarios and time periods (S1 = WD, S2 = WW, S3 = HD, S4 = HW, S5 = Central).

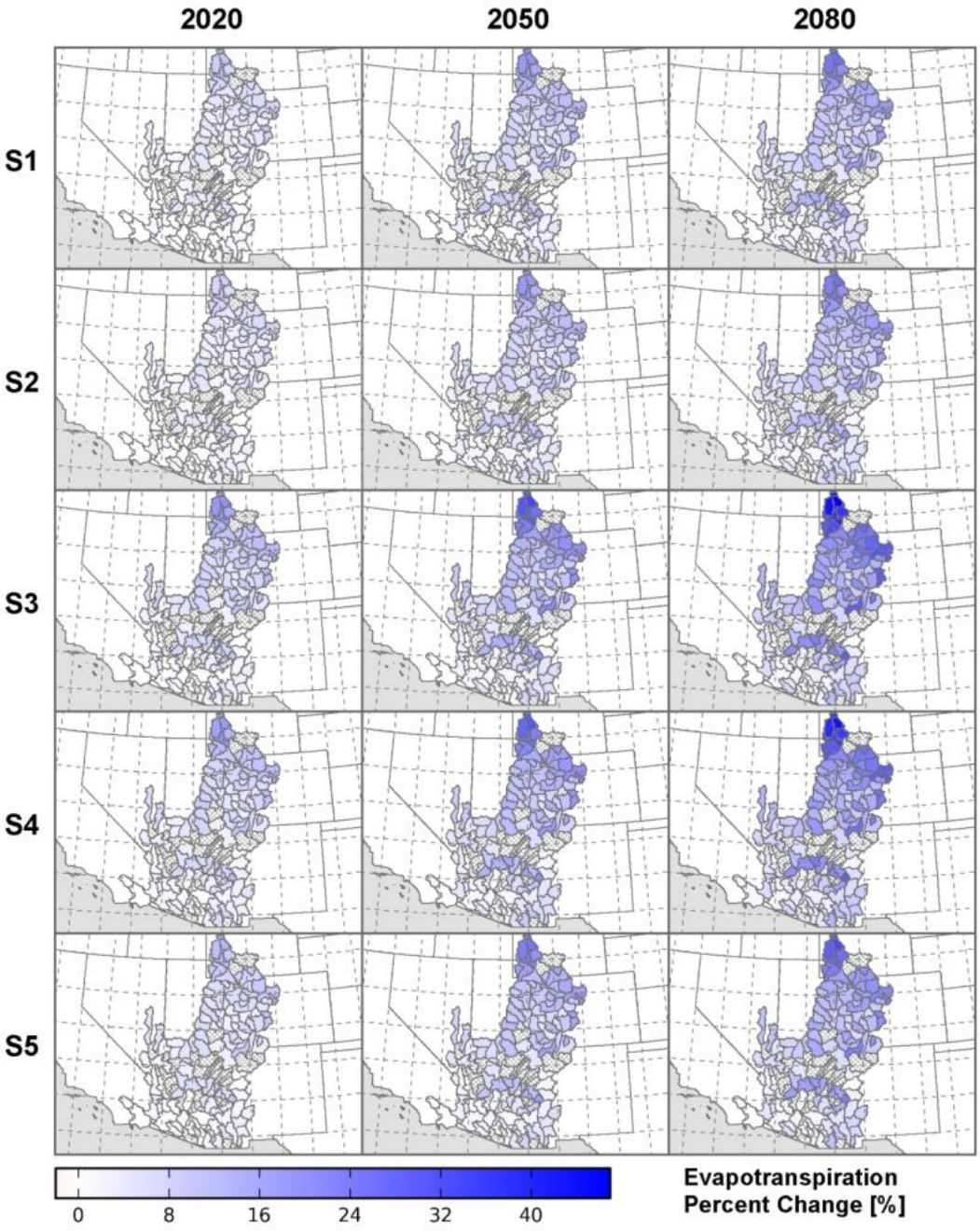

Figure 16.—Colorado River Basin – Spatial distribution of projected crop evapotranspiration percent change for different climate scenarios and time periods (S1 = WD, S2 = WW, S3 = HD, S4 = HW, S5 = Central).

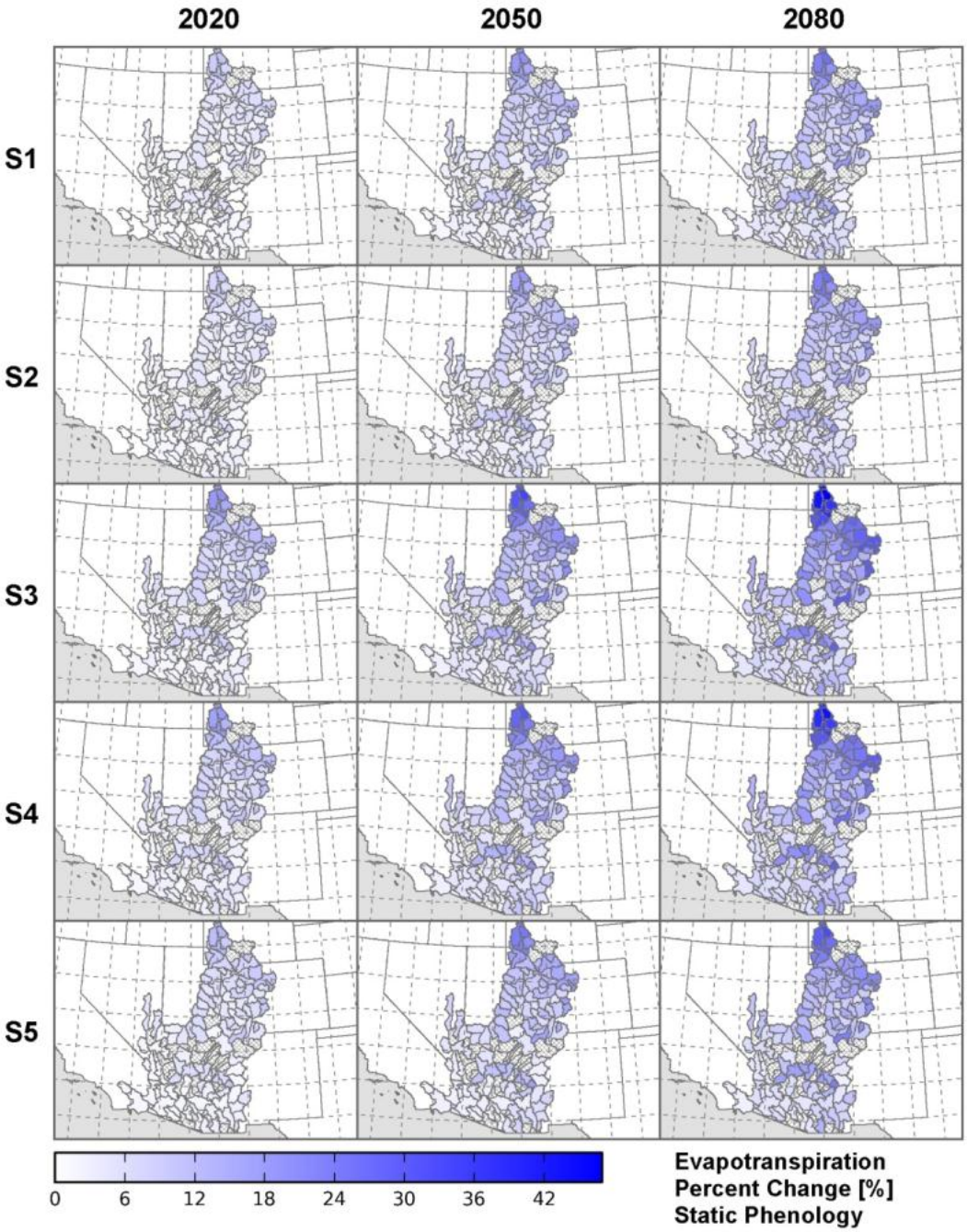

Figure 17.—Colorado River Basin – Spatial distribution of projected crop evapotranspiration percent change for different climate scenarios and time periods assuming static phenology for annual crops (S1 = WD, S2 = WW, S3 = HD, S4 = HW, S5 = Central).

The spatial distribution of projected NIWR percent change for different climate scenarios and time periods is shown on figures 18 and 19. The NIWR incorporates growing-season and non-growing-season soil moisture gains and losses from precipitation, bare soil evaporation, and ET. Therefore, spatial variations in the distribution of NIWR percent change for different time periods and scenarios are a function of respective ET_c (figures 16 and 17) and precipitation (figure 14) distributions. For example, in the northern portion of the basin, scenario S3 (hotter drier) precipitation is projected to decrease whereas scenario S4 (hotter wetter) precipitation is projected to increase. This results in NIWR increasing more under S4 than under S3, even though S3 and S4 ET_c changes are nearly identical. For more illustrations on unit changes (degrees F and inches) in spatial projections of mean temperature, precipitation, ET_0, ET_c, and NIWR for different time periods and scenarios, see appendix 9.

Figures 20, 21, and 22 illustrate the baseline and projected temporal distribution of mean daily ET_c for selected Met Nodes, crops, scenarios, and time periods. At NWS/COOP Met Node WY6555 (Mountain View, WY), the simulated mean daily ET_c of pasture grass for the 2020 time period shows slight but noticeable shifts in the growing-season length relative to baseline conditions (figure 20, left). By the 2080 time period (figure 20, right), significant shifts in growing-season length and crop development are noticeable relative to baseline conditions (again, assuming unlimited water availability), with scenarios S3 and S4 exhibiting the most extreme changes. At NWS/COOP Met Node UT5969 (Myton, UT), the simulated mean daily ET_c of alfalfa for the 2020 time period shows slight but noticeable shifts in the growing-season length and alfalfa cutting cycles relative to baseline conditions (figure 21, left). By the 2080 time period (figure 21, right) significant shifts in growing-season length, crop development, and cutting cycles are noticeable relative to baseline conditions, with scenarios S3 and S4 exhibiting the most extreme changes. Figure 22 shows simulated mean daily ET_c of cotton at NWS/COOP Met Node AZ9656 under different scenarios for the 2020 and 2080 time periods assuming non-static phenology. However, because planting dates for annual crops are temperature dependent in the non-static phenology simulations, shifts in planting, development, and harvest dates are similar to those shown for cotton and are clearly evident, especially by the 2080 time period. The uncertainty in such potential shifts in planting dates, accelerated crop development, and harvest was a primary reason for using baseline temperatures for annual crop static phenology simulations (figures 17 and 19). In static phenology simulations, because baseline temperatures are used for estimating planting, crop development, and harvest dates, all scenarios and time periods have identical seasonal K_{cb} shapes, and only exhibit differences in daily ET_c magnitudes due to daily ET_0 and precipitation differences.

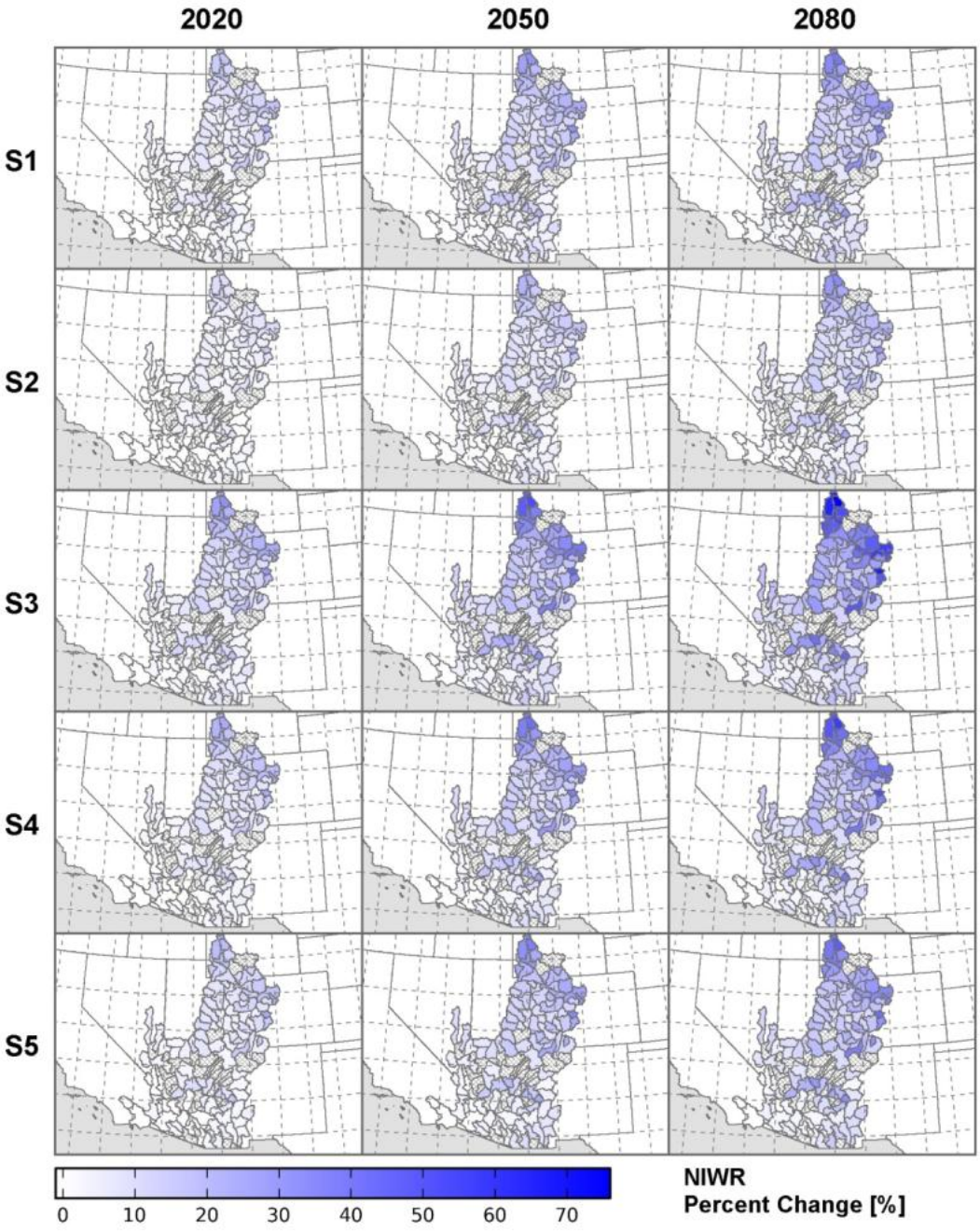

Figure 18.—Colorado River Basin – Spatial distribution of projected net irrigation water requirements (NIWR) percent change for different climate scenarios and time periods (S1 = WD, S2 = WW, S3 = HD, S4 = HW, S5 = Central).

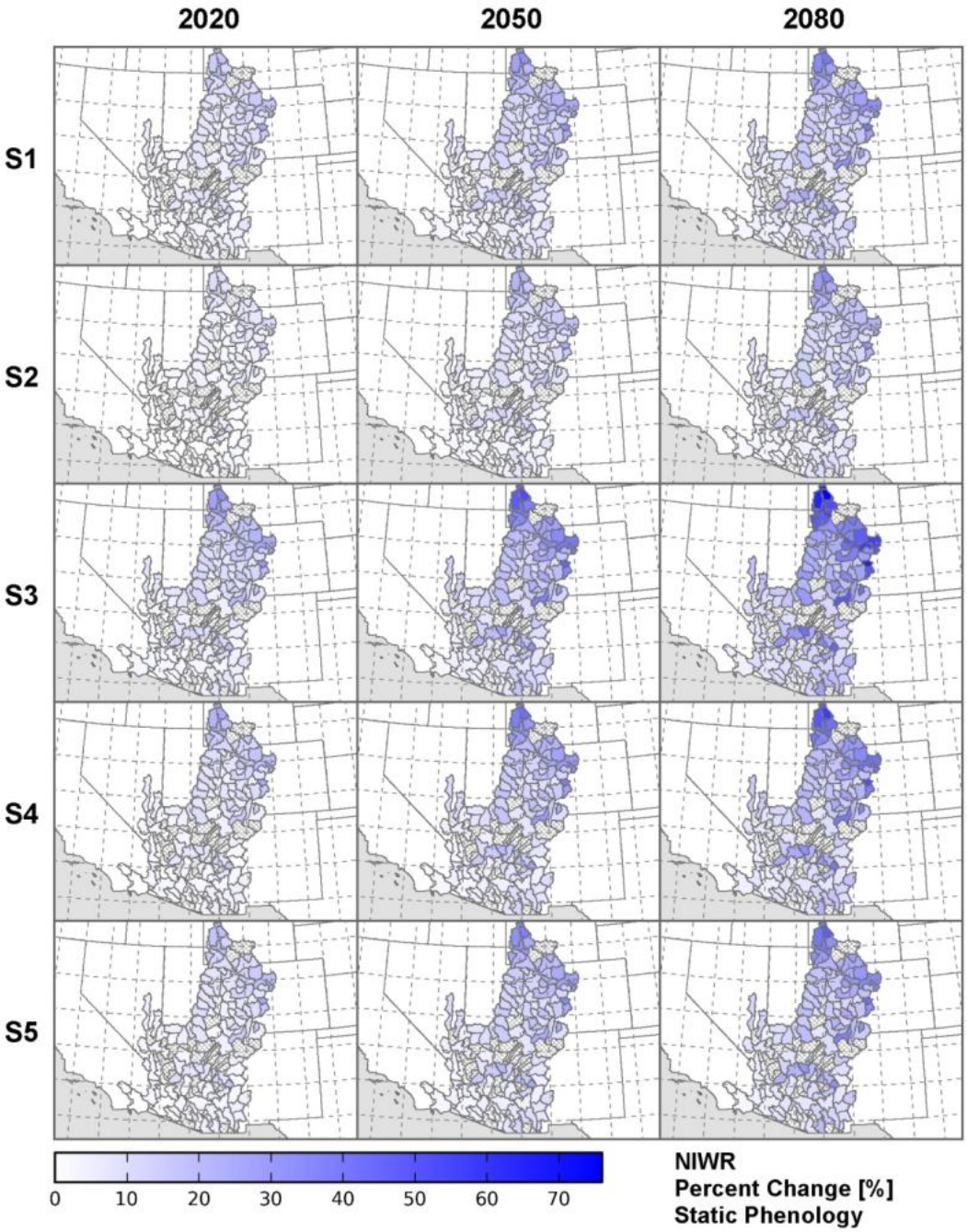

Figure 19.—Colorado River Basin – Spatial distribution of projected net irrigation water requirements (NIWR) percent change for different climate scenarios and time periods assuming static phenology for annual crops (S1 = WD, S2 = WW, S3 = HD, S4 = HW, S5 = Central).

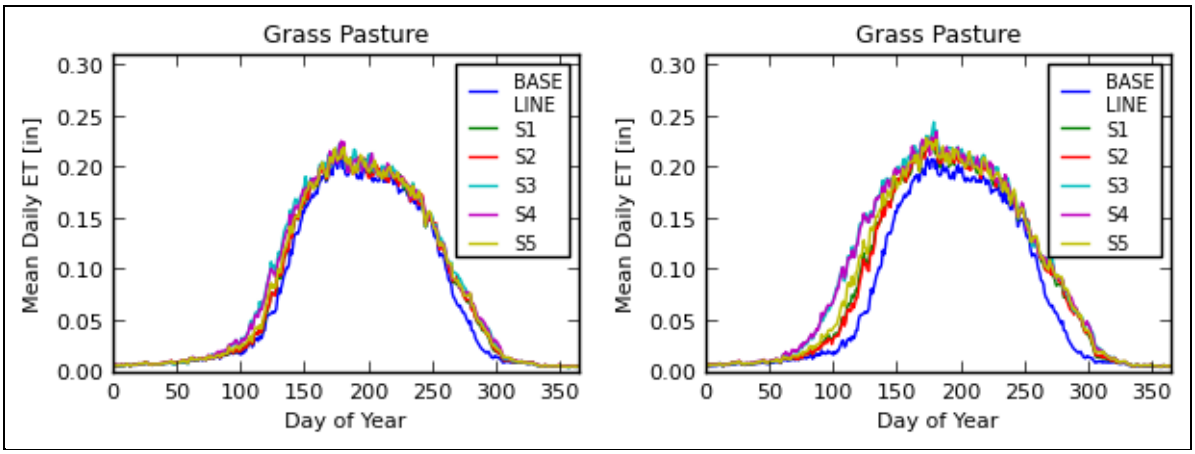

Figure 20.—Colorado River Basin – COOP station WY6555 (Mountain View, WY). Baseline and projected mean daily grass pasture evapotranspiration for all scenarios and for time periods 2020 (left) and 2080 (right).

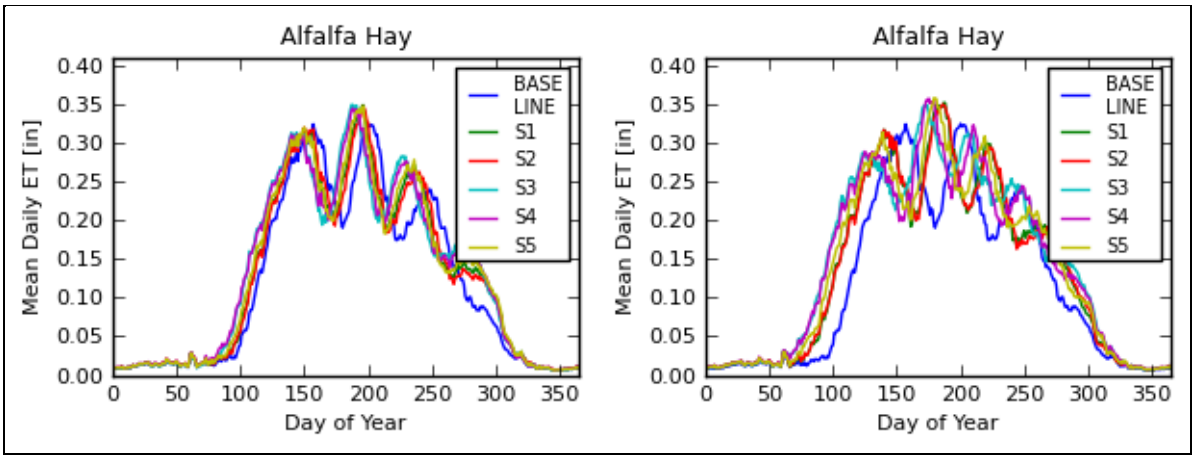

Figure 21.—Colorado River Basin – COOP station UT5969 (Myton, UT). Baseline and projected mean daily alfalfa evapotranspiration for all scenarios and for time periods 2020 (left) and 2080 (right).

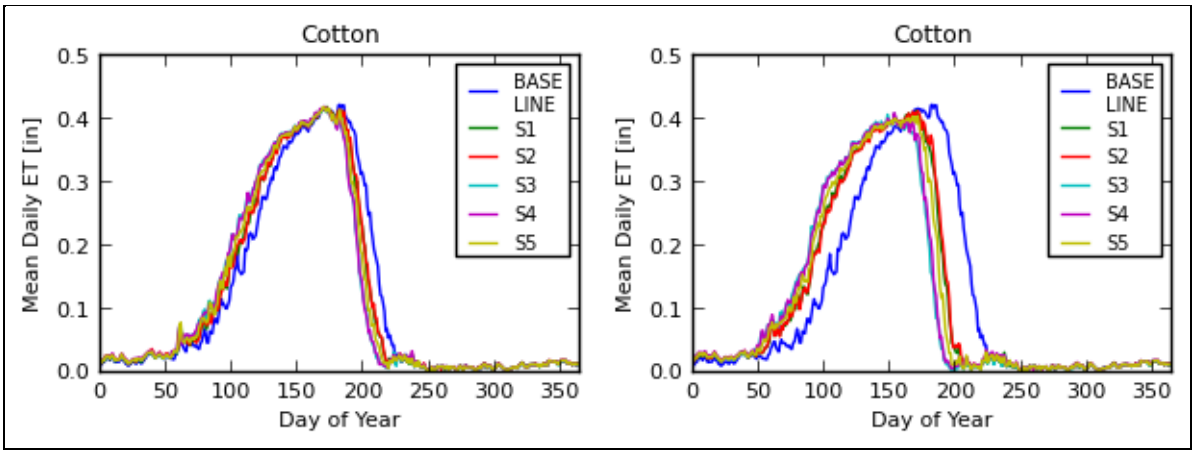

Figure 22.—Colorado River Basin – COOP station AZ9656 (Yuma, AZ). Baseline and projected mean daily cotton evapotranspiration for all scenarios and for time periods 2020 (left) and 2080 (right).

5.2.2 Baseline and Projected Reservoir Evaporation

Figures 23 and 24 illustrate baseline and projected annual precipitation (top left), annual mean temperature (top right), annual evaporation (bottom left), and annual net evaporation (bottom right) for Lake Powell and Lake Mead. The heavy black line for each variable is the annual time series for 50 percentile values (i.e., ensemble-median). The shaded area for each variable is the annual time series of 5th to 95th percentiles or the 90-percent range of variability.

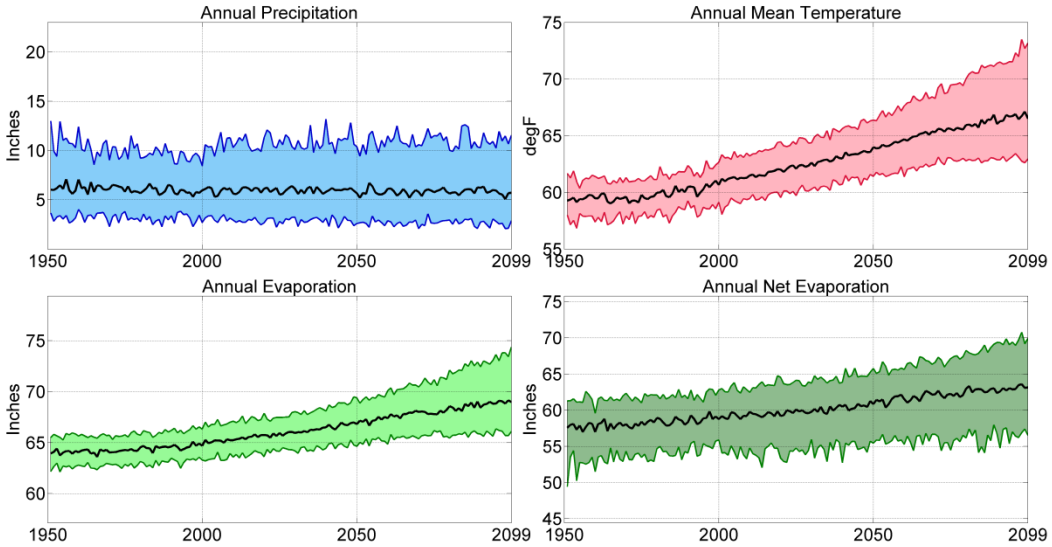

Figure 23.—Colorado River Basin – Lake Powell ensemble median and 5th and 95th percentile annual precipitation, temperature, reservoir evaporation, and net evaporation.

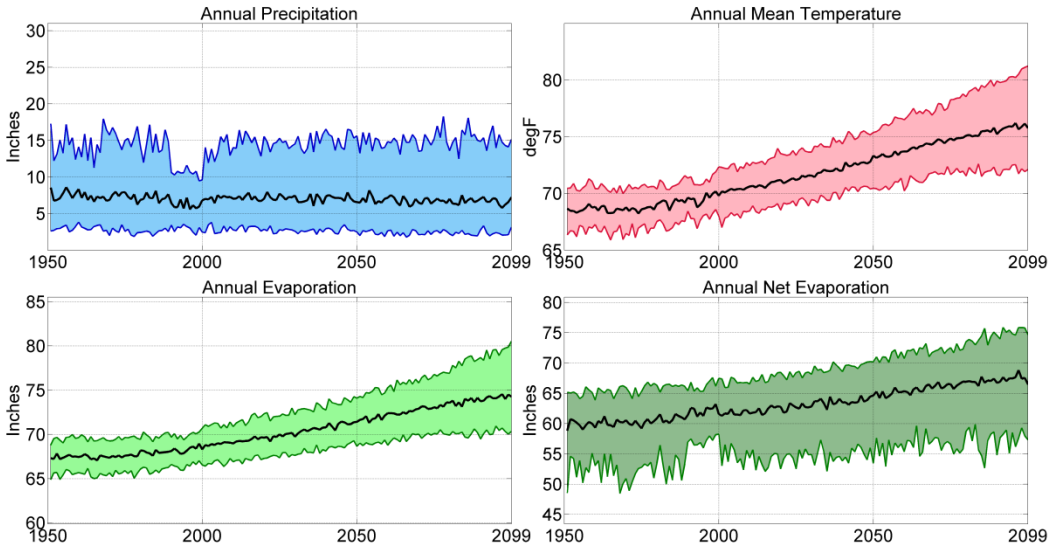

Figure 24.—Colorado River Basin – Lake Mead ensemble median and 5th and 95th percentile annual precipitation, temperature, reservoir evaporation, and net evaporation.

Annual precipitation over Lake Powell and Lake Mead has a very nominal decline over the transient period going out to 2099. The 5th to 95th percentile envelope for annual precipitation is fairly large (~40% of the ensemble median) for both reservoirs, and shows no trend over time, implying that there is no increase or decrease in the uncertainty from the present. The mean annual temperature and annual evaporation both show increasing trends and diverging variability over time at both reservoirs. The ensemble-median and variability for net evaporation (i.e., evaporation minus precipitation) are affected by both precipitation and temperature projections. It is evident, for instance, that the upper envelope bound in precipitation causes the lower bound of net evaporation to be highly variable, while the diverging variability is caused primarily by the diverging temperature projections.

Advection of heat from river inflow and outflow occurs in Lake Powell and Lake Mead. Annual net advection of heat on large rivers and reservoir systems is often positive, inasmuch as the inflows have an average water temperature that is commonly higher than the outflow temperature due to dam releases of relatively deep and cool water. Because the CRLE model does not consider the impact of net advected heat, it was estimated from previous work. Based on an estimate of the annual average net advected heat of 12 inches reported by Morton (1979), Lake Mead and Lake Powell monthly CRLE evaporation estimates were adjusted for historical and projected time periods. Morton's estimate of the average annual net advected heat is in the range of results from a recent energy balance study on Lake Mead, where annual net advected heat ranged from 0 to 15 inches for 2010–2012 (Moreo et al. 2013). The average monthly distribution of net advected heat reported by Moreo et al. (2013) was used to distribute the annual average estimate by Morton (1979) to average monthly values used in this report. Average monthly values ranged from –0.5 inches per month (March) to 3.4 inches per month (August).

In Figures 25 and 26, representing Lake Powell and Lake Mead, respectively, the solid lines show the ensemble-median mean monthly evaporation and net evaporation for the baseline period (1950–1999) and for the 2020s, 2050s, and 2080s, and the shaded areas show the decadal spread of mean monthly evaporation and net evaporation for the baseline period (gray shading) and the 2080s (magenta shading), where the spread is bound by the ensemble's 5th to 95th percentile values for each month. The simulated impact of heat storage is clearly evident, as the peak evaporation occurs in August and the minimum occurs between February and March. The magnitude of projected monthly evaporation and net evaporation is greatest during the summer months and least during the fall and winter months. The increase in annual evaporation and net evaporation from baseline to the 2080 time period is 6.3 and 7.1 percent (4.1 and 4.1 in) for Lake Powell, and 8.4 and 10.1 percent (5.7 and 6.1 in) for Lake Mead, respectively (appendix 10).

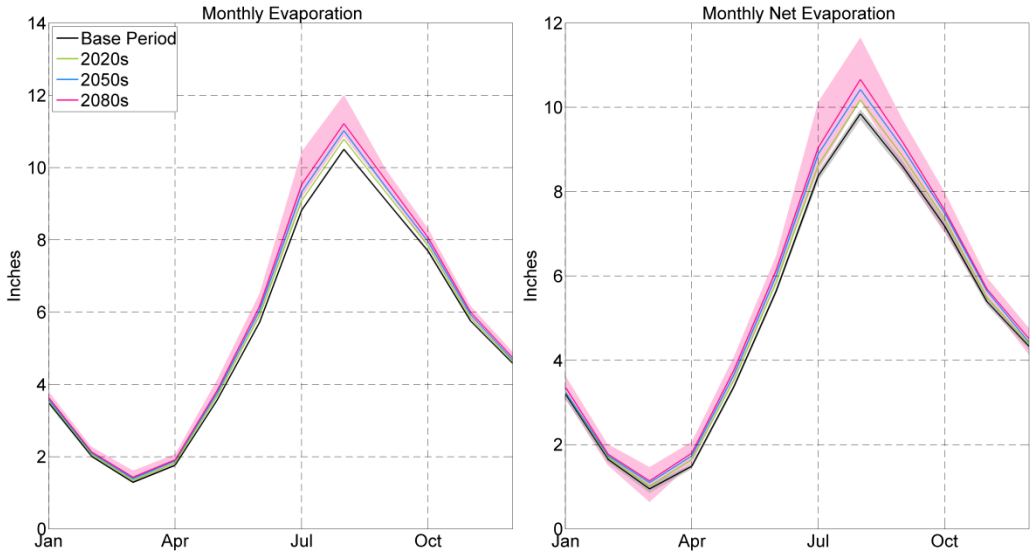

Figure 25.—Colorado River Basin – Lake Powell mean monthly ensemble median and 5th and 95th percentile reservoir evaporation and net evaporation.

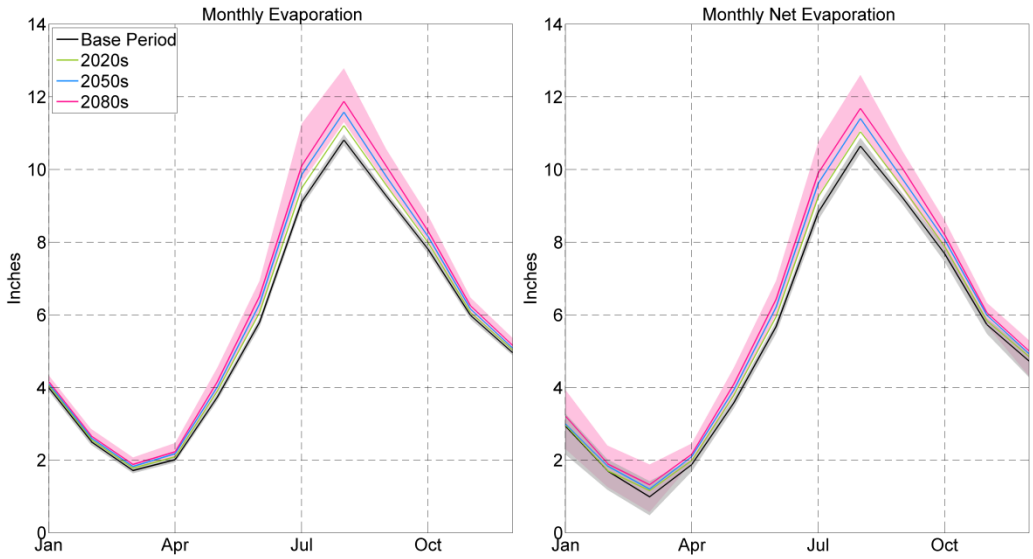

Figure 26.—Colorado River Basin – Lake Mead mean monthly ensemble median and 5th and 95th percentile reservoir evaporation and net evaporation.

5.3 Columbia River Basin

5.3.1 Baseline and Projected Irrigation Water Demands

Figure 27 illustrates COOP station based Met Nodes that were used to estimate irrigation water demands, as well as HUC8 boundaries used to upscale Met Node estimates in the Columbia River Basin. Figure 28 illustrates the spatial distribution of baseline (1950–1999) mean annual temperature (top left) and mean annual precipitation (top right) derived from BCSD data, mean annual dewpoint depression (bottom left) and mean annual windspeed (bottom right) estimated from historical agricultural weather data (discussed in section 4.2.1). Gray-hatched HUC8 polygons illustrated on figure 28 (and other results figures) represent areas where no significant crop acreage was present, so baseline and projected climate and irrigation water demands were not simulated for those areas.

Figure 28 illustrates mean annual temperatures ranging from cool in the east to warm in the west, while precipitation varies from low or moderately low in the majority of the basin to relatively high in the extreme western portion. The mean annual dewpoint depression (i.e., $T_{min} - T_{dew}$) is used here as a simple approximation of the humidity of the lower air mass that is consistent and representative of agricultural areas while preserving regional and local advection effects. Its spatial distribution clearly shows a more arid region in the south-central part of the basin, a moderately dry portion in the northwest, and less arid conditions in the remainder of the basin. Mean annual windspeeds are generally higher in the southeast portion of the basin, moderate in the center, and relatively low in the remaining areas.

Figure 29 illustrates reference ET (ET_0) (top left), crop evapotranspiration (ET_c) (top right), net irrigation water requirement (NIWR) (bottom left), and total crop acreage (bottom right) within each HUC8 boundary. ET_0, ET_c, and NIWR are all higher in the southern and west-central portions of the basin, where mean temperature, dewpoint depression, and windspeeds are significantly larger than in the northern and western portions of the basin. The projected values range from 25.6 to 50.3 in/yr for ET_0, 19.4 to 44.6 in/yr for ET_c, and 7.1 to 34.1 in/yr for NIWR.

Figure 30 shows the spatial distribution of projected mean temperature change for different climate scenarios and time periods, and it is evident that the changes shown there are generally spatially uniform for all scenarios, with scenario S3 (hot-dry) having the largest change. Figure 31 illustrates the spatial distribution of projected precipitation percent change for different scenarios and time periods. Depending on the scenario, precipitation percent changes range from –12.2 to 30.3 percent for the 2080 time period, with the ensemble median scenario (S5) generally showing a slight increase throughout the basin, ranging from 1.9 to 15.7 percent.

Figure 27.—Columbia River Basin – COOP Stations used to simulate baseline and projected irrigation demands.

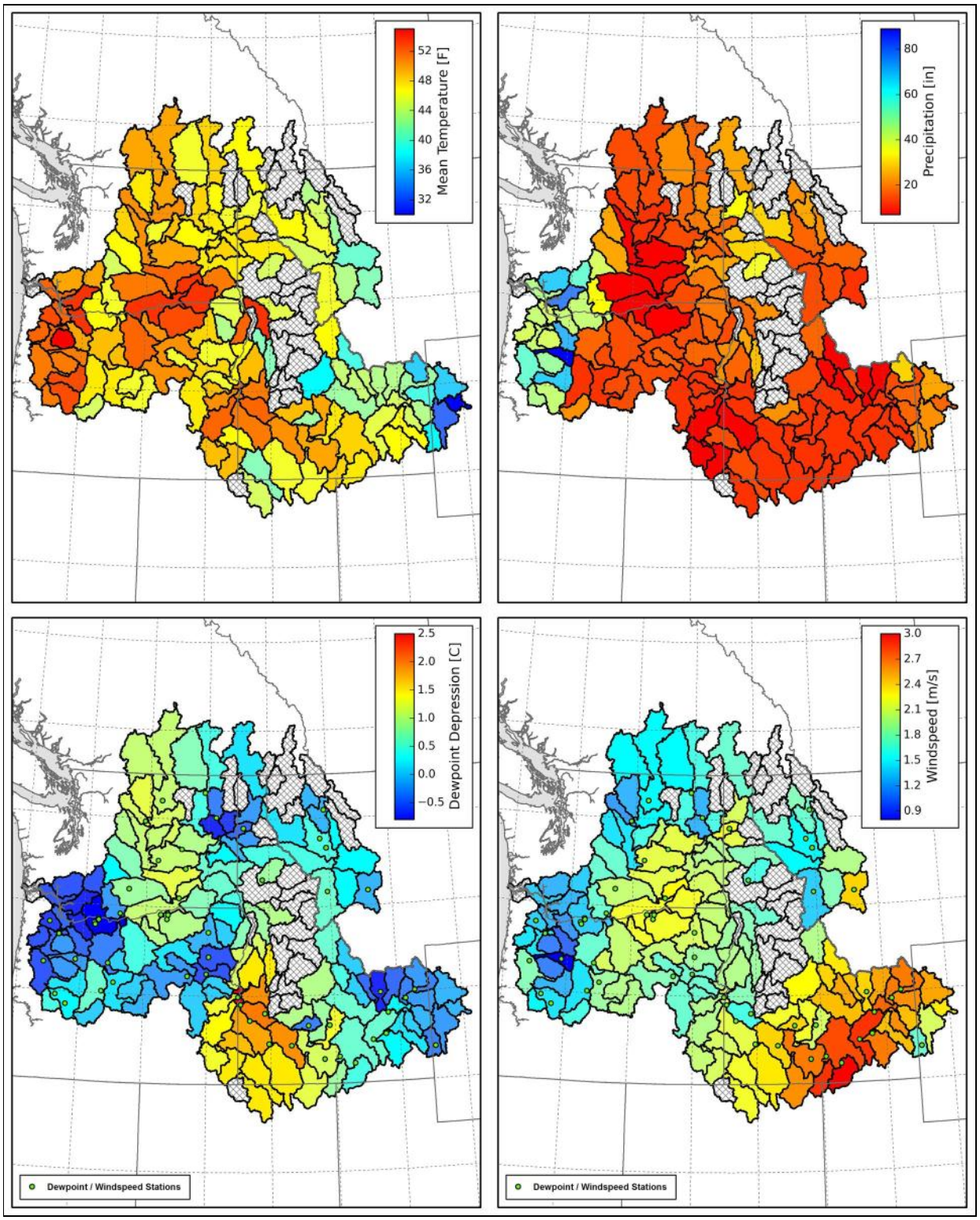

Figure 28.—Columbia River Basin – Spatial distribution of baseline temperature, precipitation, dewpoint depression, and windspeed.

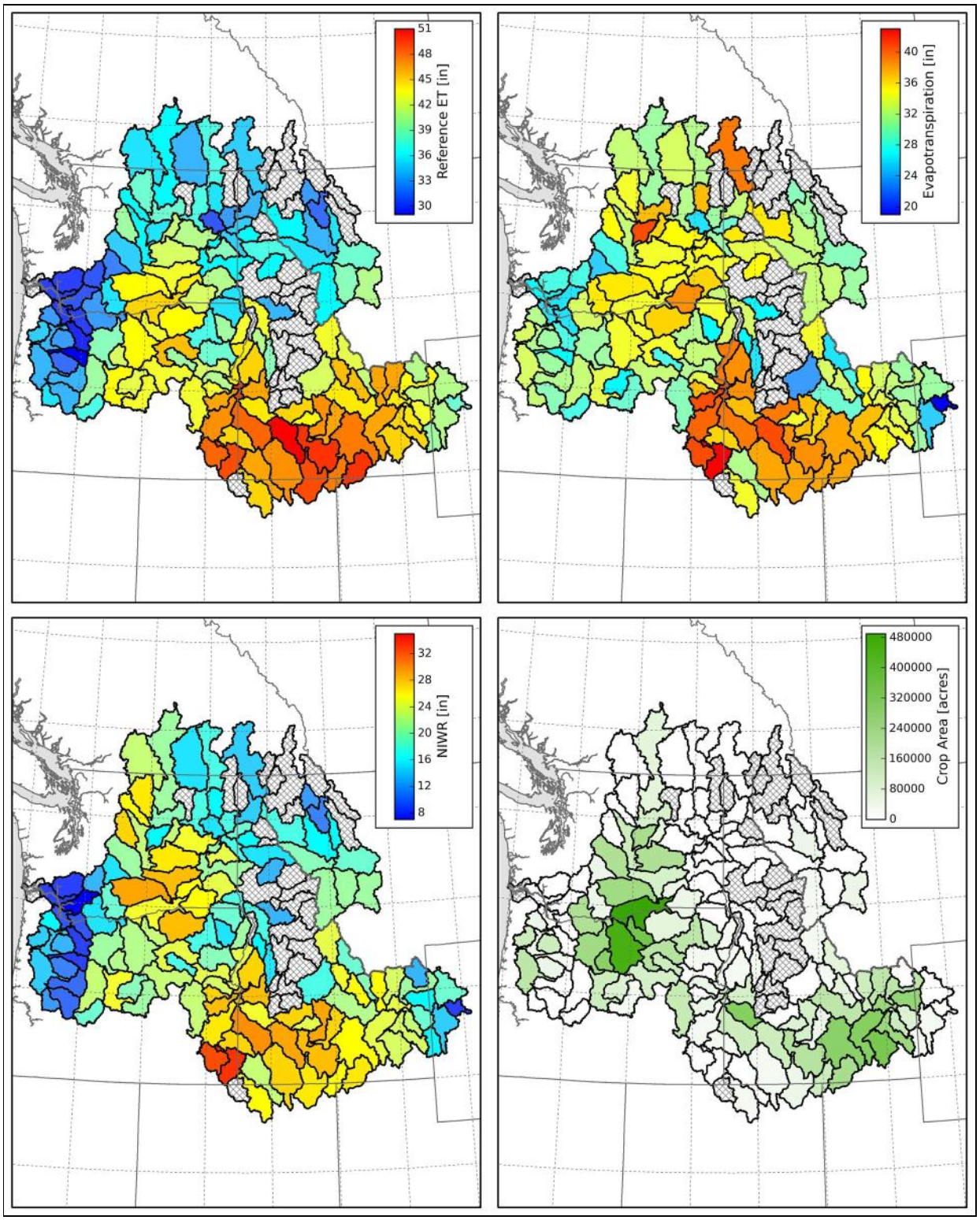

Figure 29.—Columbia River Basin – Spatial distribution of baseline reference evapotranspiration, crop evapotranspiration, net irrigation water requirements (NIWR), and crop acreage. Gray hatch areas represent HUCs with no crop acreage.

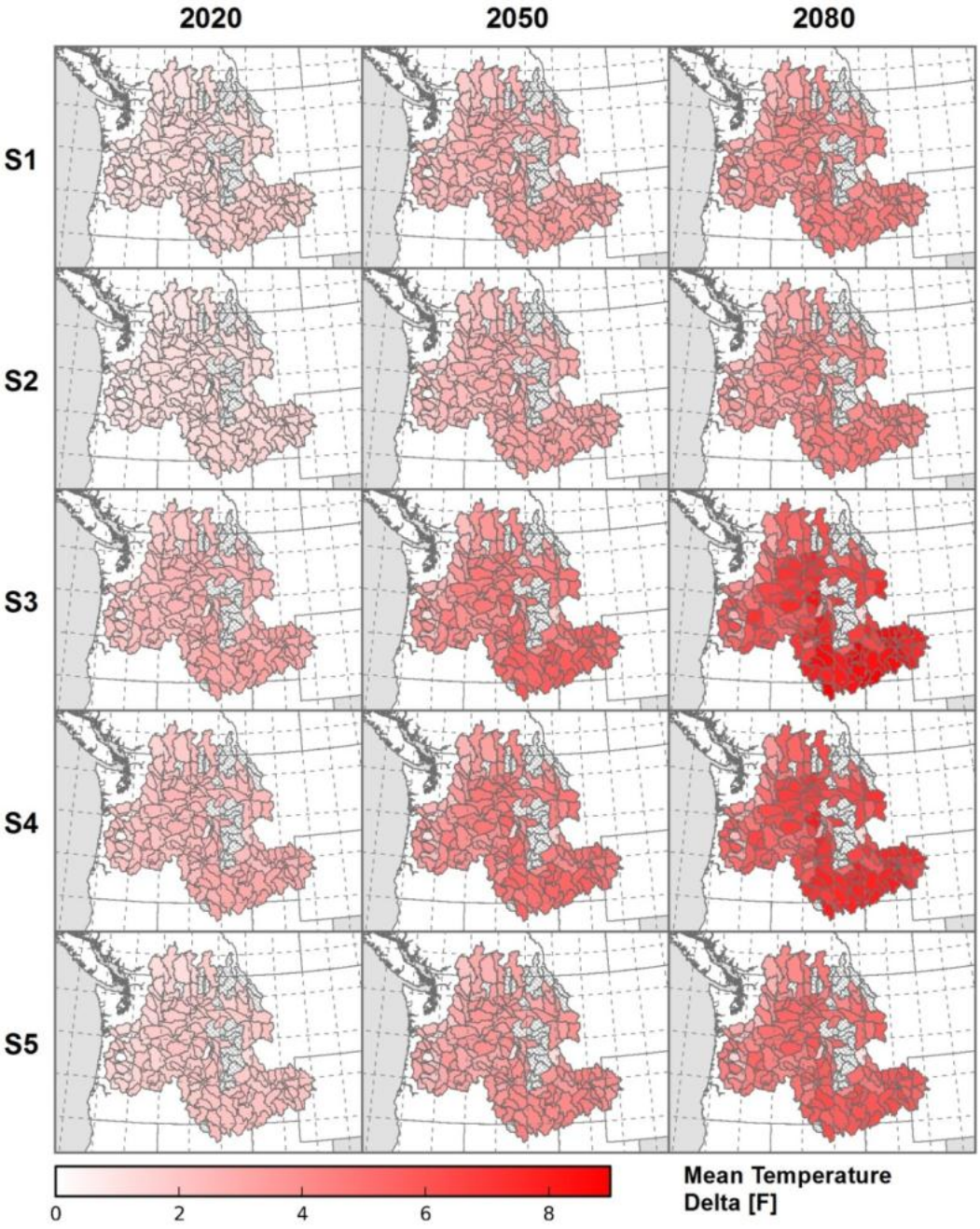

Figure 30.—Columbia River Basin – Spatial distribution of temperature change for different climate scenarios and time periods (S1 = WD, S2 = WW, S3 = HD, S4 = HW, S5 = Central).

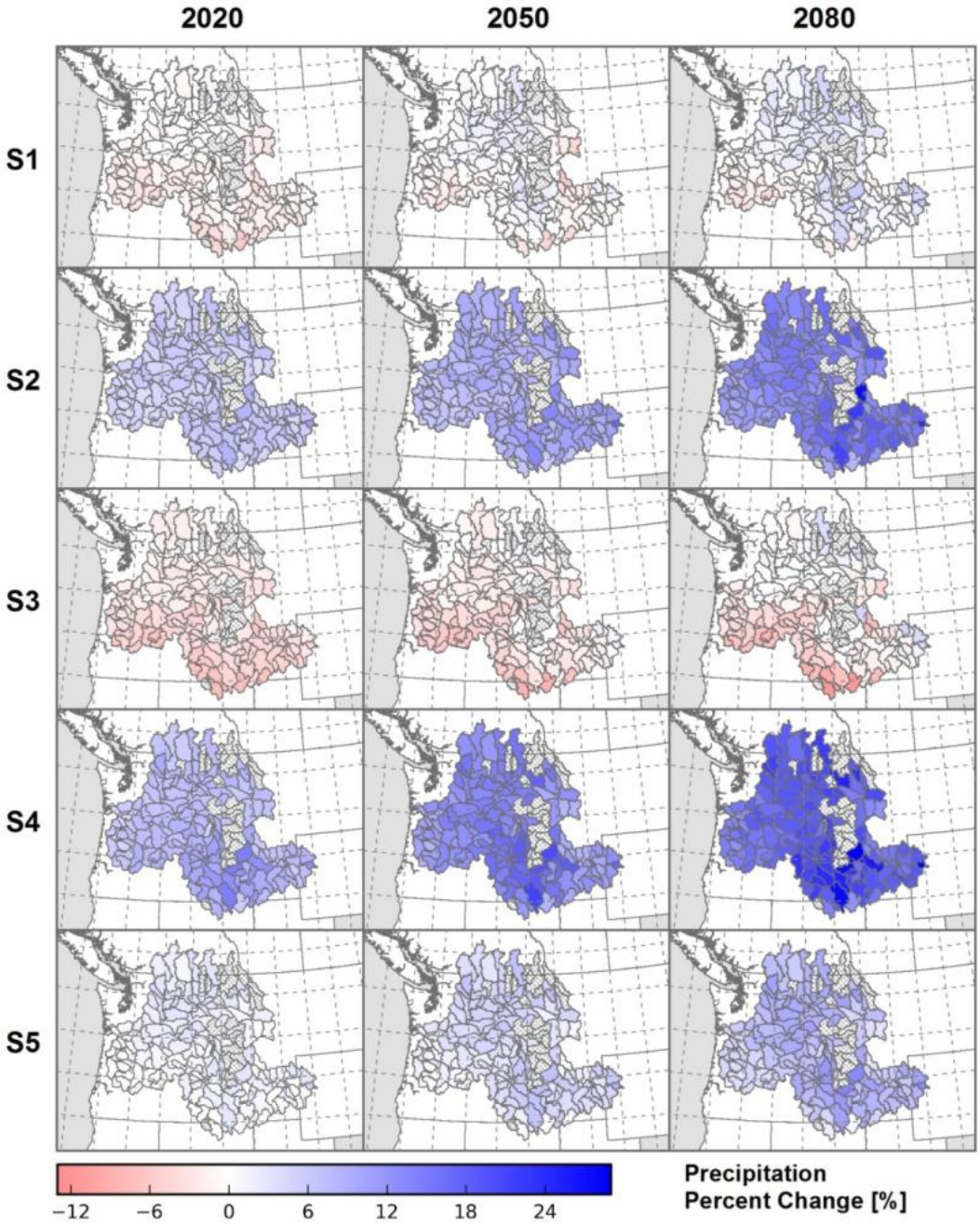

Figure 31.—Columbia River Basin – Spatial distribution of projected precipitation percent change for different climate scenarios and time periods (S1 = WD, S2 = WW, S3 = HD, S4 = HW, S5 = Central).

Figure 32 shows the spatial distribution of projected ET_0 percent change for different climate scenarios and time periods. Similar to temperature, the projected percent change in ET_0 is generally spatially uniform for all scenarios, with scenario S3 (HD) having the largest change. The higher elevation regions of the southeastern portion of the basin (in Wyoming and eastern Idaho) exhibit the largest percent change because the differences between the projected and baseline ET_0 are relatively large compared to the relatively low baseline estimates for ET_0. Figure 33 illustrates the spatial distribution of projected ET_c percent change for different climate scenarios and time periods assuming non-static crop phenology for annual crops, where projected future temperatures were used for simulating projected planting, crop coefficient development, and termination as described in section 4.2.1. Spatial differences in the distribution of projected percent change in ET_c are largely due to differences in crop type and baseline ET_c. The southern and southeastern portions of the basin are projected to experience the largest percent change for all projected time periods, largely due to the fact that the differences between the projected and baseline ET_c are fairly large relative to the baseline estimates of ET_c (figure 29). ET_c is projected to decrease by as much as 8.8 percent in about 23 HUC8s (encompassing all climate change scenarios), spread throughout the western and northern portions of the basin. This decrease is attributed to significant winter wheat acreage in the 23 HUCs in question, inasmuch as winter wheat is simulated to be planted and harvested earlier in the season, which therefore lowers the ET_c.

Figure 34 shows the spatial distribution of projected ET_c percent change for different climate scenarios and time periods assuming static crop phenology for annual crops. Baseline temperatures were used for simulating projected planting, crop coefficient development, and termination for all future time periods and scenarios as described in section 4.2.1. All HUCs show ET_c increases or no change, with the exception of two HUCs in the western part of the basin that exhibit slight (less than 1%) decreases in ET_c by 2080 due to earlier harvest of perennial grass hay.

The spatial distribution of projected NIWR percent change for different climate scenarios and time periods is shown on figures 35 and 36. The NIWR incorporates growing-season and non-growing-season soil moisture gains and losses from precipitation, bare soil evaporation, and ET. Therefore, spatial variations in the distribution of NIWR percent change for different time periods and scenarios are a function of respective ET_c (figures 33 and 34) and precipitation (figure 31) distributions. For example, in the southeastern portion of the basin, S3 (HD) precipitation is projected to decrease or to increase only slightly (in the case of the extreme eastern, mountainous areas), whereas S4 (HW) precipitation is projected to largely and uniformly increase. This results in S4 NIWR increasing less than S3 NIWR, even though S3 and S4 ET_c changes are very similar. For more illustrations on unit changes (degrees F and inches) in spatial projections of mean temperature, precipitation, ET_0, ET_c, and NIWR for different time periods and scenarios, see appendix 9.

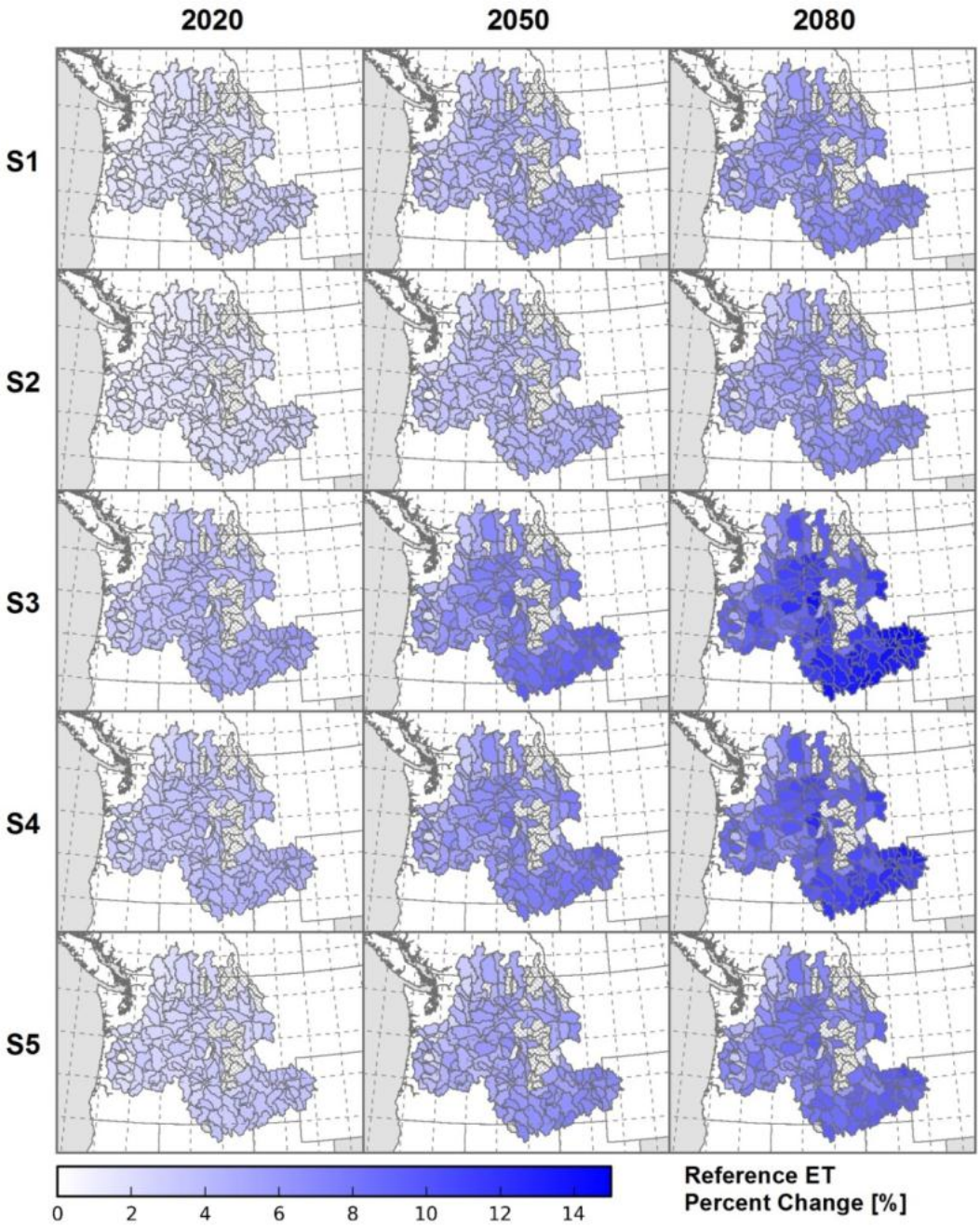

Figure 32.—Columbia River Basin – Spatial distribution of projected reference evapotranspiration percent change for different climate scenarios and time periods (S1 = WD, S2 = WW, S3 = HD, S4 = HW, S5 = Central).

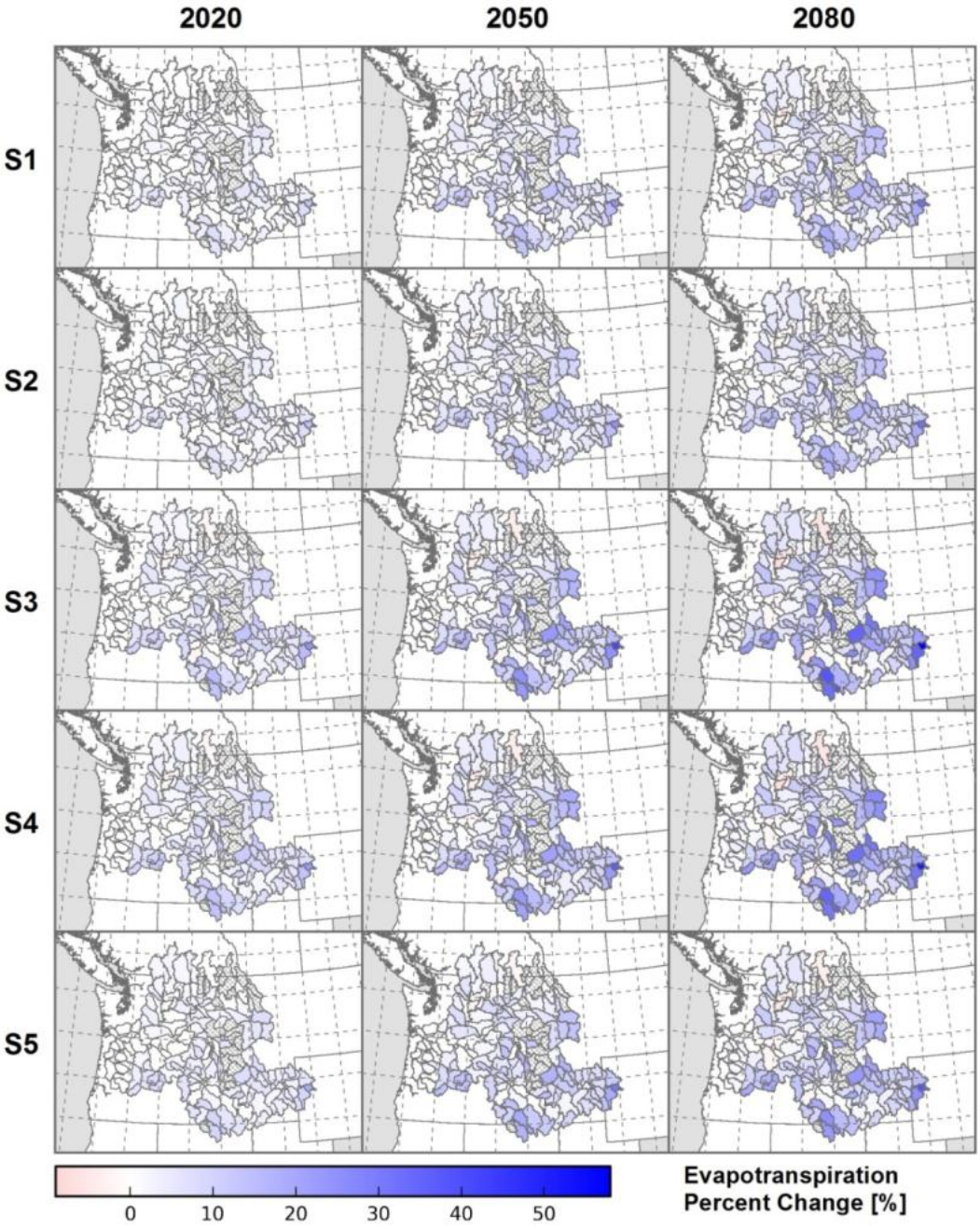

Figure 33.—Columbia River Basin – Spatial distribution of projected crop evapotranspiration percent change for different climate scenarios and time periods (S1 = WD, S2 = WW, S3 = HD, S4 = HW, S5 = Central).

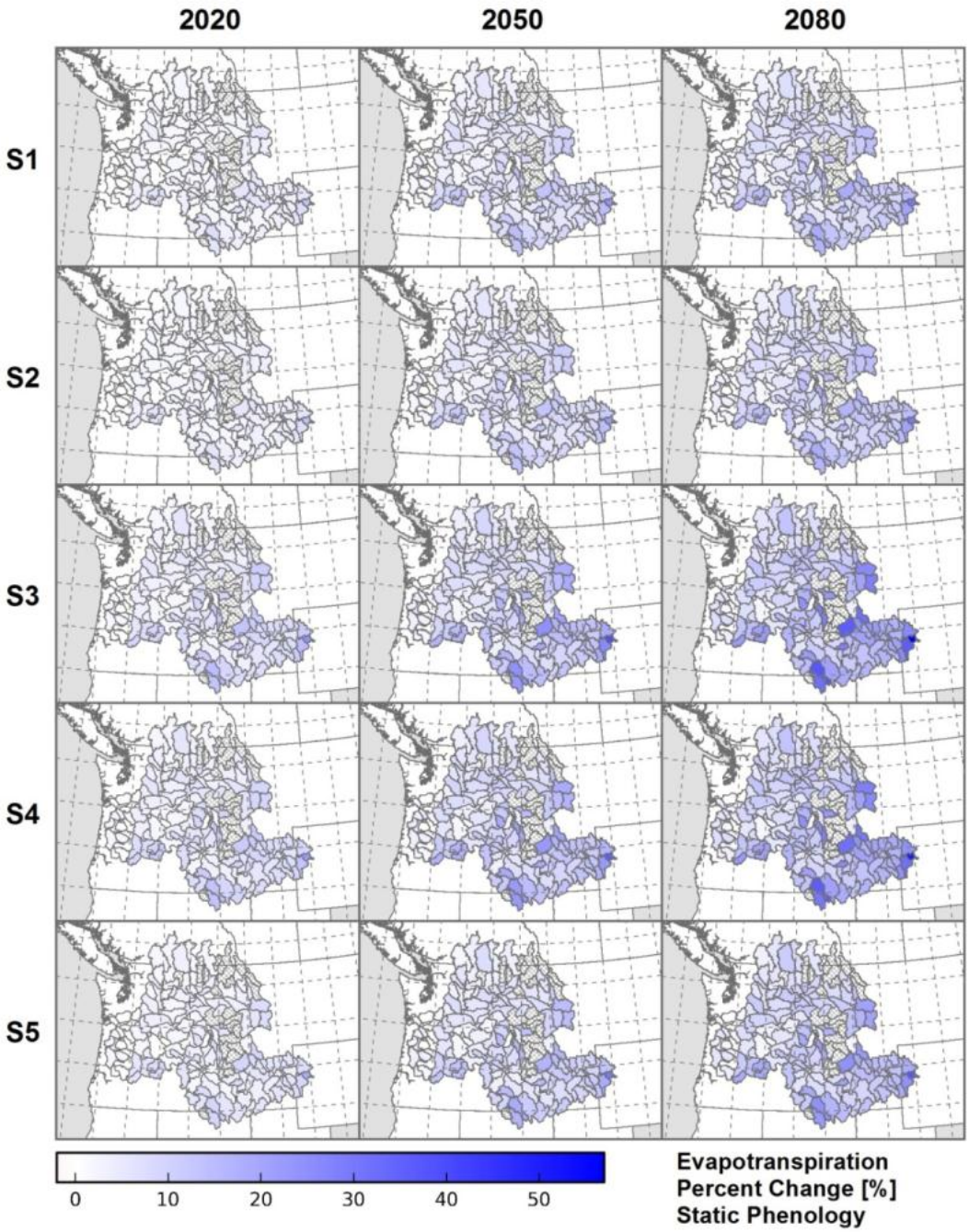

Figure 34.—Columbia River Basin – Spatial distribution of projected crop evapotranspiration percent change for different climate scenarios and time periods assuming static phenology for annual crops (S1 = WD, S2 = WW, S3 = HD, S4 = HW, S5 = Central).

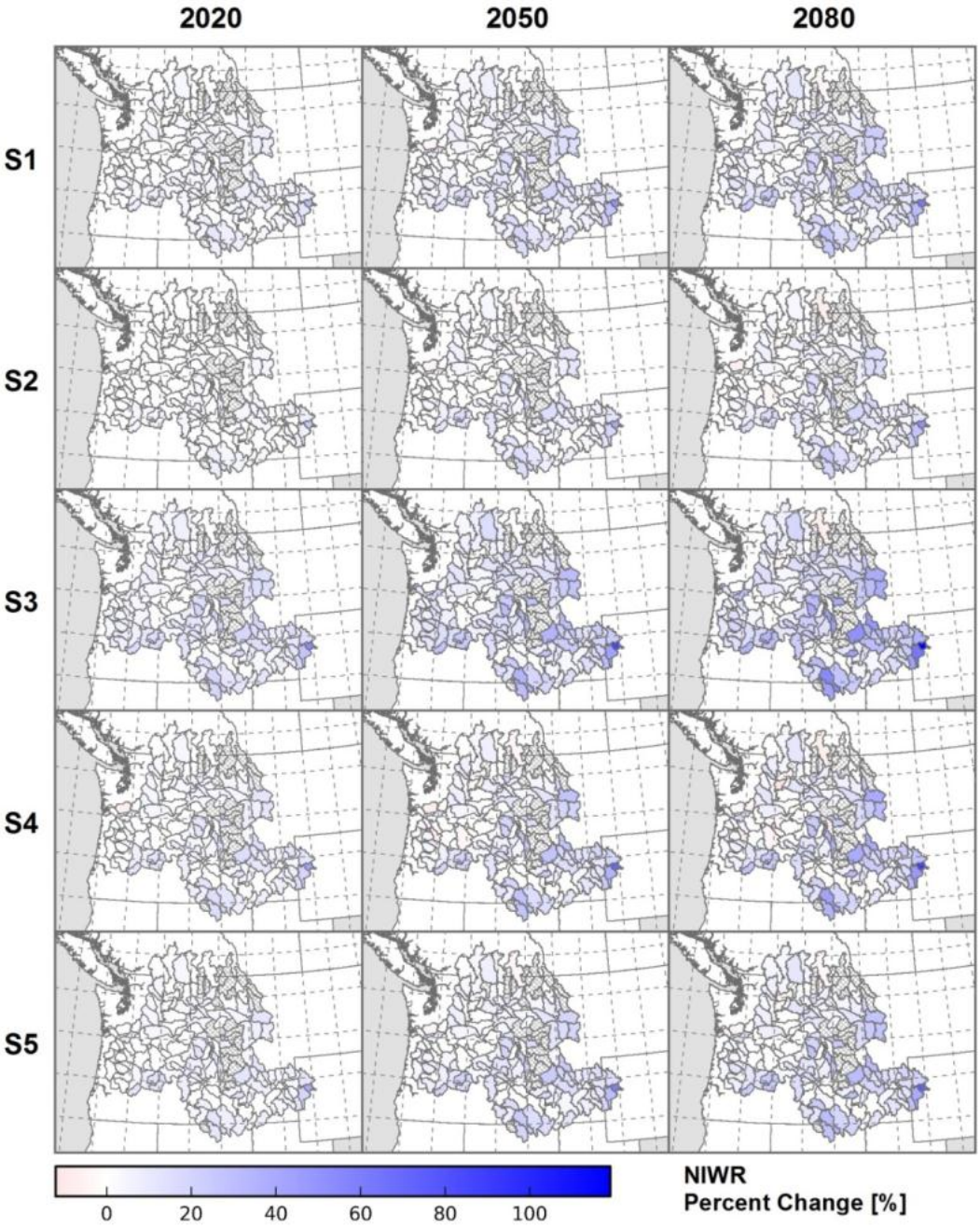

Figure 35.—Columbia River Basin – Spatial distribution of projected net irrigation water requirements (NIWR) percent change for different climate scenarios and time periods (S1 = WD, S2 = WW, S3 = HD, S4 = HW, S5 = Central).

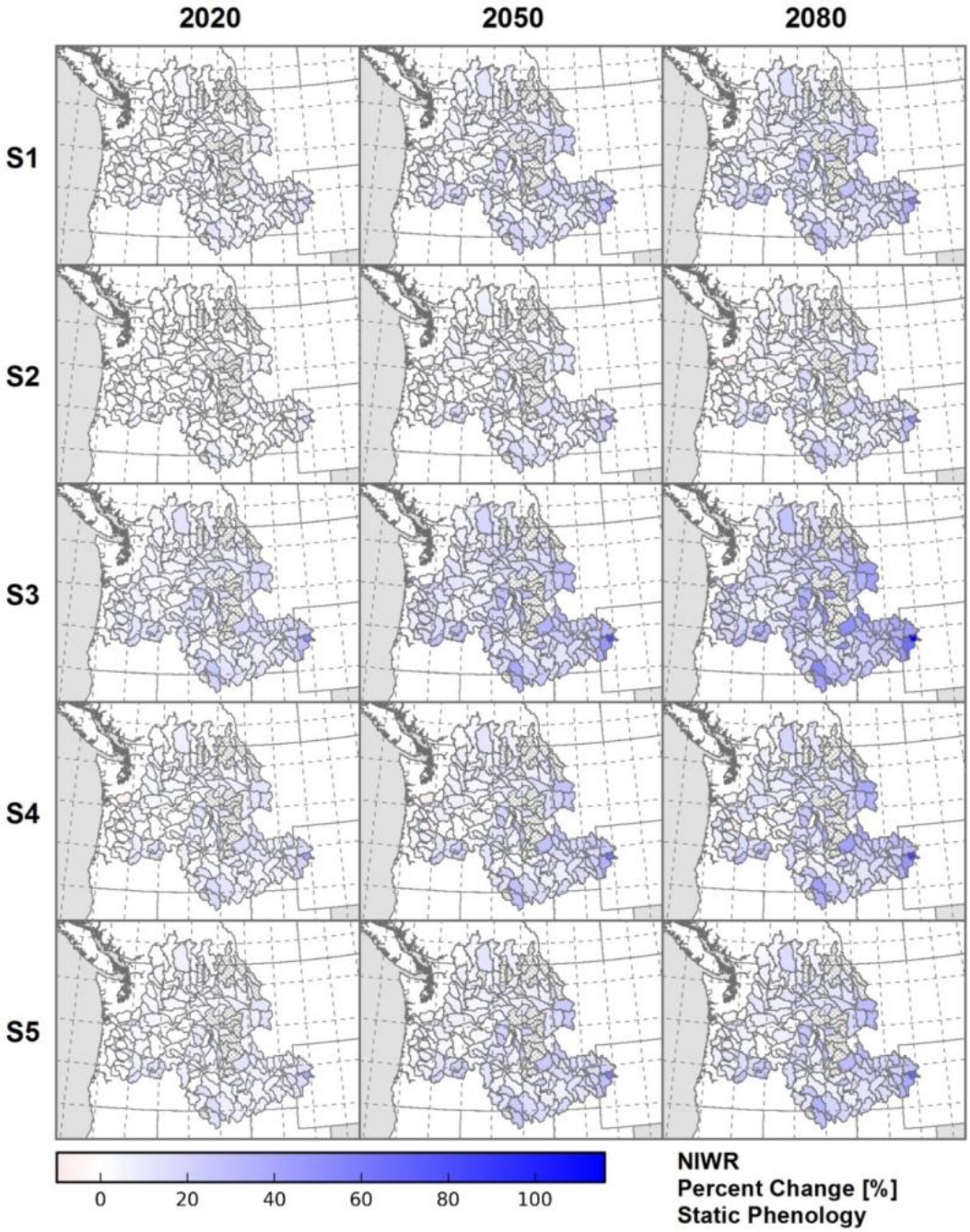

Figure 36.—Columbia River Basin – Spatial distribution of projected net irrigation water requirements (NIWR) percent change for different climate scenarios and time periods assuming static phenology for annual crops (S1 = WD, S2 = WW, S3 = HD, S4 = HW, S5 = Central).

Figures 37, 38, and 39 illustrate the baseline and projected temporal distribution of mean daily ET_c for selected Met Nodes, crops, scenarios, and time periods. The simulated mean daily ET_c of alfalfa for the 2020 time period, Met Node ID9303 (COOP Twin Falls 6E), shows slight but noticeable shifts in the growing-season length and alfalfa cutting cycles relative to baseline conditions (figure 37, left). By the 2080 time period (figure 37, right) significant shifts in growing-season length, crop development, and cutting cycles are noticeable relative to baseline conditions, with scenarios S3 and S4 exhibiting the most extreme changes. Figure 38 shows simulated mean daily ET_c of spring grain at Met Node ID9303 (Twin Falls 6E), under different scenarios, for the 2020 and 2080 time periods. Because planting dates for annual crops are temperature dependent in the non-static phenology simulations, shifts in planting, development, and harvest dates of spring grain are clearly evident, especially by the 2080 time period, in which peak ET for spring grain is shifted as much as 40 days earlier and the peak rate is reduced by about 15 percent due to its movement into a lower ET_0 period. The uncertainty associated with such potential shifts in planting dates, accelerated crop development, and harvest was a primary reason for using baseline temperatures for static phenology simulations (figures 34 and 36). In static phenology simulations, because baseline temperatures are used for estimating planting, crop development, and harvest dates, all scenarios and time periods have identical seasonal K_{cb} shapes, and show differences only in daily ET_c magnitudes due to daily ET_0 and precipitation differences. Figure 39 illustrates simulated mean daily ET_c of potatoes at Met Node ID9303 (Twin Falls 6E) for different scenarios and time periods. Similar but less extreme seasonal changes in planting, development, harvest dates, and ET_c are projected when compared to spring grain, with S3 and S4 having the most extreme seasonal changes.

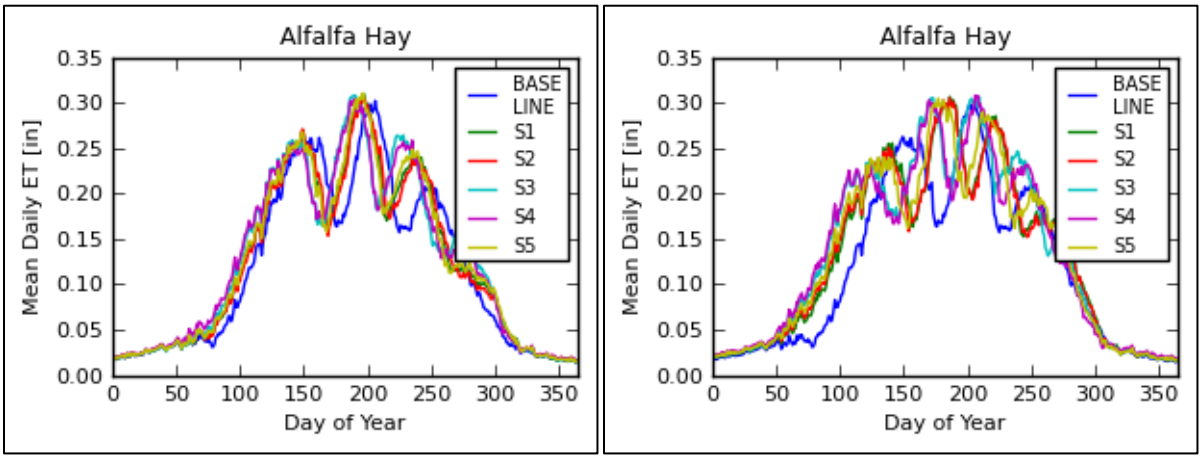

Figure 37.—Columbia River Basin – COOP station ID9303 (Twin Falls 6E). Baseline and projected mean daily alfalfa evapotranspiration for all scenarios and for time periods 2020 (left) and 2080 (right).

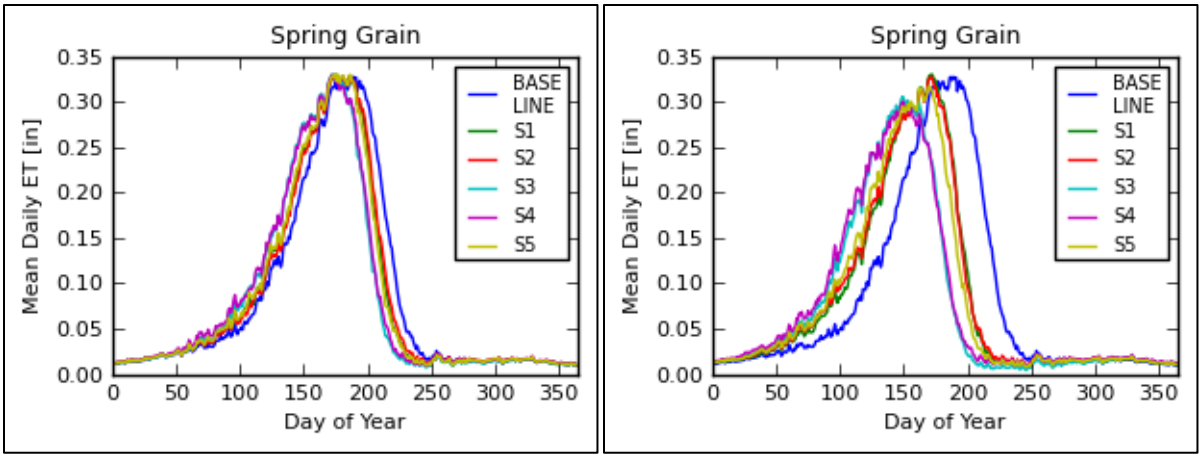

Figure 38.—Columbia River Basin – COOP station ID9303 (Twin Falls 6E). Baseline and projected mean daily spring grain evapotranspiration for all scenarios and for time periods 2020 (left) and 2080 (right).

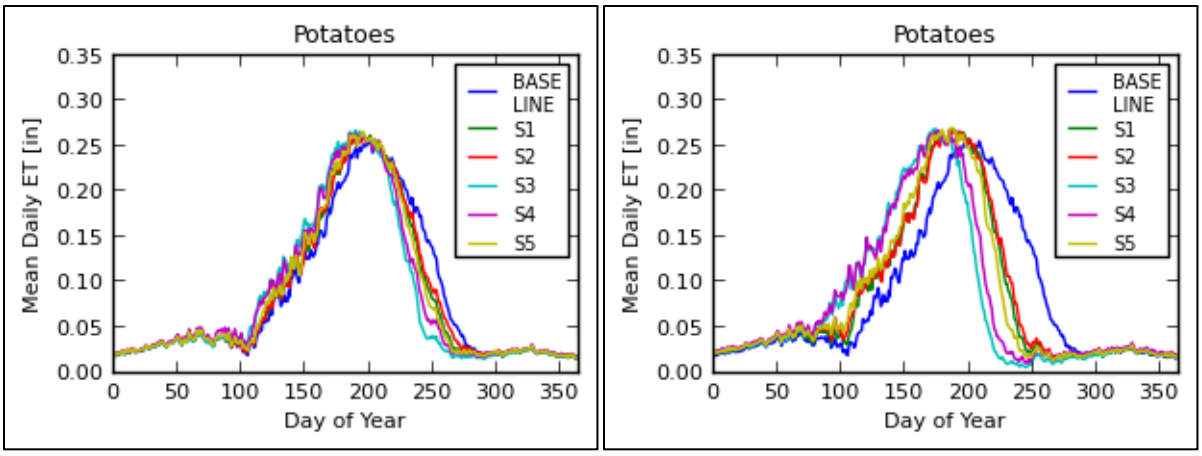

Figure 39.—Columbia River Basin – COOP station ID9303 (Twin Falls 6E). Baseline and projected mean daily potatoes evapotranspiration for all scenarios and for time periods 2020 (left) and 2080 (right).

5.3.2 Baseline and Projected Reservoir Evaporation

Figures 40 and 41 illustrate baseline and projected annual precipitation (top left), annual mean temperature (top right), annual evaporation (bottom left), and annual net evaporation (bottom right) at American Falls Reservoir and Grand Coulee (Franklin Delano Roosevelt Lake). The heavy black line for each variable is the annual time series of 50 percentile values (i.e., ensemble-median). The shaded area for each variable is the annual time series of 5th to 95th percentiles representing the 90-percent variability. Annual precipitation over American Falls and Grand Coulee has a very slight increase over the transient period going out to 2099. The variability for annual precipitation is fairly large (~50% of the ensemble median) for both reservoirs and shows an increase over time, implying

that there is increasing uncertainty from the present. The mean annual temperature and annual evaporation both show increasing trends and a diverging variability over time for both reservoirs. The ensemble-median and variability for net evaporation (i.e., evaporation minus precipitation) are affected by characteristics of both precipitation and temperature projections. It is evident, for instance, that the upper envelope bound in precipitation causes the lower bound of net evaporation to be highly variable, while the slightly diverging variability is caused primarily by the diverging temperature projections.

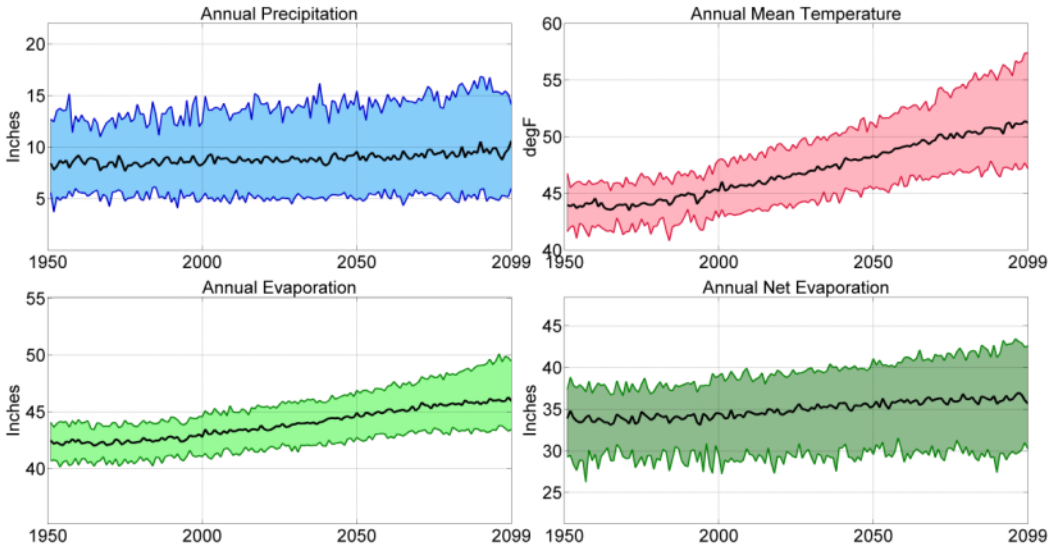

Figure 40.—Columbia River Basin – American Falls ensemble median and 5th and 95th percentile annual precipitation, temperature, reservoir evaporation, and net evaporation.

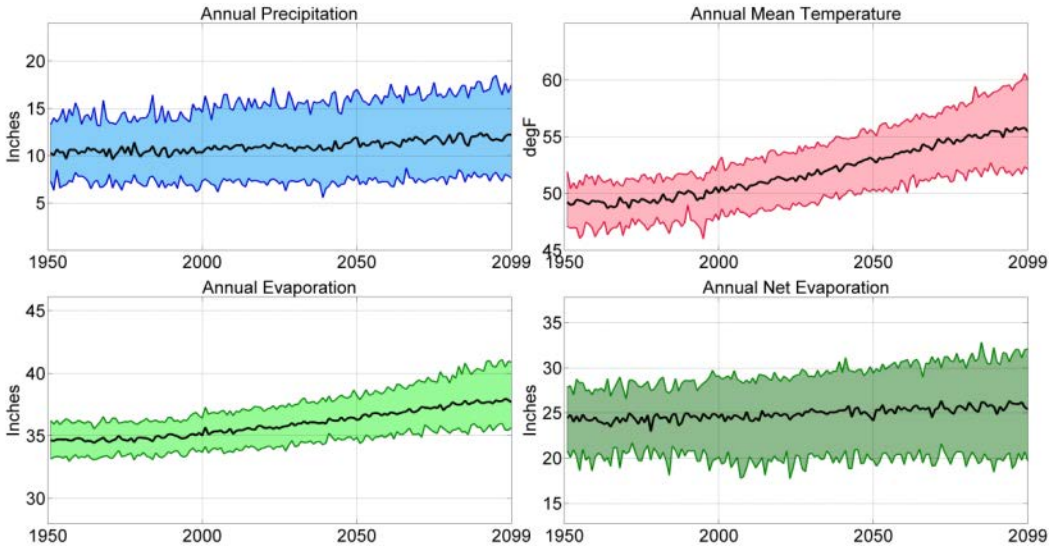

Figure 41.—Columbia River Basin – Grand Coulee ensemble median and 5th and 95th percentile annual precipitation, temperature, reservoir evaporation, and net evaporation.

In Figures 42 and 43, representing American Falls Reservoir and Grand Coulee (Franklin Delano Roosevelt Lake), respectively, the solid lines show the ensemble-median mean monthly evaporation and net evaporation for the baseline period (1950–1999) and for the 2020s, 2050s, and 2080s, and the shaded areas show the decadal spread of mean monthly evaporation and net evaporation for the baseline (gray shading) and 2080s (magenta shading), where the spread is bound by the ensemble's 5^{th} to 95^{th} percentile values for each month. The simulated impact of heat storage is clearly evident, as the peak evaporation occurs in August and the minimum evaporation occurs during February (at American Falls Reservoir) or March (at Grand Coulee). The magnitude of projected monthly evaporation and net evaporation increases is greatest during the summer months, and least during the fall and winter months. The increase in annual evaporation and net evaporation from baseline to the 2080 time period is 7.8 and 6.0 percent (3.3 and 2.0 in) for American Falls, and 7.4 and 5.4 percent (2.6 and 1.3 in) for Grand Coulee, respectively (appendix 10).

5.4 Klamath River Basin

5.4.1 Baseline and Projected Irrigation Water Demands

Figure 44 illustrates COOP station based Met Nodes that were used to estimate irrigation water demands, as well as HUC8 boundaries used to upscale Met Node estimates in the Klamath River Basin. Figure 45 illustrates the spatial distribution of baseline (1950–1999) mean annual temperature (top left) and mean annual precipitation (top right) derived from BCSD data (discussed in section 3.2), mean annual dewpoint depression (bottom left) and mean annual windspeed (bottom right) estimated from historical agricultural weather data (discussed in section 4.2.1). Gray-hatched HUC8 polygons illustrated on figure 45 (and other results figures) represent areas where no significant crop acreage was present, so baseline and projected climate and irrigation water demands were not simulated for those areas. Figure 45 illustrates mean annual temperatures ranging from cool in the west-southwest to warm in the northeast, while precipitation varies from moderately high in the southwest-central area to low amounts in the northeast. The mean annual dewpoint depression (i.e., $T_{min} - T_{dew}$) is used here as a simple approximation of the humidity of the lower air mass that is consistent and representative of agricultural areas while preserving regional and local advection effects. Its spatial distribution clearly shows that northeast areas are more arid and southwest-central areas are more humid. Mean annual windspeeds are generally lower in the west and southwest areas, and higher in the northeast portion of the basin. Figure 46 illustrates reference ET (ET_0) (top left), crop evapotranspiration (ET_c) (top right), net irrigation water requirement (NIWR) (bottom left), and total crop acreage (bottom right) within each HUC8 boundary. ET_0, ET_c, and NIWR are all higher in the southwest portion of the basin, where air temperature, solar radiation, and dewpoint depression are significantly larger than in the southwest-

central portion of the basin. The projected values range from 41 to 52 in/yr for ET_0, 29 to 52 in/yr for ET_c, and 18 to 37 in/yr for NIWR.

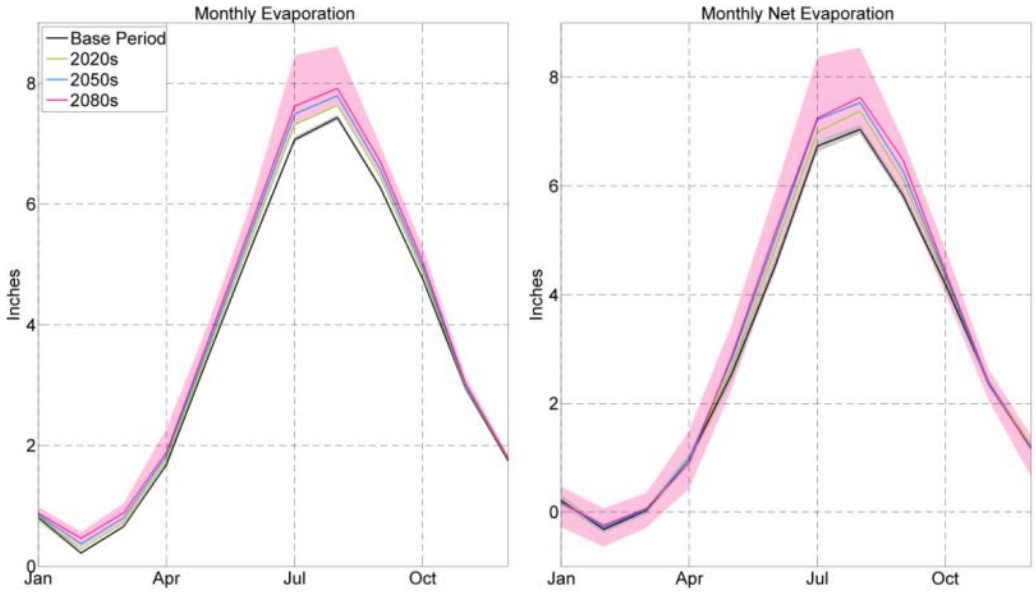

Figure 42.—Columbia River Basin – American Falls mean monthly ensemble median and 5th and 95th percentile reservoir evaporation and net evaporation.

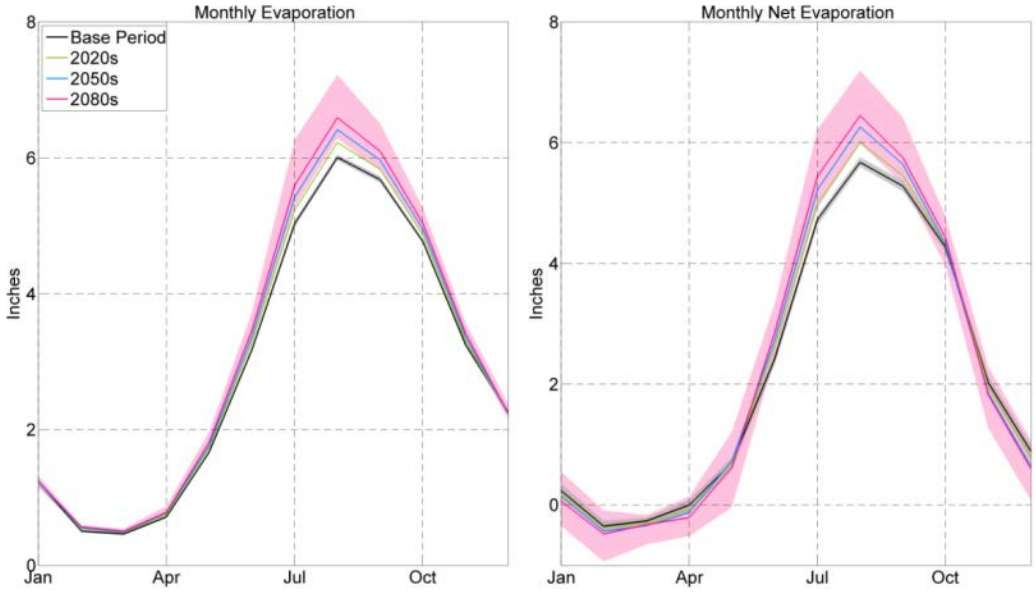

Figure 43.—Columbia River Basin – Grand Coulee mean monthly ensemble median and 5th and 95th percentile reservoir evaporation and net evaporation.

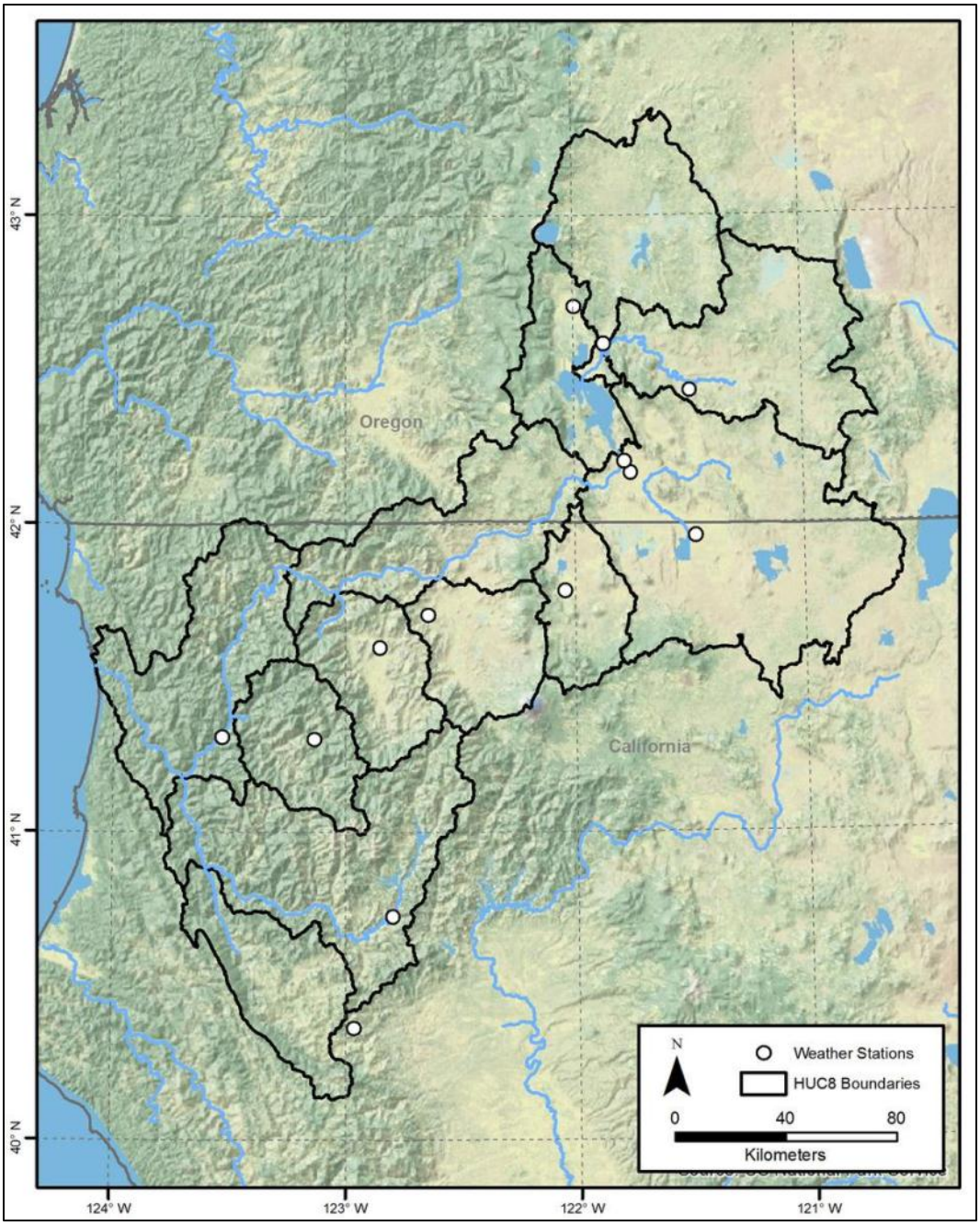

Figure 44.—Klamath River Basin – COOP stations used to simulate baseline and projected irrigation demands.

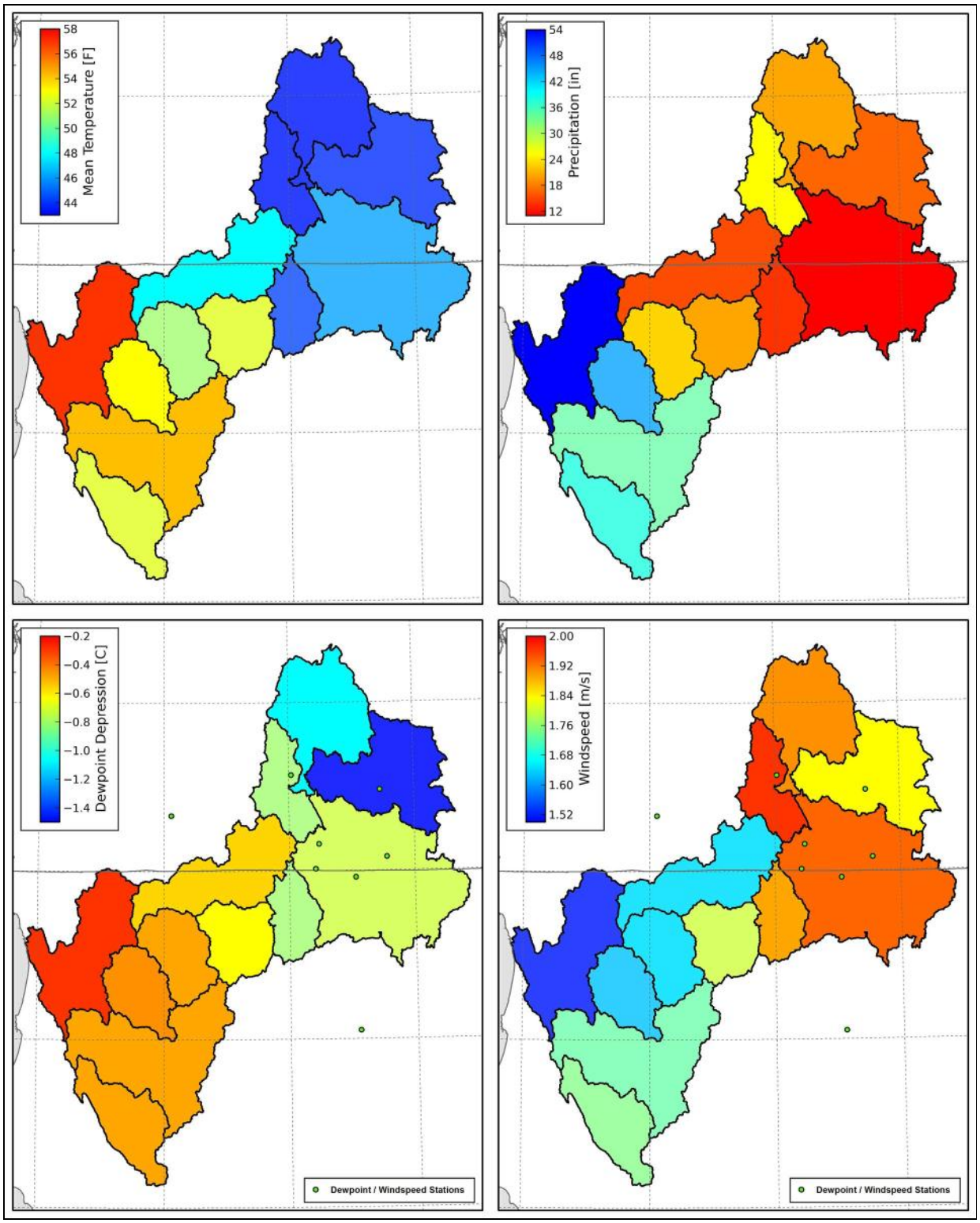

Figure 45.—Klamath River Basin – Spatial distribution of baseline temperature, precipitation, dewpoint depression, and windspeed.

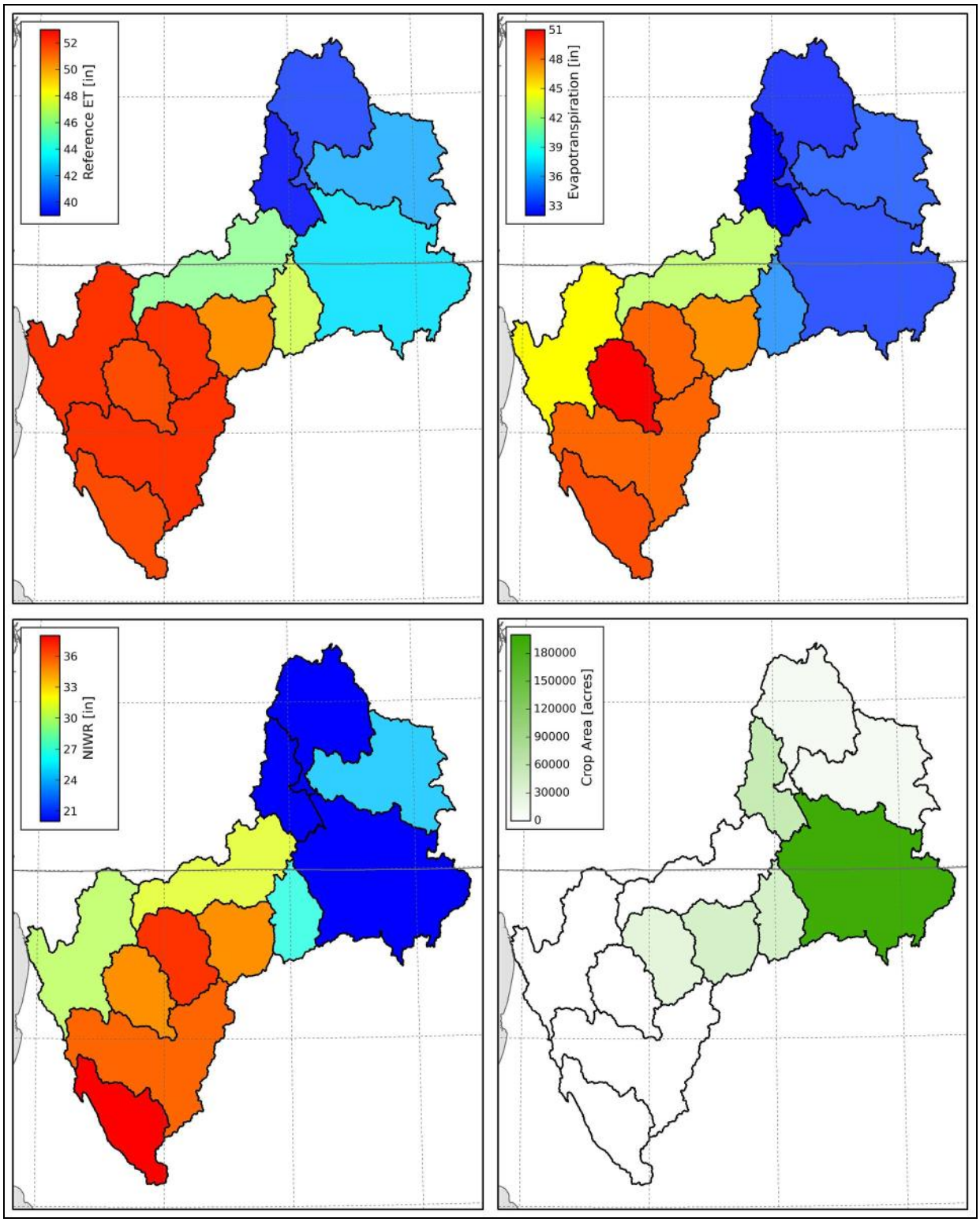

Figure 46.—Klamath River Basin – Spatial distribution of baseline reference evapotranspiration, crop evapotranspiration, net irrigation water requirements (NIWR), and crop acreage.

Figure 47 shows the spatial distribution of projected mean temperature change for different climate scenarios and time periods, and it is evident that the changes shown there are generally spatially uniform for all scenarios, with scenario S3 (hot-dry) having the largest change. Figure 48 illustrates the spatial distribution of projected precipitation percent change for different scenarios and time periods. Depending on the scenario, precipitation percent changes range from –14 to 17 percent for the 2080 time period, with the ensemble median scenario (S5) generally showing a slight decrease and increase in the southwest and an increase in the northeast portion of the basin.

Figure 49 shows the spatial distribution of projected ET_0 percent change for different climate scenarios and time periods. Similar to temperature, the projected percent change in ET_0 is generally spatially uniform for all scenarios, with scenario S3 having the largest change. The northeast portions of the basin exhibit the largest percent change due to the fact that the difference between the projected and baseline ET_0 is relatively large compared to the relatively low baseline estimates for ET_0. Figure 50 illustrates the spatial distribution of projected ET_c percent change for different climate scenarios and time periods assuming non-static crop phenology for annual crops, where projected future temperatures were used for simulating projected planting, crop coefficient development, and termination as described in section 4.2.1. Spatial differences in the distribution of projected percent change in ET_c are largely due to differences in crop type and baseline ET_c. The northeast portion of the basin is projected to experience the largest percent change for all projected time periods, largely due to the fact that the difference between the projected and baseline ET_c is fairly large relative to the baseline estimate of ET_c (figure 46). ET_c in the southwest portion of the basin is projected to slightly decrease or to remain relatively static, depending on the scenario. This is largely because significantly more annual variety crops are grown in the southwest portion of the basin, and they are projected to have fairly static or reduced growing-season lengths due to increased temperatures. Therefore the dates of planting, crop coefficient development, and harvest may be advanced. Perennial forage crops are primarily grown in the northeast, and are projected to have earlier greenup, longer harvest periods (i.e., more cuttings), and later killing frosts, leading to longer growing seasons and large percent increases relative to baseline ET_c. Figure 51 shows the spatial distribution of projected ET_c percent change for different climate scenarios and time periods assuming static crop phenology for annual crops. Baseline temperatures were used for simulating projected planting, crop coefficient development, and termination for all future time periods and scenarios as described in section 4.2.1. All HUCs show positive ET_c increases or no change, with the exception of the westernmost HUC in the basin that exhibits slight decreases in ET_c under all scenarios by 2080 due to earlier harvest of grass hay.

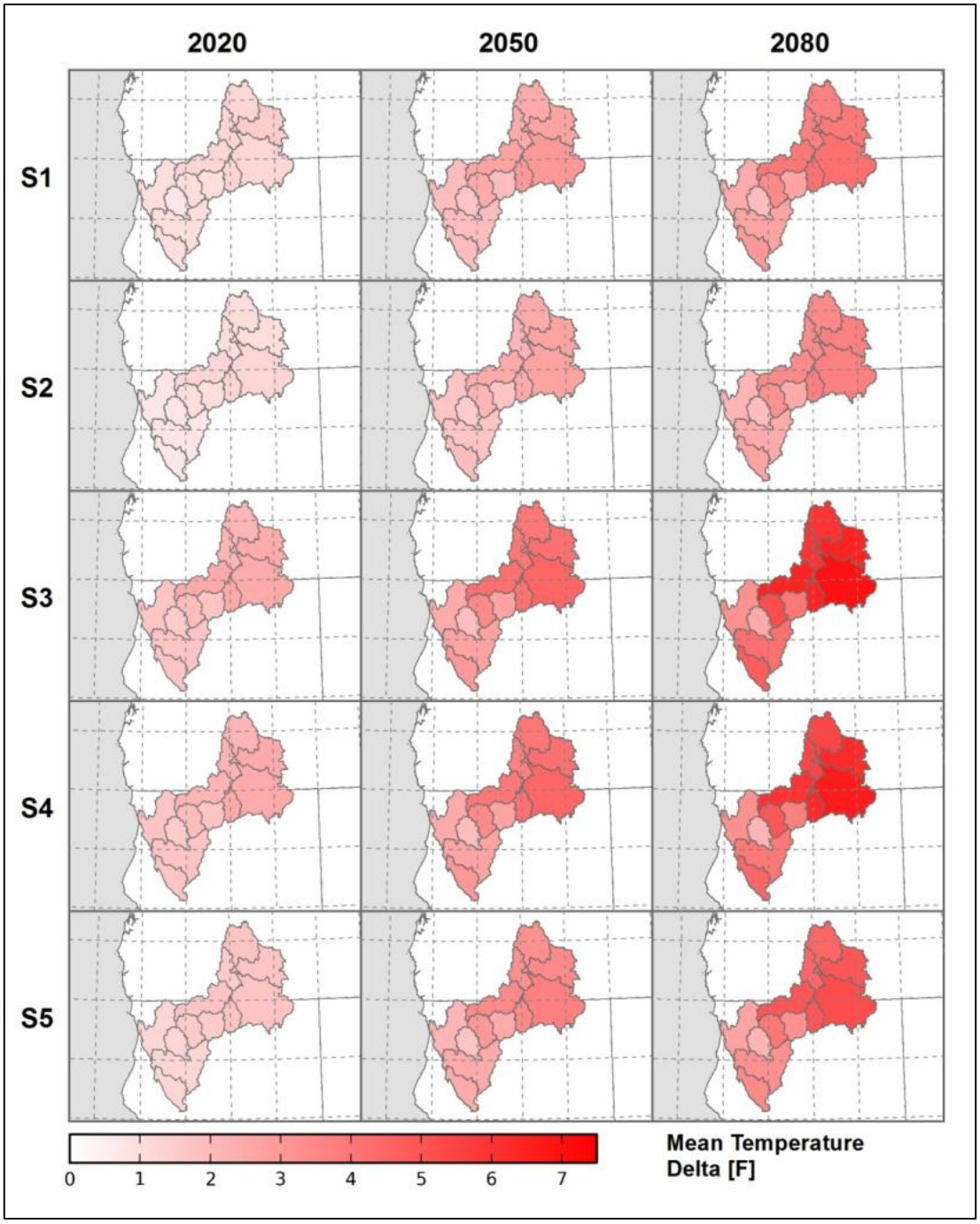

Figure 47.—Klamath River Basin – Spatial distribution of temperature change for different climate scenarios and time periods (S1 = WD, S2 = WW, S3 = HD, S4 = HW, S5 = Central).

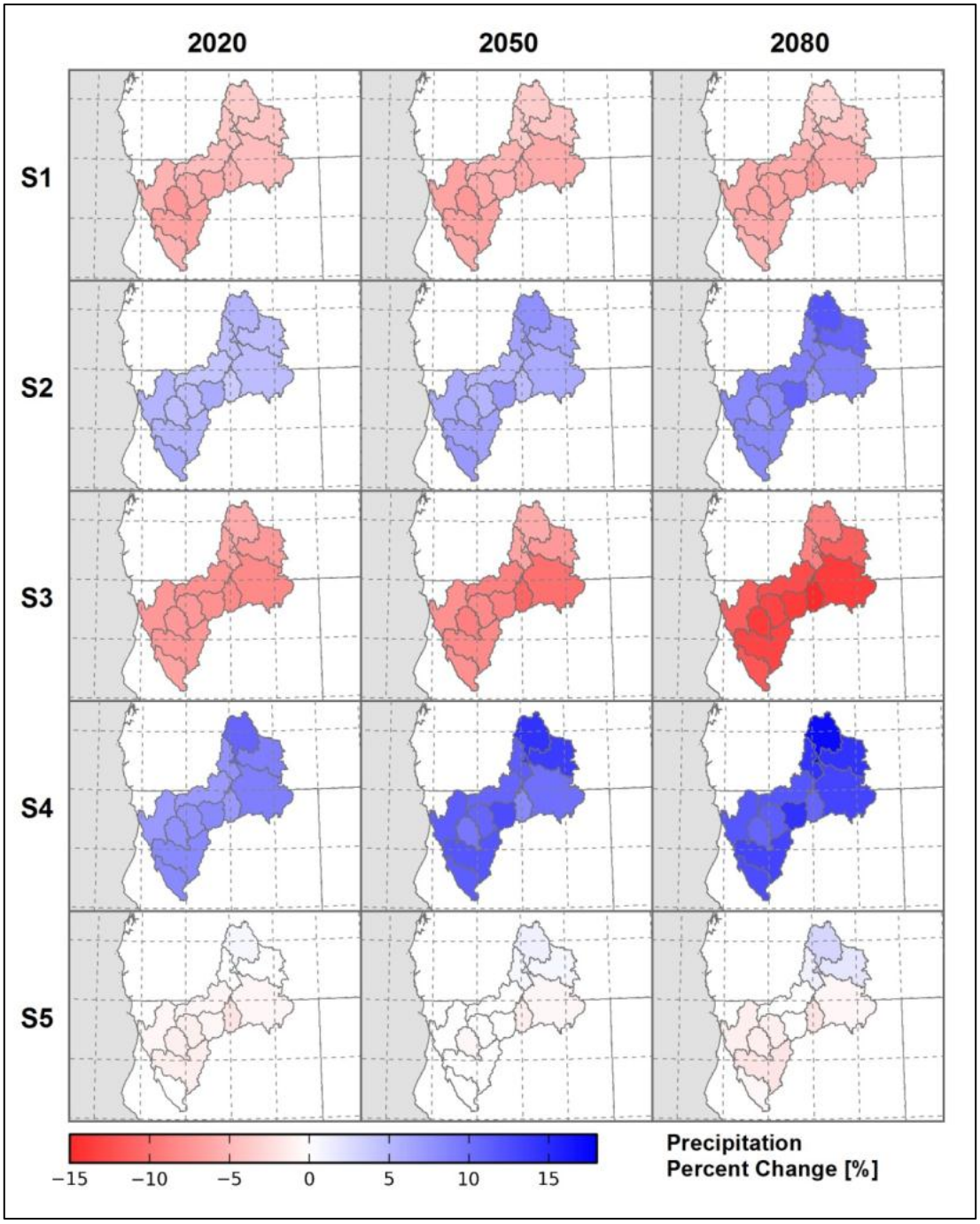

Figure 48.—Klamath River Basin – Spatial distribution of projected precipitation percent change for different climate scenarios and time periods (S1 = WD, S2 = WW, S3 = HD, S4 = HW, S5 = Central).

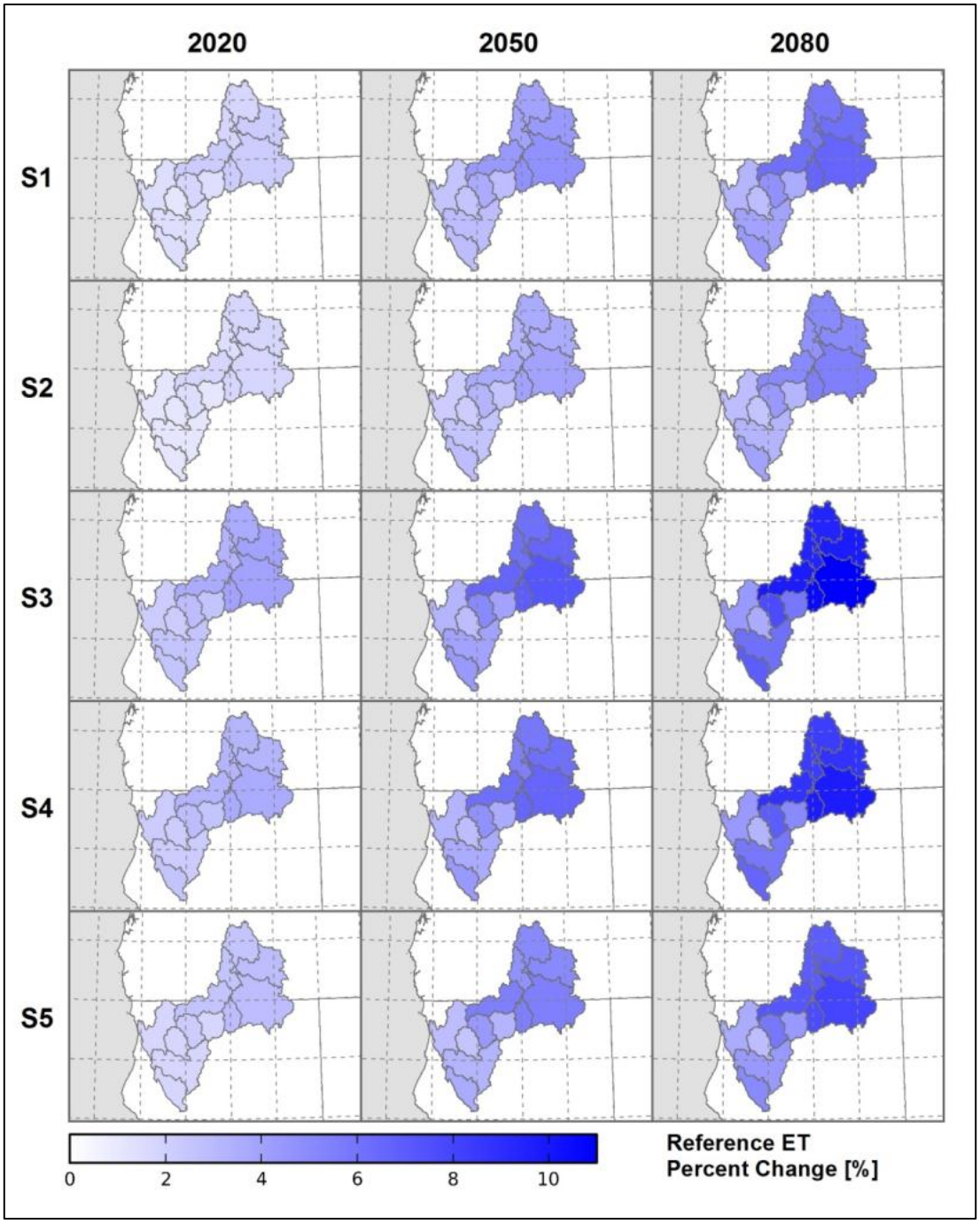

Figure 49.—Klamath River Basin – Spatial distribution of projected reference evapotranspiration percent change for different climate scenarios and time periods (S1 = WD, S2 = WW, S3 = HD, S4 = HW, S5 = Central).

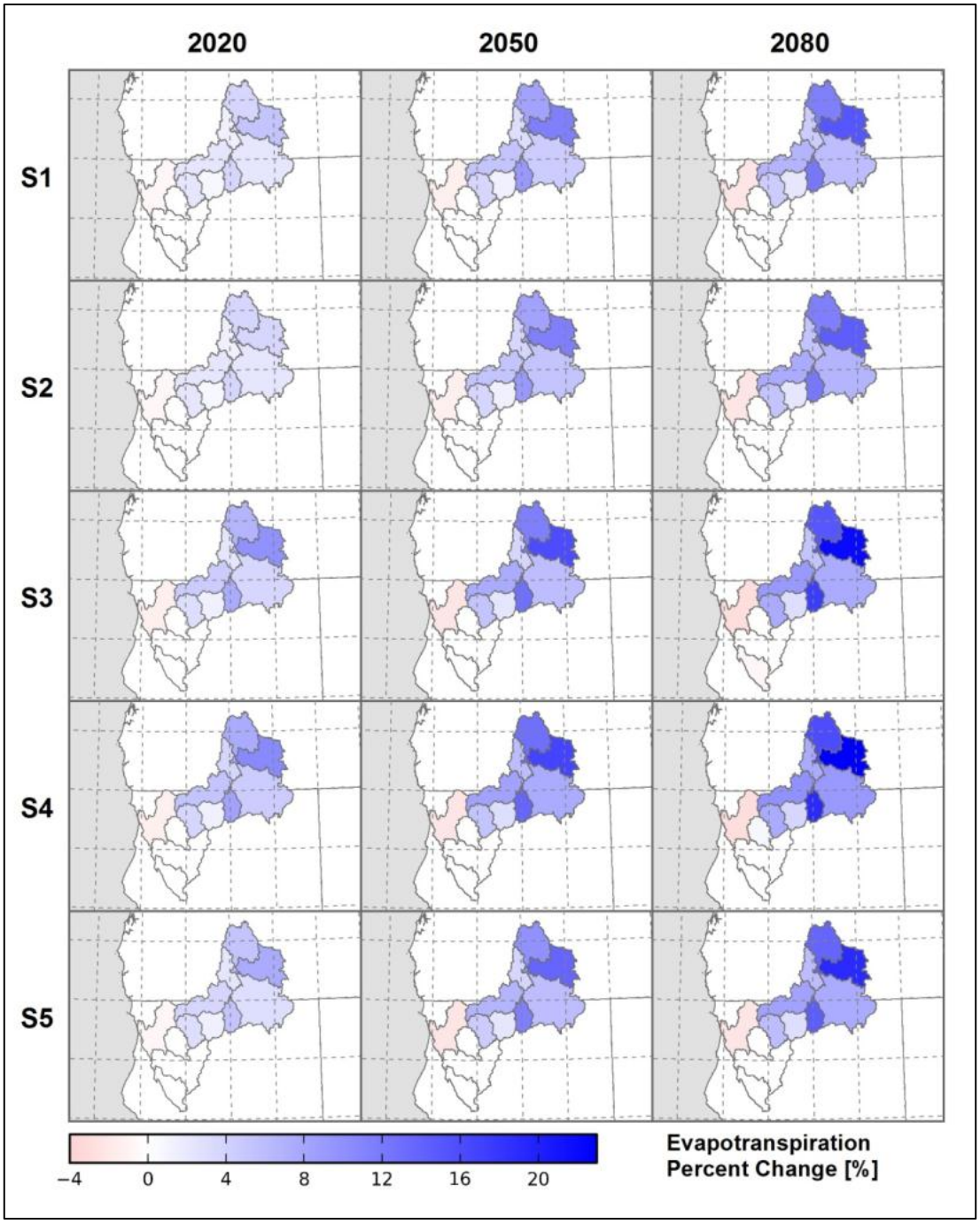

Figure 50.—Klamath River Basin – Spatial distribution of projected crop evapotranspiration percent change for different climate scenarios and time periods (S1 = WD, S2 = WW, S3 = HD, S4 = HW, S5 = Central).

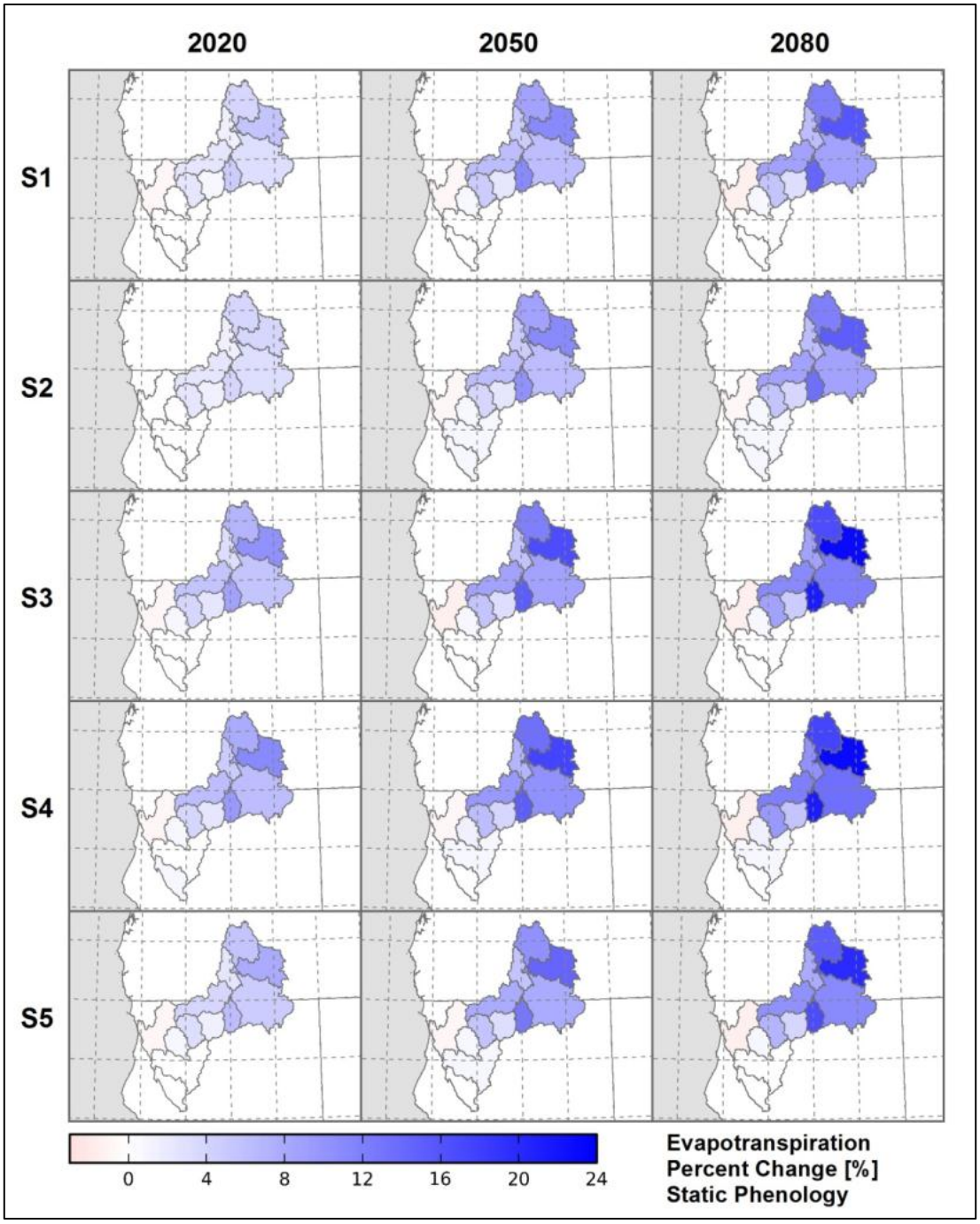

Figure 51.—Klamath River Basin – Spatial distribution of projected crop evapotranspiration percent change for different climate scenarios and time periods assuming static phenology for annual crops (S1 = WD, S2 = WW, S3 = HD, S4 = HW, S5 = Central).

The spatial distribution of projected NIWR percent change for different climate scenarios and time periods is shown on figures 52 and 53. The NIWR incorporates growing-season and non-growing-season soil moisture gains and losses from precipitation, bare soil evaporation, and ET. Therefore, spatial variations in the distribution of NIWR percent change for different time periods and scenarios are a function of respective ET_c (figures 50 and 51) and precipitation (figure 48) distributions. For example, under the S3 (hotter drier) scenario, precipitation is projected to decrease whereas, under S4 (hotter wetter), it is projected to increase. This results in S4 NIWR increasing less than S3 NIWR, even though S3 and S4 ET_c changes are nearly identical. For more illustrations on unit changes (degrees F and inches) in spatial projections of mean temperature, precipitation, ET_0, ET_c, and NIWR for different time periods and scenarios, see appendix 9.

Figures 54, 55, and 56 illustrate the baseline and projected temporal distribution of mean daily ET_c for selected Met Nodes, crops, scenarios, and time periods. The simulated mean daily ET_c of alfalfa for the 2020 time period, Met Node OR4511 (NWS/COOP Klamath Falls Ag. Station), shows slight but noticeable shifts in the growing-season length and alfalfa cutting cycles relative to baseline conditions (figure 54, left). By the 2080 time period (figure 54, right) significant shifts in growing-season length, crop development, and cutting cycles are noticeable relative to baseline conditions, with scenarios S3 and S4 exhibiting the most extreme changes. Figure 55 shows simulated mean daily ET_c of spring grain at Met Node OR4511, under different scenarios, for the 2020 and 2080 time periods. Because planting dates for annual crops are temperature dependent in the non-static phenology simulations, shifts in planting, development, and harvest dates of spring grain are clearly evident, especially by the 2080 time period. The uncertainty in such potential shifts in planting dates, accelerated crop development, and harvest was a primary reason for using baseline temperatures for static phenology simulations (figures 51 and 53). In static phenology simulations, because baseline temperatures are used for estimating planting, crop development, and harvest dates, all scenarios and time periods have identical seasonal K_{cb} and ET_c shapes, and show differences only in daily ET_c magnitudes due to daily ET_0 and precipitation differences. Figure 56 illustrates simulated mean daily ET_c of pasture grass at Met Node OR4511 for different scenarios and time periods. Similar changes in greenup timing and increases in growing-season length and ET_c are projected when compared to alfalfa, with S3 and S4 having the most extreme seasonal changes.

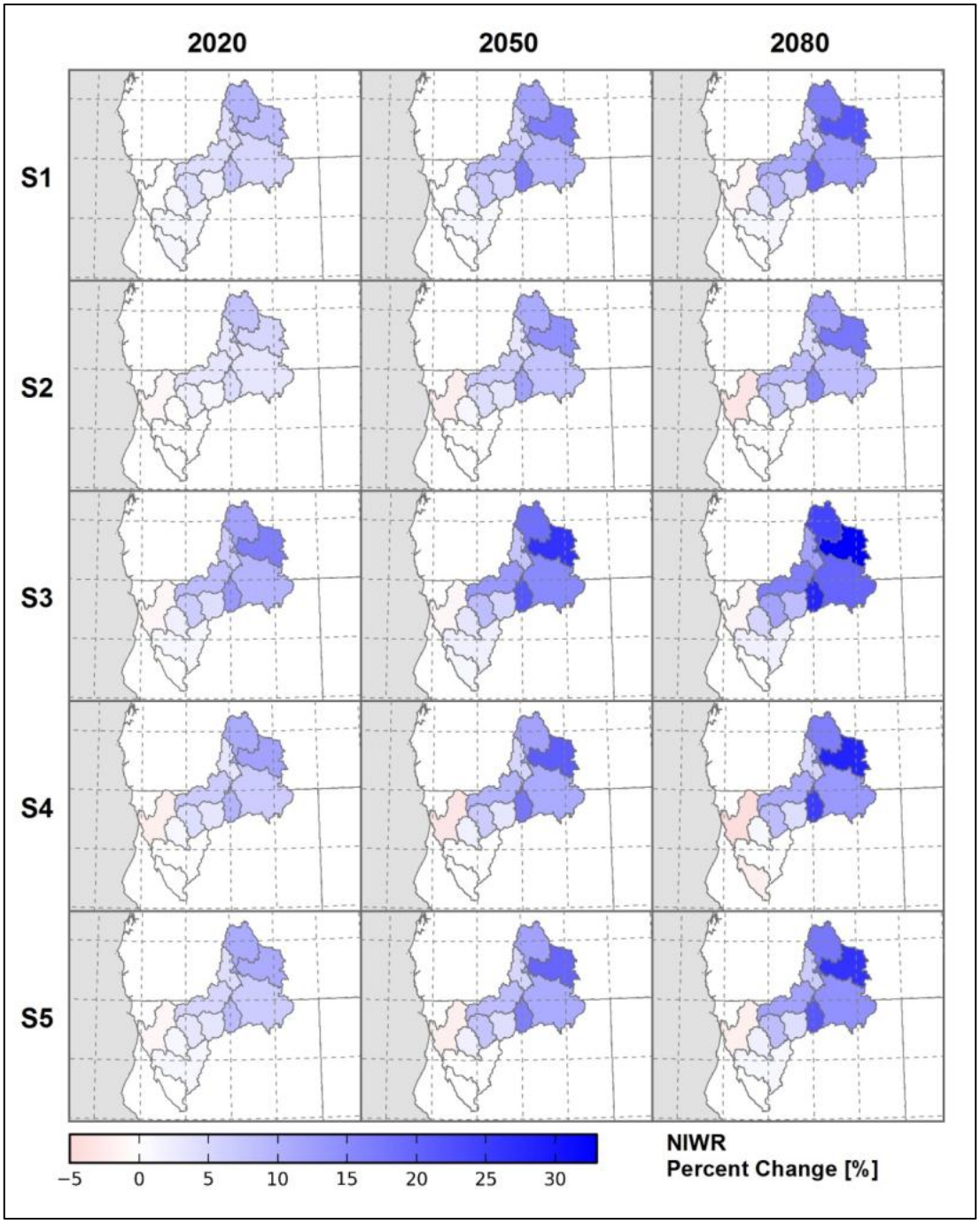

Figure 52.—Klamath River Basin – Spatial distribution of projected net irrigation water requirements (NIWR) percent change for different climate scenarios and time periods (S1 = WD, S2 = WW, S3 = HD, S4 = HW, S5 = Central).

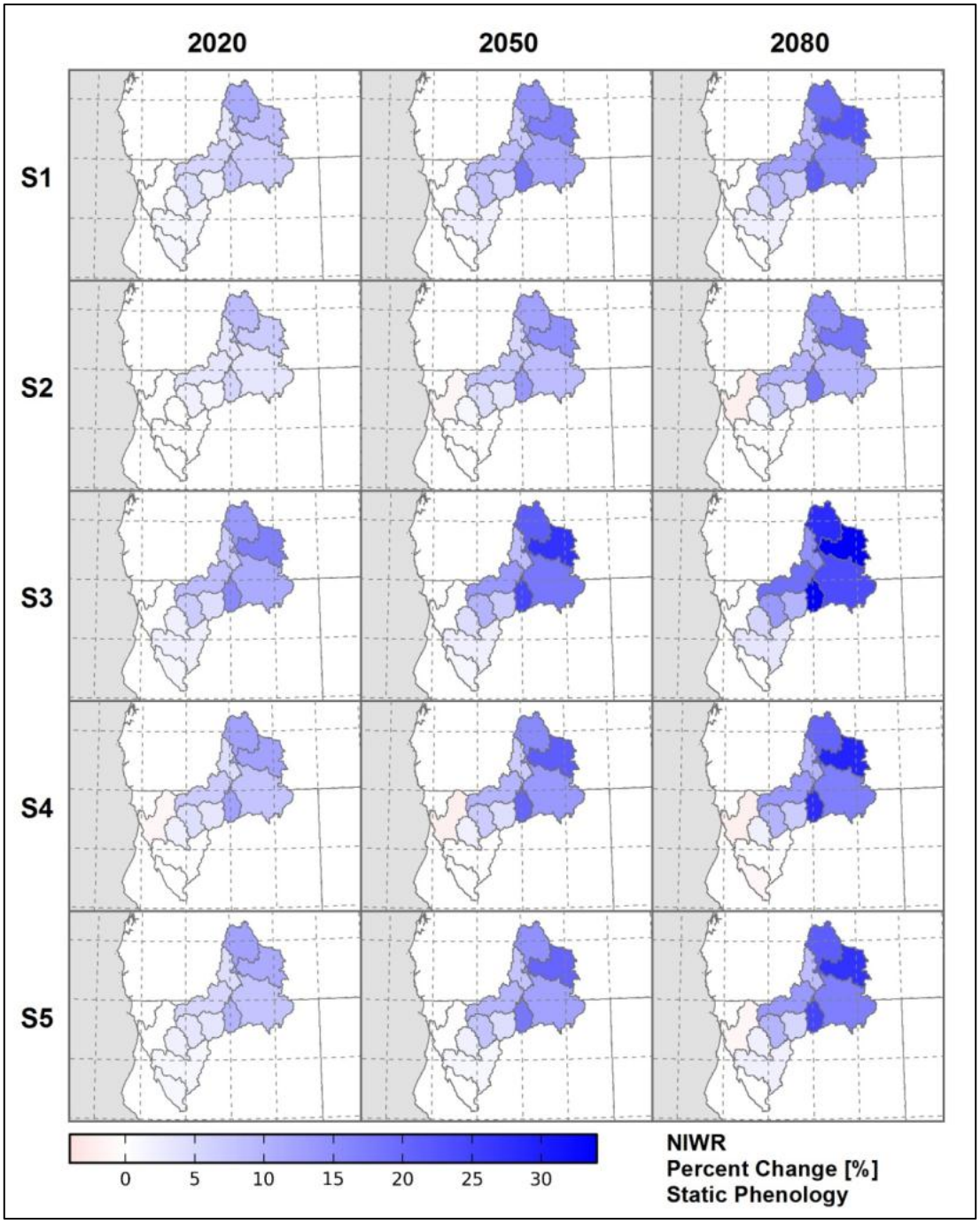

Figure 53.—Klamath River Basin – Spatial distribution of projected net irrigation water requirements (NIWR) percent change for different climate scenarios and time periods assuming static phenology for annual crops (S1 = WD, S2 = WW, S3 = HD, S4 = HW, S5 = Central).

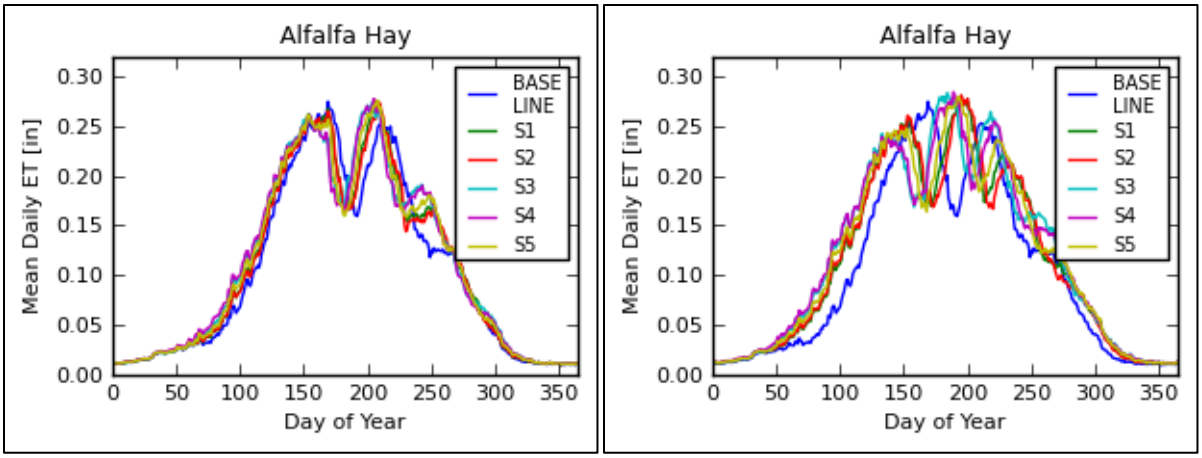

Figure 54.—Klamath River Basin – COOP Station OR4511 (NWS/COOP Klamath Falls Ag. Station). Baseline and projected mean daily alfalfa evapotranspiration for all scenarios and for time periods 2020 (left) and 2080 (right).

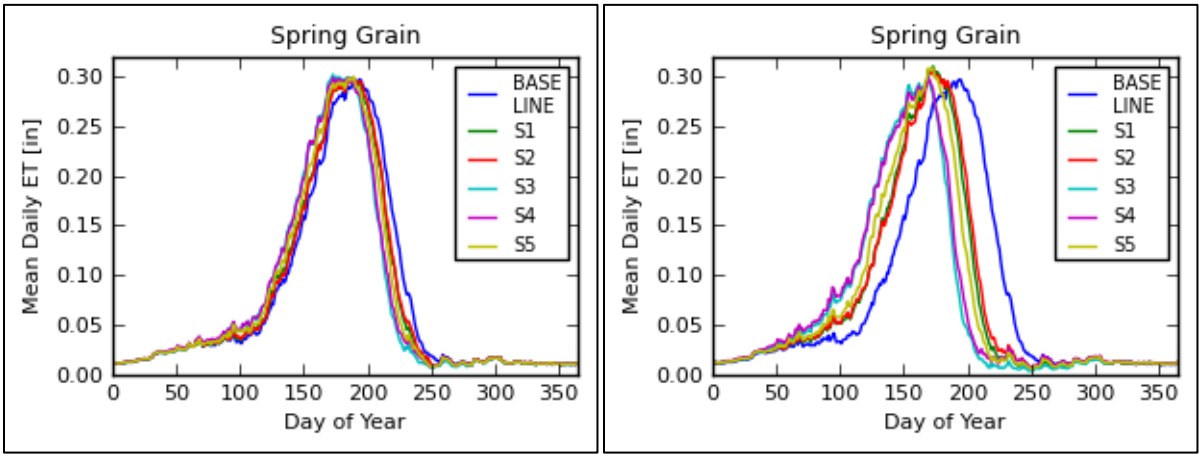

Figure 55.—Klamath River Basin – COOP Station OR4511 (NWS/COOP Klamath Falls Ag. Station). Baseline and projected mean daily spring grain evapotranspiration for all scenarios and for time periods 2020 (left) and 2080 (right).

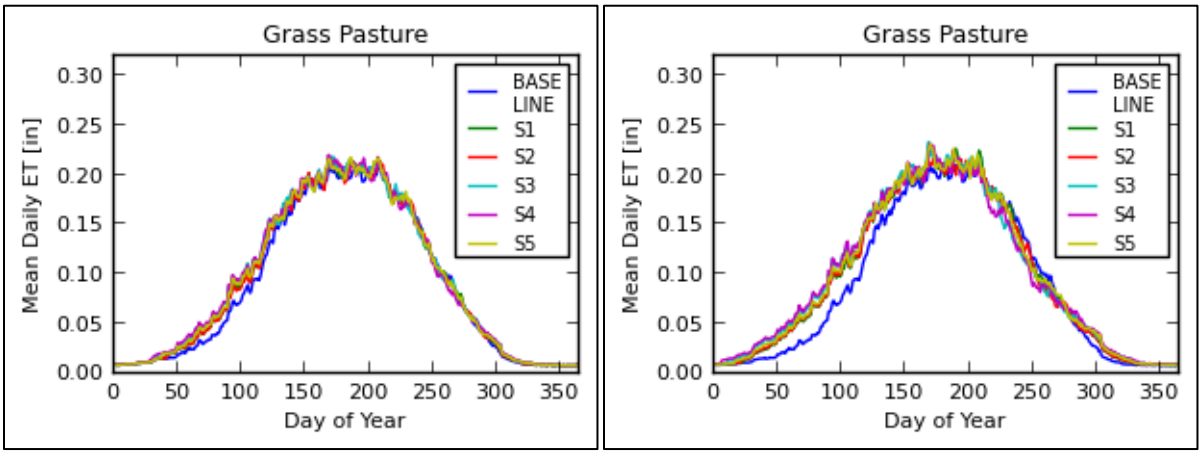

Figure 56.—Klamath River Basin – COOP Station OR4511 (NWS/COOP Klamath Falls Ag. Station). Baseline and projected mean daily grass pasture evapotranspiration for all scenarios and for time periods 2020 (left) and 2080 (right).

5.4.2 Baseline and Projected Reservoir Evaporation

Figure 57 illustrates baseline and projected Upper Klamath Lake annual precipitation (top left), annual mean temperature (top right), annual evaporation (bottom left), and annual net evaporation (bottom right). The heavy black line for each variable is the annual time series of 50 percentile values (i.e., ensemble-median). The shaded area for each variable is the annual time series of 5th to 95th percentiles or the 90-percent variability. Annual precipitation over Upper Klamath Lake is seen to have a very nominal decline over the transient period going out to 2099. The variability for annual precipitation is fairly large (~40% of the ensemble median) and shows no trend over time, implying that there is no increase or decrease in the confidence from the present. The mean annual temperature and annual evaporation both show increasing trends and a diverging variability over time. The ensemble-median and variability for net evaporation (i.e., evaporation minus precipitation) are affected by characteristics of both precipitation and temperature projections. It is evident, for instance, that the upper envelope bounds in precipitation cause the lower bound of net evaporation to be highly variable, while the diverging variability is caused primarily by the diverging temperature projections.

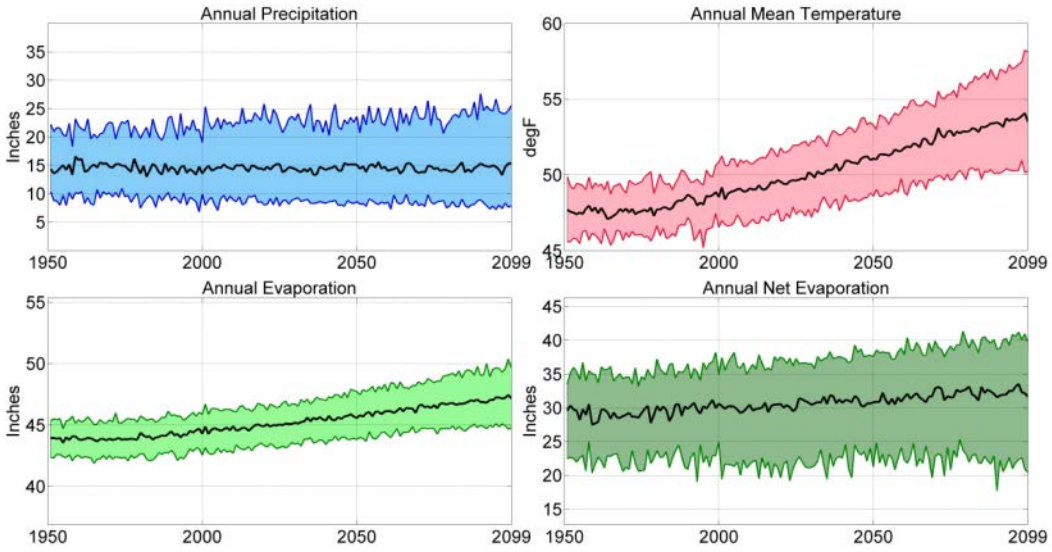

Figure 57.—Klamath River Basin – Upper Klamath Lake ensemble median and 5th and 95th percentile annual precipitation, temperature, reservoir evaporation, and net evaporation.

Figure 58 shows evaporation and net evaporation at Upper Klamath Lake. The solid lines represent the ensemble-median mean monthly evaporation and net evaporation for the baseline period (1950–1999) and for the 2020s, 2050s, and 2080s, and the shaded areas show the decadal spread of mean monthly evaporation and net evaporation for the baseline period (gray shading) and 2080s (magenta shading), where the spread is bound by the ensemble's 5th to 95th percentile values for each month. The simulated impact of heat storage is

negligible due to the shallow depth of Upper Klamath Lake. The magnitude of projected monthly evaporation and net evaporation increase is greatest during July and least during the fall and winter months. The magnitude of annual evaporation and net evaporation increase from the baseline to the 2080 time period for Upper Klamath Lake is 6.3 and 8.2 percent (2.8 and 2.4 in), respectively (appendix 10).

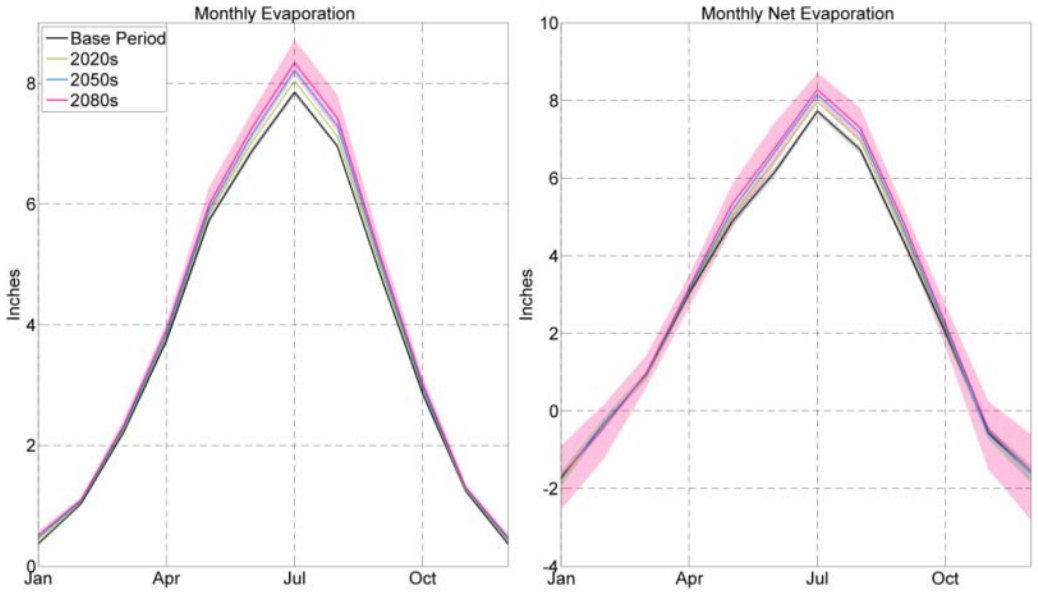

Figure 58.—Klamath River Basin – Upper Klamath Lake mean monthly ensemble median and 5th and 95th percentile reservoir evaporation and net evaporation.

5.5 Missouri River Basin

5.5.1 Baseline and Projected Irrigation Water Demands

Figure 59 illustrates COOP station based Met Nodes that were used to estimate irrigation water demands, as well as HUC8 boundaries used to upscale Met Node estimates in the Missouri River Basin. Figure 60 illustrates the spatial distribution of baseline (1950–1999) mean annual temperature (top left) and mean annual precipitation (top right) derived from BCSD data (discussed in section 3.2), mean annual dewpoint depression (bottom left), and mean annual windspeed (bottom right) estimated from historical agricultural weather data (discussed in section 4.2.1). Gray-hatched HUC8 polygons illustrated on figure 60 (and other results figures) represent areas where no significant crop acreage was present, so baseline and projected climate and irrigation water demands were not simulated for those areas. Figure 60 illustrates mean annual temperatures ranging from warm in the south to cool in the north and in the mountainous areas in the western portions of the basin. Precipitation is shown to vary in general from moderately high in the southeast to low amounts in the northwest. The mean annual dewpoint depression

(i.e., $T_{min} - T_{dew}$) is used here as a simple approximation of the humidity of the lower air mass that is consistent and representative of agricultural areas while preserving regional and local advection effects. Its spatial distribution clearly shows that southeastern areas are more humid and northwestern areas are more arid. Mean annual windspeeds are generally lower in the northwestern and southeastern areas, and higher in the central portion of the basin. Figure 61 illustrates reference ET (ET_0) (top left), crop evapotranspiration (ET_c) (top right), net irrigation water requirement (NIWR) (bottom left), and total crop acreage (bottom right) within each HUC8 boundary. ET_0, ET_c, and NIWR are all higher in the southern portion of the basin, where air temperature and solar radiation are both higher than in the northern portions of the basin. The projected values range from 33.0 to 54.7 in/yr for ET_0, 28.3 to 45.1 in/yr for ET_c, and 5.6 to 28.6 in/yr for NIWR.

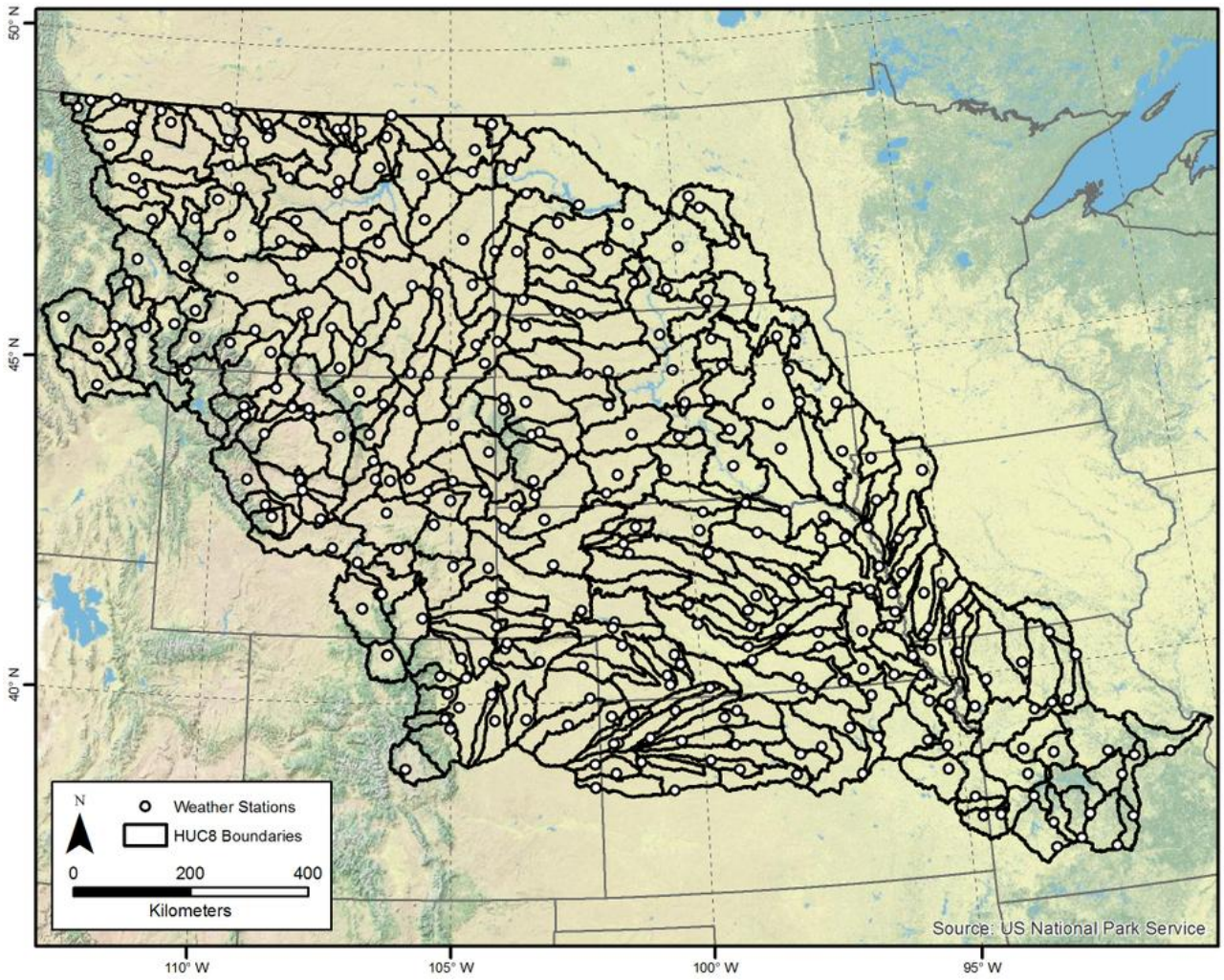

Figure 59.—Missouri River Basin – COOP stations used to simulate baseline and projected irrigation demands.

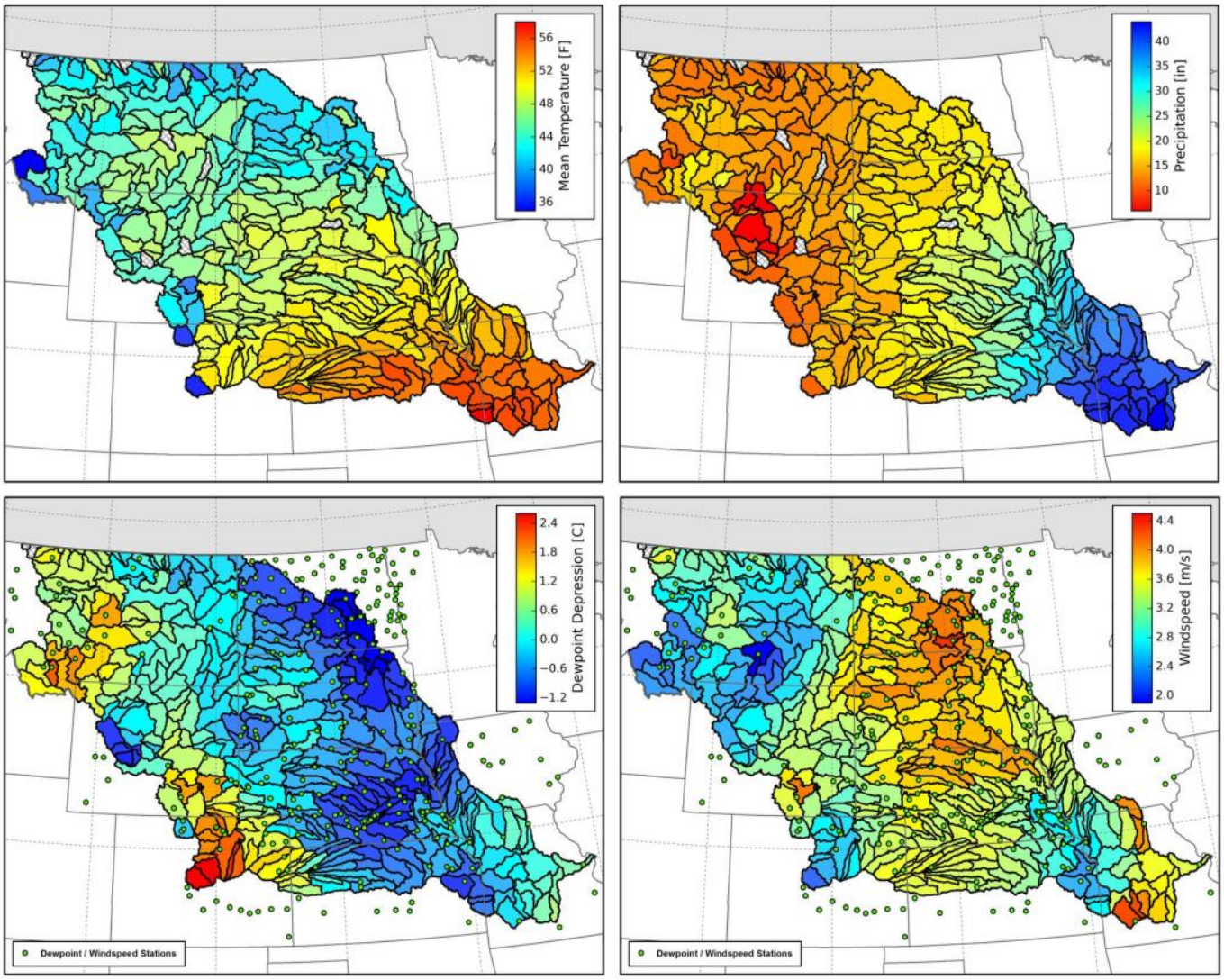

Figure 60.—Missouri River Basin – Spatial distribution of baseline temperature, precipitation, dewpoint depression, and windspeed.

Figure 62 shows the spatial distribution of projected mean temperature change for different climate scenarios and time periods, and it is evident that the changes shown there are generally spatially uniform for all scenarios, with scenario S3 (hot-dry) having the largest change. Figure 63 illustrates the spatial distribution of projected precipitation percent change for different scenarios and time periods. Depending on the scenario, precipitation percent changes range from –6.0 to 9.1 percent for the 2080 time period, with the ensemble median scenario (S5) showing a general increase throughout the basin, with the greatest increase in the east and northeast portions.

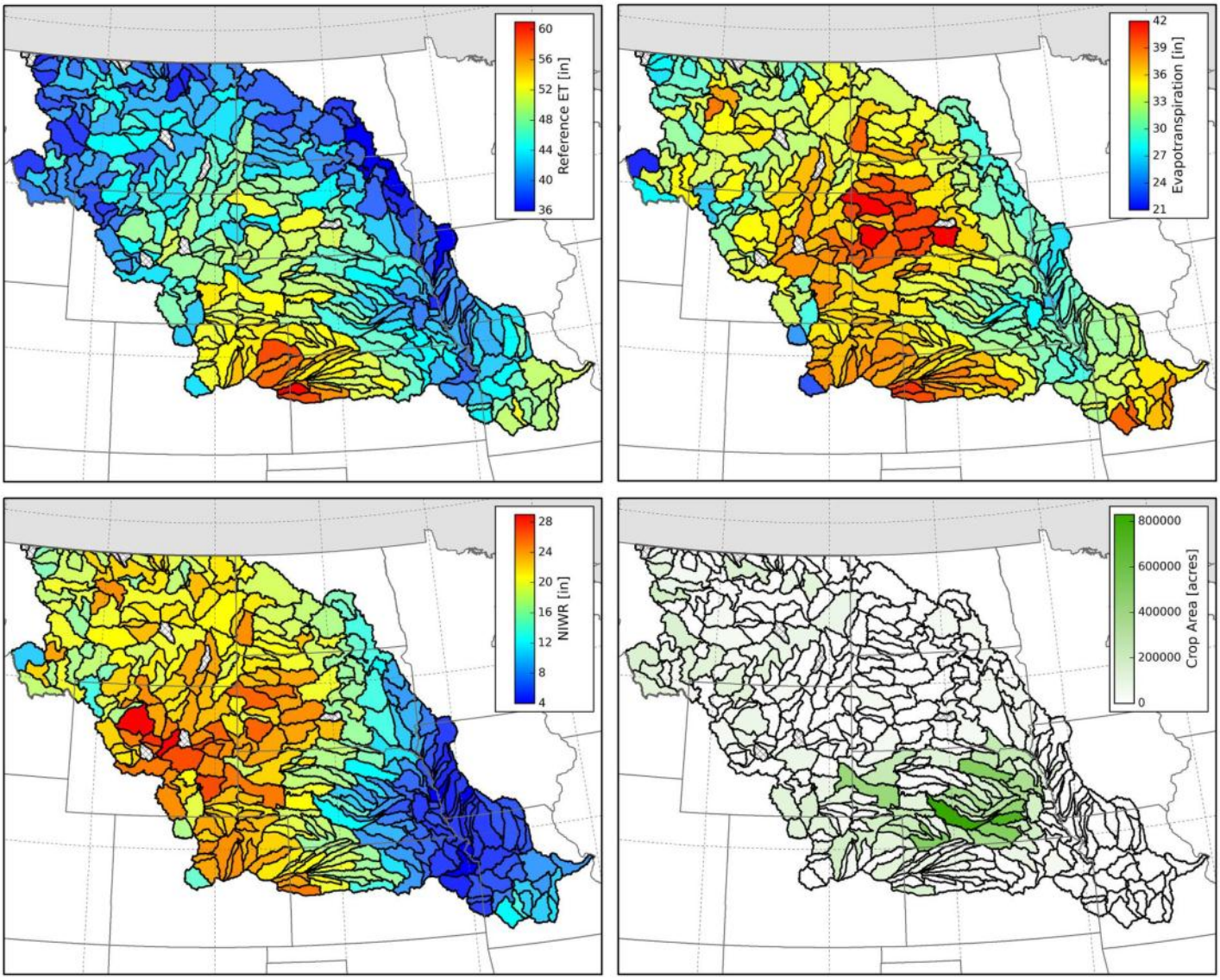

Figure 61.—Missouri River Basin – Spatial distribution of baseline reference evapotranspiration, crop evapotranspiration, net irrigation water requirements (NIWR), and crop acreage. Gray hatch areas represent HUCs with no crop acreage.

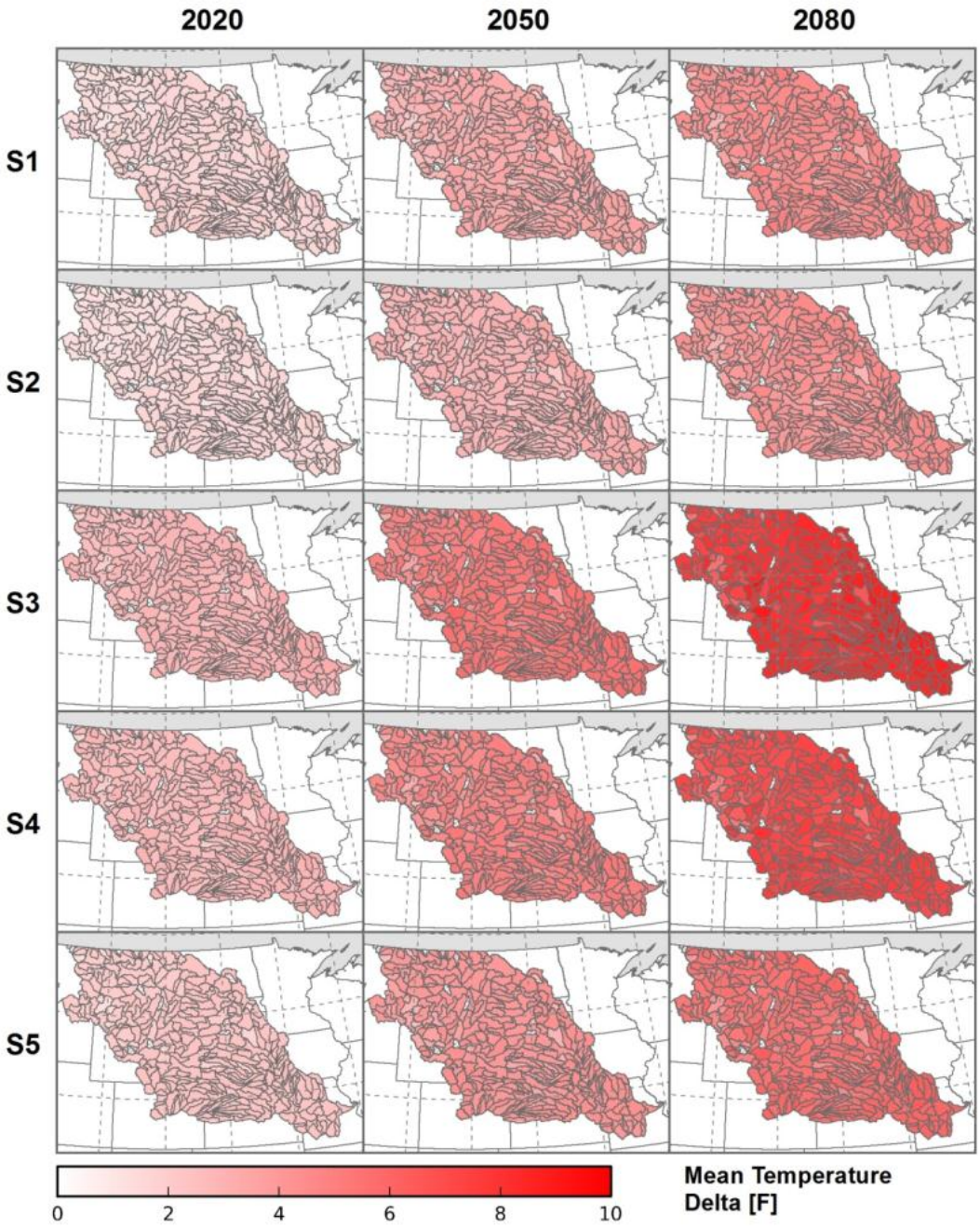

Figure 62.—Missouri River Basin – Spatial distribution of temperature change for different climate scenarios and time periods (S1 = WD, S2 = WW, S3 = HD, S4 = HW, S5 = Central).

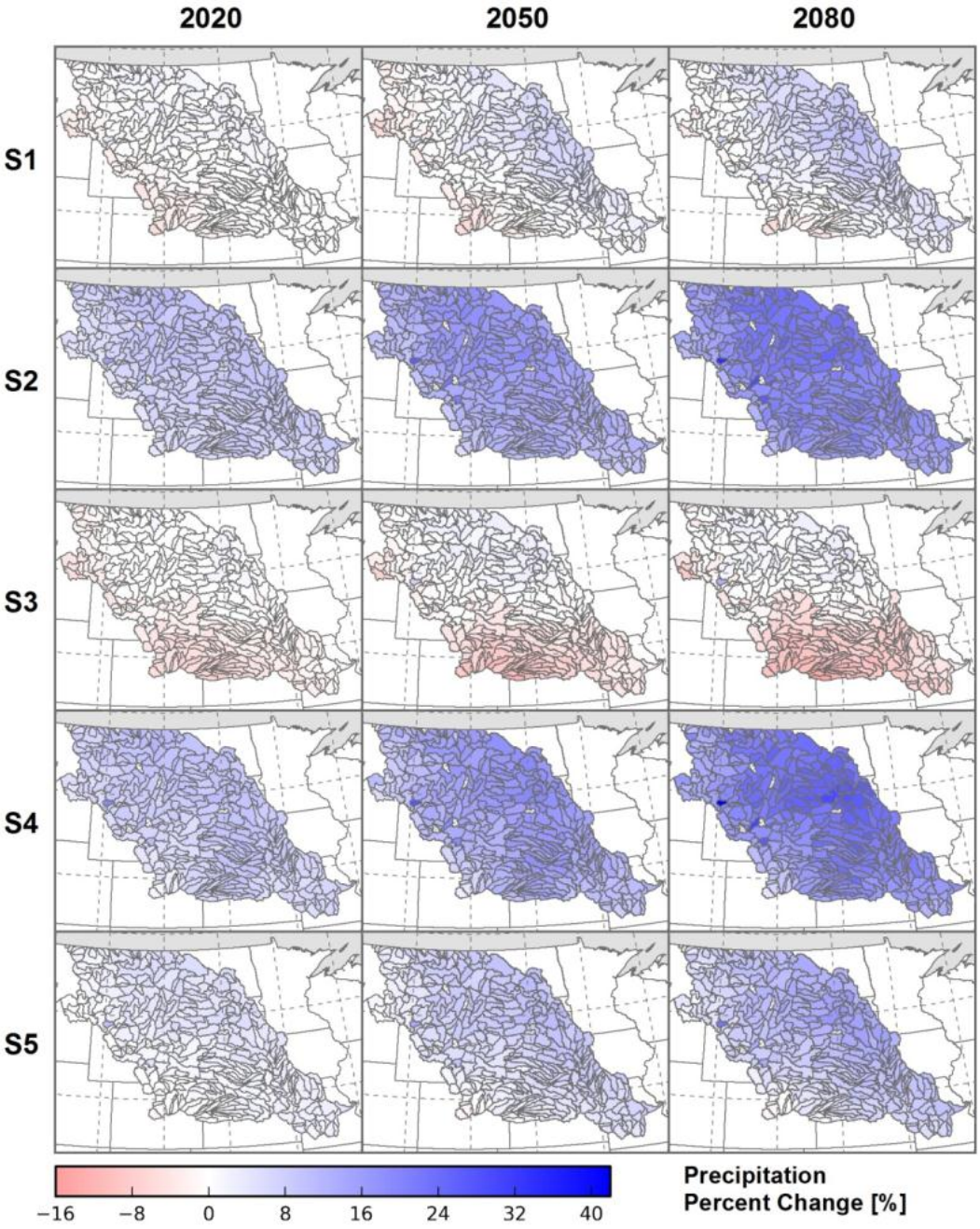

Figure 63.—Missouri River Basin – Spatial distribution of projected precipitation percent change for different climate scenarios and time periods (S1 = WD, S2 = WW, S3 = HD, S4 = HW, S5 = Central).

Figure 64 shows the spatial distribution of projected ET_0 percent change for different climate scenarios and time periods. Similar to temperature, the projected percent change in ET_0 is generally spatially uniform for all scenarios, with scenario S3 having the largest change. Figure 65 illustrates the spatial distribution of projected ET_c percent change for different climate scenarios and time periods assuming non-static crop phenology for annual crops, where projected future temperatures were used for simulating projected planting, crop coefficient development, and termination as described in section 4.2.1. Spatial differences in the distribution of projected percent change in ET_c are largely due to differences in crop type and baseline ET_c. The portions of the basin that are projected to experience the largest percent change are in the west-northwest, where perennial crops are predominant. ET_c in the southeastern portion of the basin is projected to change less or remain unchanged, depending on the scenario. This is largely because significantly more annual variety crops are grown in the southeast, and these crops are projected to have fairly static or reduced growing-season lengths due to increased temperatures. Therefore, they may have advanced dates for planting, crop coefficient development, and harvest. Perennial forage crops are primarily grown in the northwest and are projected to have earlier greenup, longer harvest periods (i.e., more cuttings), and later killing frosts, leading to longer growing seasons and large percent increases relative to baseline ET_c. Figure 66 shows the spatial distribution of projected ET_c percent change for different climate scenarios and time periods assuming static crop phenology for annual crops. Baseline temperatures were used for simulating projected planting, crop coefficient development, and termination for all future time periods and scenarios as described in section 4.2.1. Under static phenology conditions, ET_c increases are slightly greater than under non-static phenology conditions due to the assumption of baseline planting and harvest dates for future periods.

The spatial distribution of projected NIWR percent change for different climate scenarios and time periods is shown on figures 67 and 68. The NIWR incorporates growing-season and non-growing-season soil moisture gains and losses from precipitation, bare soil evaporation, and ET. Therefore, spatial variations in the distribution of NIWR percent change for different time periods and scenarios are a function of respective ET_c (figures 65 and 66) and precipitation (figure 64) distributions. For example, in the southern portion of the basin, S3 (hotter drier) precipitation is projected to decrease whereas S4 (hotter wetter) precipitation is projected to increase. This results in S4 NIWR increasing less than S3 NIWR, even though S3 and S4 ET_c changes are nearly identical. For more illustrations on unit changes (degrees F and inches) in spatial projections of mean temperature, precipitation, ET_0, ET_c, and NIWR for different time periods and scenarios, see appendix 9.

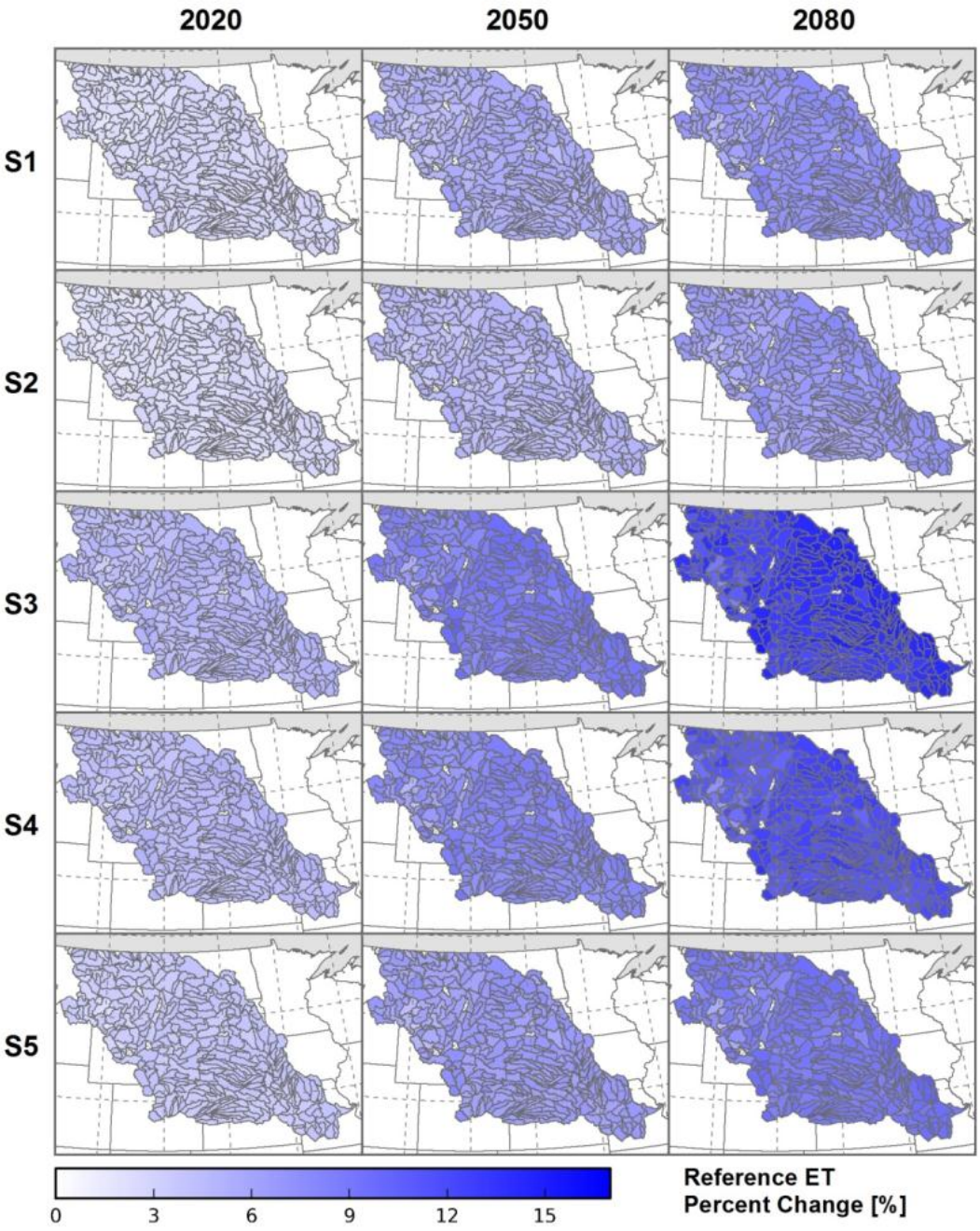

Figure 64.—Missouri River Basin – Spatial distribution of projected reference evapotranspiration percent change for different climate scenarios and time periods (S1 = WD, S2 = WW, S3 = HD, S4 = HW, S5 = Central).

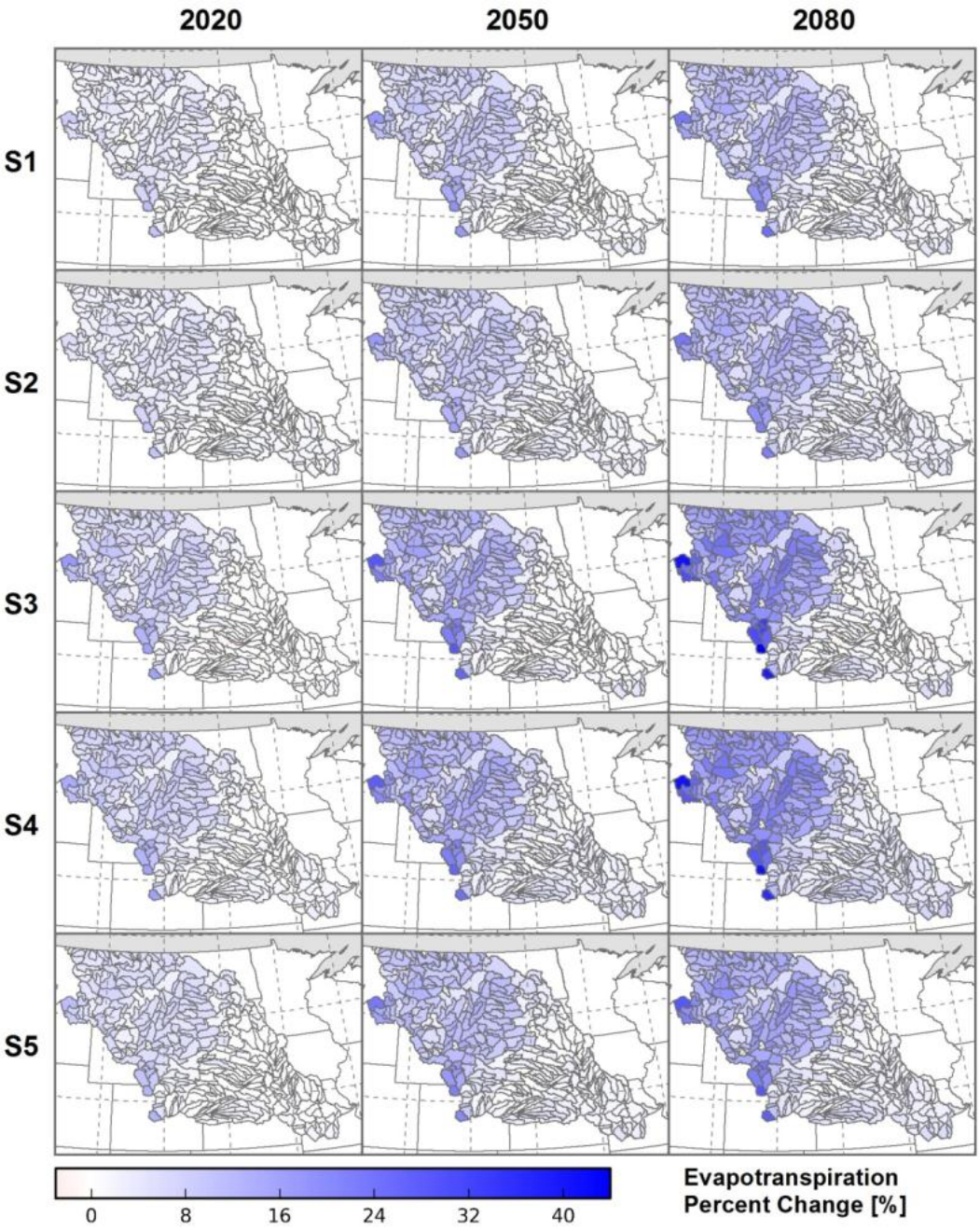

Figure 65.—Missouri River Basin – Spatial distribution of projected crop evapotranspiration percent change for different climate scenarios and time periods (S1 = WD, S2 = WW, S3 = HD, S4 = HW, S5 = Central).

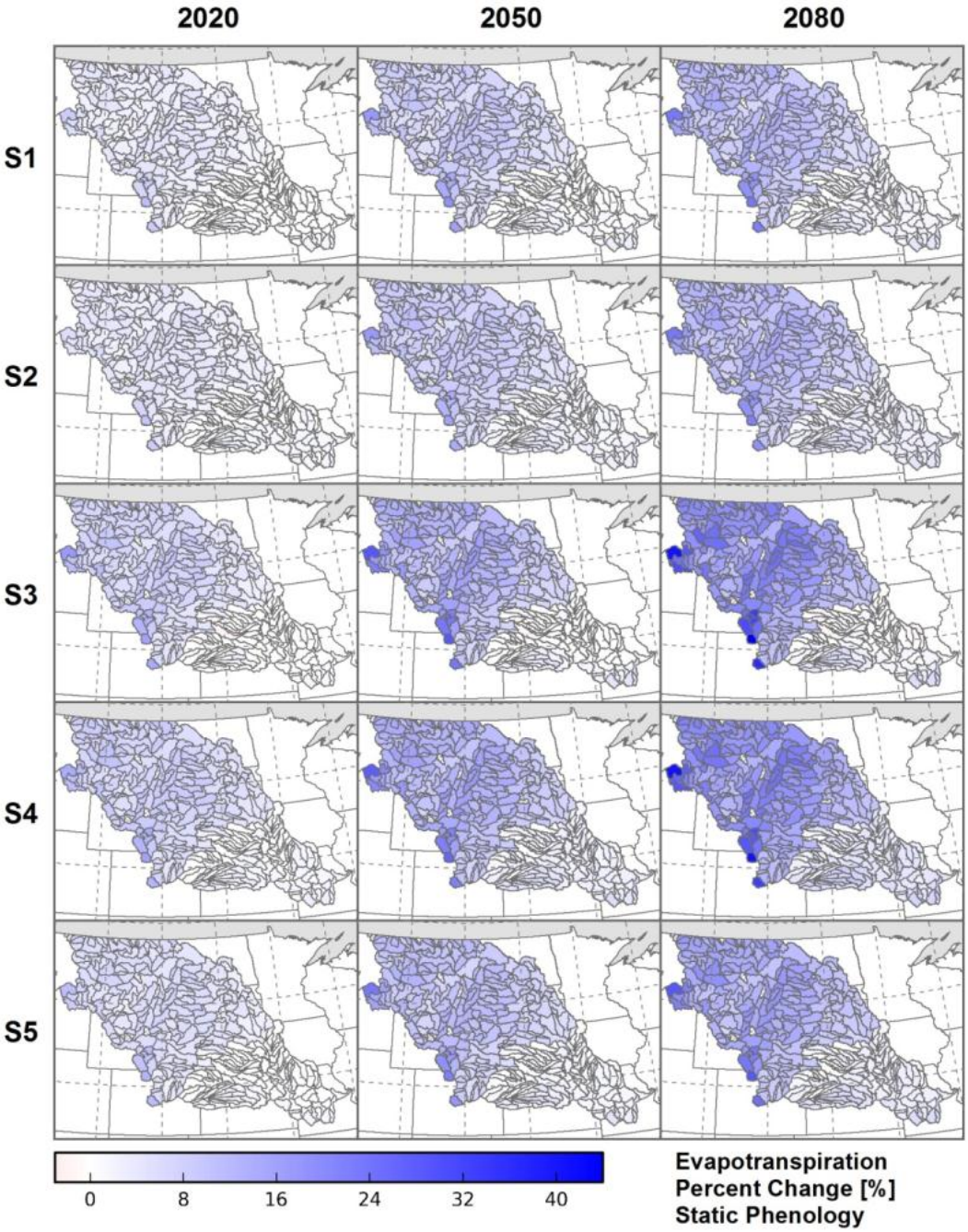

Figure 66.—Missouri River Basin – Spatial distribution of projected crop evapotranspiration percent change for different climate scenarios and time periods assuming static phenology for annual crops (S1 = WD, S2 = WW, S3 = HD, S4 = HW, S5 = Central).

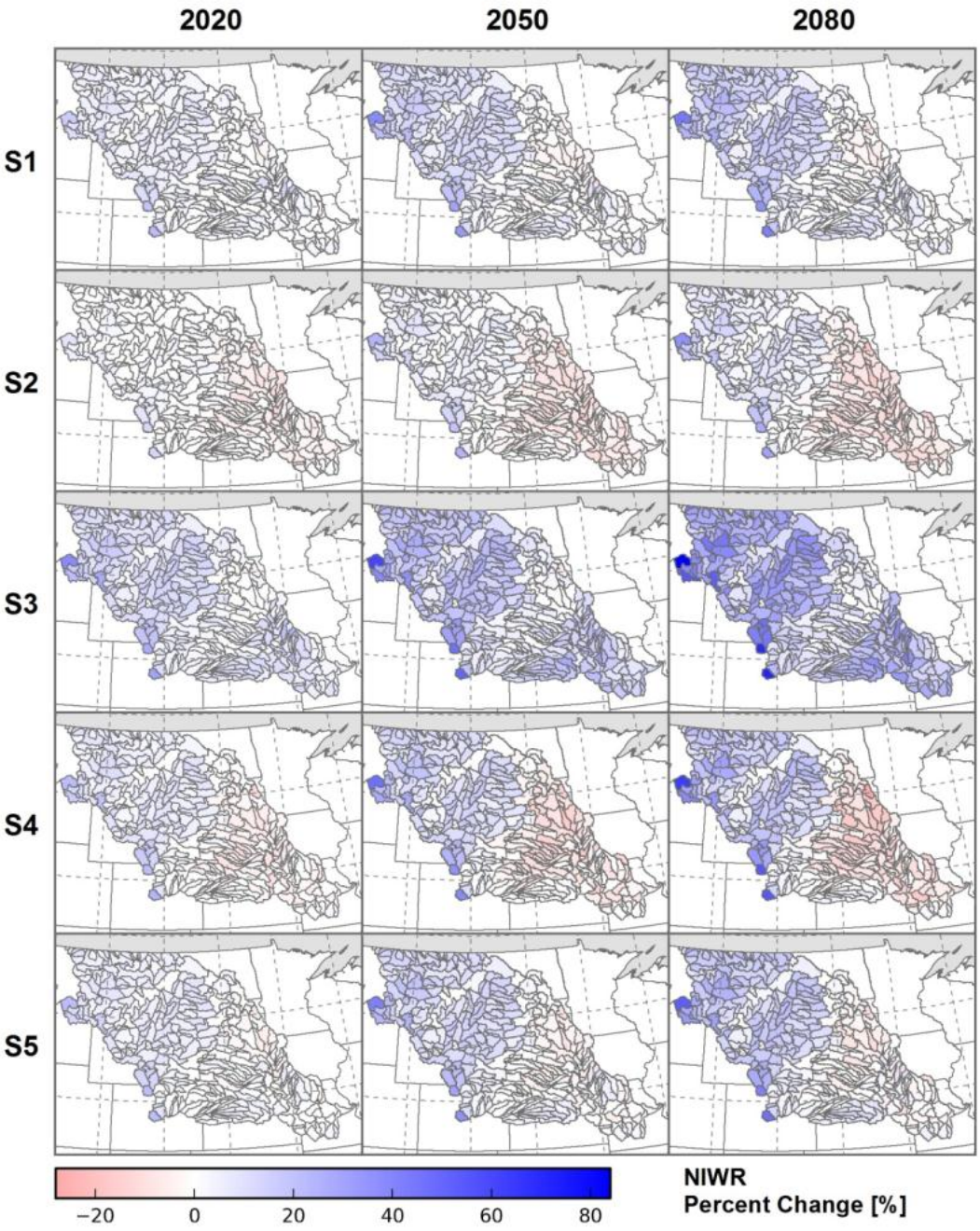

Figure 67.—Missouri River Basin – Spatial distribution of projected net irrigation water requirements (NIWR) percent change for different climate scenarios and time periods (S1 = WD, S2 = WW, S3 = HD, S4 = HW, S5 = Central).

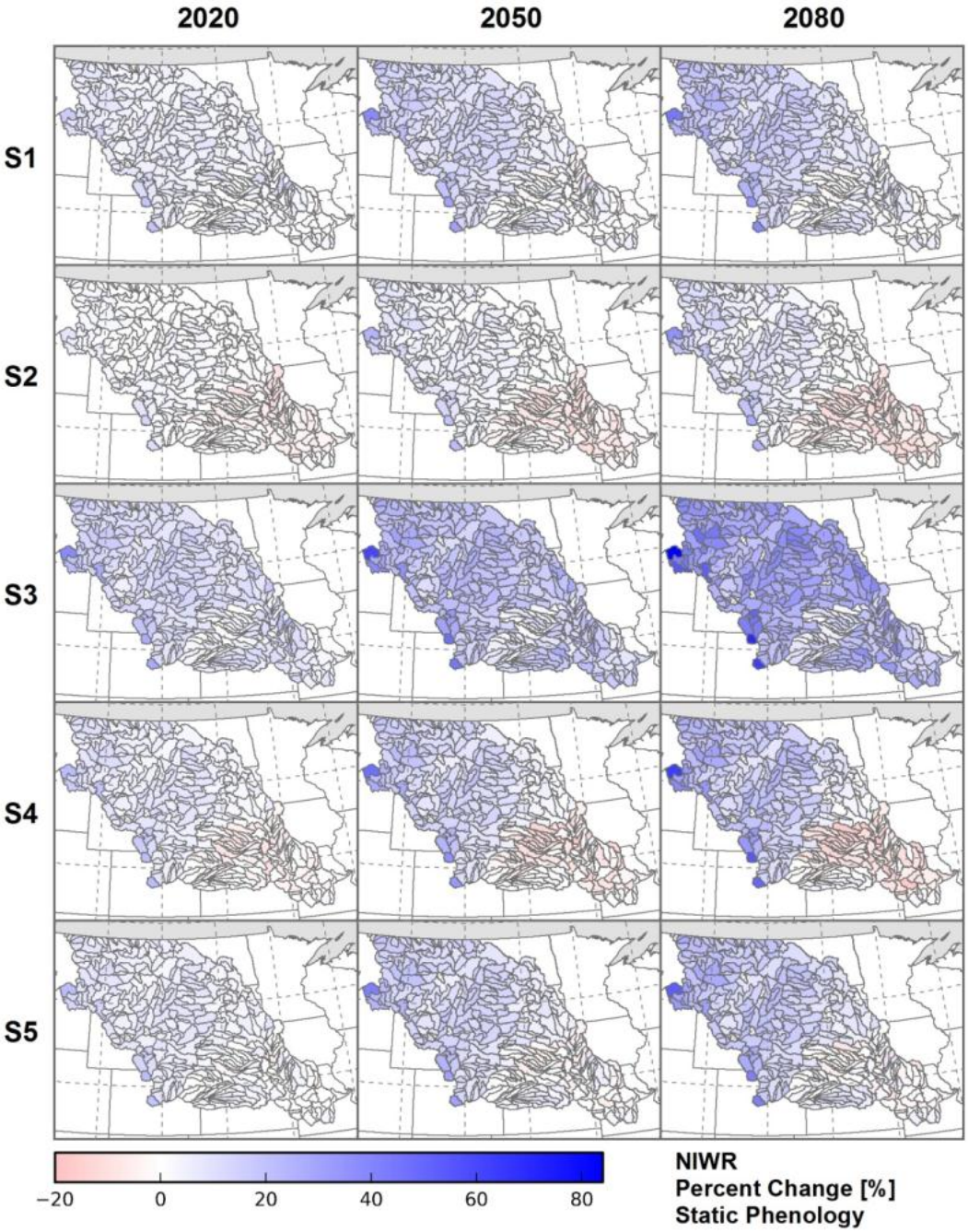

Figure 68.—Missouri River Basin – Spatial distribution of projected net irrigation water requirements (NIWR) percent change for different climate scenarios and time periods assuming static phenology for annual crops (S1 = WD, S2 = WW, S3 = HD, S4 = HW, S5 = Central).

Figures 69, 70, and 71 illustrate the baseline and projected temporal distribution of mean daily ET_c for selected Met Nodes, crops, scenarios, and time periods. The simulated mean daily ET_c of alfalfa for the 2020 time period, COOP/NWS Met Node MT 4305 (Huntley Exp. Stn., MT), shows slight but noticeable shifts in the growing-season length and alfalfa cutting cycles relative to baseline conditions (figure 69, left). By the 2080 time period (figure 69, right) significant shifts in growing-season length, crop development, and cutting cycles are noticeable relative to baseline conditions, with scenarios S3 and S4 exhibiting the most extreme changes. Figure 70 shows simulated mean daily ET_c of spring grain at NWS/COOP Met Node CO3553 (Greeley UNC, CO), under different scenarios, for the 2020 and 2080 time periods. Because planting dates for annual crops are temperature dependent in the non-static phenology simulations, shifts in planting, development, and harvest dates of spring grain are clearly evident, especially by the 2080 time period. The uncertainty in such potential shifts in planting dates, accelerated crop development, and harvest was a primary reason for using baseline temperatures for static phenology simulations (figures 66 and 68). In static phenology simulations, because baseline temperatures are used for estimating planting, crop development, and harvest dates, all scenarios and time periods have identical seasonal K_{cb} and ET_c shapes, and show differences only in daily ET_c magnitudes due to daily ET_0 and precipitation differences. Figure 71 illustrates simulated mean daily ET_c of soybeans at NWS/COOP Met Node KS4712 (Lincoln 2 ESE, KS) for different scenarios and time periods. Similar seasonal changes in planting, development, harvest dates, and ET_c are projected when compared to spring grain, with S3 and S4 having the most extreme seasonal changes.

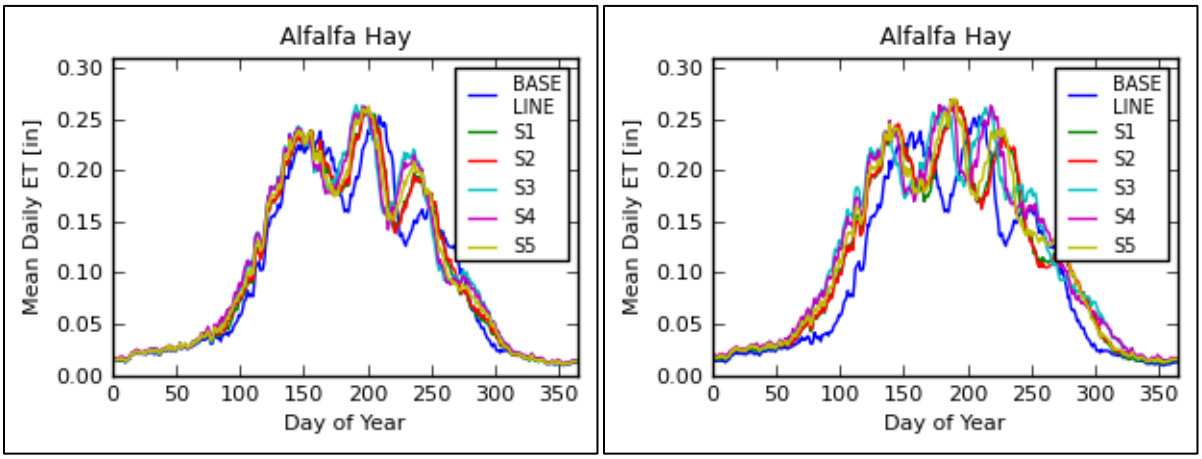

Figure 69.—Missouri River Basin – COOP station MT4305 (Huntley Exp. Stn., MT). Baseline and projected mean daily alfalfa evapotranspiration for all scenarios and for time periods 2020 (left) and 2080 (right).

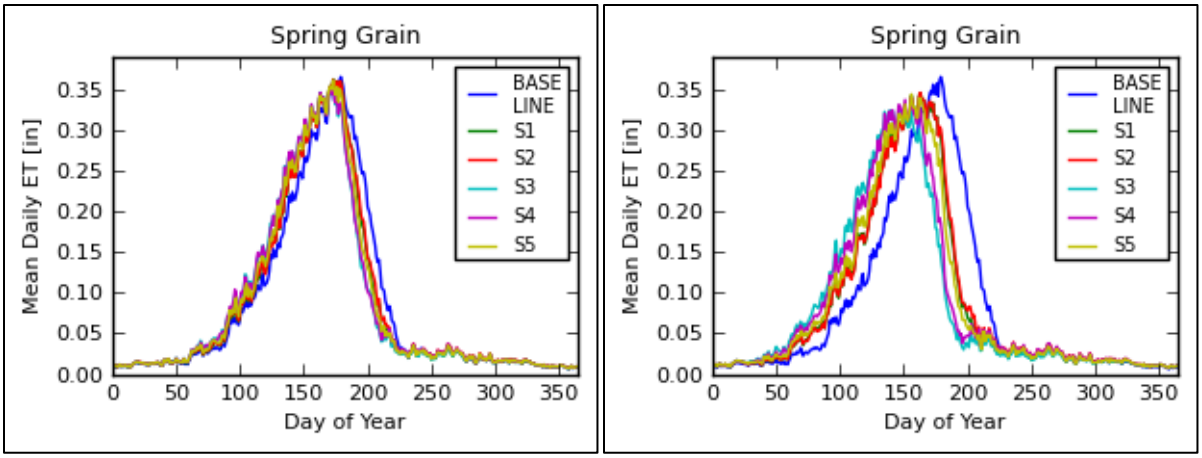

Figure 70.—Missouri River Basin – COOP station CO3553 (Greeley UNC, CO). Baseline and projected mean daily spring grain evapotranspiration for all scenarios and for time periods 2020 (left) and 2080 (right).

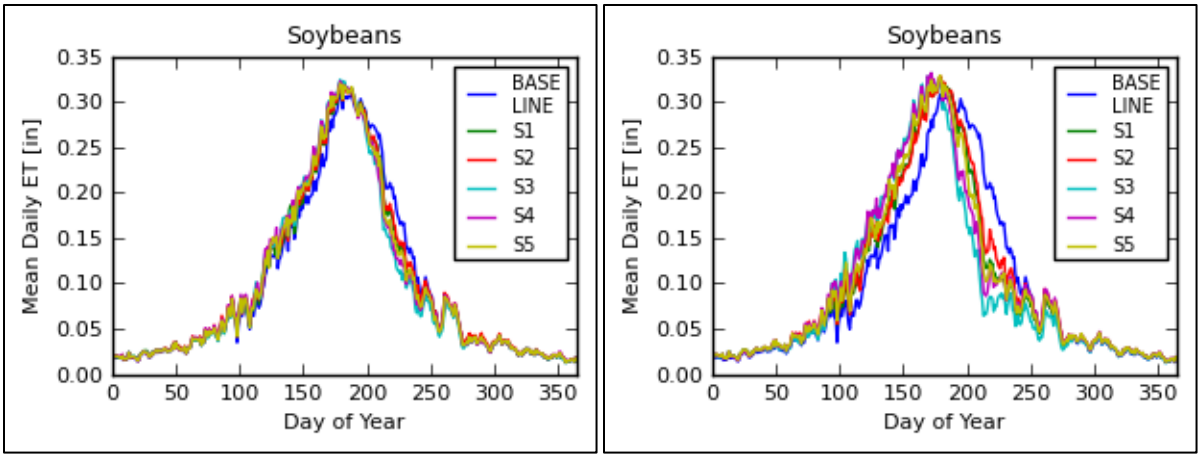

Figure 71.—Missouri River Basin – COOP Station KS4712 (Lincoln 2 ESE, KS). Baseline and projected mean daily soybean evapotranspiration for all scenarios and for time periods 2020 (left) and 2080 (right).

5.5.2 Baseline and Projected Reservoir Evaporation

Figures 72 and 73 illustrate baseline and projected annual precipitation (top left), annual mean temperature (top right), annual evaporation (bottom left), and annual net evaporation (bottom right) at Boysen Reservoir and Canyon Ferry Reservoir. The heavy black line for each variable is the annual time series of 50 percentile values (i.e., ensemble-median). The shaded area for each variable is the annual time series of 5th to 95th percentiles or the 90-percent variability. Annual precipitation over Boysen Reservoir and Canyon Ferry Reservoir is seen to have a slight increase over the transient period going out to 2099. The variability for annual precipitation is fairly large (~40% of the ensemble median) for both reservoirs, and slightly increases over time. The mean annual temperature and

annual evaporation both show increasing trends and a diverging variability over time for both reservoirs. The ensemble-median and variability for net evaporation (i.e., evaporation minus precipitation) are affected by characteristics of both precipitation and temperature projections. It is evident, for instance, that the upper envelope bound in precipitation causes the lower bound of net evaporation to be highly variable, while the diverging variability is caused primarily by the diverging temperature projections.

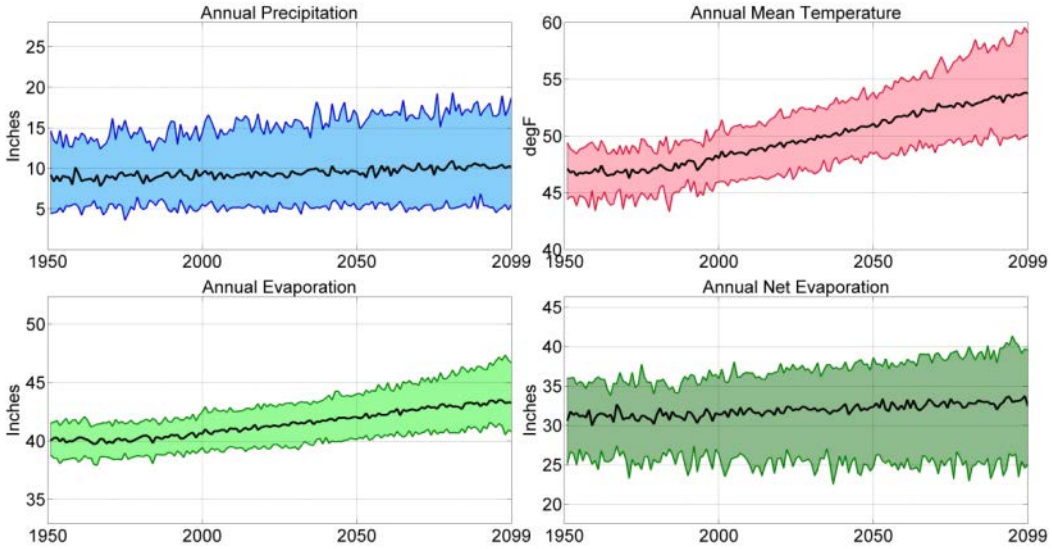

Figure 72.—Missouri River Basin – Boysen ensemble median and 5th and 95th percentile annual precipitation, temperature, reservoir evaporation, and net evaporation.

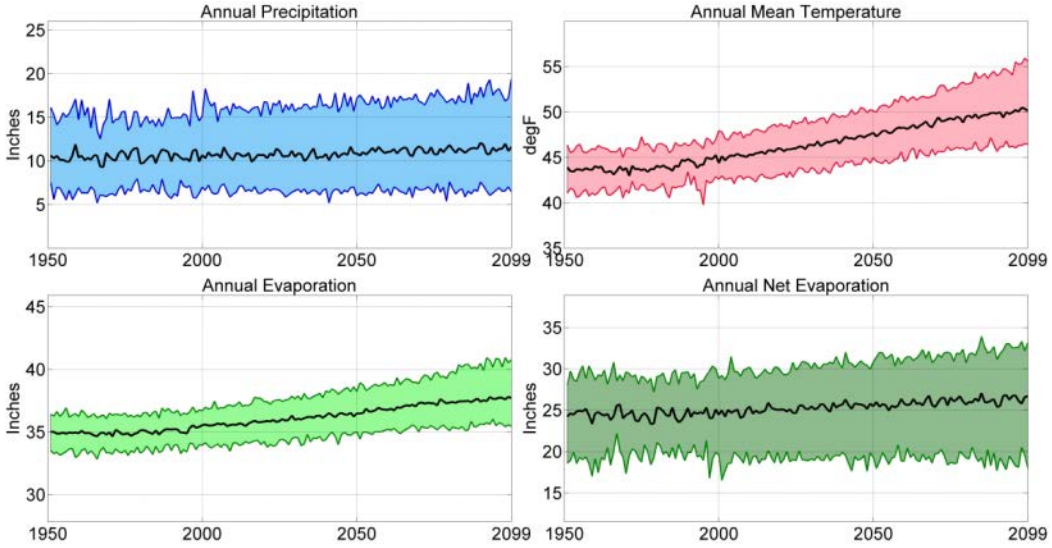

Figure 73.—Missouri River Basin – Canyon Ferry ensemble median and 5th and 95th percentile annual precipitation, temperature, reservoir evaporation, and net evaporation.

In Figures 74 and 75, representing Boysen Reservoir and Canyon Ferry Reservoir, respectively, the solid lines show the ensemble-median mean monthly evaporation and net evaporation for the baseline period (1950–2099) and for the 2020s, 2050s, and 2080s, and the shaded areas show the decadal spread of mean monthly evaporation and net evaporation for the baseline (gray shading) and 2080s (magenta shading), where the spread is bound by the ensemble's 5^{th} to 95^{th} percentile values for each month. The simulated impact of heat storage is clearly evident, as the peak evaporation occurs in August and the minimum evaporation occurs during February or March. The magnitude of projected monthly evaporation and net evaporation increase is greatest during the summer months and least during the fall and winter months. The increase in annual evaporation and net evaporation from baseline to the 2080 time period is 7.0 and 4.3 percent (2.8 and 1.3 in) for Boysen Reservoir, and 6.8 and 6.9 percent (2.4 and 1.7 in) for Canyon Ferry Reservoir, respectively (appendix 10).

5.6 Rio Grande Basin

5.6.1 Baseline and Projected Irrigation Water Demands

Figure 76 illustrates COOP station based Met Nodes that were used to estimate irrigation water demands, as well as HUC8 boundaries used to upscale Met Node estimates in the Rio Grande River Basin. Figure 77 illustrates the spatial distribution of baseline (1950–1999) mean annual temperature (top left) and mean annual precipitation (top right) derived from BCSD data discussed in section 3.2, mean annual dewpoint depression (bottom left), and mean annual windspeed (bottom right) estimated from historical agricultural weather data (discussed in section 4.2.1). Figure 77 shows mean annual temperatures ranging from cool in the higher elevations in the northern of the basin to warm in the lower elevations to the south. Annual precipitation is generally low (~ 10 inches) throughout the basin. The mean annual dewpoint depression (i.e., $T_{min} - T_{dew}$) is used here as a simple approximation of the humidity of the lower air mass that is consistent and representative of agricultural areas while preserving regional and local advection effects. In the Rio Grande basin, its distribution was simplified to two regions due to the sparsity of agricultural weather stations in the area. The dewpoint depression does show, however, that the Middle Rio Grande region, to the south, is significantly dryer than the San Luis Valley region. Similar to dewpoint depression, the spatial distribution of windspeed was simplified to two regions, and it is evident that the windspeed is slightly lower in the Middle Rio Grande region than in the San Luis Valley to the north. Figure 78 illustrates reference ET (ET_0) (top left), crop evapotranspiration (ET_c) (top right), net irrigation water requirement (NIWR) (bottom left), and total crop acreage (bottom right) within each HUC8 boundary. ET_0, ET_c, and NIWR are all higher in the southern portion of the basin, where air temperature, solar radiation, and dewpoint depression are

larger than in the north. The projected values range from 49 to 67 in/yr for ET_0, 32 to 54 in/yr for ET_c, and 22 to 44 in/yr for NIWR.

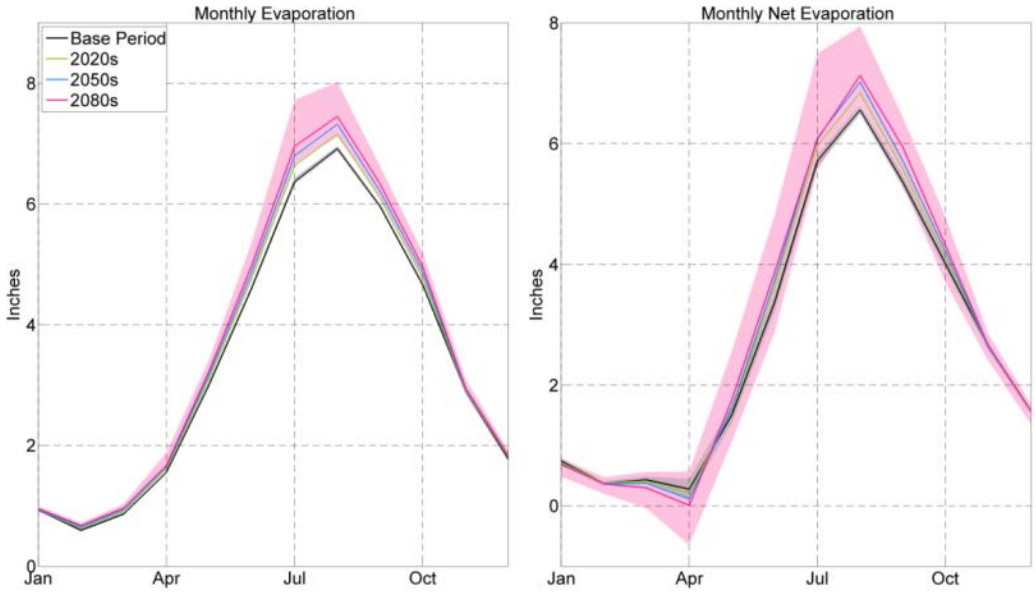

Figure 74.—Missouri River Basin – Boysen mean monthly ensemble median and 5th and 95th percentile reservoir evaporation and net evaporation.

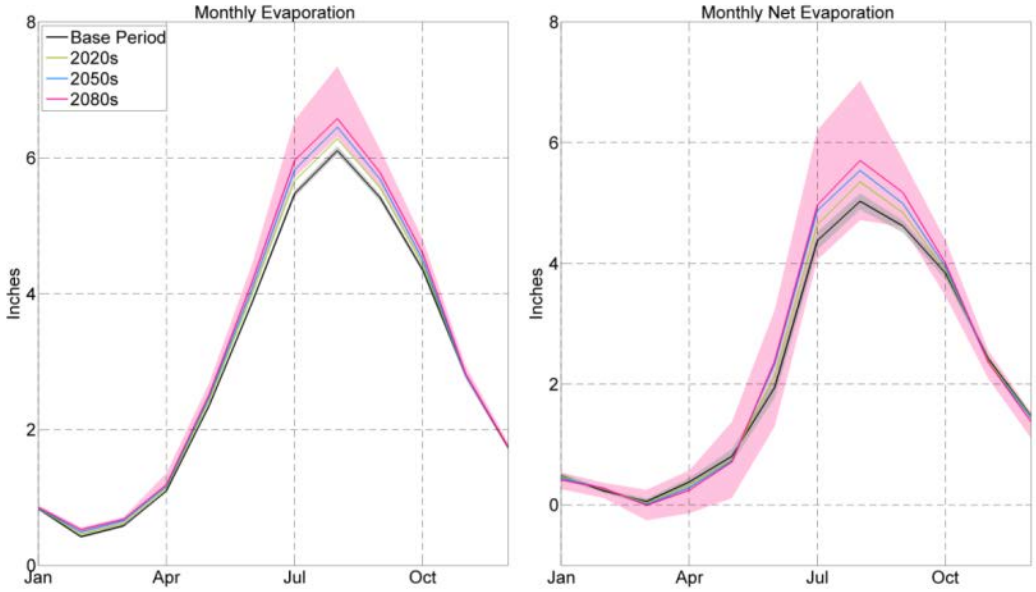

Figure 75.—Missouri River Basin – Canyon Ferry mean monthly ensemble median and 5th and 95th percentile reservoir evaporation and net evaporation.

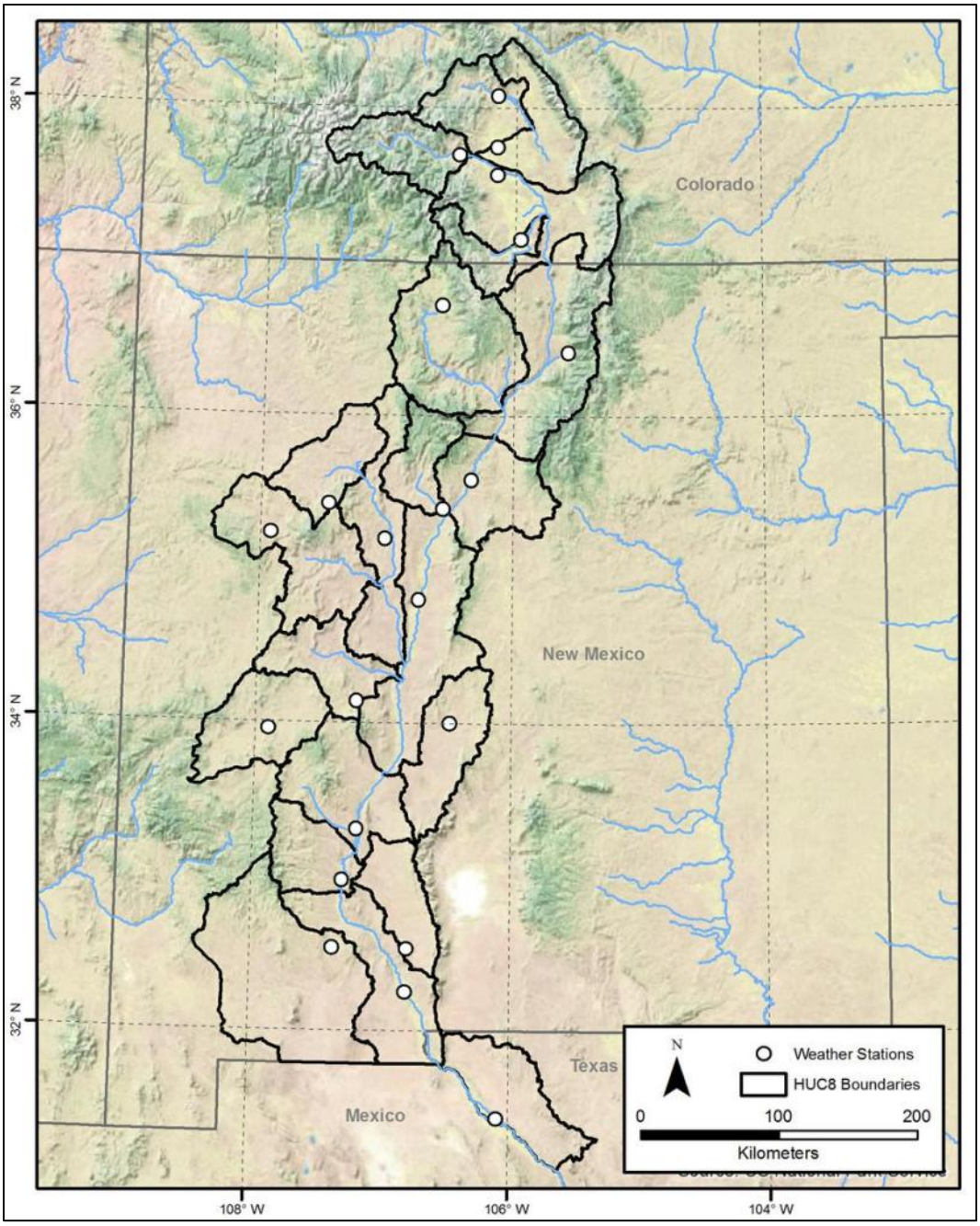

Figure 76.—Rio Grande River Basin – COOP stations used to simulate baseline and projected irrigation demands.

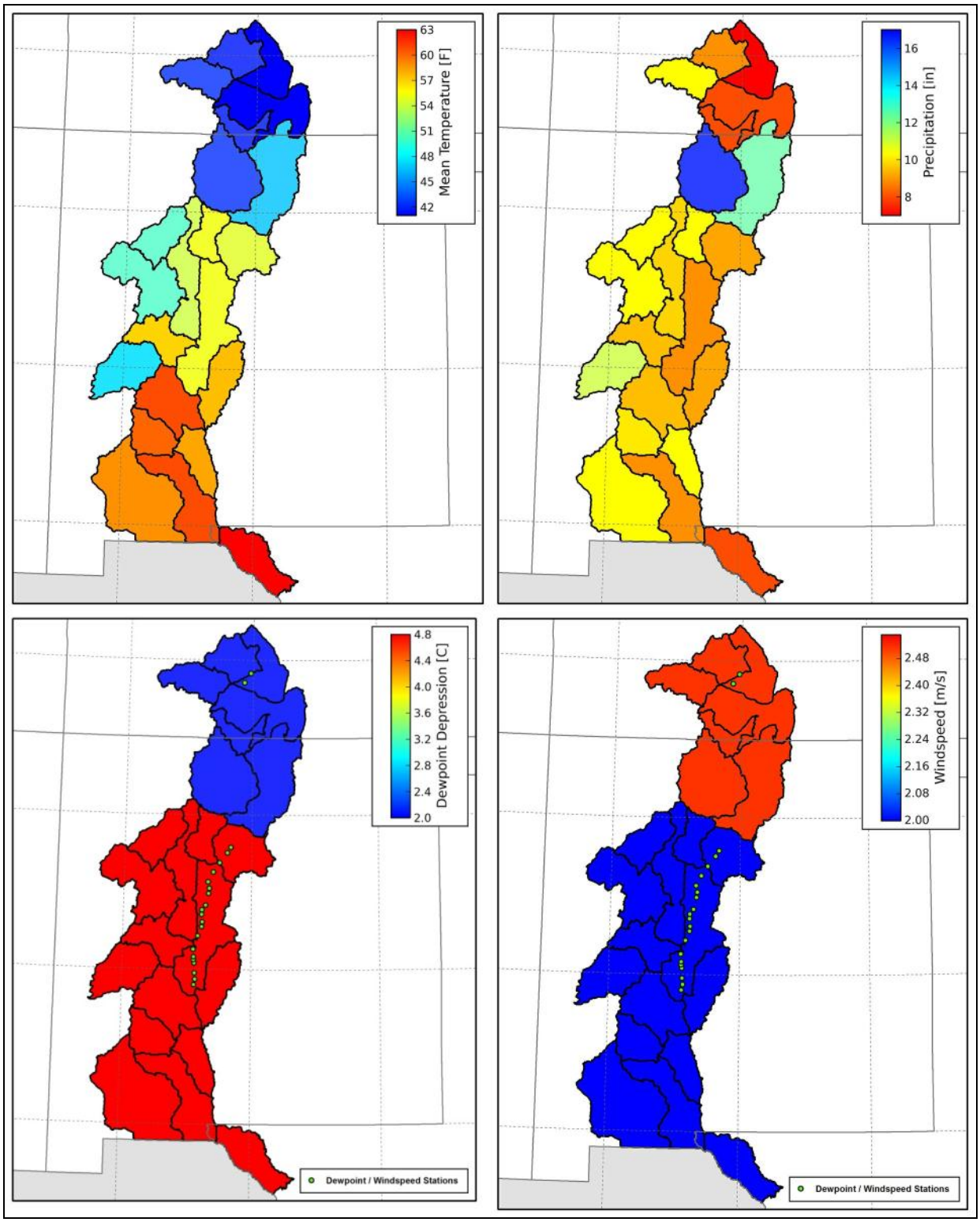

Figure 77.—Rio Grande River Basin – Spatial distribution of baseline temperature, precipitation, dewpoint depression, and windspeed.

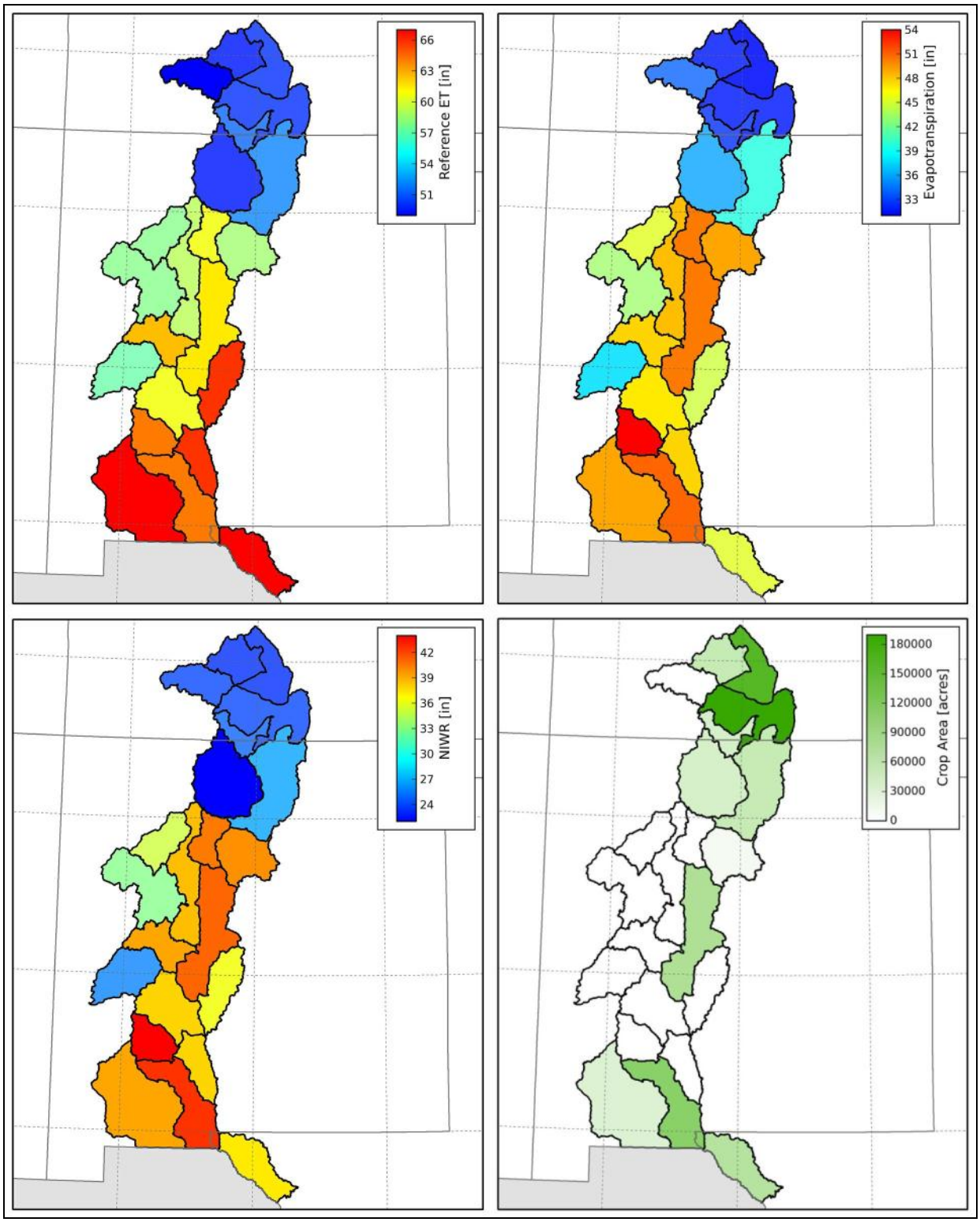

Figure 78.—Rio Grande River Basin – Spatial distribution of baseline reference evapotranspiration, crop evapotranspiration, net irrigation water requirements (NIWR), and crop acreage.

Figure 79 shows the spatial distribution of projected mean temperature change for different climate scenarios and time periods, and it is evident that the changes shown there are generally spatially uniform for all scenarios, with scenario S3 (hot-dry) having the largest change. Figure 80 illustrates the spatial distribution of projected precipitation percent change for different scenarios and time periods. Depending on the scenario, precipitation percent changes range from –19 percent (S3 or hot-dry scenario) to 16 percent (S4 or hot-wet scenario) for the 2080 time period, with the central tendency scenario (S5) generally showing some decrease (~5%) throughout the basin.

Figure 81 shows the spatial distribution of projected ET_0 percent change for different climate scenarios and time periods. Similar to temperature, the projected percent change in ET_0 is generally spatially uniform for all scenarios, with scenario S3 (hot-dry) having the largest change. The northern portions of the basin exhibit the largest percent change due to the fact that the difference between the projected and baseline ET_0 is relatively large compared to the relatively low baseline estimate of ET_0. Figure 82 illustrates the spatial distribution of projected ET_c percent change for different climate scenarios and time periods assuming non-static crop phenology for annual crops, where projected future temperatures were used for simulating projected planting, crop coefficient development, and termination as described in section 4.2.1. Spatial differences in the distribution of projected percent change in ET_c are largely due to differences in crop type and baseline ET_c. The northern portion of the basin is projected to experience the largest percent change for all projected time periods, largely due to the fact that the difference between the projected and baseline ET_c is fairly large relative to the baseline estimate of ET_c (figure 78). ET_c in the southern portion of the basin is also projected to increase. Figure 83 shows the spatial distribution of projected ET_c percent change for different climate scenarios and time periods assuming static crop phenology for annual crops. Baseline (1950–1999) temperatures were used for simulating projected planting, crop coefficient development, and termination for all future time periods and scenarios as described in section 4.2.1. All HUCs show ET_c increases under the static crop phenology assumption.

The spatial distribution of projected NIWR percent change for different climate scenarios and time periods is shown on figures 84 and 85. The NIWR incorporates growing-season and non-growing-season soil moisture gains and losses from precipitation, bare soil evaporation, and ET. Therefore, spatial variations in the distribution of NIWR percent change for different time periods and scenarios are a function of respective ET_c (figures 82 and 83) and precipitation (figure 80) distributions. The basin shows an increase in NIWR under all climate change scenarios. For more illustrations on unit changes (degrees F and inches) in spatial projections of mean temperature, precipitation, ET_0, ET_c, and NIWR for different time periods and scenarios, see appendix 9.

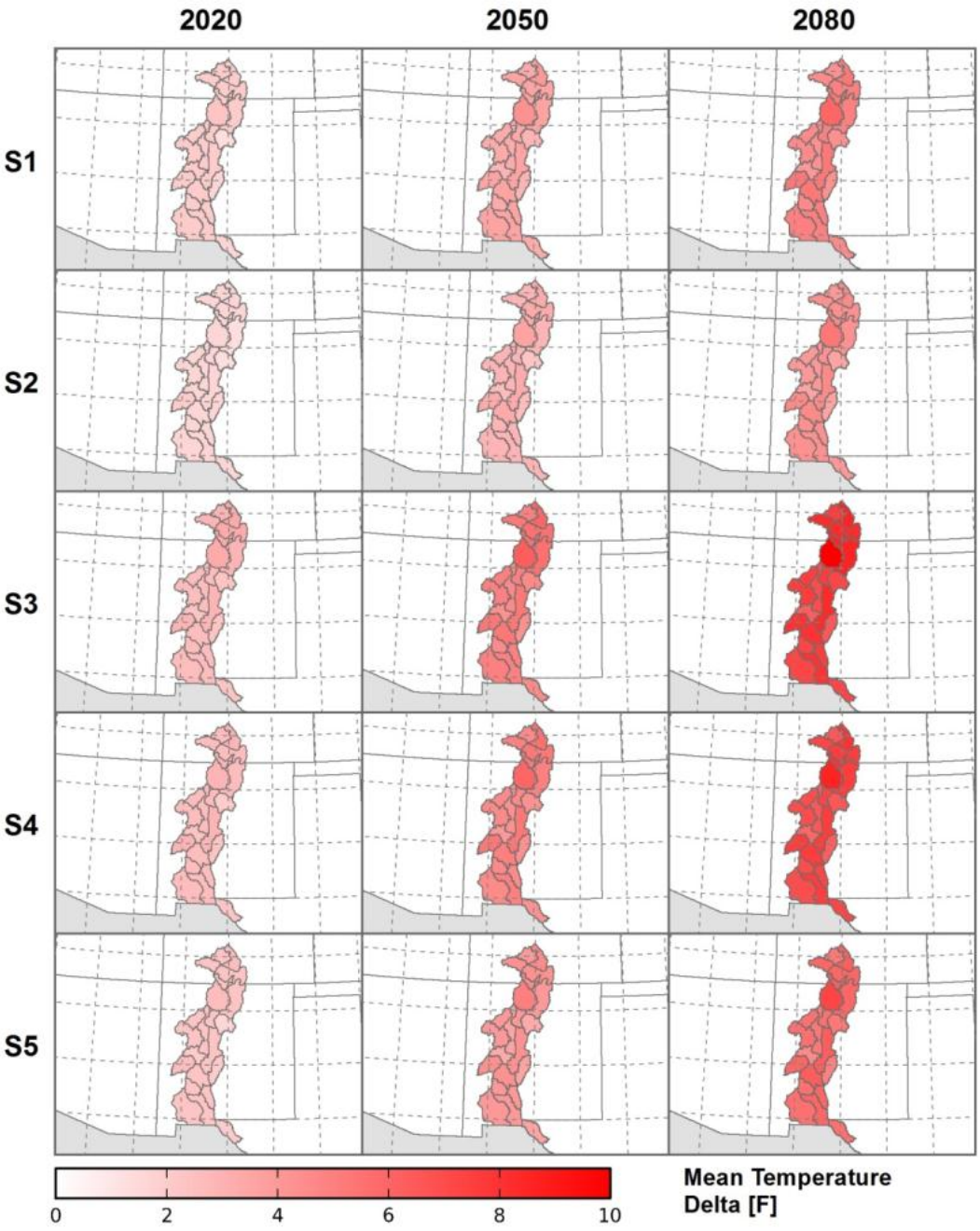

Figure 79.—Rio Grande River Basin – Spatial distribution of temperature change for different climate scenarios and time periods (S1 = WD, S2 = WW, S3 = HD, S4 = HW, S5 = Central).

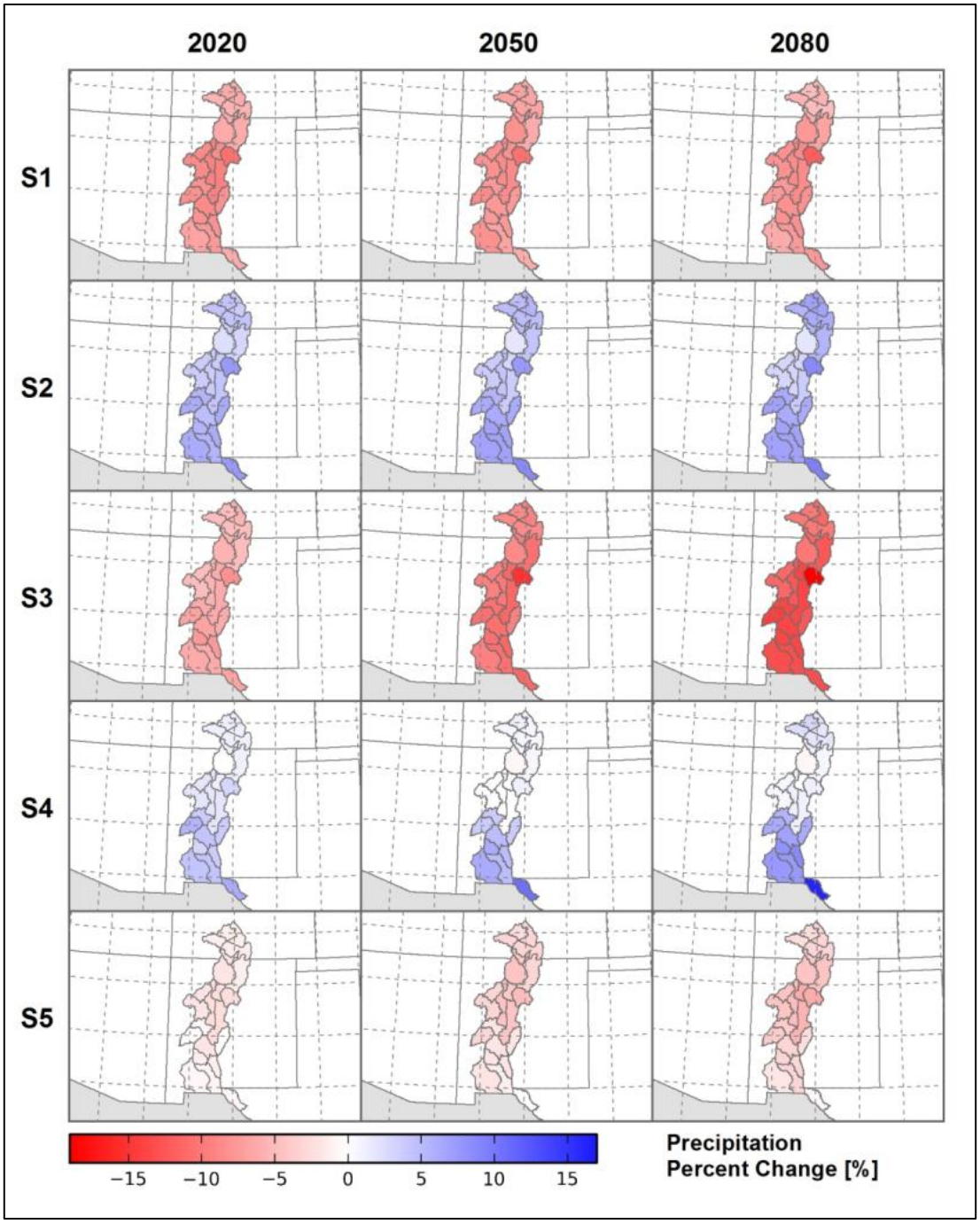

Figure 80.—Rio Grande River Basin – Spatial distribution of projected precipitation percent change for different climate scenarios and time periods (S1 = WD, S2 = WW, S3 = HD, S4 = HW, S5 = Central).

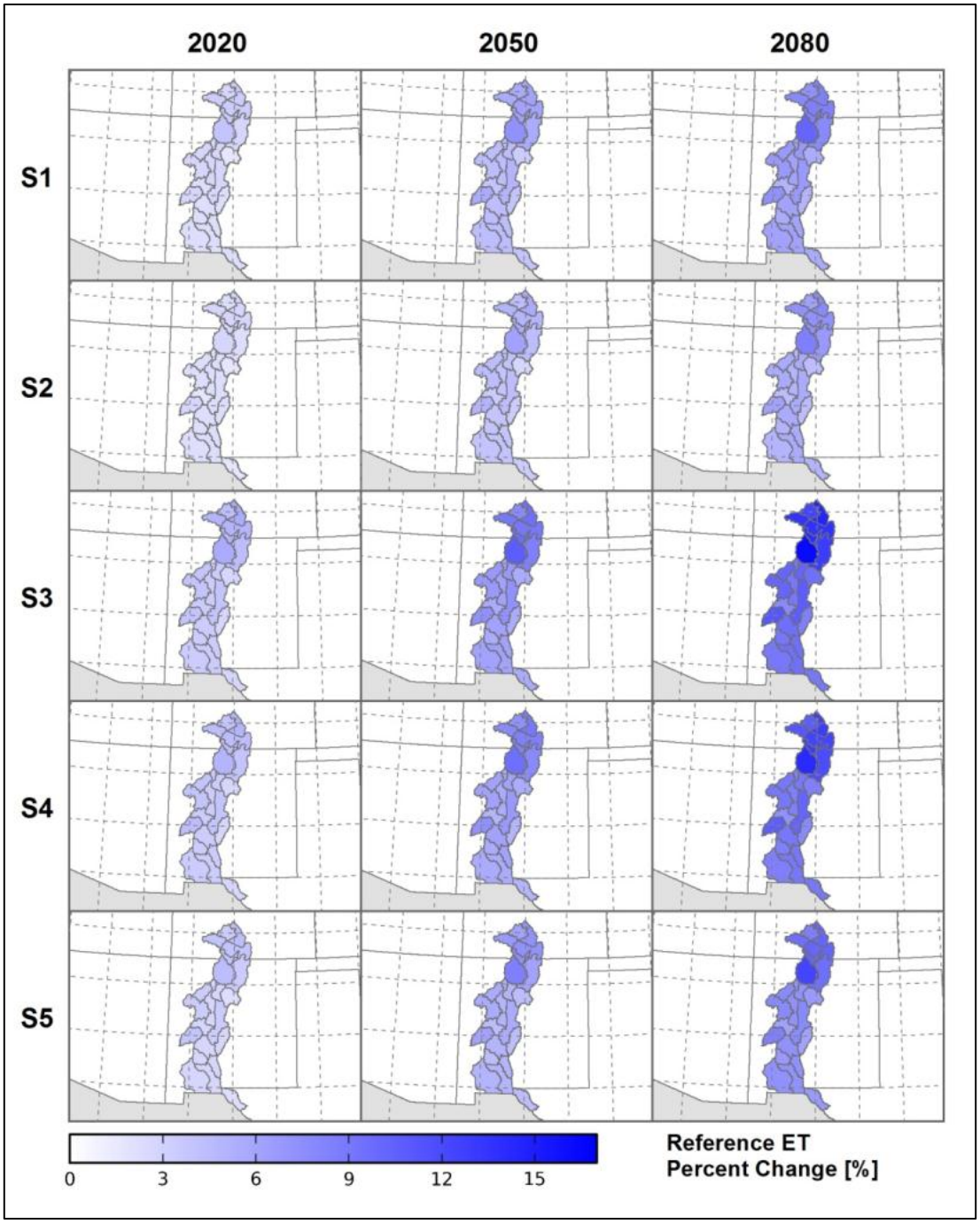

Figure 81.—Rio Grande River Basin – Spatial distribution of projected reference evapotranspiration percent change for different climate scenarios and time periods (S1 = WD, S2 = WW, S3 = HD, S4 = HW, S5 = Central).

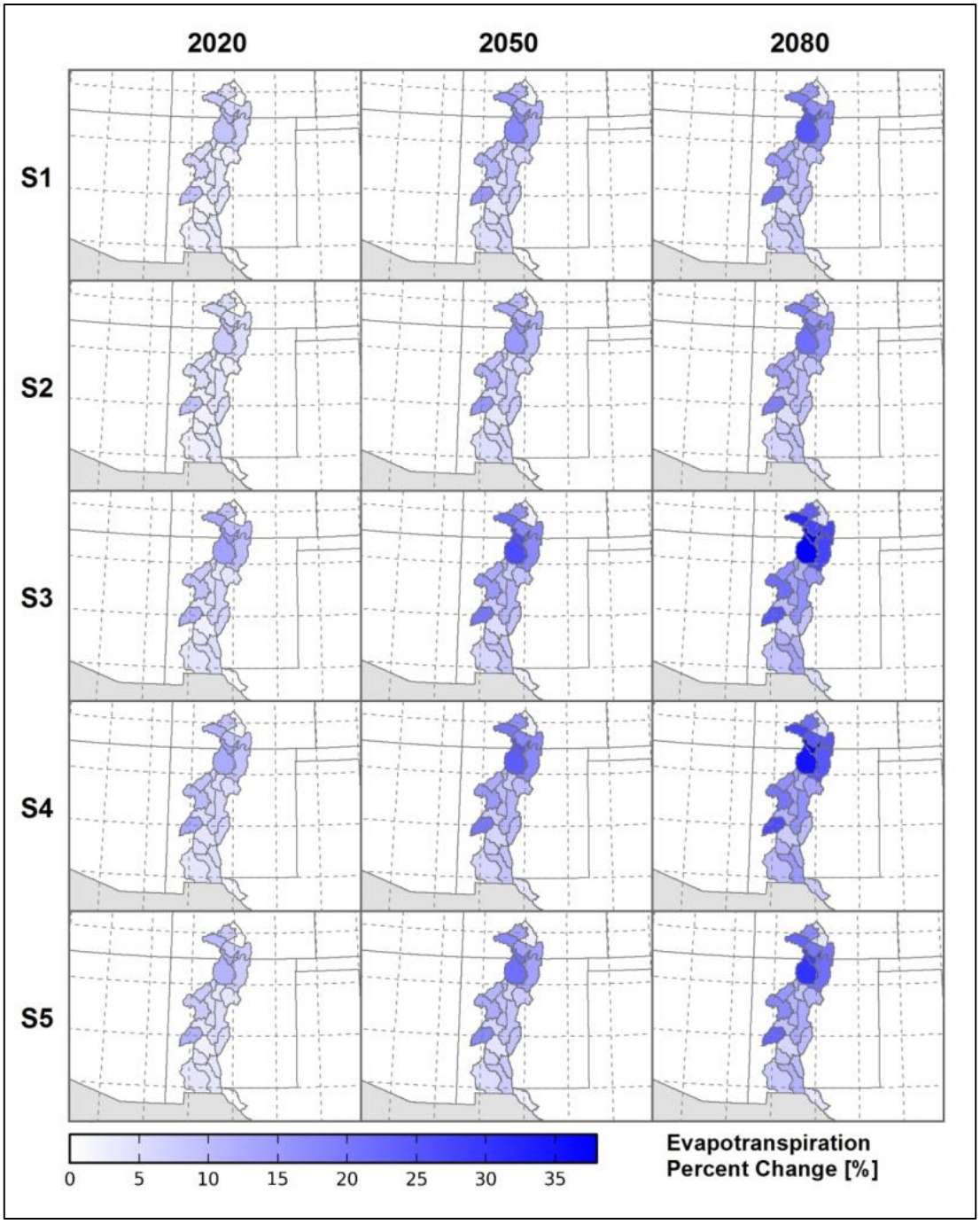

Figure 82.—Rio Grande River Basin – Spatial distribution of projected crop evapotranspiration percent change for different climate scenarios and time periods (S1 = WD, S2 = WW, S3 = HD, S4 = HW, S5 = Central).

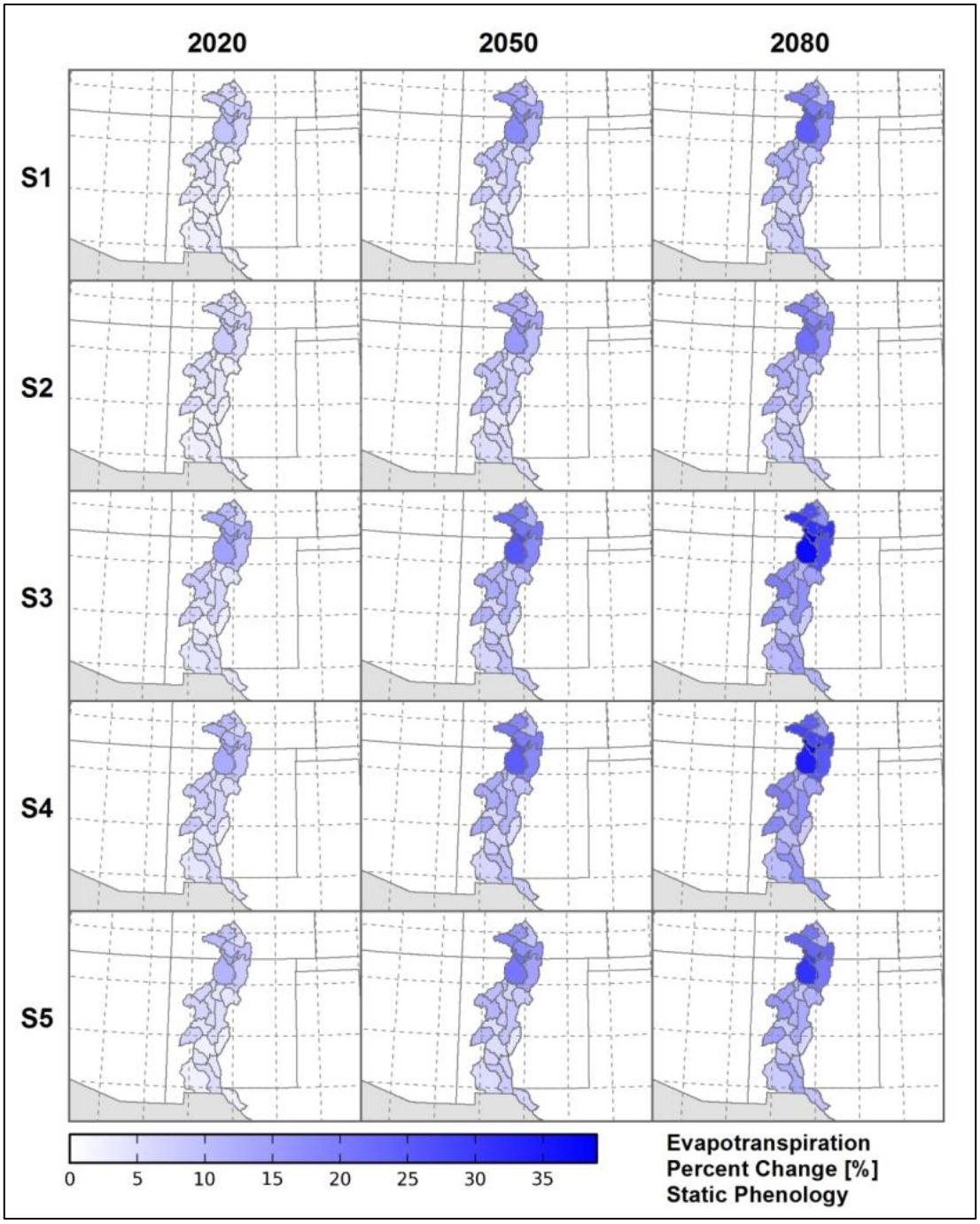

Figure 83.—Rio Grande River Basin – Spatial distribution of projected crop evapotranspiration percent change for different climate scenarios and time periods assuming static phenology for annual crops (S1 = WD, S2 = WW, S3 = HD, S4 = HW, S5 = Central).

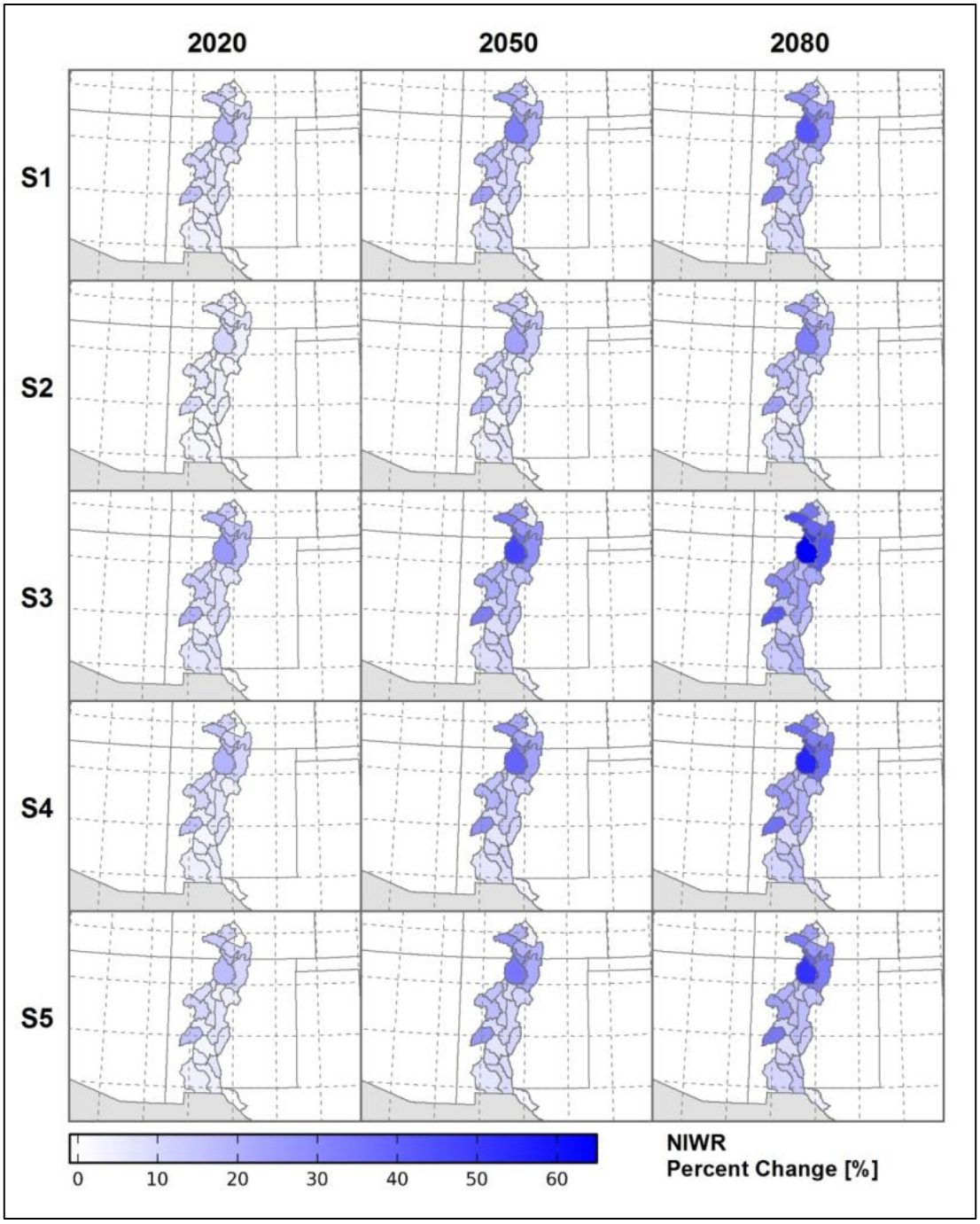

Figure 84.—Rio Grande River Basin – Spatial distribution of projected net irrigation water requirements (NIWR) percent change for different climate scenarios and time periods (S1 = WD, S2 = WW, S3 = HD, S4 = HW, S5 = Central).

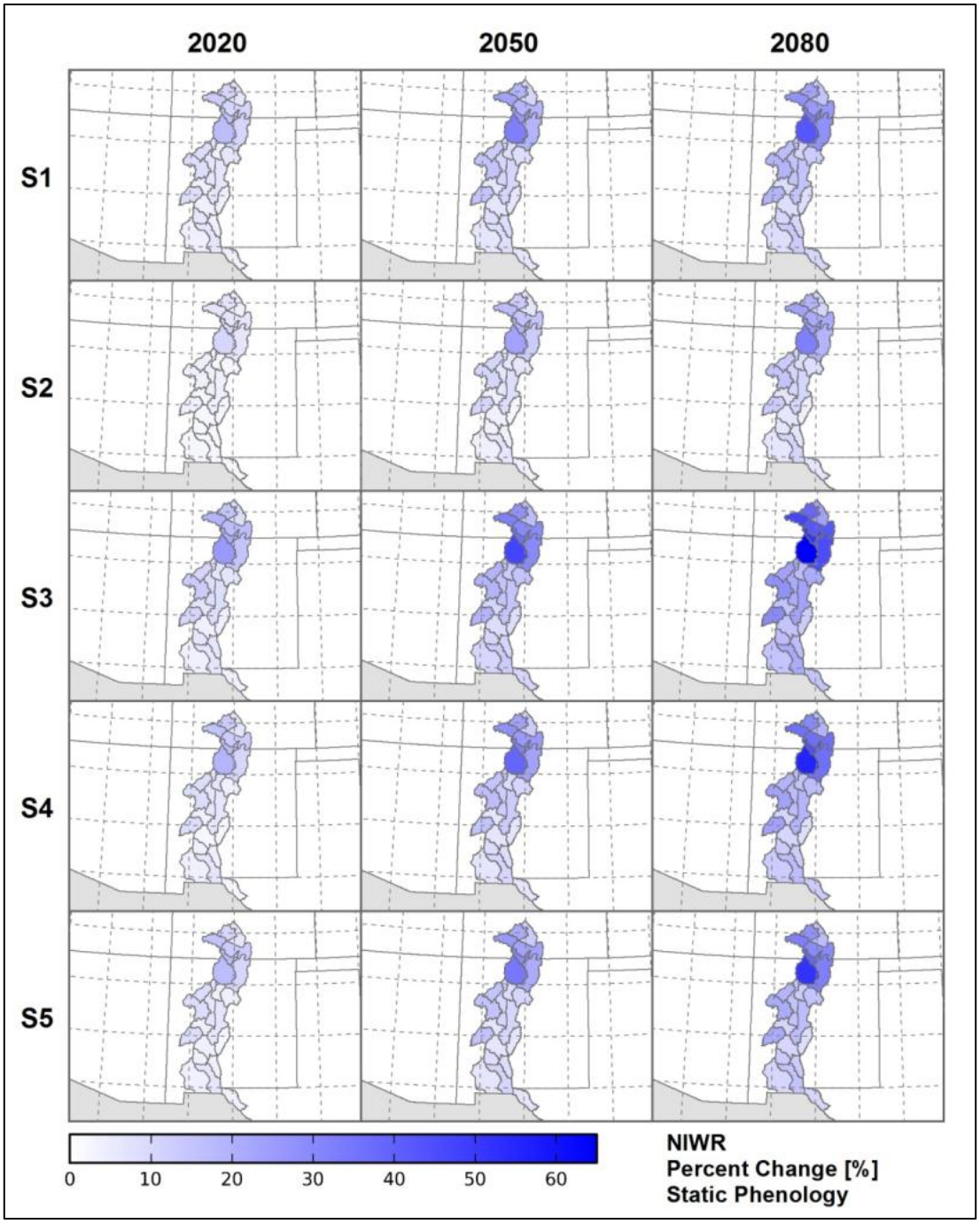

Figure 85.—Rio Grande River Basin – Spatial distribution of projected net irrigation water requirements (NIWR) percent change for different climate scenarios and time periods assuming static phenology for annual crops (S1 = WD, S2 = WW, S3 = HD, S4 = HW, S5 = Central).

Figures 86, 87, and 88 illustrate the baseline and projected temporal distribution of mean daily ET_c for selected Met Nodes, crops, scenarios, and time periods. The simulated mean daily ET_c of alfalfa for the 2020 time period, NWS/COOP Met Node NM5147 (Middle RG – Los Lunas, NM), shows slight but noticeable shifts in the growing-season length and alfalfa cutting cycles relative to baseline conditions (figure 86, left). By the 2080 time period (figure 86, right) significant shifts in growing-season length, crop development, and cutting cycles are noticeable relative to baseline conditions, with scenarios S3 and S4 exhibiting the most extreme changes. Figure 87 shows simulated mean daily ET_c of spring grain at Met Node NM5147 (Middle RG – Los Lunas, NM), under different scenarios, for the 2020 and 2080 time periods. Because planting dates for annual crops are temperature dependent in the non-static phenology simulations, shifts in planting, development, and harvest dates of spring grain are clearly evident, especially by the 2080 time period. The uncertainty in such potential shifts in planting dates, accelerated crop development, and harvest was a primary reason for using baseline temperatures for static phenology simulations (figures 83 and 85). In static phenology simulations, because baseline temperatures are used for estimating planting, crop development, and harvest dates, all scenarios and time periods have identical seasonal K_{cb} and ET_c shapes, and show differences only in daily ET_c magnitudes due to daily ET_0 and precipitation differences. Figure 88 illustrates simulated mean daily ET_c of peppers at Met Node NM5147 (Middle RG – Los Lunas, NM) for different scenarios and time periods. Significant seasonal changes in planting, development, harvest dates, and ET_c are projected by 2080, with S3 and S4 having the most extreme seasonal changes. Large midsummer increases in ET_c occur because peppers are traditionally planted relatively late in the season compared to other crops such as spring grain, and also because full cover is simulated to occur earlier, during a time when reference ET (ET_0) is larger.

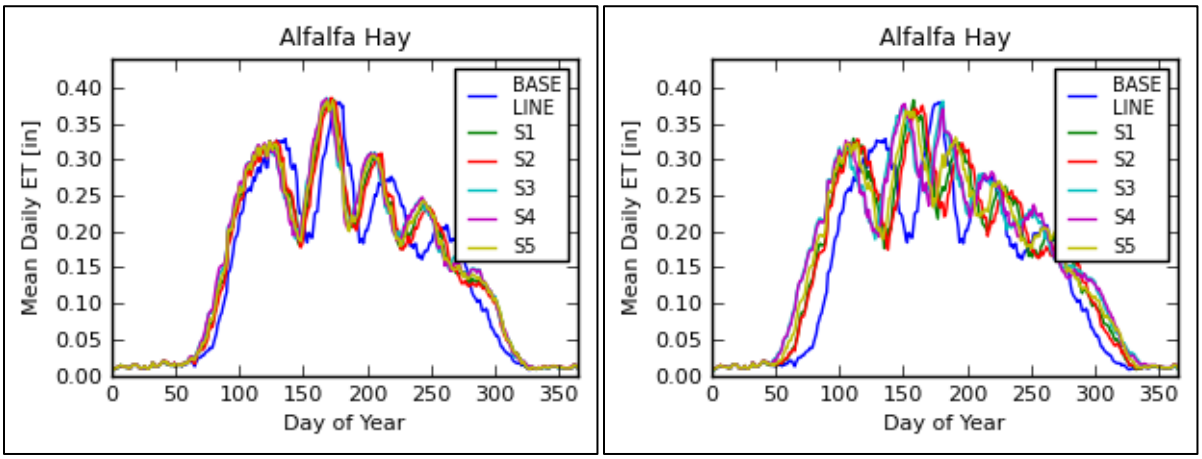

Figure 86.—Rio Grande River Basin – COOP station NM5147 (Los Lunas, NM). Baseline and projected mean daily alfalfa evapotranspiration for all scenarios and for time periods 2020 (left) and 2080 (right).

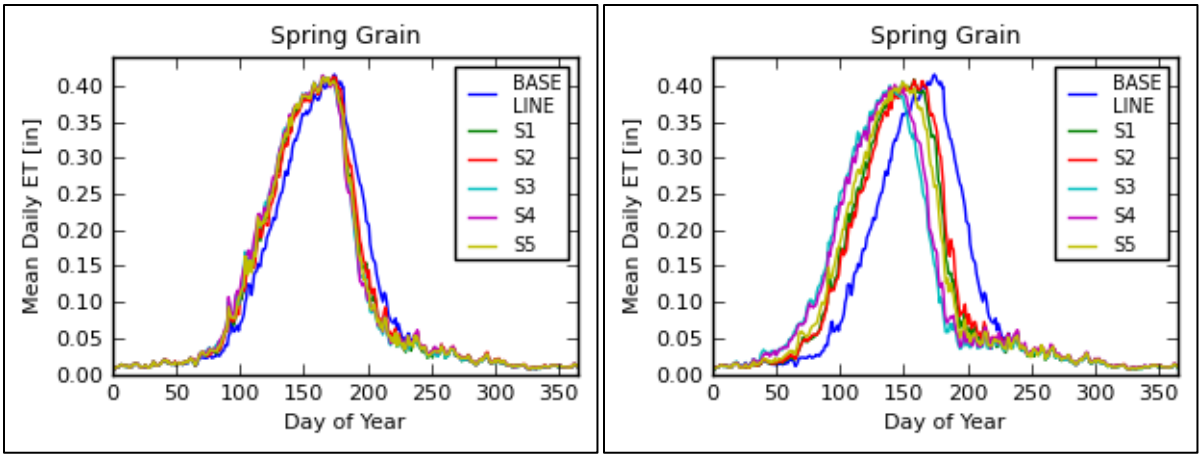

Figure 87.—Rio Grande River Basin – COOP Station NM5147 (Los Lunas, NM). Baseline and projected mean daily spring grain evapotranspiration for all scenarios and for time periods 2020 (left) and 2080 (right).

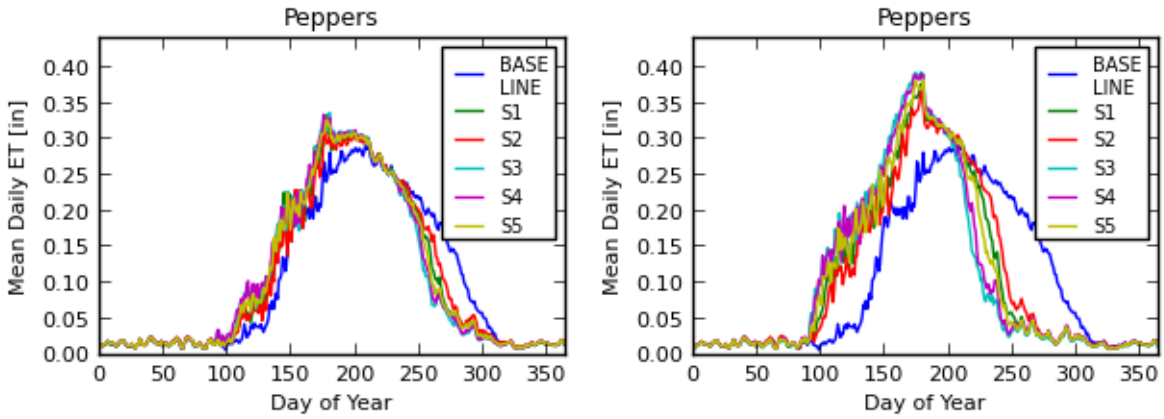

Figure 88.—Rio Grande River Basin – COOP station NM5147 (Los Lunas, NM). Baseline and projected mean daily garden peppers evapotranspiration for all scenarios and for time periods 2020 (left) and 2080 (right).

5.6.2 Baseline and Projected Reservoir Evaporation

Figure 89 illustrates baseline and projected Elephant Butte Reservoir annual precipitation (top left), annual mean temperature (top right), annual evaporation (bottom left), and annual net evaporation (bottom right). The heavy black line for each variable is the annual time series of 50-percentile values (i.e., ensemble-median). The shaded area for each variable is the annual time series of 5th to 95th percentiles or the 90-percent variability. Annual precipitation over the Elephant Butte Reservoir is seen to have a very nominal decline over the transient period going out to 2099. The variability for annual precipitation is somewhat large and shows some divergence with time. However, the mean annual temperature and annual evaporation both show increasing trends and a diverging variability over time. The ensemble-median and variability for net evaporation (i.e., evaporation

minus precipitation) are affected by characteristics of both precipitation and temperature projections. It is evident, for instance, that the upper confidence bound in precipitation causes the lower bound of net evaporation to be highly variable, while the diverging variability is caused primarily by the diverging temperature projections.

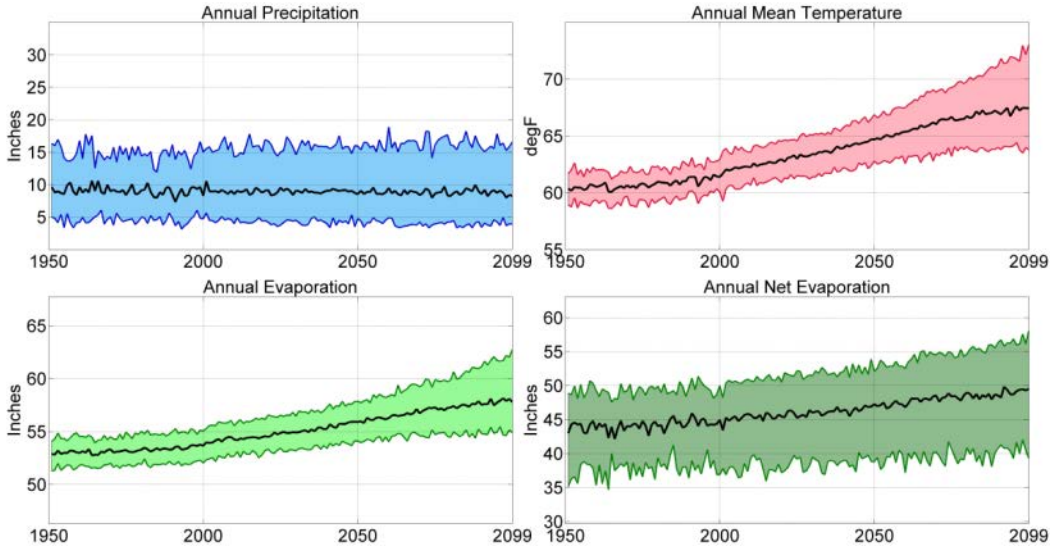

Figure 89.—Rio Grande River Basin – Elephant Butte ensemble median and 5th and 95th percentile annual precipitation, temperature, reservoir evaporation, and net evaporation.

Figure 90 shows evaporation and net evaporation at Elephant Butte Reservoir. The solid lines represent the ensemble-median mean-monthly evaporation and net evaporation for the baseline period (1950–1999) and for the 2020s, 2050s, and 2080s, and the shaded areas show the decadal spread of mean monthly evaporation and net evaporation for the baseline period (gray shading) and 2080s (magenta shading), where the spread is bound by the ensemble's 5th to 95th percentile values for each month. The simulated impact of heat storage is evident, as the peak evaporation occurs in August and the minimum evaporation occurs in February. The magnitude of projected monthly evaporation and net evaporation increase is greatest during the summer months, and least during the fall and winter months. The increase in annual evaporation and net evaporation for Elephant Butte, from baseline to the 2080 time period, is 7.7 and 9.5 percent (4.1 and 4.2 in), respectively (appendix 10).

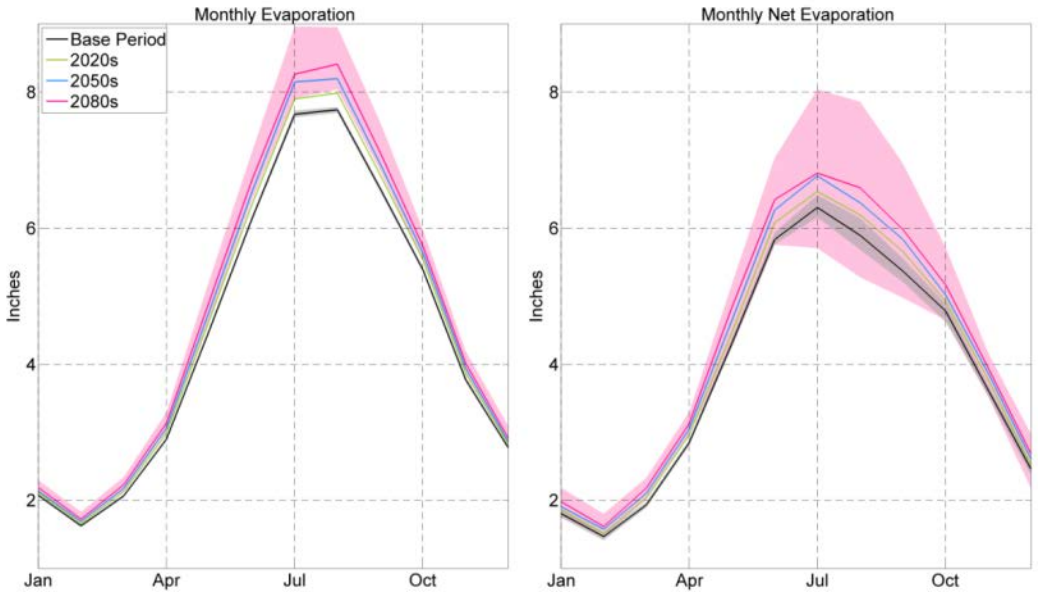

Figure 90.—Rio Grande River Basin – Elephant Butte ensemble median and 5th and 95th percentile annual precipitation, temperature, reservoir evaporation, and net evaporation.

5.7 Sacramento and San Joaquin River Basins

5.7.1 Baseline and Projected Irrigation Water Demands

Figure 91 illustrates COOP station based Met Nodes that were used to estimates irrigation water demands, as well as planning area boundaries used to upscale Met Node estimates in the Central Valley Basins of the Sacramento and San Joaquin Rivers. Although only in hydrologic connection with the San Joaquin River during exceptionally wet years, the Tulare Lake Basin in the southernmost part of the Central Valley is also included because it is a major agricultural area within Reclamation's Central Valley Project service area. Figure 92 illustrates the spatial distribution of baseline (1950–1999) mean annual temperature (top left) and mean annual precipitation (top right) derived from BCSD data (discussed in section 3.2), mean annual dewpoint depression (bottom left) and mean annual windspeed (bottom right) estimated from historical agricultural weather station data (discussed in section 4.2.1). Figure 92 shows an overall trend in mean annual temperatures from cool in the north to warm in the south. Precipitation varies from high in the north to low amounts in the south, but also shows an increasing trend across the valley from west to east. The mean annual dewpoint depression (i.e., $T_{min} - T_{dew}$) is used here as a simple approximation of the humidity of the lower air mass that is consistent and representative of agricultural areas while preserving regional and local advection effects. Its spatial distribution

clearly shows that southwestern areas are typically more arid while most northern and eastern areas tend toward being somewhat more humid. Mean annual windspeeds are generally lower in southeastern areas, and higher in the western and northern portions of the basin. The highest windspeeds occur near the Sacramento–San Joaquin Delta, where the influence of topography and large temperature gradients between the coast and the valley combine to generate strong winds during the summer months. Figure 93 illustrates reference ET (ET_0) (top left), crop evapotranspiration (ET_c) (top right), net irrigation water requirement (NIWR) (bottom left), and total crop acreage (bottom right) within each planning area boundary. ET_0, ET_c, and NIWR are mostly higher in the southern portion of the basin, where air temperature, solar radiation, windspeed, and dewpoint depression are larger than in the northern portions. The projected values range from about 53 to 62 in/yr for ET_0, 42 to 57 in/yr for ET_c, and 30 to 45 in/yr for NIWR. In many areas, a trend from higher to lower rates of ET_0 occurs from west to east across the valley. The spatial distribution of ET_0 compares well to that previously mapped by California Department of Water Resources (1999). The planning areas with the larger crop acreages typically occur along the western and southern portions of the valley.

Figure 94 shows the spatial distribution of projected mean temperature change for different climate scenarios and time periods; the changes shown there are generally spatially uniform for all scenarios, with the hotter scenarios S3 (hot-dry) and S4 (hot-wet) having the largest change. Figure 95 illustrates the spatial distribution of projected precipitation percent change for different scenarios and time periods. Depending on the scenario, precipitation percent changes range from –21 percent under the S3 (hot-dry) scenario to 17 percent under the S4 (hot-wet) scenario for the 2080 time period, with the central tendency scenario (S5) generally showing little change in the northern areas but some decrease in the southern portions of the valley.

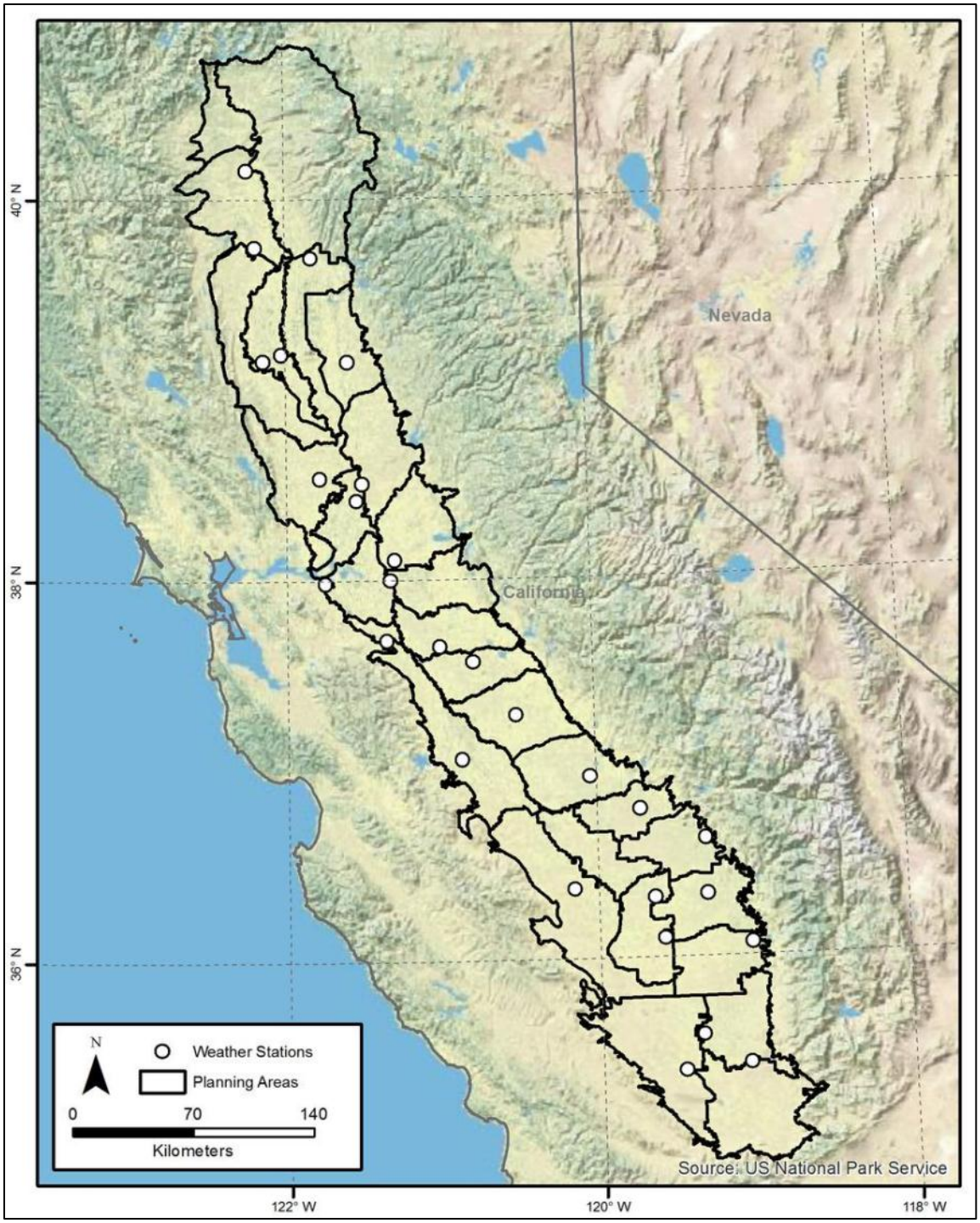

Figure 91.—Sacramento and San Joaquin River Basins – COOP stations used to simulate baseline and projected irrigation demands.

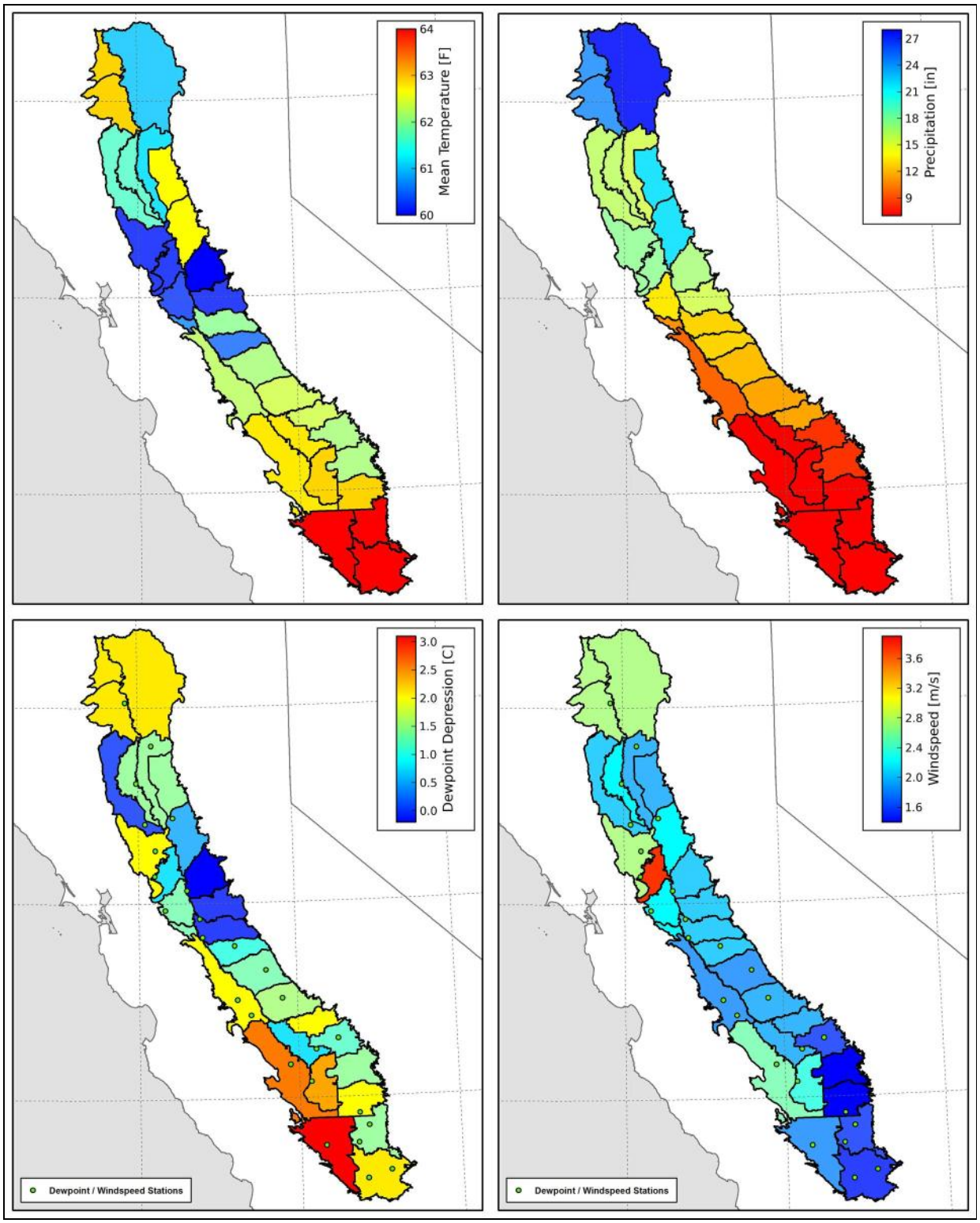

Figure 92.—Sacramento and San Joaquin River Basins – Spatial distribution of baseline temperature, precipitation, dewpoint depression, and windspeed.

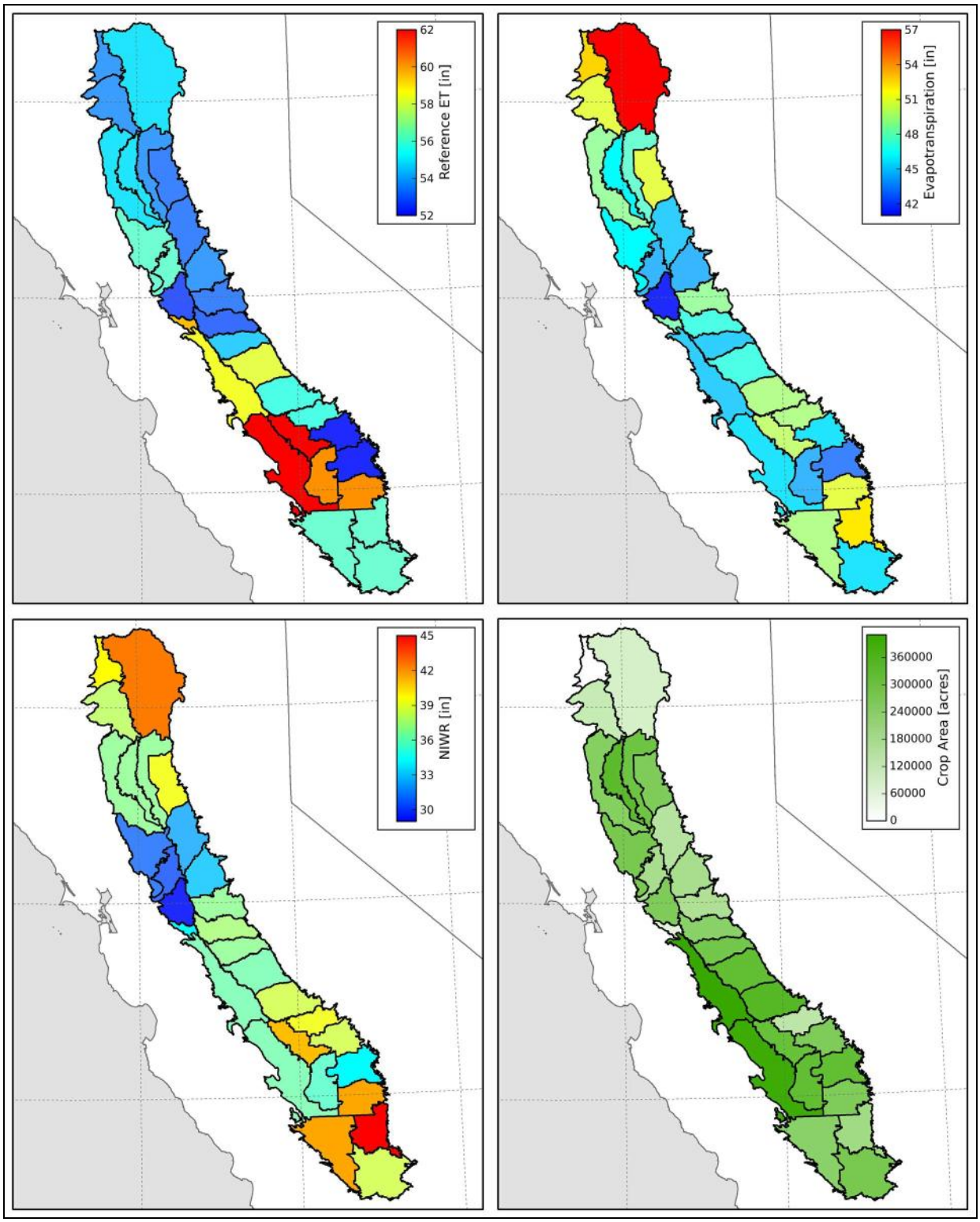

Figure 93.—Sacramento and San Joaquin River Basins – Spatial distribution of baseline reference evapotranspiration, crop evapotranspiration, net irrigation water requirements (NIWR), and crop acreage.

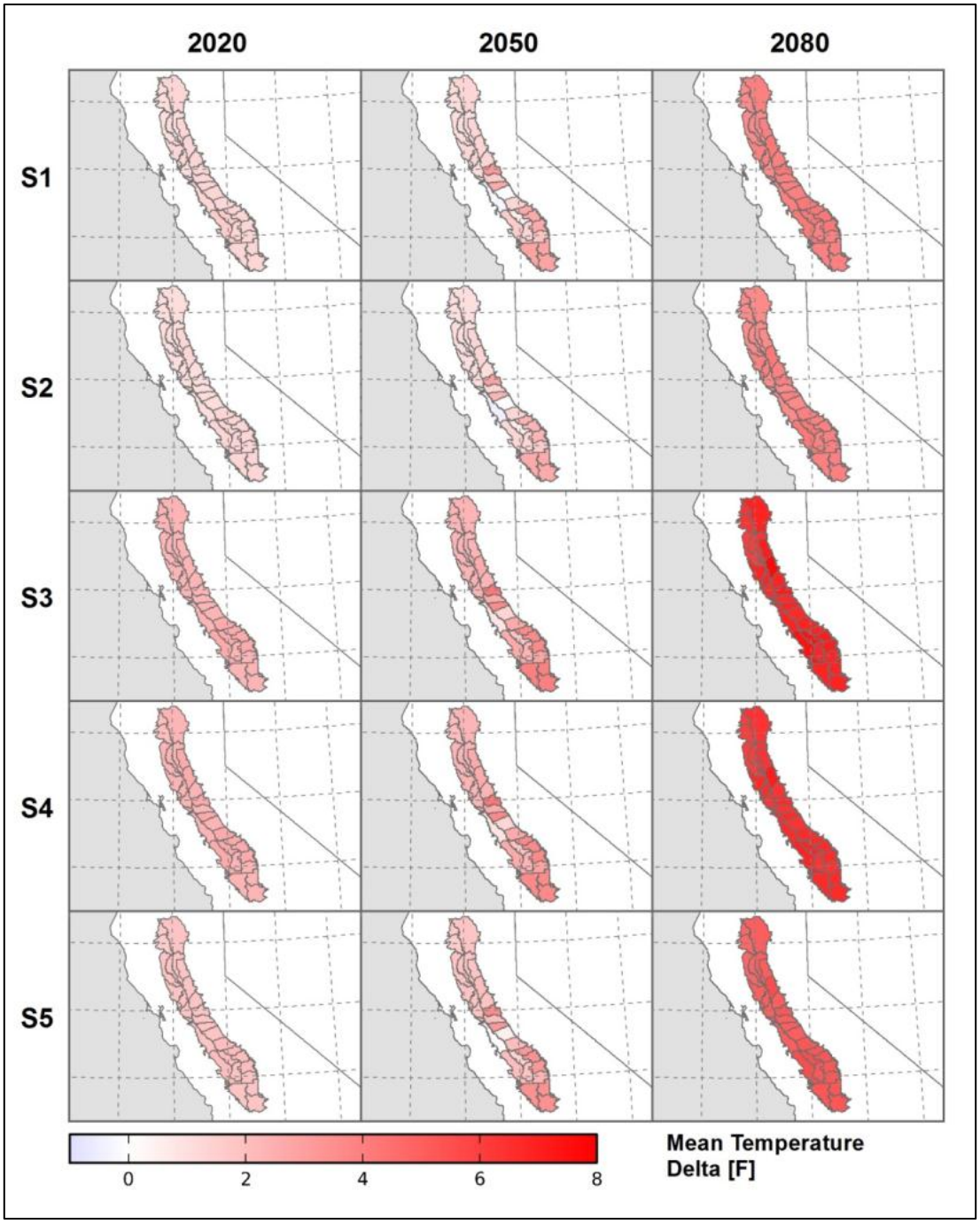

Figure 94.—Sacramento and San Joaquin River Basins – Spatial distribution of temperature change for different climate scenarios and time periods (S1 = WD, S2 = WW, S3 = HD, S4 = HW, S5 = Central).

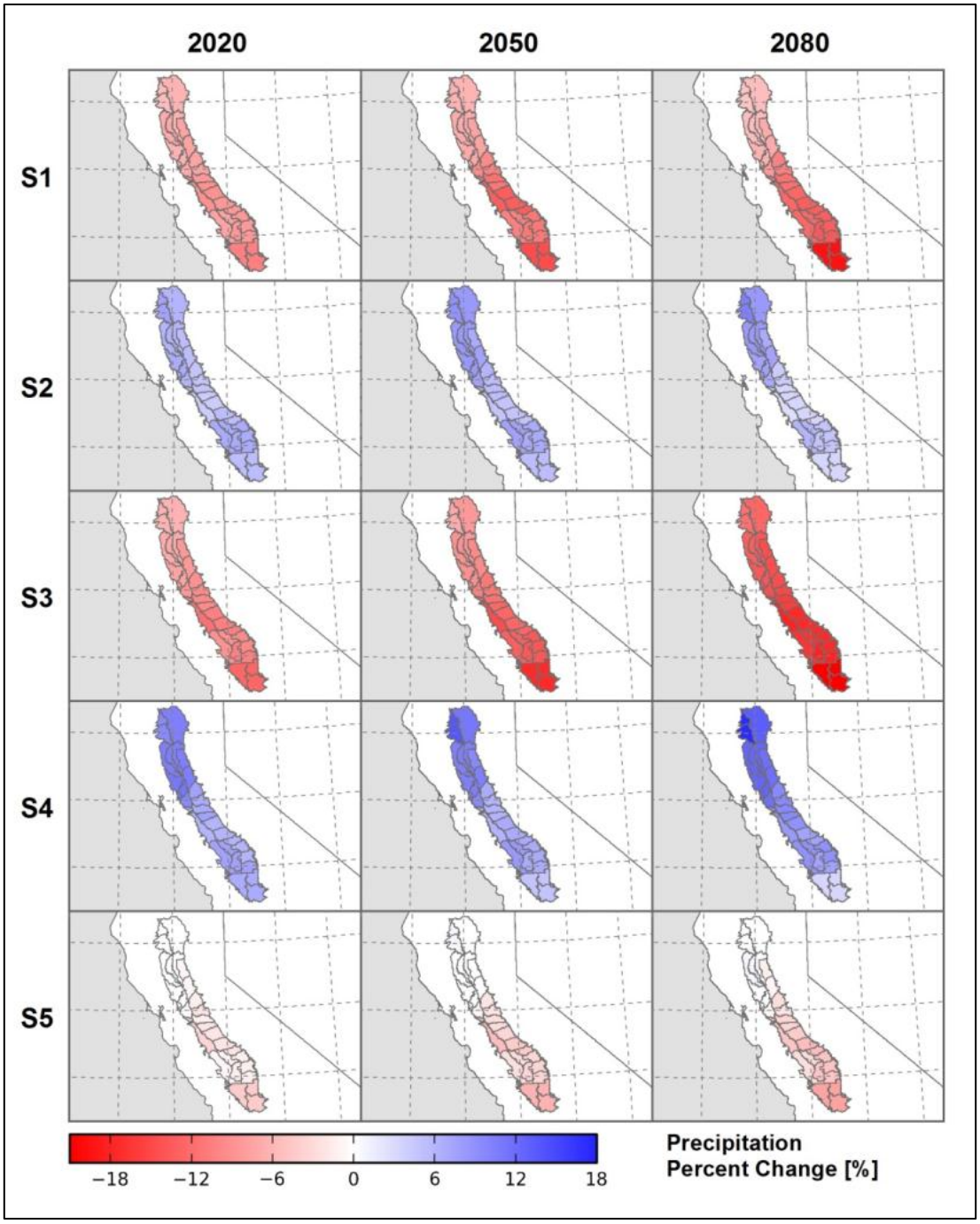

Figure 95.—Sacramento and San Joaquin River Basins – Spatial distribution of projected precipitation percent change for different climate scenarios and time periods (S1 = WD, S2 = WW, S3 = HD, S4 = HW, S5 = Central).

Figure 96 shows the spatial distribution of projected ET_0 percent change for different climate scenarios and time periods. Similar to temperature, the projected percent change in ET_0 is generally spatially uniform for all scenarios, with scenario S3 (hot-dry) having the largest change. Figure 97 illustrates the spatial distribution of projected ET_c percent change for different climate scenarios and time periods, assuming non-static crop phenology for annual crops, where projected future temperatures were used to simulate projected planting, crop coefficient development, and termination as described in section 4.2.1. Spatial differences in the distribution of projected percent change in ET_c are largely due to differences in crop type and baseline ET_c. The most northerly portion of the basin is projected to experience the largest percent change for all projected time periods, due to large acreages of perennial nut and olive orchards. ET_c in the southern portion of the basin is projected to slightly decrease or increase, depending on the scenario. This is largely because significantly more annual variety crops are grown in the south, and they are projected to have earlier planting dates, slightly reduced growing-season lengths due to increased temperatures, and advanced crop coefficient development and harvest dates. Perennial forage crops are primarily grown in the north, and projected to have earlier greenup, longer growing seasons, and therefore a larger percent increase than in other planning areas. Figure 98 shows the spatial distribution of projected ET_c percent change for different climate scenarios and time periods assuming static crop phenology for annual crops. Baseline temperatures were used for simulating projected planting, crop coefficient development, and termination for all future time periods and scenarios as described in section 4.2.1. Under static crop phenology conditions (for annual crops only), the percent change in ET_c generally increases uniformly across the basin for different time periods, with the exception of one planning area near Lodi, CA, where perennial grass hay and grapes make up over 50 percent of the acreage. Those crops are simulated to greenup earlier and have earlier harvest and reduced K_{cb} thereafter (grass hay) and earlier senescence (grapes).

The spatial distribution of projected percent change in NIWR for different climate scenarios and time periods is shown on figures 99 and 100. The NIWR incorporates growing-season and non-growing-season soil moisture gains and losses from precipitation, bare soil evaporation, and ET. Therefore, spatial variations in the distribution of NIWR percent change for different time periods and scenarios are a function of respective ET_c (figures 97 and 98) and precipitation (figure 95) distributions. For example, throughout the valley precipitation is projected to decrease under scenario S3 (hot dry) but to increase under scenario S4 (hot wet). This results in S4 NIWR increasing less than S3 NIWR, even though S3 and S4 ET_c changes are nearly identical. For more illustrations on unit changes (degrees F and inches) in spatial projections of mean temperature, precipitation, ET_0, ET_c, and NIWR for different time periods and scenarios, see appendix 9.

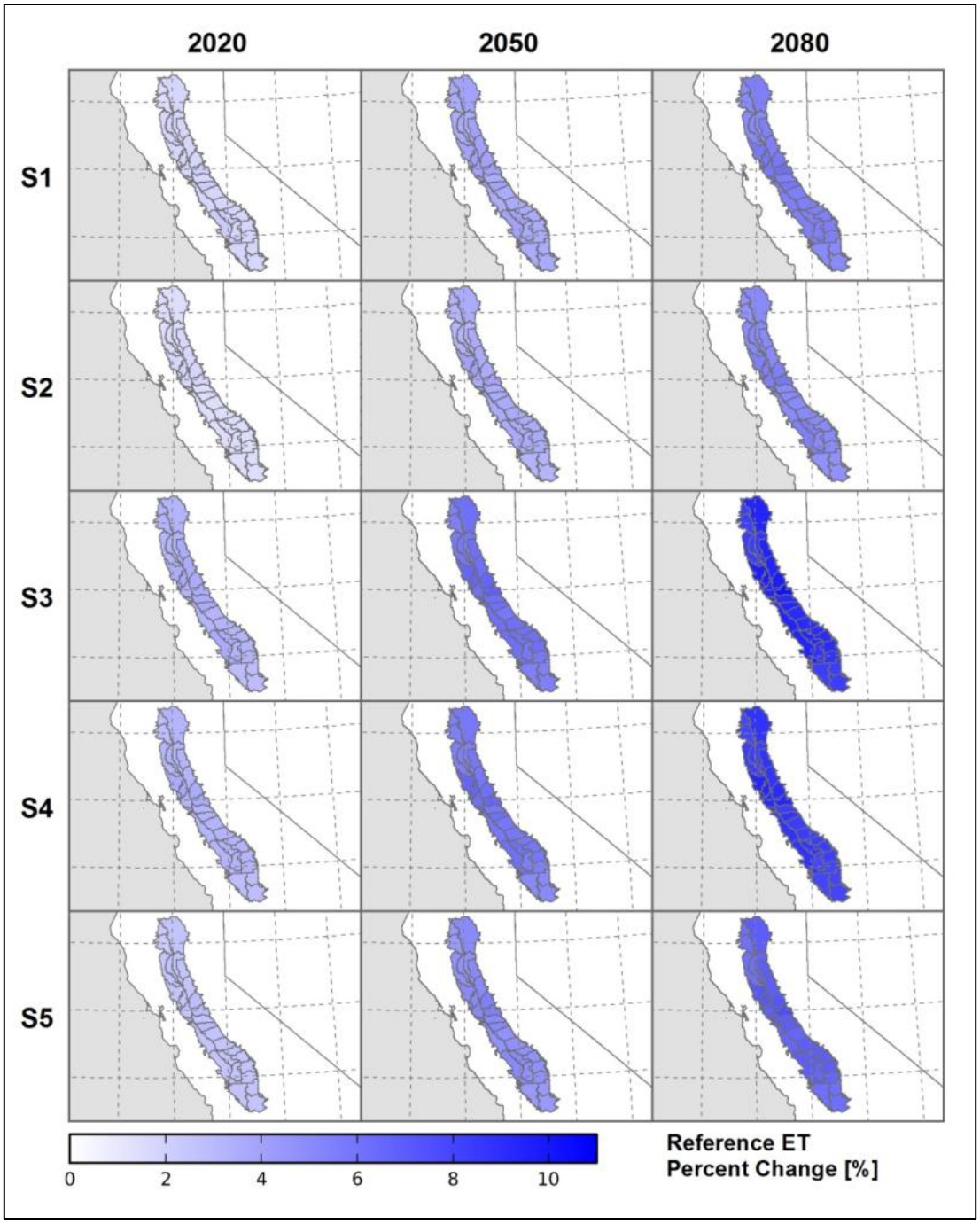

Figure 96.—Sacramento and San Joaquin River Basins – Spatial distribution of projected reference evapotranspiration percent change for different climate scenarios and time periods (S1 = WD, S2 = WW, S3 = HD, S4 = HW, S5 = Central).

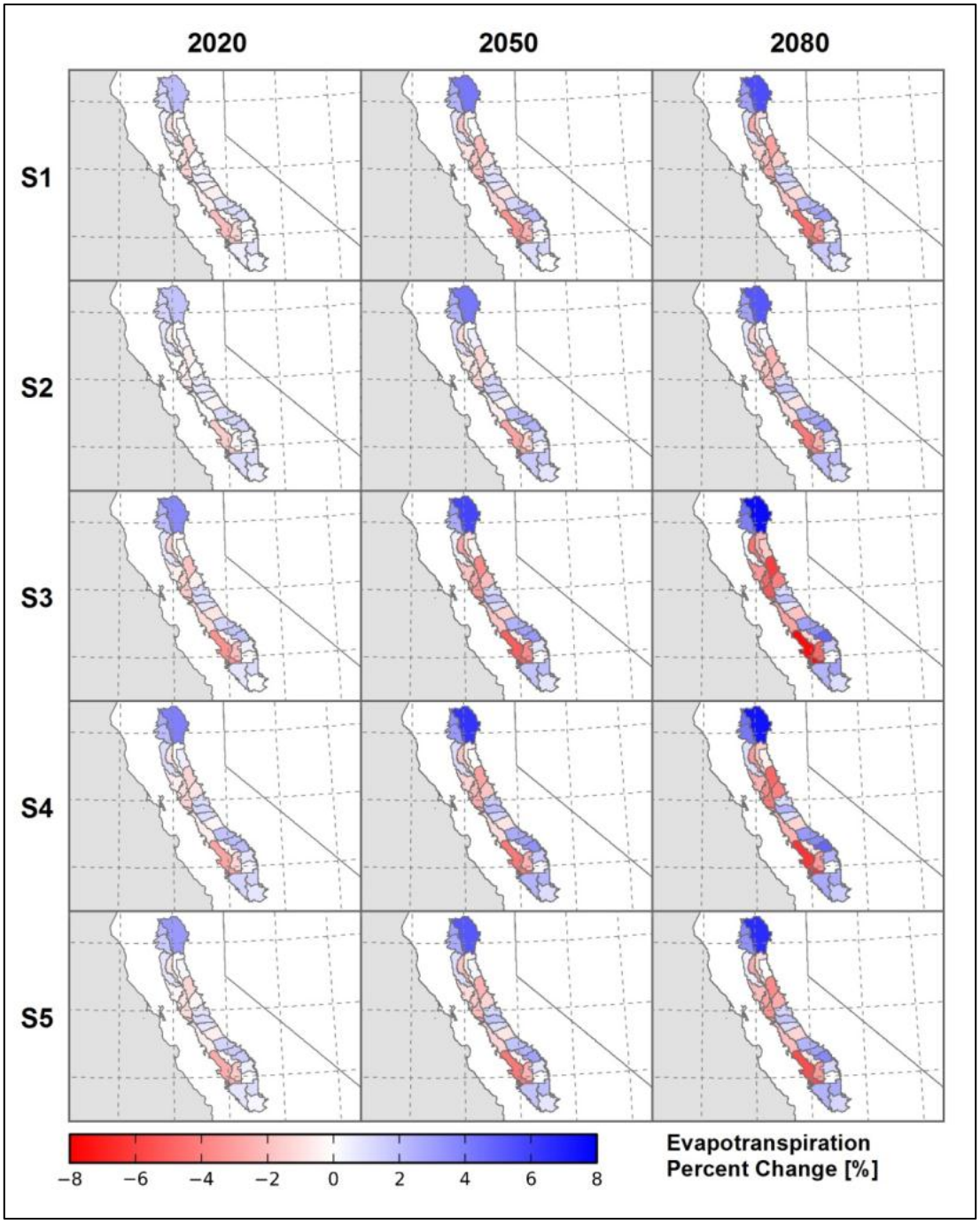

Figure 97.—Sacramento and San Joaquin River Basins – Spatial distribution of projected crop evapotranspiration percent change for different climate scenarios and time periods (S1 = WD, S2 = WW, S3 = HD, S4 = HW, S5 = Central).

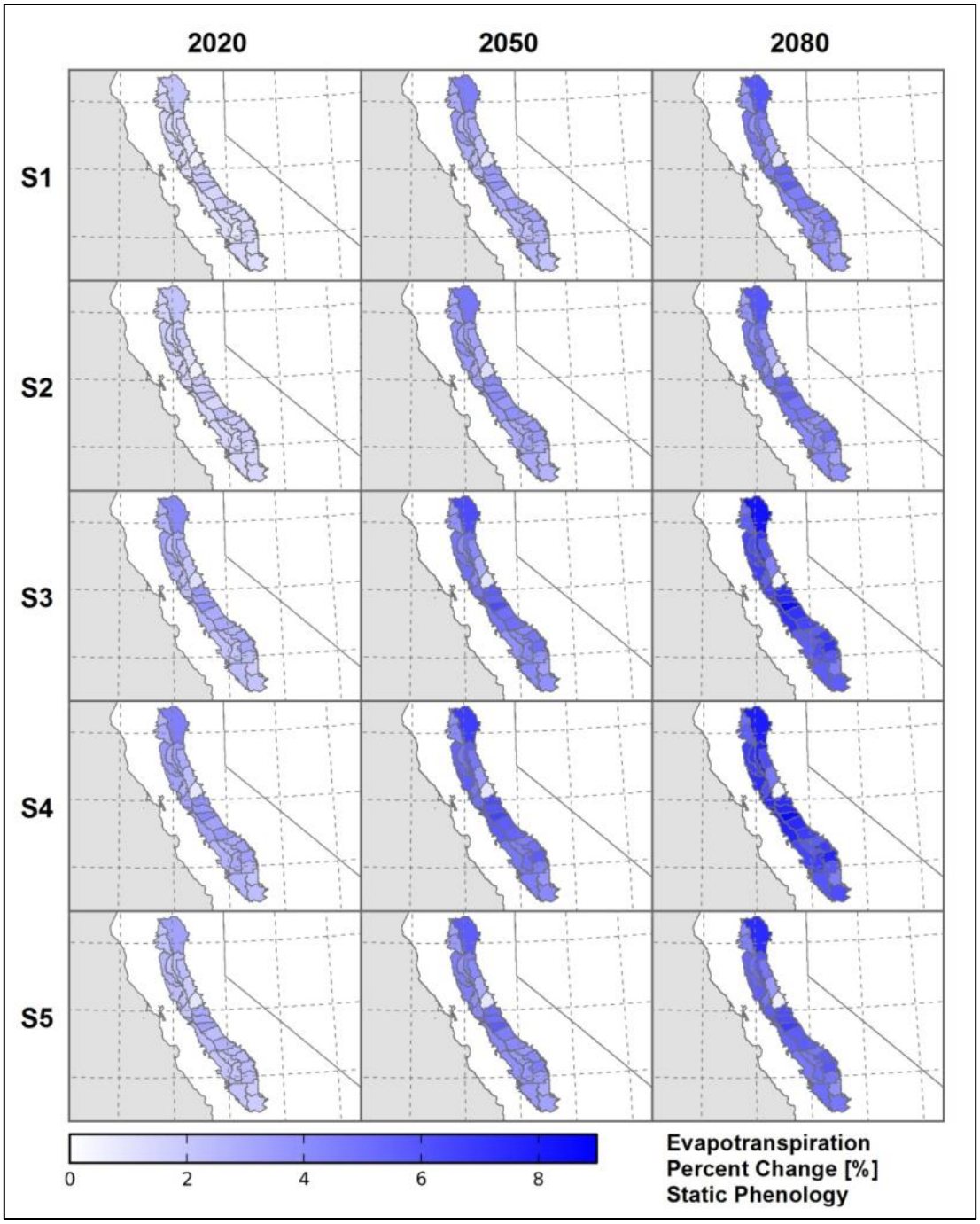

Figure 98.—Sacramento and San Joaquin River Basins – Spatial distribution of projected crop evapotranspiration percent change for different climate scenarios and time periods assuming static phenology for annual crops (S1 = WD, S2 = WW, S3 = HD, S4 = HW, S5 = Central).

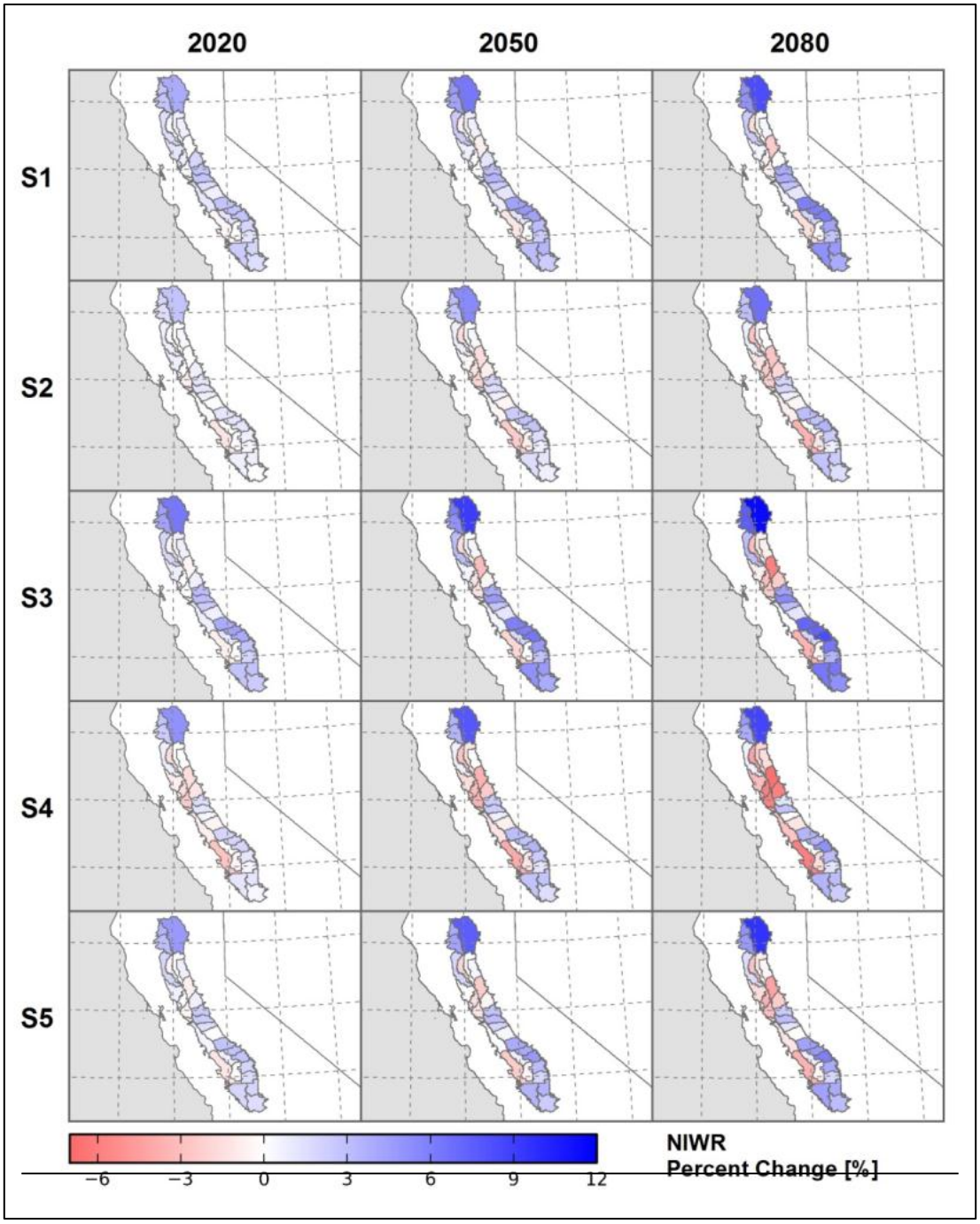

Figure 99.—Sacramento and San Joaquin River Basins – Spatial distribution of projected net irrigation water requirements (NIWR) percent change for different climate scenarios and time periods (S1 = WD, S2 = WW, S3 = HD, S4 = HW, S5 = Central).

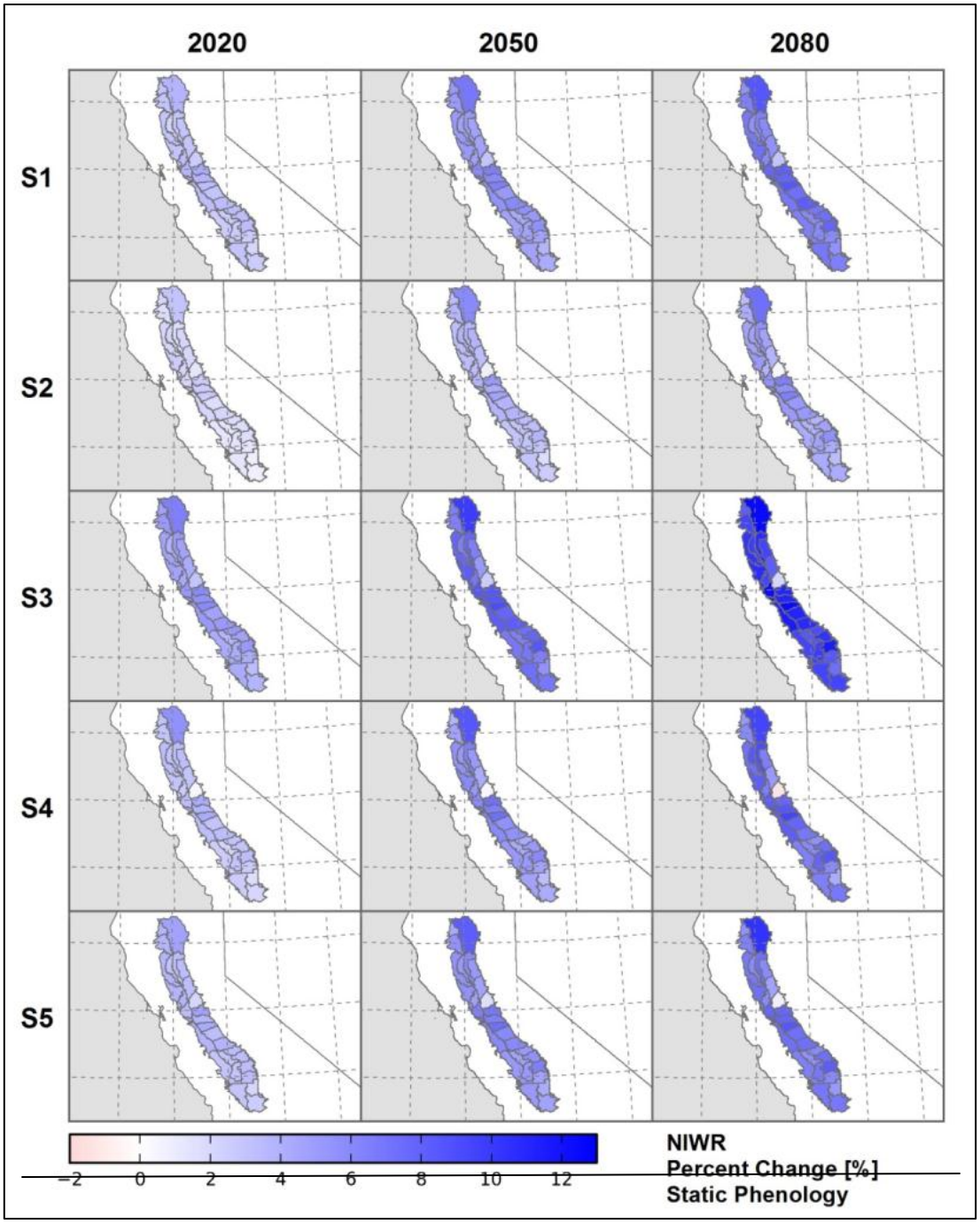

Figure 100.—Sacramento and San Joaquin River Basins – Spatial distribution of projected net irrigation water requirements (NIWR) percent change for different climate scenarios and time periods assuming static phenology for annual crops (S1 = WD, S2 = WW, S3 = HD, S4 = HW, S5 = Central).

Figures 101, 102, and 103 illustrate the baseline and projected temporal distribution of mean daily ET_c for selected Met Nodes, crops, scenarios, and time periods. The simulated mean daily ET_c of alfalfa for the 2020 time period, NWS/COOP Met Node CA2294 (Davis 2WSW Exp. Farm), shows slight but noticeable shifts in the growing-season length and alfalfa cutting cycles relative to baseline conditions (figure 101, left). By the 2080 time period (figure 101, right) significant shifts in growing-season length, crop development, and cutting cycles are noticeable relative to baseline conditions, with scenarios S3 and S4 exhibiting the most extreme changes. Figure 102 shows simulated mean daily ET_c of field corn at Met Node CA2294, under different scenarios, for the 2020 and 2080 time periods. Because planting dates for annual crops are temperature dependent in the non-static phenology simulations, shifts in planting, development, and harvest dates of spring grain are clearly evident, especially by the 2080 time period. The uncertainty in such potential shifts in planting dates, accelerated crop development, and harvest was a primary reason for using baseline temperatures for static phenology simulations (figures 98 and 100). In static phenology simulations, because baseline temperatures are used for estimating planting, crop development, and harvest dates, all scenarios and time periods have identical seasonal K_{cb} shapes, and show differences only in daily ET_c magnitudes due to daily ET_0 and precipitation differences. Figure 103 illustrates simulated mean daily ET_c of nuts at Met Node CA2294 for different scenarios and time periods. Simulated seasonal changes in greenup, development, and senescence are evident in Figure 103, with S3 and S4 exhibiting the most extreme seasonal changes.

5.7.2 Baseline and Projected Open-Water Evaporation

Figures 104 and 105 illustrate baseline and projected annual precipitation (top left), annual mean temperature (top right), annual evaporation (bottom left), and annual net evaporation (bottom right) at Lake Shasta and Millerton Lake. The heavy black line for each variable is the annual time series of 50 percentile values (i.e., ensemble-median). The shaded area for each variable is the annual time series of 5^{th} to 95^{th} percentiles. Annual median precipitation over Lake Shasta and Millerton Lake is projected to decline slightly over the transient period going out to 2099. The uncertainty envelope for annual precipitation is fairly large for both reservoirs, and shows no significant trend over time, implying that there is no increase or decrease in the uncertainty from the present. The mean annual temperature and annual evaporation both show increasing trends and a diverging uncertainty envelope over time for both reservoirs. The ensemble-median and uncertainty envelopes for net evaporation (i.e., evaporation minus precipitation) are affected by characteristics of both precipitation and temperature projections. It is evident, for instance, that the upper uncertainty bound in precipitation causes the lower bound of net evaporation to be highly variable, while the diverging uncertainty envelope is caused primarily by the diverging temperature projections.

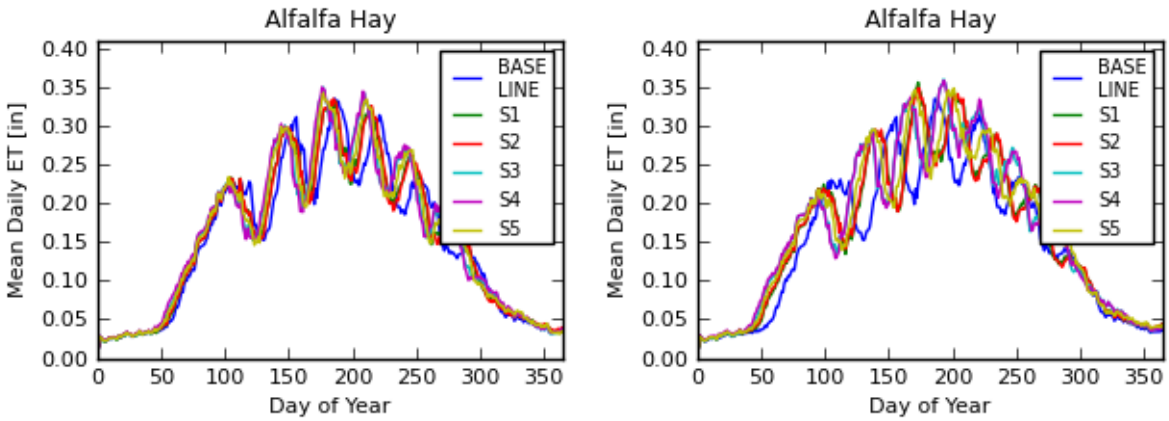

Figure 101.—Sacramento and San Joaquin River Basins – COOP station CA2294 (Davis 2WSW Exp. Farm). Baseline and projected mean daily alfalfa evapo-transpiration for all scenarios and for time periods 2020 (left) and 2080 (right).

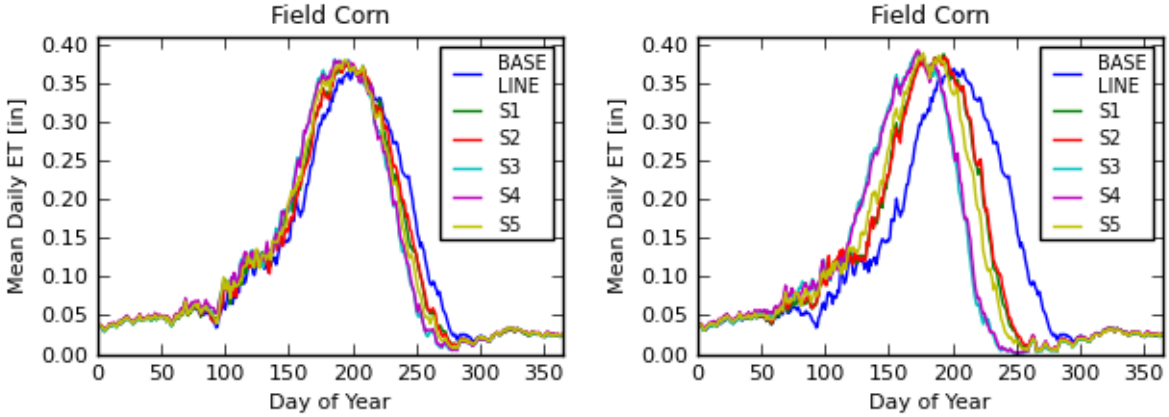

Figure 102.—Sacramento and San Joaquin River Basins – COOP station CA2294 (Davis 2WSW Exp. Farm). Baseline and projected mean daily field corn evapo-transpiration for all scenarios and for time periods 2020 (left) and 2080 (right).

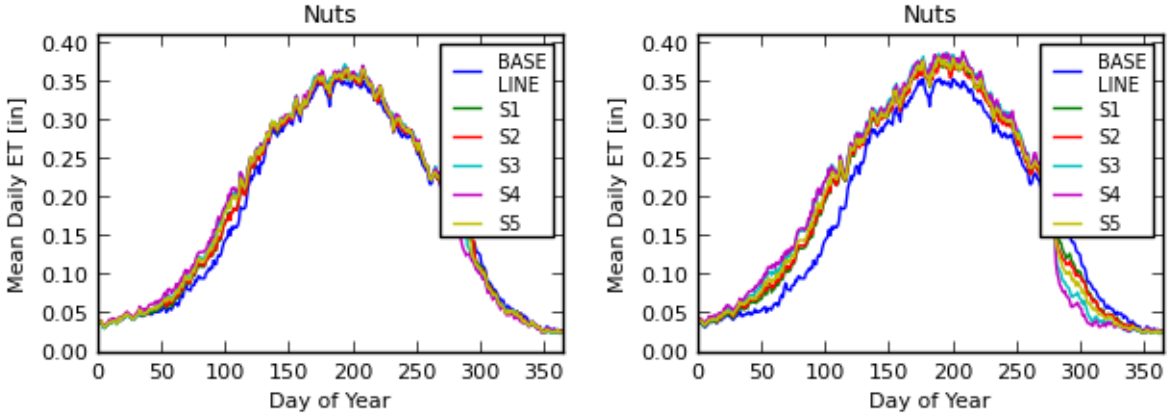

Figure 103.—Sacramento and San Joaquin River Basins – COOP station CA2294 (Davis 2WSW Exp. Farm). Baseline and projected mean daily evapotranspiration from nut trees for all scenarios and for time periods 2020 (left) and 2080 (right).

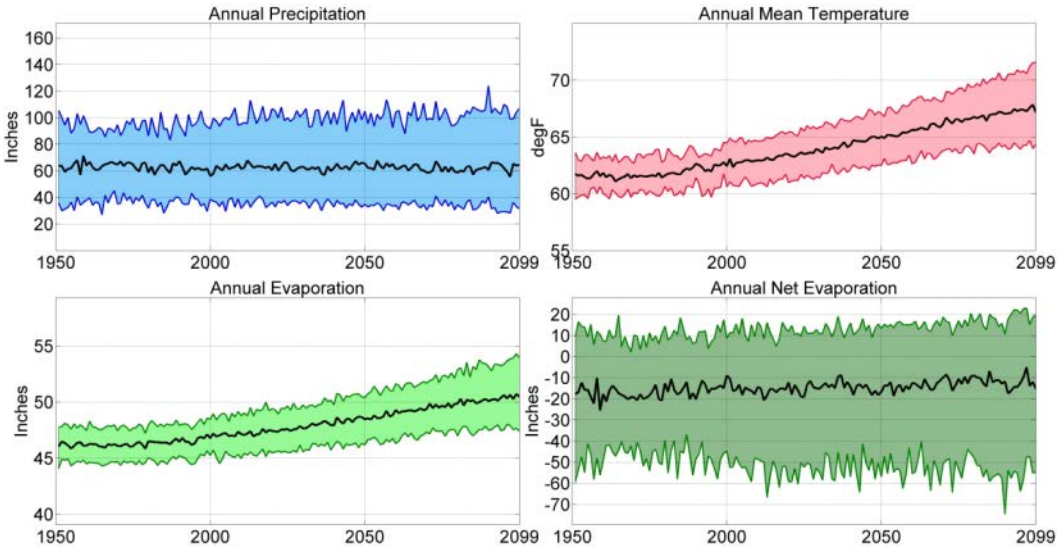

Figure 104.—Sacramento and San Joaquin River Basins – Lake Shasta ensemble median and 5th and 95th percentile annual precipitation, temperature, reservoir evaporation, and net evaporation.

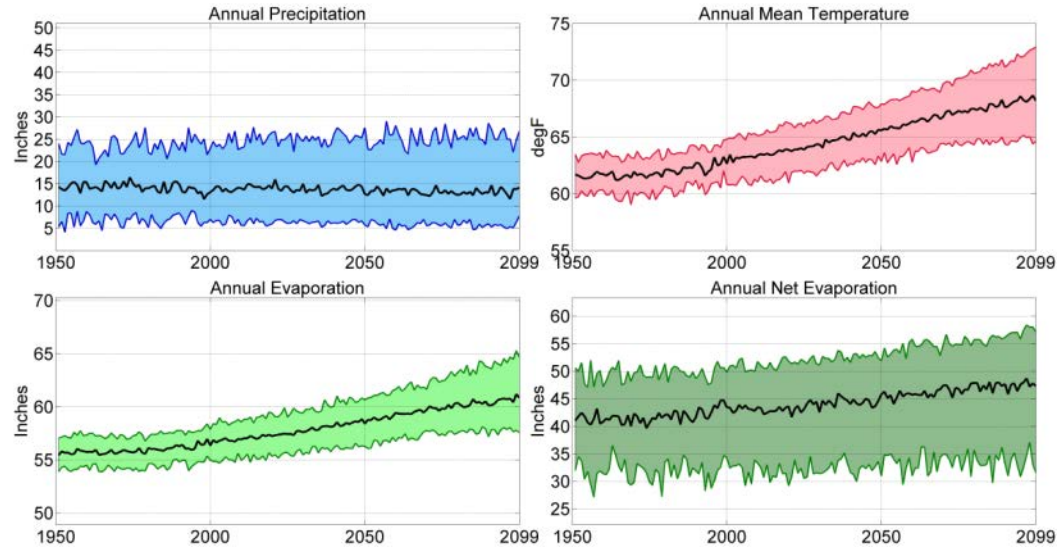

Figure 105.—Sacramento and San Joaquin River Basins – Millerton Lake ensemble median and 5th and 95th percentile annual precipitation, temperature, reservoir evaporation, and net evaporation.

In Figures 106 and 107, representing Lake Shasta and Millerton Lake, respectively, the solid lines show the ensemble-median mean monthly evaporation and net evaporation for the baseline period (1950–1999) and for the 2020s, 2050s, and 2080s, and the shaded areas show the decadal spread of mean monthly evaporation and net evaporation for the baseline period (gray shading) and 2080s (magenta shading), where the spread is bound by the ensemble's 5th to 95th percentile values for each month. The simulated impact of increasing heat storage during spring and early summer on delaying the availability of energy to evaporation is clearly evident, as the peak evaporation occurs in August and

September, and the minimum evaporation occurs between February and April. The magnitude of projected monthly evaporation and net evaporation increase is greatest during the summer months and least during the fall and winter months. The change in annual evaporation and net evaporation from the baseline to the 2080 time period is 7.6 and 14.7 percent (3.5 and 2.5 in) for Lake Shasta, and 7.7 and 12.3 percent (4.3 and 5.0 in) for Millerton Lake, respectively (appendix 10).

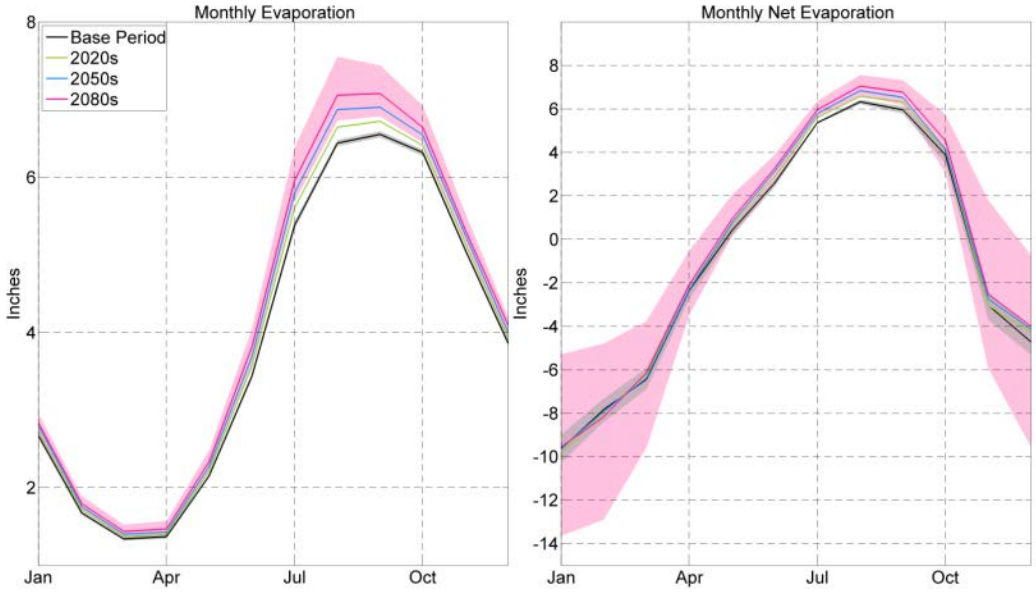

Figure 106.—Sacramento and San Joaquin River Basins – Lake Shasta mean monthly ensemble median and 5th and 95th percentile reservoir evaporation and net evaporation.

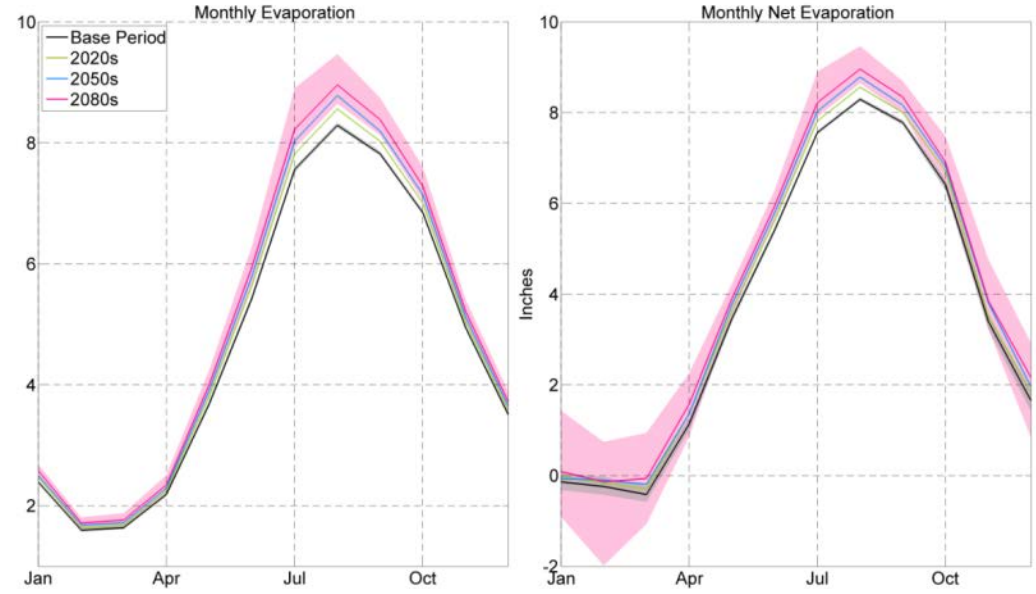

Figure 107.—Sacramento and San Joaquin River Basins – Millerton Lake mean monthly ensemble median and 5th and 95th percentile reservoir evaporation and net evaporation.

5.8 Truckee and Carson River Basins

5.8.1 Baseline and Projected Irrigation Water Demands

Figure 108 illustrates COOP station based Met Nodes that were used to estimate irrigation water demands, as well as HUC8 boundaries used to upscale Met Node estimates in the Truckee and Carson Basins. Figure 109 illustrates the spatial distribution of baseline (1950–1999) mean annual temperature (top left) and mean annual precipitation (top right) derived from BCSD data (discussed in section 3.2), mean annual dewpoint depression (bottom left) and mean annual windspeed (bottom right) estimated from historical agricultural weather data (discussed in section 4.2.1). Figure 109 illustrates cool to warm mean annual temperatures ranging from cool in the west-southwest to warm in the northeast. Precipitation varies from moderately high in the southwest-central part of the basin to low amounts in the northeast. The mean annual dewpoint depression (i.e., $T_{min} - T_{dew}$) is used here as a simple approximation of the humidity of the lower air mass that is consistent and representative of agricultural areas while preserving regional and local advection effects. Its spatial distribution clearly shows that eastern areas are more arid and western areas are more humid. The mean annual windspeeds are generally lower in southern and eastern area, and higher in the northeastern and northwestern portions of the basin. Figure 110 illustrates reference ET (ET_0) (top left), crop evapotranspiration (ET_c) (top right), net irrigation water requirement (NIWR) (bottom left), and total crop acreage (bottom right) within each HUC8 boundary. ET_0, ET_c, and NIWR range from about 44 to 56, 37 to 49, and 28 to 42 in/yr, respectively, with higher rates occurring in the north and eastern portions of the basin where air temperature, solar radiation, and dewpoint depression are significantly larger relative to the south and western portions of the basin. The projected values range from about 44 to 56 in/yr for ET_0, 37 to 49 in/yr for ET_c, and 28 to 42 in/yr for NIWR.

Figure 111 shows the spatial distribution of projected mean temperature change for different climate scenarios and time periods, and it is evident that the changes shown there are greatest for the Pyramid Lake, Middle Carson, and Fallon area HUCs, with scenario S3 (hot-dry) having the largest change. Figure 112 illustrates the spatial distribution of projected precipitation percent change for different scenarios and time periods. Depending on the scenario, precipitation percent changes range from about –19 to 20 percent for the 2080 time period, with the ensemble median scenario (S5) generally showing a slight decrease in the western portion of the basin, with more significant declines in the eastern and northern portions of the basin.

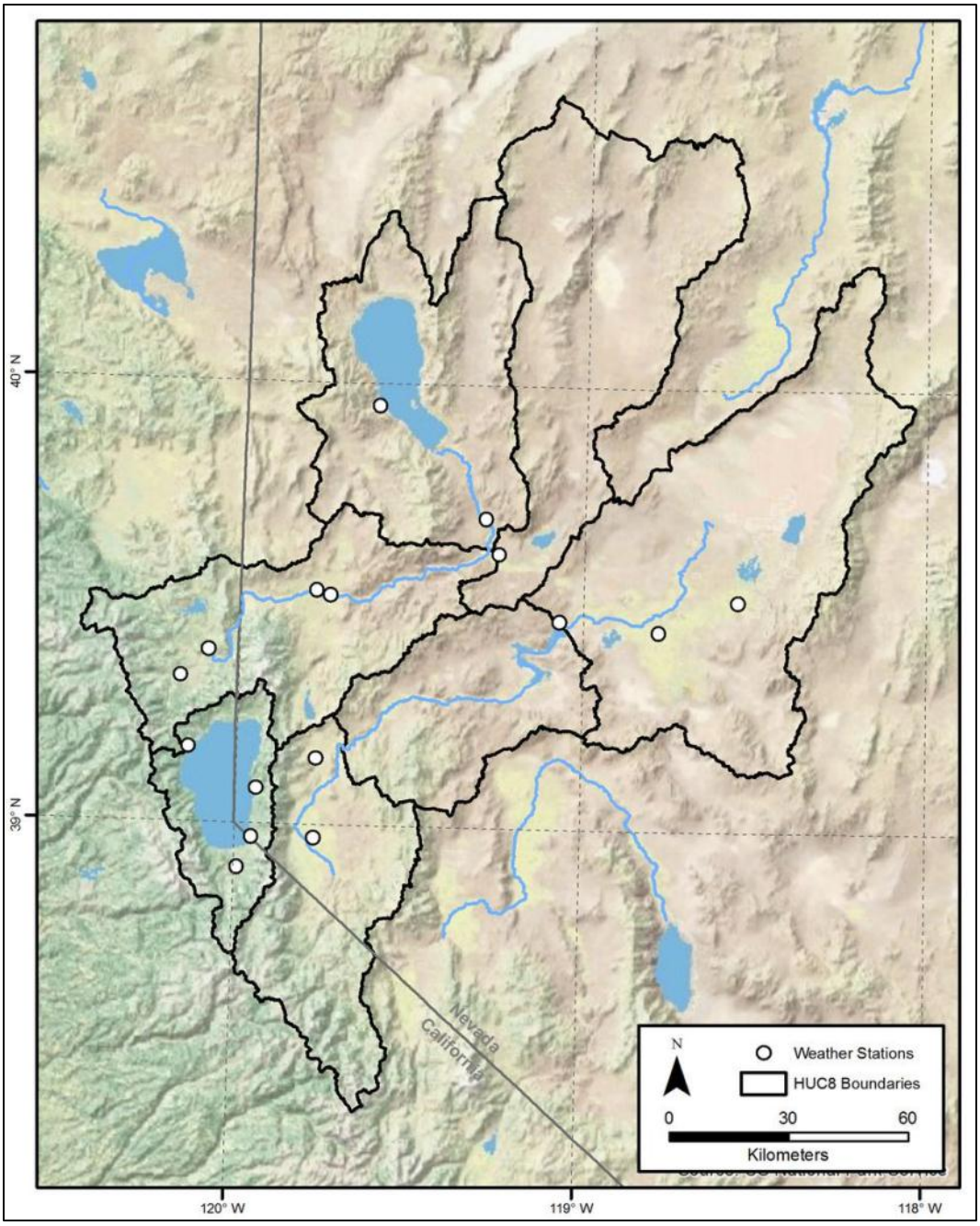

Figure 108.—Truckee and Carson River Basins – COOP stations used to simulate baseline and projected irrigation demands.

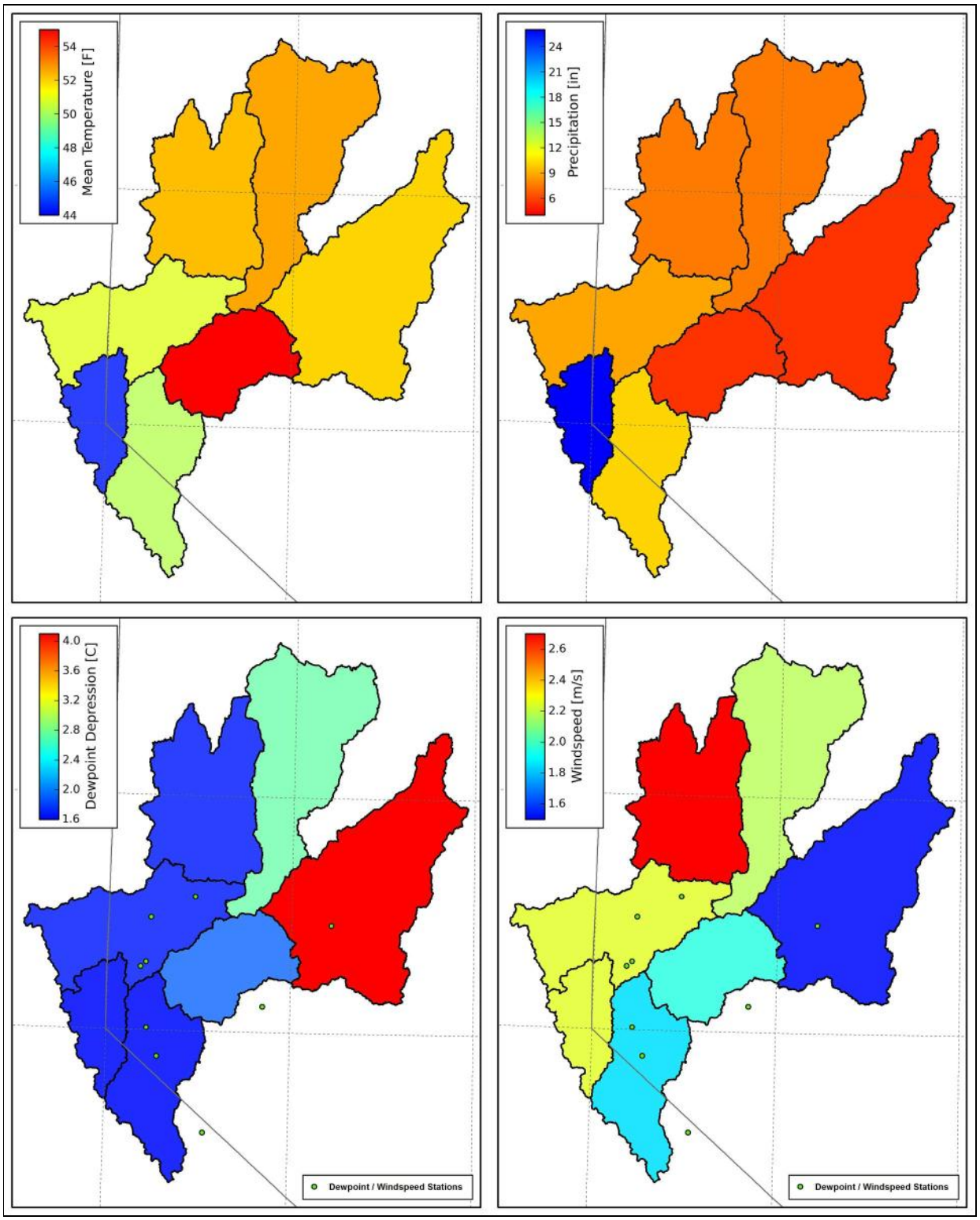

Figure 109.—Truckee and Carson River Basins – Spatial distribution of baseline temperature, precipitation, dewpoint depression, and windspeed.

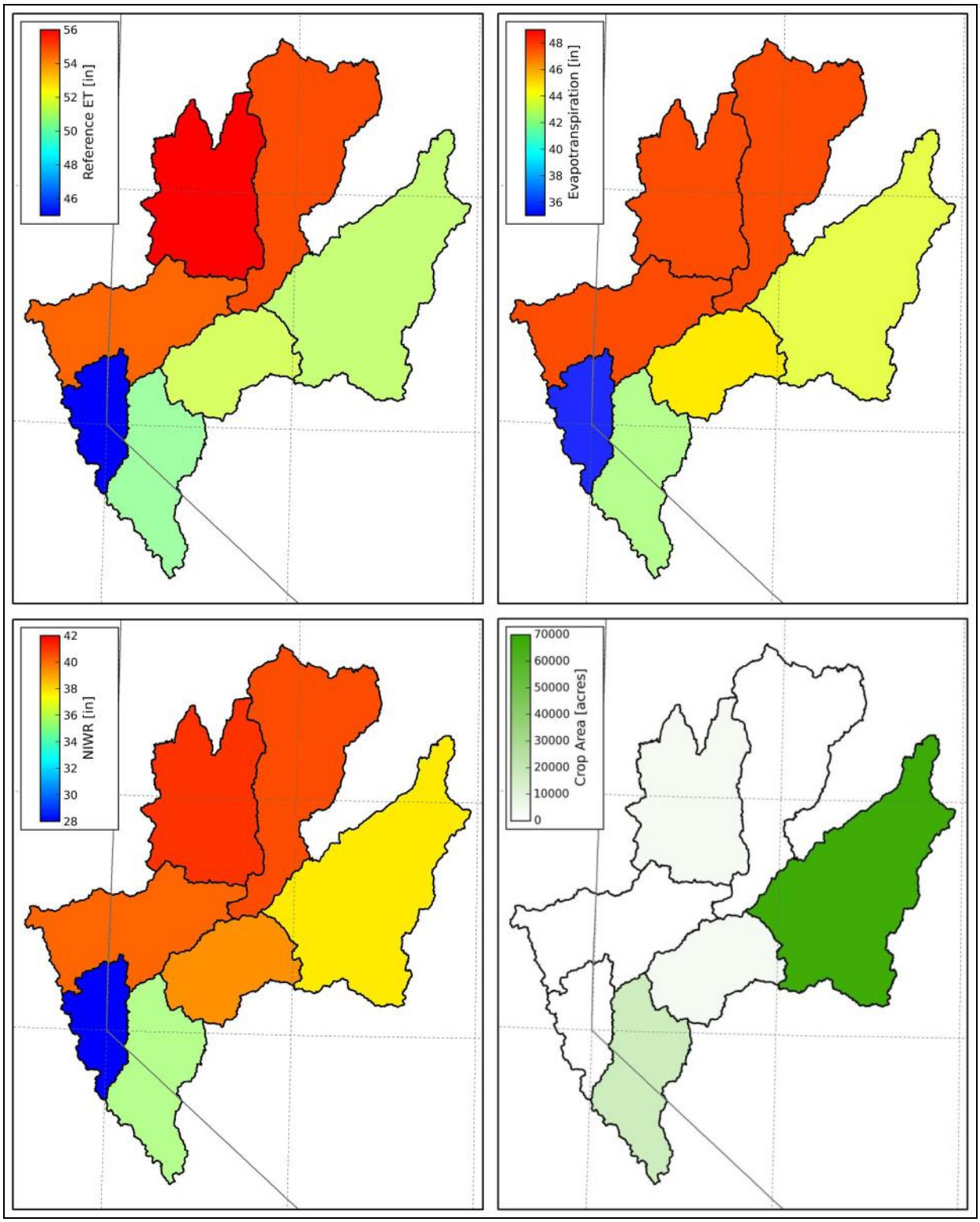

Figure 110.—Truckee and Carson River Basins – Spatial distribution of baseline reference evapotranspiration, crop evapotranspiration, net irrigation water requirements (NIWR), and crop acreage.

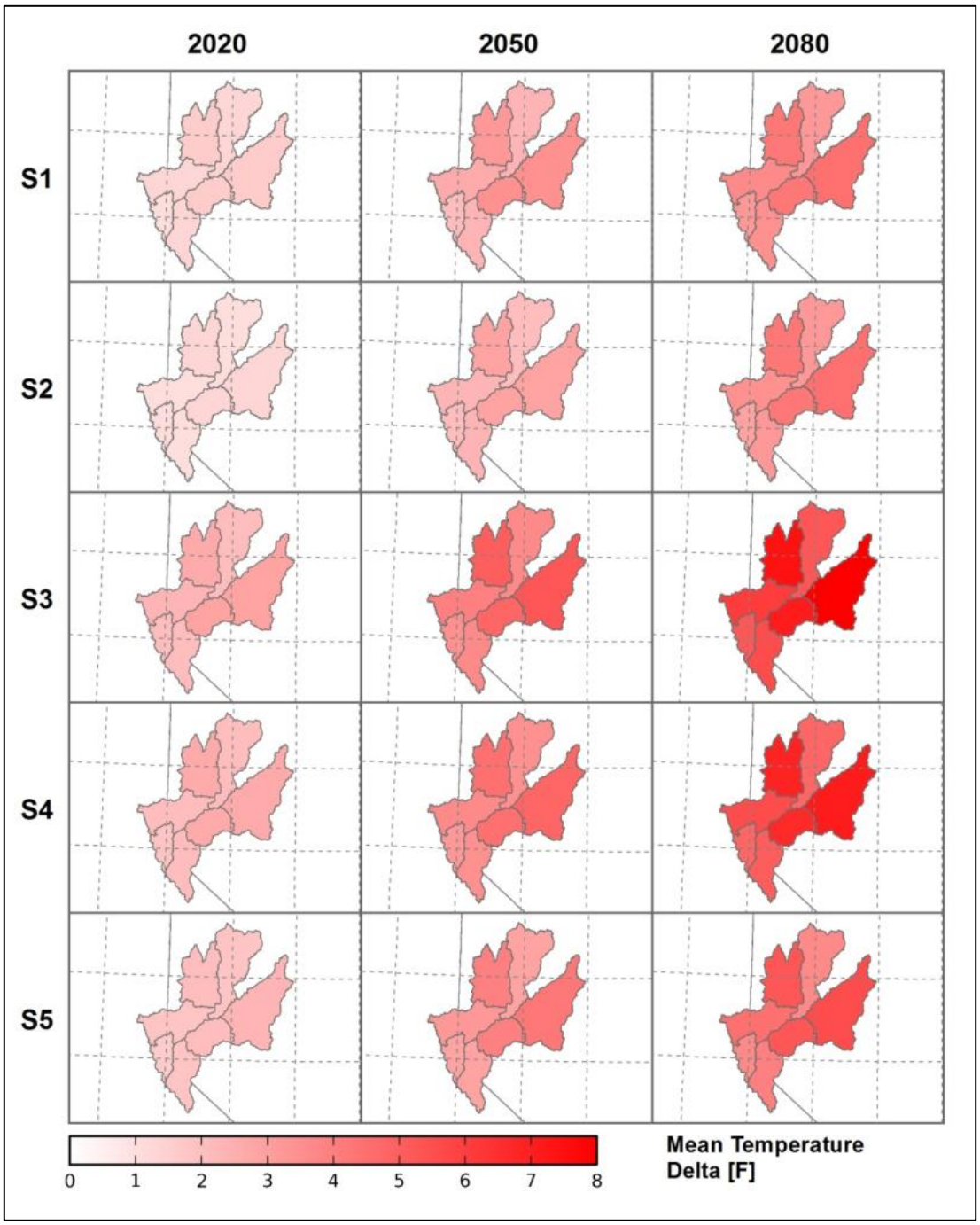

Figure 111.—Truckee and Carson River Basins – Spatial distribution of temperature change for different climate scenarios and time periods (S1 = WD, S2 = WW, S3 = HD, S4 = HW, S5 = Central).

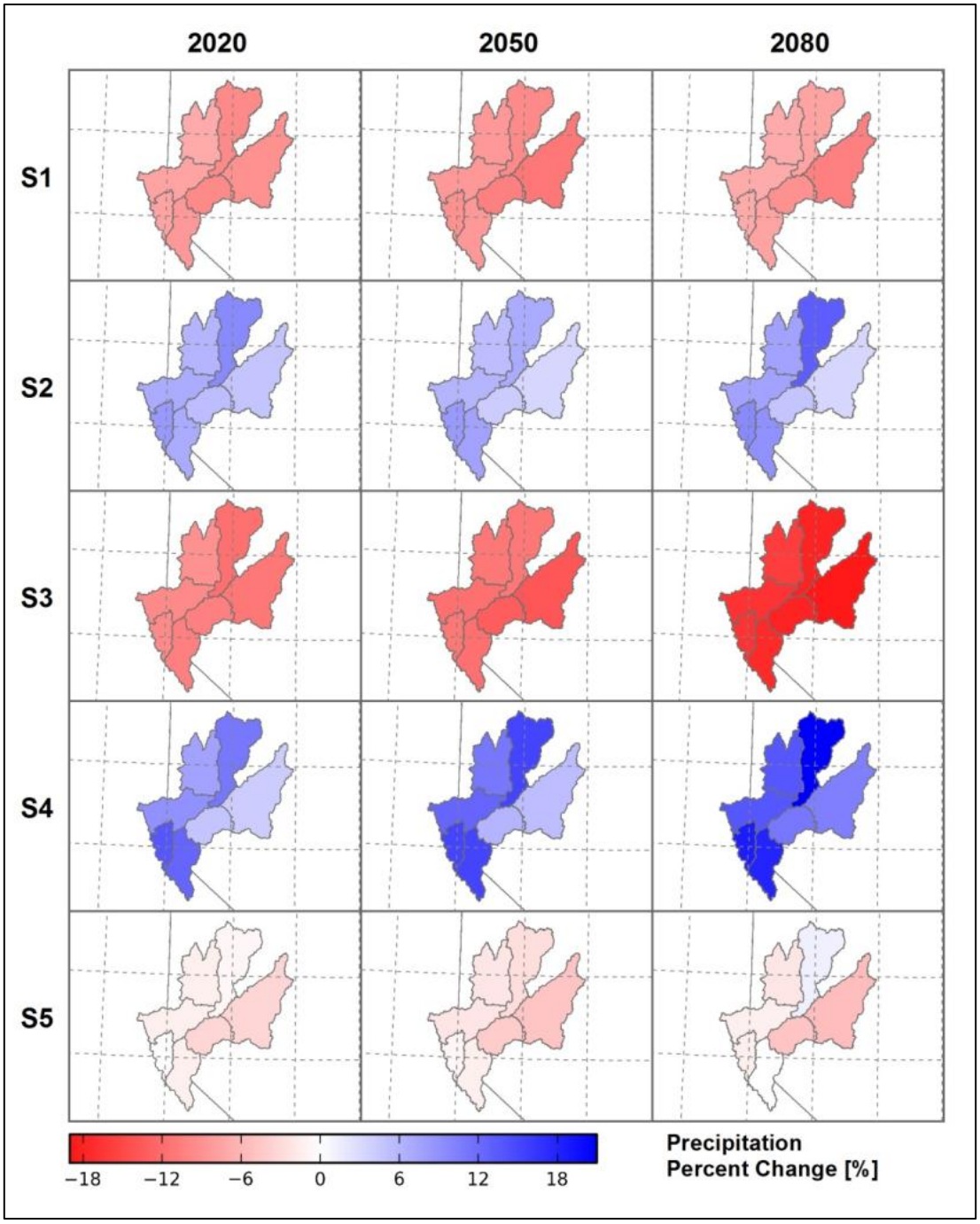

Figure 112.—Truckee and Carson River Basins – Spatial distribution of projected precipitation percent change for different climate scenarios and time periods (S1 = WD, S2 = WW, S3 = HD, S4 = HW, S5 = Central).

Figure 113 shows the spatial distribution of projected ET_0 percent change for different climate scenarios and time periods. Similar to temperature, the projected percent change in ET_0 is generally spatially uniform for all scenarios, with scenario S3 having the largest change. Figure 114 illustrates the spatial distribution of projected ET_c percent change for different climate scenarios and time periods assuming non-static crop phenology for annual crops, where projected future temperatures were used for simulating projected planting, crop coefficient development, and termination as described in section 4.2.1. Spatial differences in the distribution of projected percent change in ET_c are largely due to differences in crop type and baseline ET_c. The Tahoe basin is projected to experience the largest percent change for all projected time periods, largely due to the fact that the difference between the projected and baseline ET_c is fairly large relative to the baseline estimate of ET_c (figure 110). Perennial forage crops are primarily grown in the Truckee and Carson River Basins, and are projected to have earlier greenup, longer harvest periods, and later killing frosts, leading to longer growing seasons and fairly significant increases in ET_c relative to baseline ET_c by 2080. Figure 115 shows the spatial distribution of projected ET_c percent change for different climate scenarios and time periods assuming static crop phenology for annual crops. Baseline temperatures were used for simulating projected planting, crop coefficient development, and termination for all future time periods and scenarios as described in section 4.2.1. Results are nearly identical to non-static phenology results (figure 114) due to the fact that over 80 percent of the crop area is alfalfa and pasture grass.

The spatial distribution of projected NIWR percent change for different climate scenarios and time periods is shown on figures 116 and 117. The NIWR incorporates growing-season and non-growing-season soil moisture gains and losses from precipitation, bare soil evaporation, and ET. Therefore, spatial variations in the distribution of NIWR percent change for different time periods and scenarios are a function of respective ET_c (figures 114 and 115) and precipitation (figure 112) distributions. For example, under the S3 (hotter drier) scenario, precipitation is projected to decrease whereas under S4 (hotter wetter), precipitation is projected to increase. This results in S4 NIWR increasing less than S3 NIWR, even though S3 and S4 ET_c changes are nearly identical. For more illustrations on unit changes (degrees F and inches) in spatial projections of mean temperature, precipitation, ET_0, ET_c, and NIWR for different time periods and scenarios, see appendix 9.

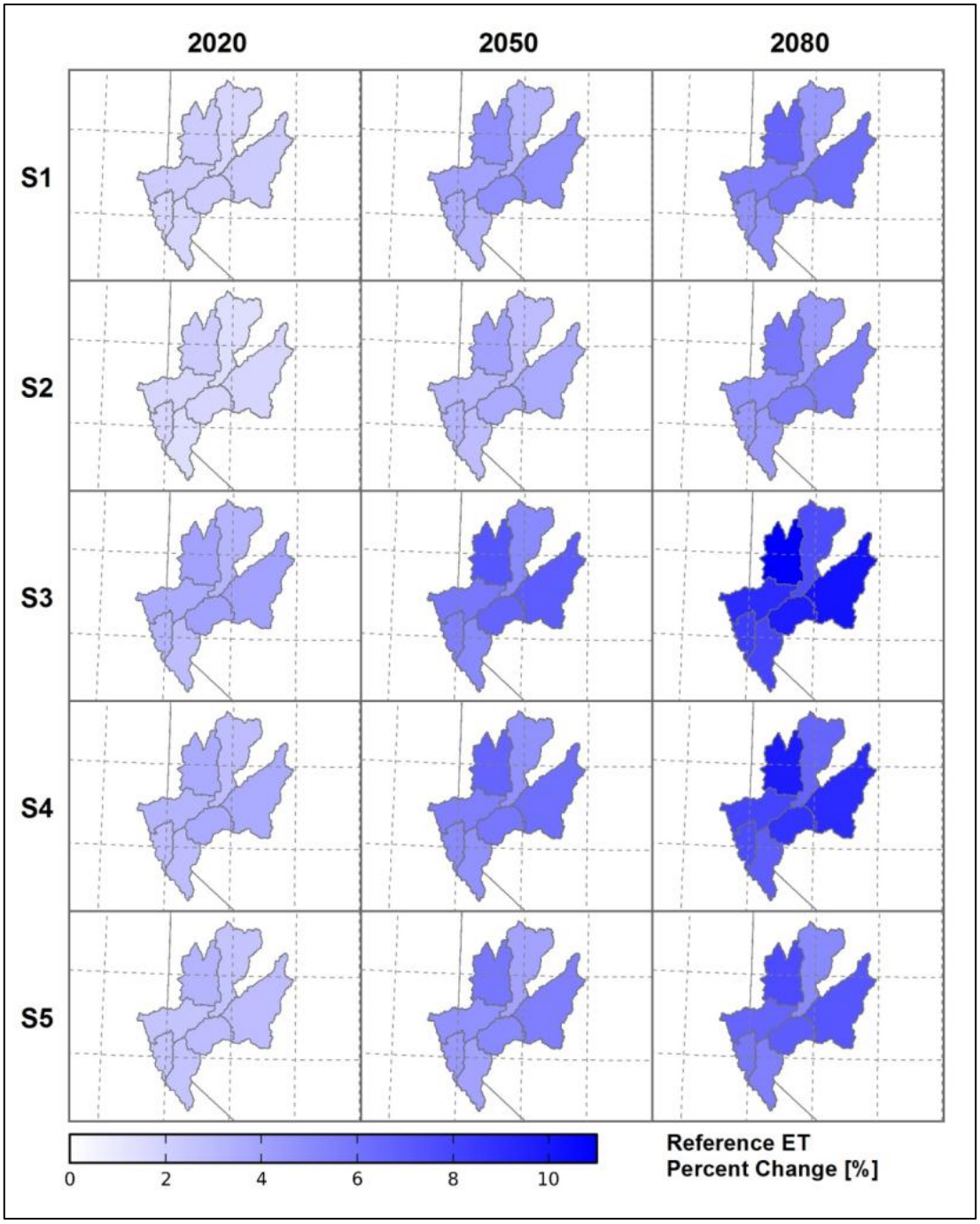

Figure 113.—Truckee and Carson River Basins – Spatial distribution of projected reference evapotranspiration percent change for different climate scenarios and time periods (S1 = WD, S2 = WW, S3 = HD, S4 = HW, S5 = Central).

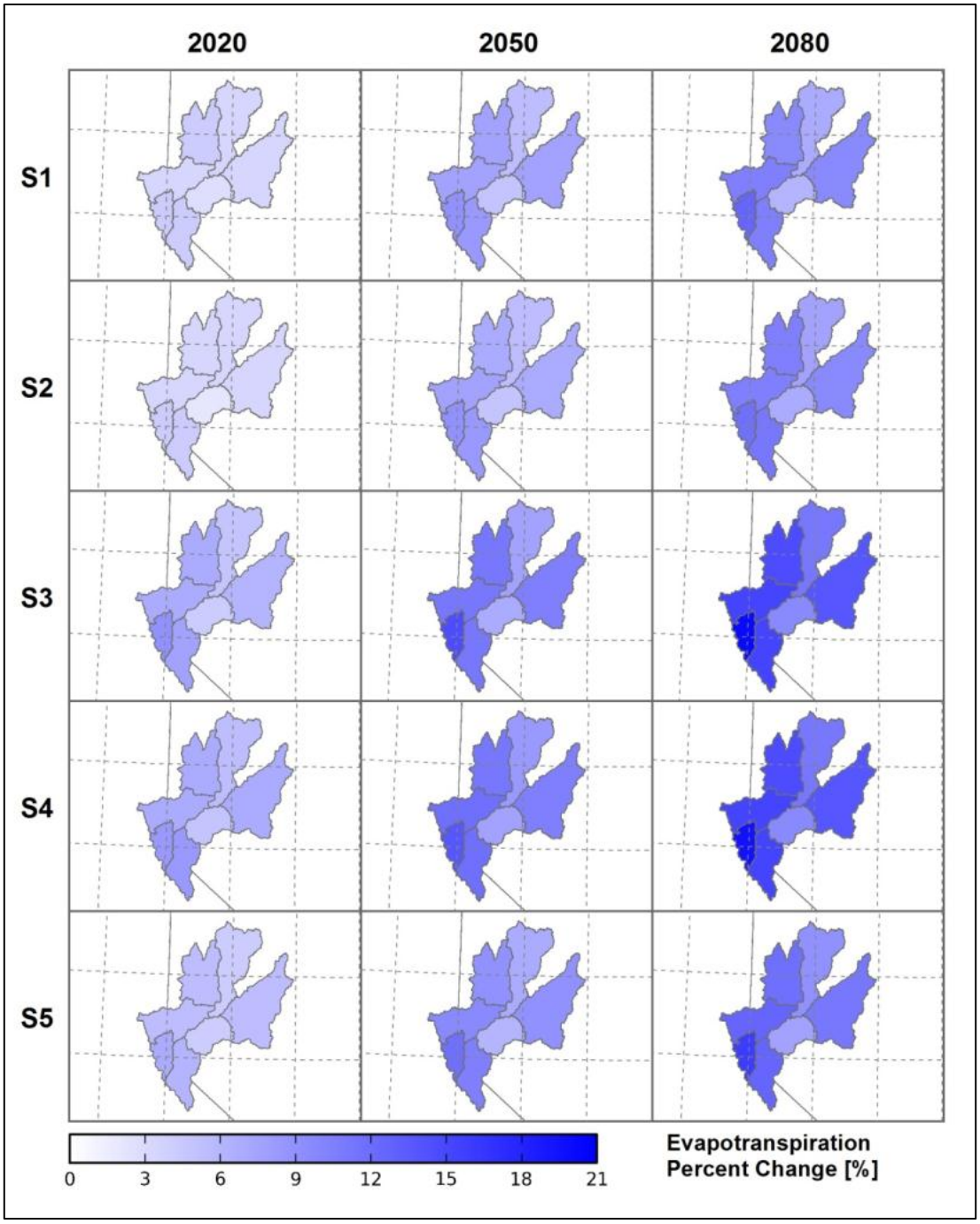

Figure 114.—Truckee and Carson River Basins – Spatial distribution of projected crop evapotranspiration percent change for different climate scenarios and time periods (S1 = WD, S2 = WW, S3 = HD, S4 = HW, S5 = Central).

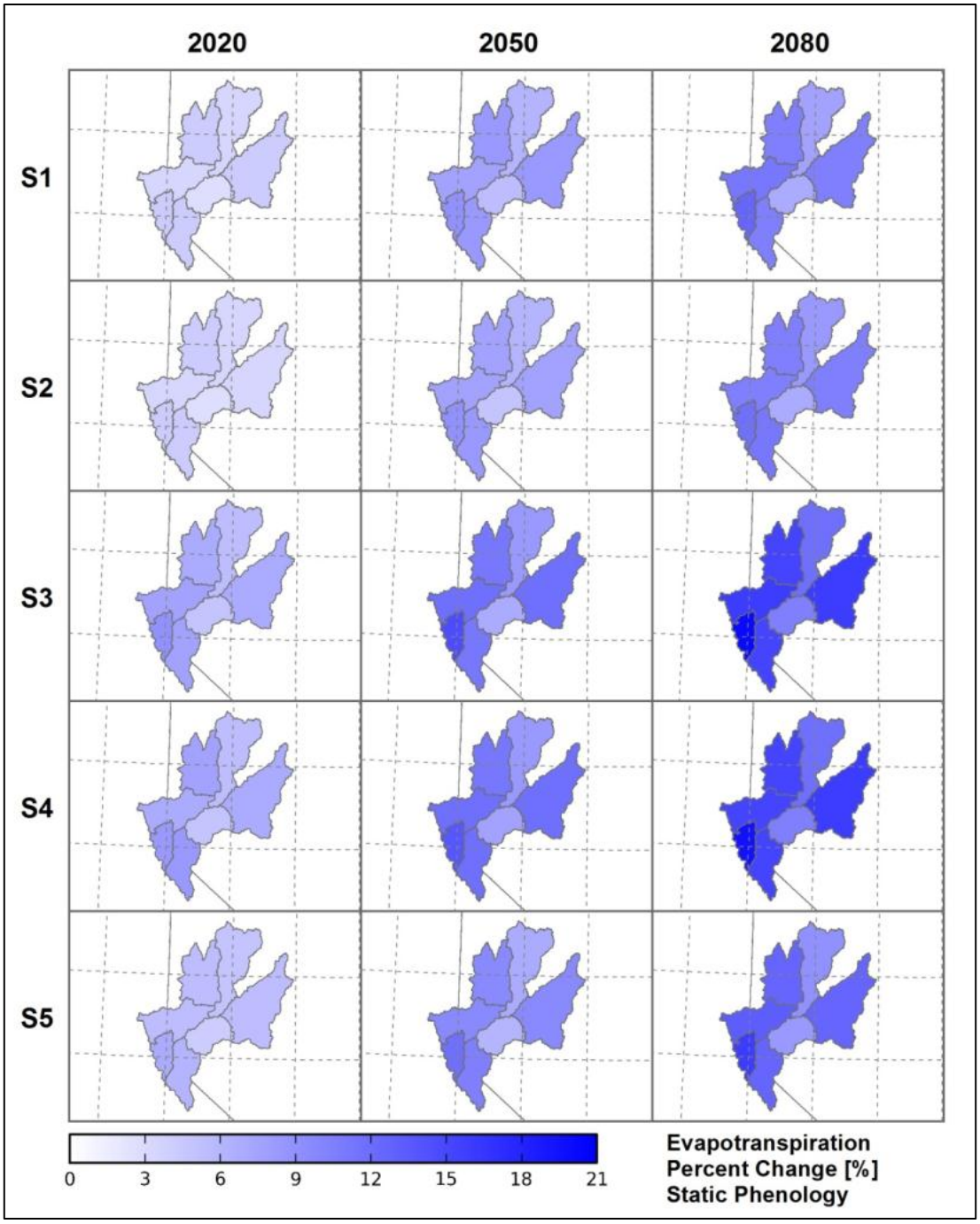

Figure 115.—Truckee and Carson River Basins – Spatial distribution of projected crop evapotranspiration percent change for different climate scenarios and time periods assuming static phenology for annual crops (S1 = WD, S2 = WW, S3 = HD, S4 = HW, S5 = Central).

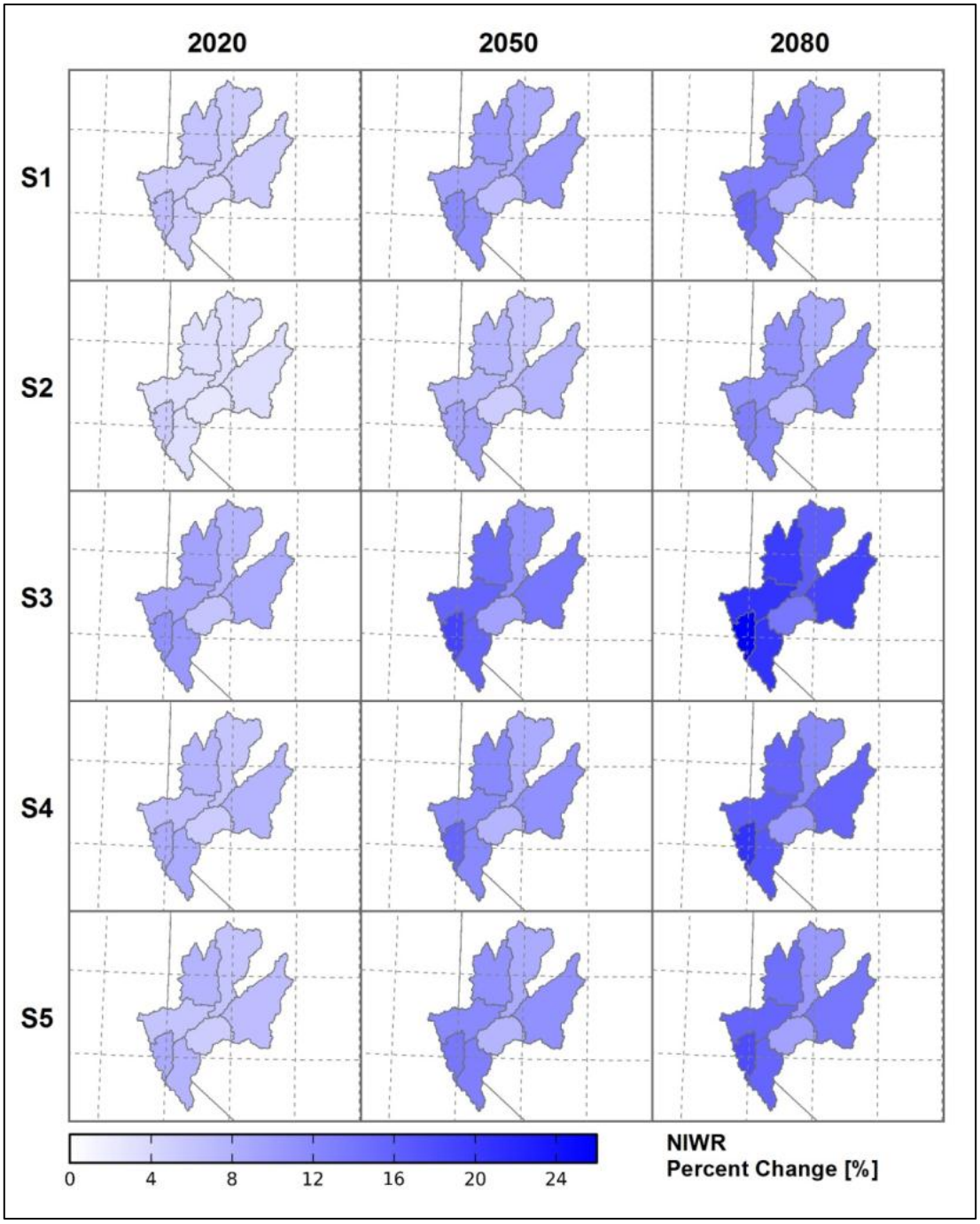

Figure 116.—Truckee and Carson River Basins – Spatial distribution of projected net irrigation water requirements (NIWR) percent change for different climate scenarios and time periods (S1 = WD, S2 = WW, S3 = HD, S4 = HW, S5 = Central).

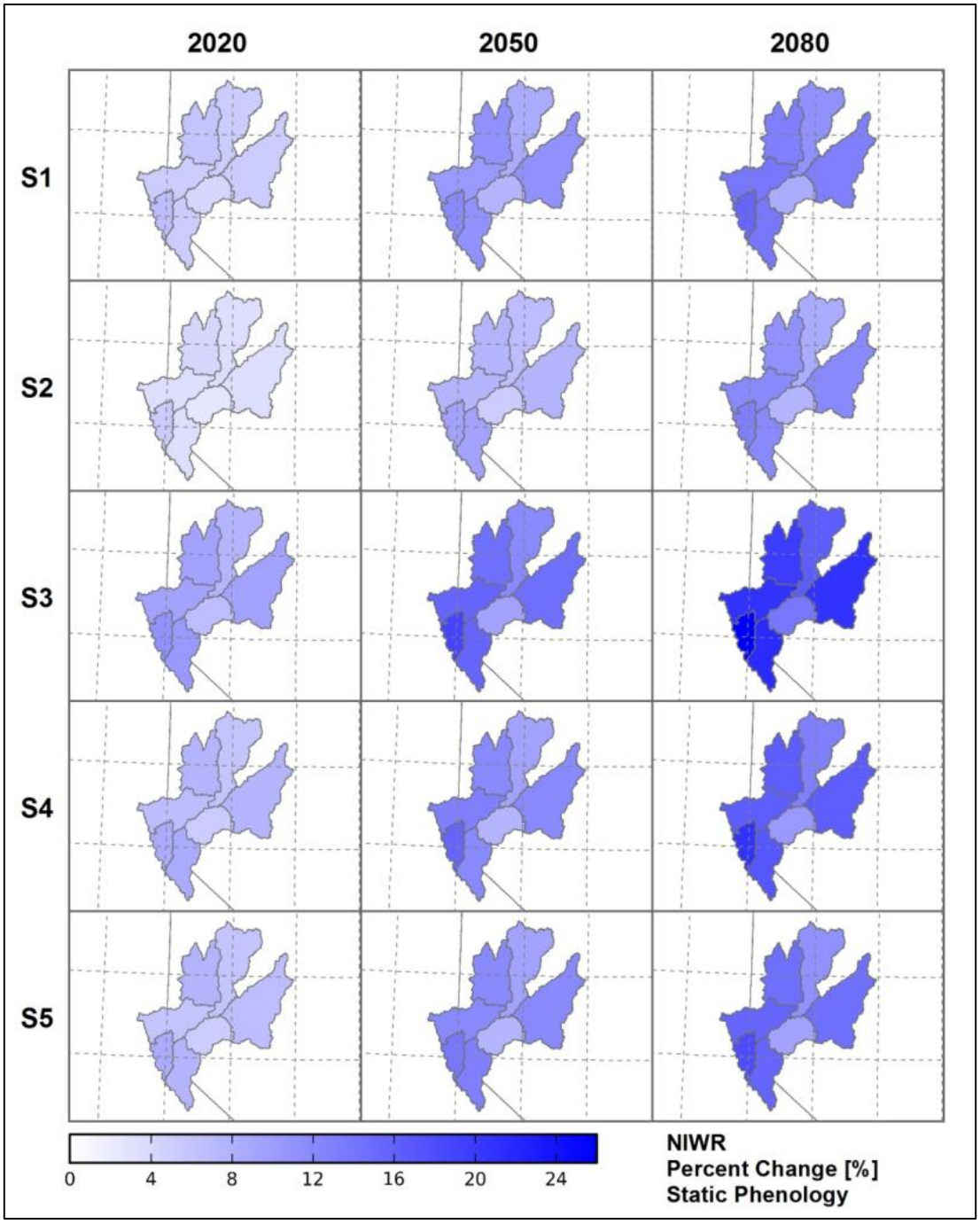

Figure 117.—Truckee and Carson River Basins – Spatial distribution of projected net irrigation water requirements (NIWR) percent change for different climate scenarios and time periods, assuming static phenology for annual crops (S1 = WD, S2 = WW, S3 = HD, S4 = HW, S5 = Central).

Figures 118, 119, and 120 illustrate the baseline and projected temporal distribution of mean daily ET_c for selected Met Nodes, crops, scenarios, and time periods. The simulated mean daily ET_c of alfalfa for the 2020 time period, NWS/COOP Met Node NV2780 (Fallon Exp. Station, NV), shows slight but noticeable shifts in the growing-season length and alfalfa cutting cycles relative to baseline conditions (figure 118, left). By the 2080 time period (figure 118, right) significant shifts in growing-season length, crop development, and cutting cycles are noticeable relative to baseline conditions, with scenarios S3 and S4 exhibiting the most extreme changes. Figure 119 shows simulated mean daily ET_c of spring grain at Met Node NV2780 for different scenarios, and for the 2020 and 2080 time periods. Because planting dates for annual crops are temperature dependent in the non-static phenology simulations, shifts in planting, development, and harvest dates of spring grain are clearly evident, especially by the 2080 time period. The uncertainty in such potential shifts in planting dates, accelerated crop development, and harvest was a primary reason for using baseline temperatures for static phenology simulations (figures 115 and 117). In static phenology simulations, because baseline temperatures are used for estimating planting, crop development, and harvest dates, all scenarios and time periods have identical seasonal K_{cb} shapes, and show differences only in daily ET_c magnitudes due to daily ET_0 and precipitation differences. Figure 120 illustrates simulated mean daily ET_c of garden vegetables at Met Node NV2780 for different scenarios and time periods. Shifts in seasonal changes of planting, development, harvest dates, and ET_c are noticeable but less pronounced than those shown for spring grain, with S3 and S4 having the most extreme seasonal changes.

5.8.2 Baseline and Projected Reservoir Evaporation

Figures 121 and 122 illustrate baseline and projected annual precipitation (top left), annual mean temperature (top right), annual evaporation (bottom left), and annual net evaporation (bottom right) at Lahontan Reservoir and Lake Tahoe. The heavy black line for each variable is the annual time series of 50 percentile values (i.e., ensemble-median). The shaded area for each variable is the annual time series of 5^{th} to 95^{th} percentiles. Due to the large precipitation gradient from west to east across Lake Tahoe, as observed from the long-term precipitation records at Tahoe City and Glenbrook NWS COOP stations, respectively, estimated historical and projected BCSD precipitation values for Tahoe City were scaled by the ratio of spatially averaged 1950 to 1999 mean monthly PRISM precipitation over Lake Tahoe to mean monthly Tahoe City precipitation for the 1950 to 1999 period. Based on energy balance estimates for Lake Tahoe reported by Myrup et al. (1979), net advected energy and the energy required to melt direct snowfall on the lake was considered to be important to include in this work. Monthly average fluxes for these two energy balance components reported by Myrup et al. (1979) were incorporated into historical and projected CRLE estimates of Lake Tahoe monthly evaporation, and amounted to a reduction of mean annual evaporation by 2.7 inches per year.

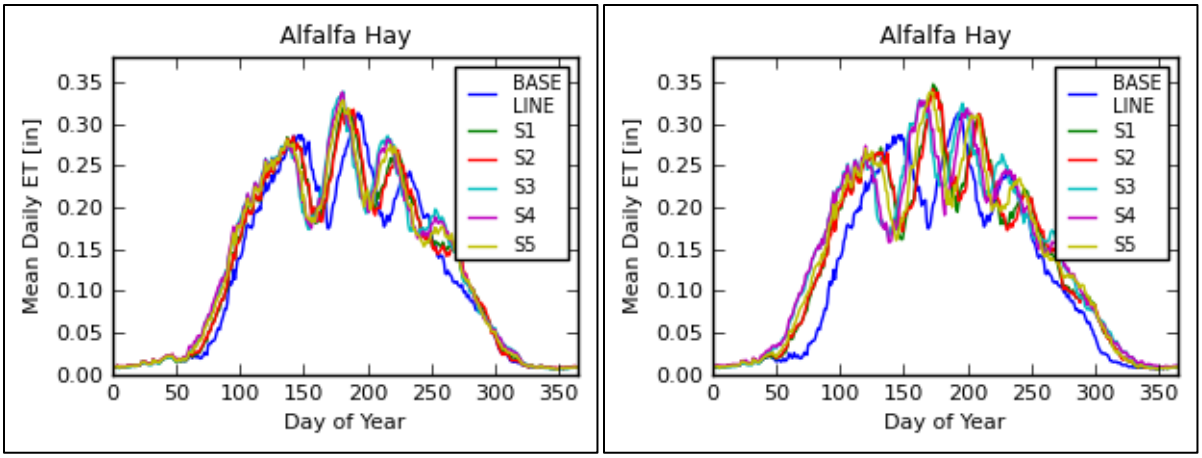

Figure 118.—Truckee and Carson River Basins – COOP station NV2780 (Fallon Exp. Sta., NV). Baseline and projected mean daily alfalfa evapotranspiration for all scenarios and for time periods 2020 (left) and 2080 (right).

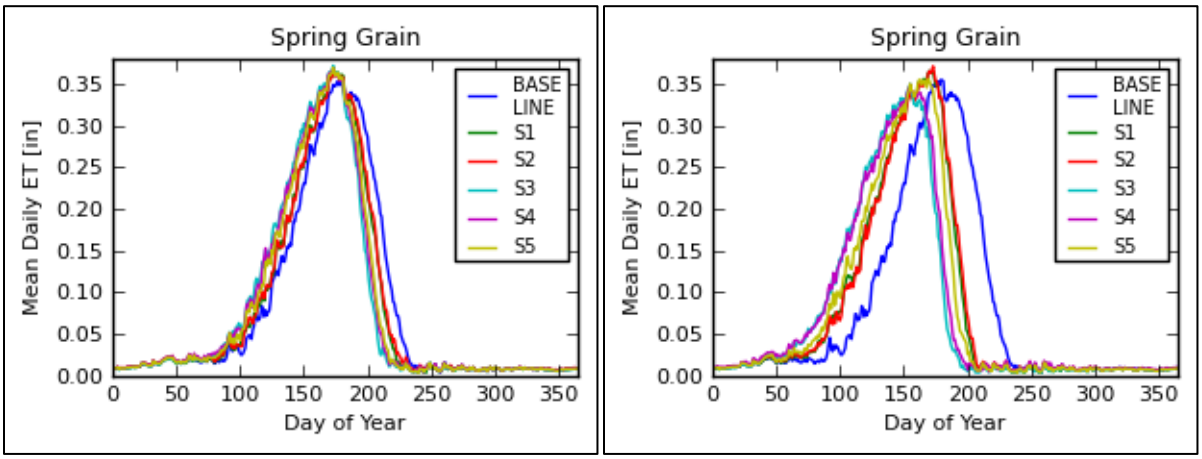

Figure 119.—Truckee and Carson River Basins – COOP station NV2780 (Fallon Exp. Sta., NV). Baseline and projected mean daily spring grain evapotranspiration for all scenarios and for time periods 2020 (left) and 2080 (right).

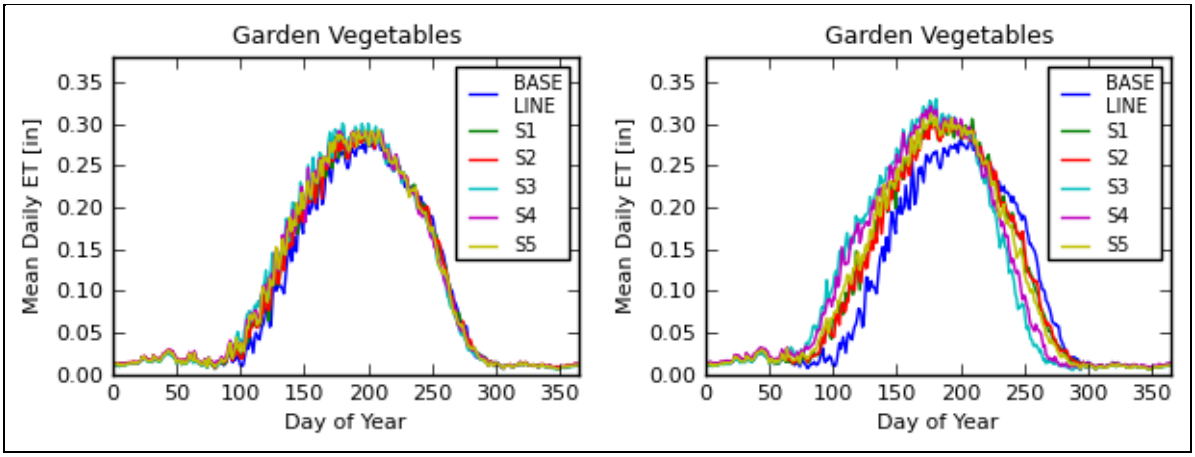

Figure 120.—Truckee and Carson River Basins – COOP station NV2780 (Fallon Exp. Sta., NV). Baseline and projected mean daily garden vegetable evapotranspiration for all scenarios and for time periods 2020 (left) and 2080 (right).

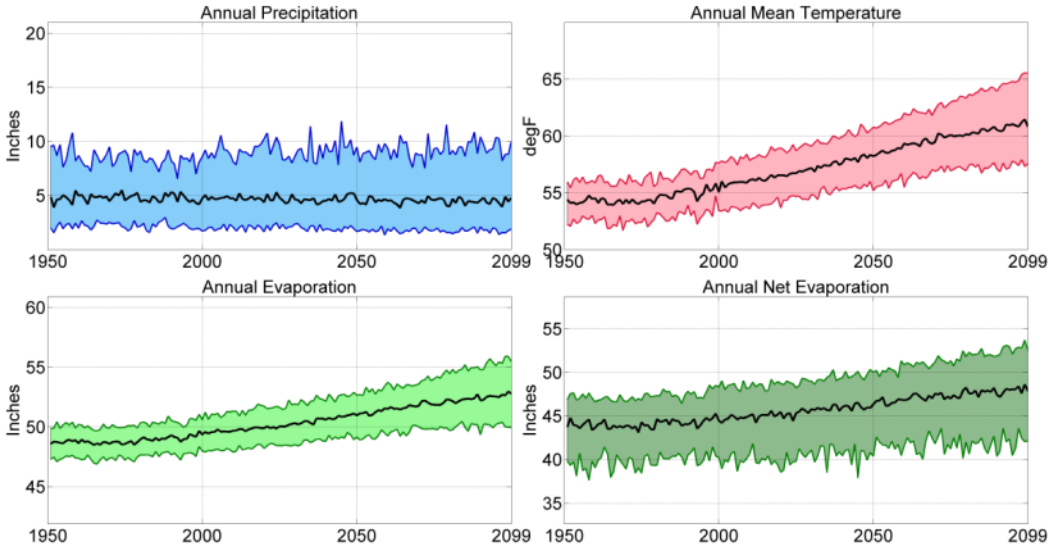

Figure 121.—Truckee and Carson River Basins – Lahontan Reservoir ensemble median and 5th and 95th percentile annual precipitation, temperature, reservoir evaporation, and net evaporation.

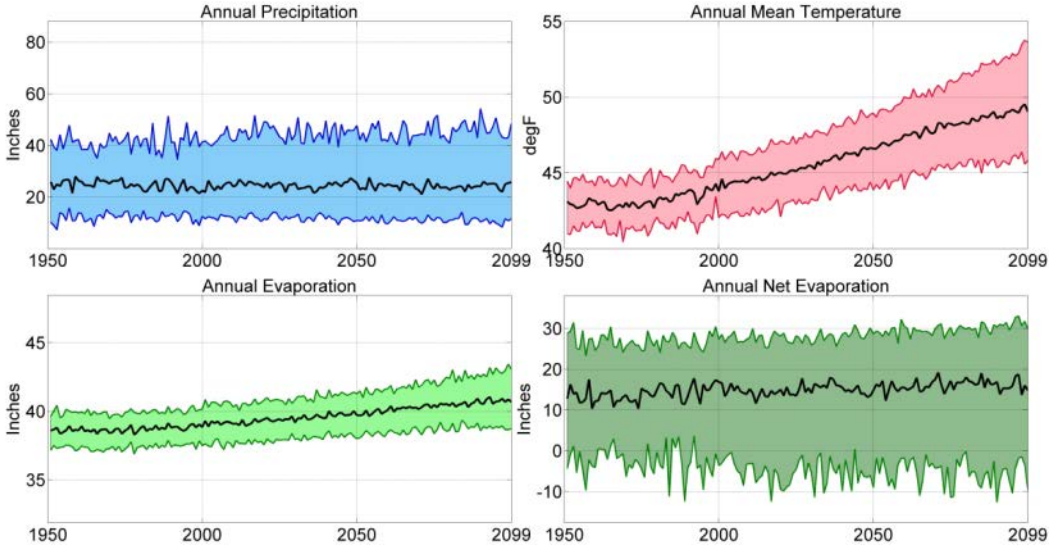

Figure 122.—Truckee and Carson River Basins – Lake Tahoe ensemble median and 5th and 95th percentile annual precipitation, temperature, reservoir evaporation, and net evaporation.

Annual precipitation over Lahontan Reservoir and Lake Tahoe decreases very slightly over the transient period going out to 2099. The uncertainty envelope for annual precipitation is fairly large (~40% of the ensemble median) for both reservoirs and shows a slight increase over time, implying that there is increasing uncertainty from the present. The mean annual temperature and annual evaporation both show increasing trends and a diverging uncertainty envelope over time for both reservoirs. The ensemble-median and uncertainty envelopes

for net evaporation (i.e., evaporation minus precipitation) are affected by characteristics of both precipitation and temperature projections. It is evident, for instance, that the upper uncertainty bound in precipitation causes the lower bound of net evaporation to be highly variable, while the slightly diverging uncertainty envelope is caused primarily by the diverging temperature projections.

In Figures 123 and 124, representing Lahontan Reservoir and Lake Tahoe, respectively, the solid lines show the ensemble-median mean monthly evaporation and net evaporation for the baseline period (1950–1999) and for the 2020s, 2050s, and 2080s, and the shaded areas show the decadal spread of mean monthly evaporation and net evaporation for the baseline period (gray shading) and 2080s (magenta shading), where the spread is bound by the ensemble's 5th to 95th percentile values for each month. The simulated impact of heat storage on evaporation from Lake Tahoe is clearly evident, as the peak evaporation occurs in September and October, and the minimum evaporation occurs during April. The large spread in net evaporation from October to March is due to the large range in projected monthly precipitation during this period. For Lahontan Reservoir, peak evaporation occurs during July and August, due to the shallow depth and reduced heat storage, and the minimum evaporation occurs during January and February. The magnitude of projected monthly evaporation and net evaporation increase is greatest during the late summer and fall months for Lake Tahoe, and during the summer months for Lahontan Reservoir. Estimated annual evaporation and net evaporation increase from baseline to the 2080 time period is 4.6 and 14.4 percent (1.8 and 1.9 in) for Lake Tahoe, and 6.9 and 7.1 percent (3.5 and 3.2 in) for Lahontan Reservoir, respectively (appendix 10).

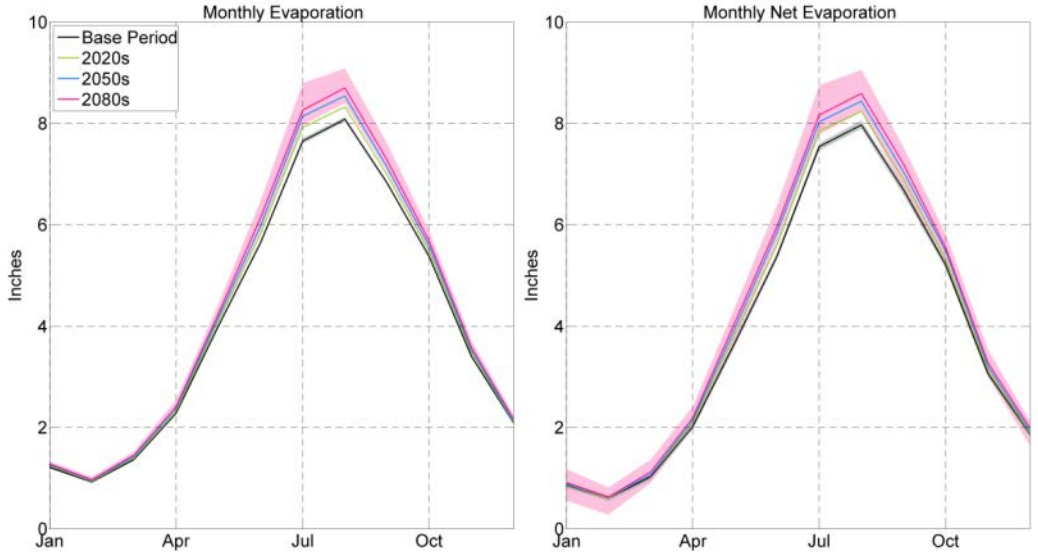

Figure 123.—Truckee and Carson River Basins – Lahontan Reservoir mean monthly ensemble median and 5th and 95th percentile reservoir evaporation and net evaporation.

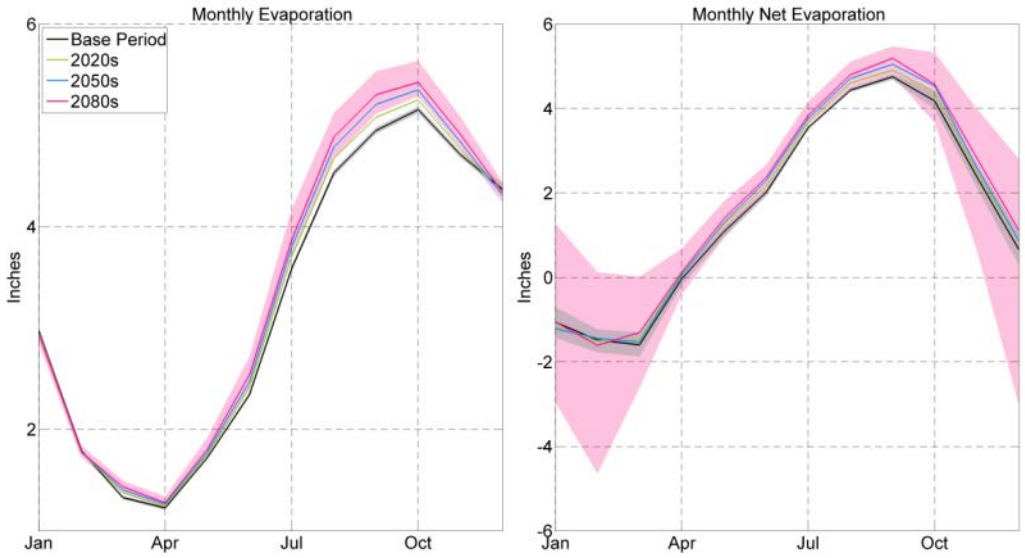

Figure 124.—Truckee and Carson River Basins – Lake Tahoe mean monthly ensemble median and 5th and 95th percentile reservoir evaporation and net evaporation.

5.9 West-Wide Summary of Results

This section summarizes the findings on irrigation demands and reservoir evaporation impacts from sections 5.2 through 5.8. The impacts across the seven basins vary, but general consistencies in results are summarized as follows:

- Precipitation projections are highly variable and basin dependent, with the ensemble median scenario (S5) showing both slight increases and slight decreases within most basins.

- Temperature shows a persistent increasing trend from the baseline level of more than 2.8°C (5°F) over the 90-year period.

- Reference evapotranspiration is projected to increase in all basins by up to about 15 percent.

- Crop evapotranspiration is projected to increase in areas where perennial crops are grown, but smaller increases, and in some cases slight decreases, are projected for areas where annual crops are grown. For the static phenology case, crop evapotranspiration in nearly all basins and subareas is projected to increase.

- Because the NIWR incorporates growing-season and non-growing-season soil moisture gains and losses from precipitation, bare soil evaporation, and crop ET, projections of NIWR are largely uncertain and heavily dependent on the precipitation scenario considered.

- The ensemble median of annual reservoir evaporation and net evaporation is projected to increase in all basins. Relatively consistent increases in evaporation are seen as a function of increasing temperatures, with varying net evaporation increases resulting from increasing or decreasing precipitation.

CHAPTER 6 — UNCERTAINTIES

This analysis is designed to provide a quantitative representation of how irrigation water demand and reservoir evaporation in the major Reclamation river basins may respond to a range of future climate projections. The activity was designed to take advantage of the best available datasets and modeling tools and to follow methodologies documented in peer-reviewed literature. However, there are a number of analytical uncertainties that should be understood in interpreting results, including uncertainties associated with the following analytical areas that can be grouped under two categories—climate projection information and assessing irrigation demand and reservoir evaporation.

6.1 Climate Projection Information

6.1.1 Global Climate Forcing

Although the assessment of irrigation demand and reservoir evaporation considers future climate projections representing a range of future greenhouse gas (GHG) emission paths, the uncertainties associated with these pathways are not explored. Such uncertainties include those introduced by assumptions about technological and economic developments, globally and regionally; how those assumptions translate into global energy use involving greenhouse gas emissions; and biogeochemical analysis to determine the fate of GHG emissions in the oceans, land, and atmosphere. Also, not all of the uncertainties associated with climate forcing involve GHG assumptions. Considerable uncertainty remains associated with natural forcings, with the cooling influence of aerosols being regarded as the most uncertain on a global scale (e.g., figure SPM-2 in IPCC 2007). This uncertainty will continue to exist even with the new sets of emissions pathways such as the representative concentration pathways used in the CMIP5 set of GCM runs.

6.1.2 Global Climate Simulation

This report has been based on climate projections produced by state-of-the-art coupled ocean-atmosphere climate models, which have shown an ability to simulate the influence of increasing GHG emissions on global climate (IPCC 2007). Nevertheless, there are still uncertainties about the scientific understanding of physical processes that affect climate (e.g., atmospheric circulation, clouds, ocean circulation, deep ocean heat uptake, ice sheet dynamics, sea level change, and land cover effects from water cycle, vegetative, and other biological changes); about how to represent such processes in climate models; and about how to do so in a mathematically efficient manner given computational limitations.

6.1.3 Climate Projection Bias Correction

This irrigation demands and reservoir evaporation projection assessment has incorporated the philosophy that GCM results biased towards being too wet, too dry, too warm, or too cool should be identified and accounted for as bias-corrected climate projections data prior to use in impact studies, in order to account for disparities in scale and climate between the global, regional, and local scales. Bias correction of climate projections to local weather stations was especially important since major irrigation demands and reservoir simulation processes are temperature and precipitation dependent.

6.1.4 Climate Projection Spatial Downscaling

This activity uses global scale climate projections that have been empirically downscaled, using spatial disaggregation on a monthly time step (following GCM bias correction on a monthly time step). Although this technique has been used to support numerous water resources impacts studies (e.g., Van Rheenan et al. 2004; Maurer 2007; Anderson et al. 2008; Reclamation 2008; Reclamation 2010; Reclamation 2012a; McGuire et al. 2010), uncertainties remain about the limitations of empirical downscaling methodologies. One potential limitation relates to how empirical methodologies require historical reference information on spatial climatic patterns, at the downscaled spatial resolution. These finer grid patterns are implicitly related to historical large-scale atmospheric circulation patterns, which presumably will change with global climate change. Application of the historical finer grid spatial patterns to guide downscaling of future climate projections implies an assumption that the historical relationship between finer grid surface climate patterns and large-scale atmospheric circulation will still be valid under the future climate. In other words, the relationship is assumed to have statistical stationarity. However, it is possible that such stationarity will not hold at various space and time scales, over multiple locations, and for various climate variables. The significance of potential non-stationarity in empirical bias correction and downscaling methods remains to be established, and it is unknown whether alternative downscaling methodologies may be preferable.

6.2 Assessing Irrigation Demand and Reservoir Evaporation

6.2.1 Generating Weather Sequences Consistent with Climate Projections

Temporal disaggregation to develop daily weather sequences from the monthly HDe climate projections used in the assessment of irrigation demand under climate change ultimately relies on historical weather station data event sequences (e.g., wet or dry spells, cool or hot spells), which are represented in the daily gridded climate of Maurer et al. (2002). This approach only accounts for changes

in the intensity of historical events and cannot account for any future changes in frequency and duration of events. For the assessment of open-water evaporation where transient projections were used (this excludes HDe projections, which are based on a non-transient period change approach), continuous precipitation and temperature sequences were disaggregated to daily values. Although historical weather data were also required for this case, the use of continuous time series introduced the ability to capture the three characteristics of a hydrologic time series – intensity, duration, and frequency. The temporal disaggregation method used in the case of reservoir evaporation estimation was adapted to the method developed by Wood et al. (2002).

6.2.2 Modeling of Irrigation Demand

Uncertainties and limitations in modeling reference ET, crop ET, and net irrigation water requirements are numerous and are discussed below. It should be noted that these discussions pertain strictly to uncertainties associated with irrigation demands under current crop conditions. Uncertainties arising from socioeconomic factors (e.g., market forces, water management and availability, land use, farming practices, technology, etc.) are recognized but are not discussed.

Climatic data used in this assessment were limited to daily maximum and minimum temperature and daily precipitation. Therefore, solar radiation, humidity, and windspeed had to be approximated for baseline and future time periods using empirical approaches. Solar radiation was simulated for baseline and future periods based on empirical relationships between solar radiation and the daily range of air temperature. That is, cloud cover generally has the effect of holding down maximum air temperature during the day but increasing the minimum temperature at night due to increased downward emission of long-wave radiation from clouds. Potential changes in solar radiation due to changes in cloudiness were not integrated into this analysis, and the potential impact of such changes on irrigation water demands was not addressed. Historical agricultural weather data were used to estimate the spatial distribution of baseline and projected mean monthly dewpoint depression and windspeed. Given the uncertainties and limited availability in future projections of humidity and windspeed, mean monthly dewpoint depression and windspeed were considered static for future periods. Increasing wind and decreasing humidity conditions would result in increased ET and NIWR under constant solar radiation and temperature. While there is considerable uncertainty in projecting future reference ET, estimation of reference ET for historical periods using the estimated weather forcings described above was shown to be robust when compared to reference ET estimated using measured weather forcings collected at agricultural weather stations (cf. section 4.4). This analysis relied on a complex, physically based method, the ASCE standardized Penman-Monteith equation (ASCE-EWRI 2005; Allen et al. 1998), to estimate reference ET, While there are simplified equations to estimate ET without consideration of solar radiation, humidity and windspeed, the ASCE-PM reference ET equation is a nationally and

internationally standardized method, is well regarded, and serves as a reproducible index approximating the climatic demand for water vapor.

Crop ET estimated from the ET Demands model is primarily a function of reference ET, precipitation, crop type, and soil type. There are many uncertainties and limitations in estimating and defining parameters that affect these variables and states, such as definition of shapes and behavior of basal crop coefficient curves; thermal based functions that simulate planting, crop development, and harvest; crop-dependent root depth and simulation of seasonal root growth; NRCS-derived soil water holding capacity and runoff parameters; simulation of irrigation amount and frequency; and consideration of wintertime surface cover and precipitation accumulation. While many generalized parameters were used in this assessment, many primary parameters, such as basal crop coefficients and thermal parameters defining growing-season length and crop development, were based on detailed field-scale lysimeter and crop water use studies. Perhaps a more important consideration, with respect to generalized approaches for estimating crop ET, is the limitations in model structure. The ET Demands model structure does incorporate more advanced processes than other crop water demand models commonly used for similar assessment studies, such as consideration of reference crop daily energy balance, daily soil water balance, seasonal crop development and harvest for different crop types, bare soil evaporation, temperature-dependent growing-season length, and non-growing-season ET and precipitation accumulation.

Nevertheless, ET Demands still has some important limitations and can benefit from future improvements. Some important limitations in the application of the ET Demands model for this assessment are the lack of consideration as to how CO_2 potentially impacts crop development and water use, the assumption of temperature-dependent and static planting and harvest dates for future periods, generalized winter cover classes, and the assumption that all precipitation is in liquid form. All of these assumptions impact seasonal and annual crop ET, effective precipitation, and net irrigation water requirements. The impact of increased CO_2 on crop transpiration, water use efficiency, and yield is of particular interest and is probably one of the largest uncertainties. Several studies have described how elevated CO_2 concentrations may reduce stomatal aperture, transpiration, and crop production processes (Rosenberg 1981; Kimball and Idso 1983; Manabe and Wetherald 1987; Kruijt et al. 2008; Islam et al. 2012). However, estimating CO_2-induced changes on irrigation demands remains an extremely difficult task because of plant dependency, adaptation, unknown non-linear near-surface boundary-layer feedbacks from reduced transpiration and resulting increased leaf temperatures and vapor pressure deficits, uncertainties of increased leaf area index, stomatal and aerodynamic resistances, and plant-dependent stomatal sensitivities (i.e., C3 versus C4 plants).

For these reasons, this study focused on major change factors and considerations such as physically based reference ET estimation, temperature-dependent growing

seasons and crop development, bare soil evaporation, and non-growing-season soil moisture accounting for better representation of monthly and annual net irrigation water requirements. Addressing the impacts of CO_2 on irrigation water demands is currently, and will be, the focus of further Reclamation studies. In addition, Reclamation plans to enhance the ET Demands model's representation of wintertime snow accumulation and melt processes in order to improve wintertime soil water accounting.

6.2.3 Modeling of Reservoir Evaporation

Uncertainties in estimated reservoir evaporation are largely centered on CRLE energy balance considerations: specifically, heat storage and advection of heat in air and water into and out of the reservoir. The conceptual basis for the heat-storage routing technique used in the CRLE, which is a function of water body depth, is oversimplified. In spite of that weakness, it is "worthwhile because it has the potential to provide reasonably realistic seasonal patterns of evaporation for many lakes and to account for the effects of great depth in reducing the annual lake evaporation" (Morton 1986). Moreover, more complex improvements are not warranted until accurate energy or water-budget benchmark datasets of monthly evaporation are available so that a more robust model can be developed and calibrated. A limitation of the CRLE model is the need to estimate net advected heat, especially for large river and reservoir systems in arid environments, where annual average volume-weighted inflow water temperatures can be higher than outflow volume-weighted water temperatures.

Another important limitation of the CRLE model is its reliance on the energy balance without consideration of the effects of windspeed on evaporation. However, one can argue that using an approach that heavily relies on windspeed, and is therefore extremely sensitive to uncertainties in windspeed (e.g., the aerodynamic mass transfer approach or a combination approach), may actually increase uncertainty in evaporation estimates, especially under future climate scenarios in which projections of near-surface local-scale windspeeds are very uncertain. While there are several limitations and uncertainties in CRLE simulated energy balance components (see Morton 1986; DosReis and Dias 1998; Sadek et al. 1997; Vallet-Coulomb et al. 2001), most are considered minor, especially when compared to the uncertainties associated with alternative evaporation approaches that would need to be applied over large areas with limited weather data (i.e., approaches that require windspeed). Because many energy balance functions of the CRLE are largely calibrated based on estimated water balance evaporation estimates, prediction uncertainty is reduced in many respects. Reclamation is currently involved in several open-water evaporation research efforts to better quantify and evaluate alternative approaches for estimating evaporation using empirical and physically based models based on weather data and remote sensing.

6.2.4 Bias and Calibration

Although bias in estimated reference ET, crop ET, and evaporation was considered small for historical periods (see section 4.4 for an assessment discussion) there is potential for increased bias under future climates due to model assumptions and uncertainties previously discussed, such as climate forcing bias, assumption of no CO_2 impacts on transpiration, bias in calibration of temperature-dependent crop planting, development, and harvest periods for annual and perennial crops, wintertime effective precipitation considerations, and heat storage and advection of heat into and out of water bodies. This study recommends that future west-wide studies place greater emphasis on model calibration and on including better informed projections of crop cultivar development and changes in farming practices under climate change, especially as they would affect the lengths of growing periods for annual crops. For perspective, such enhanced calibration likely would be required in any locality-specific analysis.

6.2.5 Spatial Resolution of the Applications

Spatial resolution of the applications is considered to be at local scale and does not account for spatial variations within each HUC8. NWS/COOP weather station data were used to bias correct BCSD HDe and transient historical and projected climate, and these data were used to force ET Demands and CRLE models. The scale of ET Demands and CRLE estimates are therefore representative of the area influencing NWS/COOP weather station measurements, which are likely on the order of hundreds of meters to kilometers. In some HUC8 cells, multiple weather stations were used to estimate net irrigation water requirements, but spatial variations of the stations within the HUC8 were not explicitly considered. Spatial variations in climate forcings of dewpoint depression, and windspeed are considered regional due to the spatial interpolation and averaging of agricultural weather station observations to the HUC8 scale. However, these interpolated variables are considered representative of local scale agricultural weather conditions (i.e., more humid and less windy than arid dry lands). Spatial variations in soil type and water holding properties within each HUC8 were averaged across cropland areas, and are therefore representative of the HUC8 scale for cropland areas only.

6.2.6 Temporal Resolution of the Applications

The application time steps for the ET Demands and CRLE models were daily and monthly, respectively. Although ET Demands simulations were conducted at daily time steps, the application was calibrated to reproduce monthly solar radiation, and approximately weekly temporal variations in crop planting, development, and harvest characteristics at general and some site-specific locations within each basin. For this reason, users should cautiously interpret daily reference ET and crop ET results. Similarly, the CRLE model calibration

was largely based on annual water balance estimates. Therefore, resulting monthly evaporation estimates should be cautiously interpreted since seasonal uncertainties in heat storage can significantly impact monthly evaporation estimates.

CHAPTER 7 — REFERENCES

Allander, K.K., J.L. Smith, and M.K. Johnson. 2009. "Evapotranspiration in the Lower Walker River Basin, West-Central Nevada, Water Years 2005–07," U.S. Geological Survey Scientific Investigations Report 2009-5079, 62 p.

Allen, R.G. 1988. IRRiSKED: Irrigation Scheduling Program for Demand and Rotation Scheduling – User's Manual, Dept. Biol. and Irrig. Eng., Utah State University, Logan, UT, 84322 U.S.A., 80 p.

_____. 1996. "Assessing Integrity of Weather Data for use in Reference Evapotranspiration estimation," *Journal of Irrigation and Drainage Engineering*, ASCE 122(2):97–106.

_____. 1997. "A Self-Calibrating Method for Estimating Solar Radiation from Air Temperature, *Journal of Hydrologic Engineering*, 2(2):56–67.

_____. 2008. "Quality assessment of weather data and micro-meteorological flux: impacts on evapotranspiration calculation," *Journal of Agricultural and Forest Meteorology*, 64 (4):191–204.

_____. 2011. "Skin layer evaporation to account for small precipitation events—An enhancement to the FAO-56 evaporation model," *Agricultural Water Management*, 99(1):8–18.

Allen, R.G., and C.E. Brockway. 1983. Estimating Consumptive Irrigation Requirements for Crops in Idaho, Research Technical Completion Report, Idaho Water and Energy Resources Research Institute, University Idaho, Moscow, ID, 130 p.

Allen, R.G., L.S. Pereira, D. Raes, and M. Smith. 1998. "Crop Evapotranspiration: Guidelines for Computing Crop Water Requirements," FAO Irrigation and Drainage Paper 56, Food and Agriculture Organization of the United Nations, Rome, 300 p. Available at: http://www.fao.org/docrep/x0490e/x0490e00.htm

Allen, R.G., and Tasumi, M. 2005. Evaporation from American Falls Reservoir in Idaho via a Combination of Bowen Ratio and Eddy Covariance, Proceedings 2005 EWRI Conf., Anchorage, Alaska, May 15–19.

Allen, R.G., L.S. Pereira, M. Smith, D. Raes, and J.L. Wright. 2005a. "FAO-56 Dual Crop Coefficient Method for Estimating Evaporation from Soil and Application Extensions," *Journal of Irrigation and Drainage Engineering*, ASCE, 131(1):2–13.

Allen, R.G., A.J. Clemmens, C.M. Burt, K. Solomon, and T. O'Halloran. 2005b. "Prediction accuracy for project-wide evapotranspiration using crop coefficients and reference evapotranspiration," *Journal of Irrigation and Drainage Engineering*, DOI: 10.1061/(ASCE)0733-9437(2005)131:1(24).

Allen, R.G., and C.W. Robison. 2009. "Evapotranspiration and Consumptive Irrigation Water Requirements for Idaho," University of Idaho Report, 222 p. Available at http://www.kimberly.uidaho.edu/ETIdaho/.

Allen, R.G., and J.L. Wright. 2009. "Estimation of evaporation and evapotranspiration during nongrowing season using a dual crop coefficient," Proceedings of the ASCE-EWRI World Environmental and Water Resources Congress, Kansas City, Missouri, May 17–21, 2009, pp. 4158–4171.

Anderson, E.A. 1973. National Weather Service River Forecast System – Snow Accumulation and Ablation Model, Technical Memorandum NWS HYDRO-17, National Oceanic Atmospheric Administration, November 1973.

_____. 2006. Snow Accumulation and Ablation Model – SNOW-17, NWS Technical Memorandum, National Oceanic Atmospheric Administration, Silver Spring, Maryland, 61 pp.

Anderson, J., F. Chung, M. Anderson, L. Brekke, D. Easton, M. Ejeta, R. Peterson, and R. Snyder. 2008. "Progress on Incorporating Climate Change into Management of California's Water Resources," Climatic Change, Springer, Netherlands, 89, Supplement 1, 91–108.

Andreadis K., P. Storck, and D.P. Lettenmaier. 2009. "Modeling snow accumulation and ablation processes in forested environments," *Water Resources Research*, 45, W05429, DOI: 10.1029/2008WR007042.

ASCE-EWRI (Environmental and Water Resources Institute of the American Society of Civil Engineers). 2005. The ASCE Standardized Reference Evapotranspiration Equation, Report 0-7844-0805-X, ASCE Task Committee on Standardization of Reference Evapotranspiration, Reston, Virginia., American Soc. Civil Engineers. Available at http://www.kimberly.uidaho.edu/water/asceewri/

Barnett, T., D.W. Pierce, H. Hidalgo, C. Bonfils, B.D. Santer, T. Das, G. Bala, A.W. Wood, T. Nazawa, A. Mirin, D. Cayan, and M. Dettinger. 2008. "Human-induced changes in the hydrology of the Western United States," Science/Science Express Reports, 10.1126/science.1152538.

Benson, L.V., and J.W.C. White. 1994. Stable isotopes of oxygen and hydrogen in the Truckee River–Pyramid Lake surface-water system. Source of water vapor overlying Pyramid Lake. *Limnology and Oceanography* 39(8):1945–1958.

Blaney, H.F. 1957. Evaporation study at Silver Lake in the Mojave Desert, California. Eos Trans. AGU, 38(2): 209–215.

Bos, M.G., R.A.L. Kselik, R.G. Allen, and D.J. Molden. 2008. Water Requirements for Irrigation and the Environment, Springer, Dordrecht, ISBN 978-1-4020-8947-3.

Brekke, L.D., M.D. Dettinger, E.P. Maurer, and M. Anderson. 2008. "Significance of model credibility in estimating climate projection distributions for regional hydroclimatological risk assessments," *Climatic Change*, 89(3–4), 371–394.

Brekke, L.D., J.E. Kiang, J.R. Olsen, R.S. Pulwarty, D.A. Raff, D.P. Turnipseed, R.S. Webb, and K.D. White. 2009a. Climate change and water resources management—A federal perspective, U.S. Geological Survey Circular 1331, 65 pp. Also available online at http://pubs.usgs.gov/circ/1331/.

Brekke, L.D., E.P. Maurer, J.D. Anderson, M.D. Dettinger, E.S. Townsley, A. Harrison, and T. Pruitt. 2009b. "Assessing Reservoir Operations Risk under Climate Change," *Water Resources Research*, DOI: 10.1029/ 2008WR006941.

Brower, A. 2008. ET Toolbox – Evapotranspiration Toolbox for the Middle Rio Grande, A Water Resources Decision Support Tool, Version 2.1. Bureau of Reclamation, Water and Environmental Resources Division, Technical Service Center, 159 p.

Brutsaert, W.H., and G.T. Yeh. 1976. Implications of a type of empirical evaporation formula for lakes and pans, *Water Resources Research*, 6:1202–1208.

Burnash, R.J.C., R.L. Ferral, and R.A. McGuire. 1973. A generalized streamflow simulation system – Conceptual modeling for digital computers, Technical Report, Joint Federal and State River Forecast Centers of the U.S. National Weather Service and California Department of Water Resources, Sacramento, California, 204 p.

Burnash, R., and L. Ferral. 1996. "Conceptualization of the Sacramento Soil Moisture Accounting Model," NWSRFS User's Manual, Part II.3, National Weather Service, National Oceanic and Atmospheric Administration, DOC, Silver Spring, Maryland.

Burt, C.M., A. Mutziger, D.J. Howes, and K.H. Solomon. 2002. "Evaporation from irrigated land in California," Rep. R02-001, Irrigation Training and Research Center, California Polytechnic State Univ., San Luis Obispo, California. Available at http://www.itrc.org/reports/ reportsindex.html&

Burt, C.M., A.J. Mutziger, R.G. Allen, and T.A. Howell. 2005. "Evaporation Research – A Review and Interpretation," *Journal of Irrigation and Drainage Engineering* 131(1):37–58.

Cherkauer, K.A., and D.P. Lettenmaier. 2003. "Simulation of spatial variability in snow and frozen soil field," *Journal of Geophysical Research* Vol. 108, No. D22, DOI: 10.1029/2003JD003575.

Christensen, N.S., A.W. Wood, D.P. Lettenmaier, and R.N. Palmer. 2004. "Effects of Climate Change on the Hydrology and Water Resources of the Colorado River Basin," *Climatic Change* Vol. 62, Issue 1–3, 337–363.

Christensen, N.S., and D.P. Lettenmaier. 2007. "A multimodel ensemble approach to assessment of climate change impacts on the hydrology and water resources of the Colorado River basin," *Hydrology and Earth System Sciences*, 11:1417–1434.

Climate Change and Water Working. 2010. "Assessing a Portfolio of Approaches for Producing Climate Change Information to Support Adaptation Decisions," Climate Change and Water Working Group Workshop, Boulder, Colorado, November 2010.

Covey, C., K.M. AchutaRao, U. Cubasch, P.D. Jones, S.J. Lambert, M.E. Mann, T.J. Phillips, and K.E. Taylor. 2003. "An Overview of Results from the Coupled Model Intercomparison Project," *Global and Planetary Change*, 769:1–31.

Crago, R.D., R.J. Qualls, and M. Feller. 2010. "A calibrated advection-aridity evaporation model requiring no humidity data," *Water Resources Research* 46, cW09519, DOI: 10.1029/2009WR008497.

Daly, C., R. P. Neilson, and D.L. Phillips. 1994. "A Statistical-Topographic Model for Mapping Climatological Precipitation over Mountainous Terrain." *Journal of Applied Meteorology*, 33, 140–158.

Department of Water Resources. 1999. Reference Evapotranspiration. California Department of Water Resources. Scale 1:1,805,000. Available at: http://wwwcimis.water.ca.gov/App_Themes/images/etozonemap.jpg

_____. 2013. California Water Plan Update 2013. California Natural Resources Agency, Department of Water Resources, Bulletin 160-13. Available from http://www.waterplan.water.ca.gov/cwpu2013/final/

deTar, W.R. 2004. "Using a Subsurface Drip Irrigation System to Measure Crop Water Use," *Irrigation Science* 23(3):111–122.

Dettinger, M.D. 2005. "From Climate Change Spaghetti to Climate Change Distributions for 21st Century," *San Francisco Estuary and Watershed Science* 3(1).

Doorenbos, J., and W.O. Pruitt. 1977. "Crop Water Requirements," Irrigation and Drainage Paper No. 24, Food and Agriculture Organization of the United Nations, Rome.

DosReis, R.J., and N.L. Dias. 1998. "Multi-season lake evaporation – energy budget estimates and CRLE model assessment with limited meteorological observations," *Journal of Hydrology* 208:135–147.

Dugan, G.L., and P.H. McGauhey. 1974. Enrichment of Surface Waters. *Journal Water Pollution Control Federation* 46(10).

Farahani, H.J., and W.C. Bausch. 1995. "Performance of evapotranspiration models for maize: Bare soil to closed canopy," *Transactions of the American Society of Agricultural Engineers* 38(4), 1049–1059.

Ficklin, D.L., Y. Luo, E. Lunedeling, and M. Zhang, 2009. "Climate change sensitivity assessment of a highly agricultural watershed using SWAT," *Journal of Hydrology* 374(1–2):16–29.

Fowler, H.J., S. Blenkinsop, and C. Tebaldi. 2007. "Linking climate change modelling to impacts studies: recent advances in downscaling techniques for hydrological modeling," *International Journal of Climatology*, 27:1547–1578, DOI: 10.1002/joc.1556.

Fuhriman, D.K., L.B. Merritt, A.W. Miller, and H.S. Stock. 1981. Hydrology and water quality of Utah Lake. *Great Basin Naturalist Memoirs*, 5:43–67

Gleckler, P.J., K.E. Taylor, and C. Doutriaux. 2008. "Performance metrics for climate models," *Journal of Geophysical Research* 113(D06104).

Guitjens, J.C., and M.T. Goodrich. 1994. "Dormancy and Nondormancy Alfalfa Yield and Evapotranspiration," *Journal of Irrigation and Drainage* 120(6):1140.

Hamlet, A.F., and D.P. Lettenmaier. 1999. "Effects of climate change on hydrology and water resources in the Columbia River Basin," *Journal of the American Water Resources Association* 35(6):1597–1623.

Hamlet A.F., S.Y. Lee, K.E.B. Mickelson, and M.M Elsner. 2010. "Effects of projected climate change on energy supply and demand in the Pacific Northwest and Washington State," *Climatic Change*, DOI: 10.1007/ s10584-010-9857-y.

Hamlet, A.F., M.M. Elsner, G.S. Mauger, S.Y. Lee, I.M. Tohver, and R.A. Norheim. 2013. An overview of the Columbia Basin Climate Change Scenarios Project:

Approach, methods, and summary of key results. *Atmosphere-Ocean* 51(4):1–24.

Harbeck, E.G. 1962. A Practical Field Technique for Measuring Reservoir Evaporation Utilizing Mass-Transfer Theory, U.S. Geological Survey Professional Paper #272-E.

Harbeck, G.E. Jr., M.A. Kohler, and G.E. Koberg. 1958. Water loss investigations: Lake Mead studies, U.S. Geological Survey Professional Paper 298.

Harding, S.T. 1935. Evaporation from large water surfaces based on records in California and Nevada. Eos. Trans. AGU, 17, 507–511.

_____. 1962. Evaporation from Pyramid and Winnemucca lakes, Nevada. *Journal of Irrigation and Drainage*, Division of the American Society of Civil Engineers, 88(IRI):1–13.

Hawkins, R.G., A.T. Hjelmfelt, and A.W. Zevenbergen. 1985. "Runoff probability, storm depth, and curve numbers," *Journal of Irrigation and Drainage Engineering* 111(4):330–340.

Hawkins, E., and R.T. Sutton. 2009. "The potential to narrow uncertainty in regional climate predictions," Bulletin of the American Meteorological Society, 90(8):1095–1107.

_____. 2010. "The potential to narrow uncertainty in projections of regional precipitation change," Climate Dynamics, DOI: 10.1007/s00382-010-0810-6.

Hewitson, B.C., and R.G. Crane. 1996. Climate downscaling: Techniques and application, *Climate Research*, 7:85–95.

Hill, R.W. 1994. Consumptive use of irrigated crops in Utah," Research Report No. 145, Utah Agricultural Experiment Station, Utah State University, Logan, Utah, revised February 1997, reprinted. Available at http://nrwrtl.nr.state.ut.us/techinfo/consumpt/default.htm

Hill, R.W., B. Barker, and C.S. Lewis. 2011. Crop and Wetland Consumptive Use and Open Water Surface Evaporation for Utah, Utah Agricultural Experiment Station Research Report 213, 138 p. Available at http://uaes.usu.edu/files/uploads/Publications/Research%20Reports/Surface%20Evaporation.pdf.

Hounam, C.E. 1973. Comparison between pan and lake evaporation, World Meteorological Organization, Technical Note No. 126, 52 p.

Howell, T.A., J.L. Steiner, A.D. Schneider, and S.R. Evett. 1995. "Evapotranspiration of irrigated winter wheat—Southern Plains," *Transactions of the American Society of Agricultural Engineers*, 38(3):745–759.

Howell, T.A., J.L. Steiner, A.D. Schneider, S.R. Evett, and J.A. Tolk. 1997. "Seasonal and Maximum Daily Evapotranspiration of Irrigated Winter Wheat, Sorghum, and Corn – Southern High Plains," *Transactions of the American Society of Agricultural Engineers*, 40(3):623–634.

Howitt, R., J. Lund, K.W. Kirby, M.W. Jenkins, A.J. Draper, P.M. Grimes, M.D. Davis, K.B. Ward, B.D. Newlin, B.J. Van Lienden, J.L. Cordua, and S.M. Msangi. 1999. Integrated Economic-Engineering Analysis of California's Future Water

Supply, Appendix K – Irrigation Water Requirements. Available at http://calvin.ucdavis.edu/files/content/page/ReportAug99.pdf

Hughes, G.H. 1967. Analysis of techniques used to measure evaporation from Salton Sea, California. Professional Paper 272-H, U.S. Geological Survey, Washington, DC.

Huntington, J.L., and R. Allen. 2010. Evapotranspiration and Net Irrigation Water Requirements for Nevada, Nevada State Engineer's Office Publication, 266 p.

Huntington, J.L., and D. McEvoy. 2011. Climatological Estimates of Open Water Evaporation from Selected Truckee and Carson River Basin Water Bodies, California and Nevada, Desert Research Institute Publication No. 41254.

IPCC (Intergovernmental Panel on Climate Change). 2000. Special Report on Emissions Scenarios. Nakićenović, N., and R. Swart (eds.). Cambridge University Press, Cambridge, United Kingdom, 599 p. Available at http://www.grida.no/climate/ipcc/emission/.

_____. 2007. Climate Change 2007: The Physical Science Basis. Contribution of Working Group I to the Fourth Assessment Report of the Intergovernmental Panel on Climate Change. Solomon, S., D. Qin, M. Manning, Z. Chen, M. Marquis, K.B. Averyt, M. Tignor, and H.L. Miller (eds.). Cambridge University Press, Cambridge and New York, 996 p. Available at http://www.ipcc.ch/ipccreports/ar4-wg1.htm.

_____. 2013. Climate Change 2013: The Physical Science Basis. Working Group I Contribution to the Fifth Assessment Report of the Intergovernmental Panel on Climate Change. Stocker, T.F., D. Qin, et al. (eds.). Intergovernmental Panel on Climate Change, 1535 p. Available at http://www.climatechange2013.org/.

Islam, Adlul, Lajpat R. Ahuja, Luis A. Garcia, Liwang Ma, Anapalli S. Saseendran, and Thomas J. Trout. 2012. Modeling the impacts of climate change on irrigated corn production in the Central Great Plains, *Agricultural Water Management*, 110, issue C, p. 94–108.

James B.W., R.J. Hanks, and J.J. Jurinar. 1982. Modern irrigated soils. Wiley, Chichester, Great Britain, 235 p.

Jensen, M.E. 1998: Coefficients for Vegetative Evapotranspiration and Open Water Evaporation for the Lower Colorado River Accounting System. Report prepared for the Bureau of Reclamation, Boulder City, Nevada.

Jones, R.N., T.A. McMahon, and J.M. Bowler. 2001. "Modelling historical lake levels and recent climate change at three closed lakes, Western Victoria, Australia (c. 840–1990)," *Journal of Hydrology*, 246:159–180.

Jones, J.W., G. Hoogenboom, C.H. Porter, K.J. Boote, W.D. Batchelor, L.A. Hunt, P.W. Wilkens, U. Singh, A.J. Gijsman, and J.T. Ritchie. 2003. DSSAT Cropping System Model, *European Journal of Agronomy* 18:235–265.

Kimball, B.A., and B.S. Idso. 1983. Increasing atmospheric CO_2: Effects on crop yield, water use, and climate. Agricultural Water Management 7(1):55–72.

Knutti R., and J. Sedláček. 2013. Robustness and uncertainties in the new CMIP5 climate model projections, *Nature Climate Change*, 3:369–373.

Ko, J., B. Kimball, S. Anapalli, L. Ma, T. Green, A. Ruane, G. Wall, P. Pinter, D. Bader. 2010. "Simulation of free air CO_2 enriched wheat growth and interactions with water, nitrogen, and temperature." *Agricultural and Forest Meteorology* 150: 1331–1346

Kohler, M.A., and L.H. Parmele. 1967. Generalized estimates of free-water evaporation, *Water Resources Research*, 3:997–1005.

Kruijt B., J.P.M. Witte, C.M.J. Jacobs, T. Kroon. 2008. Effects of rising atmospheric CO_2 on evapotranspiration and soil moisture: A practical approach for the Netherlands, *Journal of Hydrology*, 349(3-4):257–267.

Langbein, W.B. 1951. Research on Evaporation from Lakes and Reservoirs. IASH-AISH Publ. 34, 409–425.

Leavesley, G.H., R.W. Lichty, B.M. Troutman, and L.G. Saindon. 1983. Precipitation-runoff modeling system—User's Manual, U.S. Geological Survey Water-Resources Investigation Report 83-4238, 207 p.

Lettenmaier, D.P., and T.Y. Gan. 1990. "Hydrologic sensitivities of the Sacramento-San Joaquin River basin, California, to global warming," *Water Resources Research* 26:69–86.

Lettenmaier, D.P., A.W. Wood, R.N. Palmer, E.F. Wood, and E.Z. Stakhiv. 1999. "Water Resources Implications of Global Warming: A U.S. Regional Perspective," *Climatic Change* 43(3), November 537–79.

Liang, X., D.P. Lettenmaier, E.F. Wood, and S.J. Burges. 1994. "A simple hydrologically based model of land surface water and energy fluxes for general circulation models," *Journal of Geophysical Research* 99(D7), 14415–14428.

Liang X., E.F. Wood, and D.P. Lettenmaier. 1996. "Surface soil moisture parameterization of the VIC-2L model: Evaluation and modifications," *Global and Planetary Change* 13:195–206.

Llewellyn, D., and S. Vaddey. 2013. West-Wide Climate Risk Assessment: Upper Rio Grande Impact Assessment. Bureau of Reclamation, Upper Colorado Region, Albuquerque Area Office, Albuquerque, NM. 138 p. Available at http://www.usbr.gov/WaterSMART/wcra/docs/urgia/URGIAMainReport.pdf

Lohmann, D., R. Nolte-Holube, and E. Raschke. 1996. "A large-scale horizontal routing model to be coupled to land surface parameterization schemes," *Tellus* 48 A, pp. 708–72.

Lopes, T.J., and K.K. Allander. 2009. Water budgets of the Walker River basin and Walker lake, California and Nevada: U.S. Geological Survey Scientific Investigations Report 2009-5157, 44p.

Maidment, D.R. (ed.). 1993. Handbook of Hydrology, McGraw-Hill, New York, New York, 1,424 p.

Manabe, S., and R.T. Wetherald. 1987. Large-scale changes of soil wetness induced by an increase in atmospheric carbon dioxide. *Journal of the Atmospheric Sciences* 45(5):1211–1235.

Marek, T., P. Colaizzi, T.A. Howell, D. Dusek, and D. Porter. 2006. "Estimating Seasonal Crop ET Using Calendar and Heat Unit Based Crop Coefficients in the Texas High Plains Evapotranspiration Network," ASABE Paper No: 062206,

2006 ASABE Annual International Meeting, Portland, Oregon, July 9–12, 2006, 11 p.

Mastin, M.C. 2008. "Effects of potential future warming on runoff in the Yakima River Basin," U.S. Geological Survey Scientific Investigations Report 2008-5124, 12 p.

Maurer, E.P. 2007. "Uncertainty in hydrologic impacts of climate change in the Sierra Nevada, California under two emissions scenarios," *Climatic Change* 82:309–325.

Maurer, E.P., A.W. Wood, J.C. Adam, D.P. Lettenmaier, and B. Nijssen. 2002. "A Long-Term Hydrologically-Based Data Set of Land Surface Fluxes and States for the Conterminous United States," *Journal of Climate* 15(22):3237–3251.

Maurer, D.K., D.L. Berger, M.L. Tumbusch, and M.J. Johnson. 2006. "Rates of evapotranspiration, recharge from precipitation beneath selected areas of native vegetation, and streamflow gain and loss in Carson Valley, Douglas County, Nevada and Alpine County, California," U.S. Geological Survey Scientific Investigations Report 2005-5288, 70 p.

Maurer, E.P., L. Brekke, T. Pruitt, and P.B. Duffy. 2007. "Fine-resolution climate projections enhance regional climate change impact studies," Eos Trans. AGU 88(47):504.

Maurer, E.P., H.G. Hidalgo, T. Das, M.D. Dettinger, and D.R. Cayan. 2010a. "The utility of daily large-scale climate data in the assessment of climate change impacts on daily streamflow in California," *Hydrology and Earth System Sciences* 14:1125–1138, DOI: 10.5194/hess-14-1125-2010.

Maurer, E.P., L.D. Brekke, and T. Pruitt. 2010b. "Contrasting lumped and distributed hydrology models for estimating climate change impacts on California watersheds," *Journal of the American Water Resources Association* 46(5):1024–1035, DOI: 10.1111/j.1752-1688.2010.00473.x.

Maurer, E.P., L. Brekke, T. Pruitt, B. Thrasher, J. Long, P. Duffy, M. Dettinger, D. Cayan, and J. Arnold. 2013. An enhanced archive facilitating climate impacts and adaptation analysis, Bulletin of the American Meteorological Society, DOI: 10.1175/BAMS-D-13-00126.1.

McGuire, E.M., and A. Hamlet. 2010. "Hydrologic Climate Change Scenarios for the Pacific Northwest Columbia River Basin and Coastal Drainages – Chapter 5," Macro-scale Hydrologic Model Implementation, 34 p. Available at http://www.hydro.washington.edu/2860/report/.

McGuire, E.M., L. Cuo, N. Voisin, J.S. Deems, A.F. Hamlet, J.A. Vano, K.E.B. Mickelson, S.Y. Lee, and D.P. Lettenmaier. 2010. "Implications of 21st century climate change for the hydrology of Washington State," *Climatic Change*, DOI: 10.1007/s10584-010-9855-0.

Meehl, G.A., G.J. Boer, C. Covey, M. Latif, and R.J. Stouffer. 2000. "The Coupled Model Intercomparison Project (CMIP)," Bulletin of the American Meteorological Society, 81(2):313–318.

Meehl, G.A., C. Covey, T. Delworth, M. Latif, B. Mcavaney, J.F.B. Mitchell, R.J. Stouffer, and K.E. Taylor. 2007. "The WCRP CMIP3 Multimodel Dataset – A New Era in Climate Change Research," Bulletin of the American Meteorological Society, 88(9):1383–1394.

Miller, N.L., K. Bashford, and E. Strem. 2003. "Potential Climate Change Impacts on California Hydrology," *Journal of the American Water Resources Research*, 39:771–784.

Mitchell, A.R. 1997. "Irrigating Peppermint," Oregon State University Extension Service, EM 8662 Nebraska High Plains Climate Center, 2006. Crop Coefficients, Phenology, and Growing Degree Day Accumulation. http://www.hprcc.unl.edu/crop/.

Monteith, J.L. 1965. "Evaporation and environment," Symposia of the Society for Experimental Biology 19: 205–224.

Moreo, M.T., and A. Swancar. 2013. Evaporation from lake Mead, Nevada and Arizona, March 2010 through February 2012, U.S. Geological Survey Scientific Investigations Report 2013–5229, 40 p.

Morton, F.I. 1979. "Climatological estimates of lake evaporation," *Water Resources Research*, 15:64–76.

_____. 1983. "Operational estimates of lake evaporation," *Journal of Hydrology*, 66:77–100.

_____. 1986. "Practical Estimates of Lake Evaporation," *Journal of Climate and Applied Meteorology*, 25(3):371–387.

Morton, F.I., S. Fogarasi, and F. Ricard. 1985. Operational estimates of areal evapotranspiration and lake evaporation – Program WREVAP, NHRI Paper No. 24, Inland Waters Directorate, Environment Canada, Ottawa, Ontario.

Mote, P.W., and E.P. Salathé. 2010. "Future climate in the Pacific Northwest," *Climatic Change*, DOI: 10.1007/s10584-010-9848.

Murphy, J.M. 1999. An evaluation of statistical and dynamical techniques for downscaling local climate, *Journal of Climate* 12:2256–2284.

Mutziger, A.J., C.M. Burt, D.J. Howes, and R.G. Allen. 2005. "Comparison of Measured and FAO-56 Modeled Evaporation from Bare Soil," *Journal of Irrigation and Drainage Engineering*, ASCE 131(1):59–72.

Myrup, L.O., T.M. Powell, D.A. Godden, and C.R. Goldman. 1979. Climatological Estimate of the Average Monthly Energy and Water Budgets of Lake Tahoe, California-Nevada. *Water Resources Research* 15(6).

Nijssen, B., D.P. Lettenmaier, X. Liang, S.W. Wetzel, and E F. Wood. 1997. "Streamflow simulation for continental-scale river basins," *Water Resources Research* 33:711–724.

Norman, J.M.. 1979. Modeling the complete crop canopy, in: Barfield, B.J., Gerber, J.F. (eds.). Modification of the Aerial Environment of Plants, American Society of Agricultural Engineers, St. Joseph, pp. 249–277.

Parlange, M.B., and G.G. Katul. 1992. "Estimation of the diurnal variation of potential evaporation from a wet bare soil surface," *Journal of Hydrology* 132:71–89.

Payne, J.T., A.W. Wood, A.F. Hamlet, R.N. Palmer, and D.P. Lettenmaier. 2004. "Mitigating the effects of climate change on the water resources of the Columbia River basin," *Climatic Change* 62(1–3):233–256.

Penman, H.L. 1948. "Natural evaporation from open water, bare soil, and grass," Proceedings of the Royal Society. London, A193:120–146.

Peters T., L. Nelson, and T. Karimi. 2012. Consumptive Use and Irrigation Water Requirements for Washington, Draft Report, Washington State University, 103 p.

Pierce, D.W., T.P. Barnett, B.D. Santer, and P.J. Gleckler. 2009. "Selecting global climate models for regional climate change studies," *Proceedings of the National Academy of Sciences* 106(21):8441–8446.

Pochop, L., T. Teegarden, G. Kerr, R. Delaney, and V. Hasfurther. 1992. Consumptive Use and Consumptive Irrigation Requirements in Wyoming, WWRC Publication #92-06, University of Wyoming, Laramie. October.

Priestley, C.H.B., and R.J. Taylor. 1972. On the assessment of surface heat flux and evaporation using large-scale parameters, *Monthly Weather Review* 100:81–92.

Purkey D.R., A. Huber-Lee, D.N. Yates, M. Hanemann, S. Herrod-Jones. 2007. "Integrating a climate change assessment tool into stakeholder-driven water management decision-making processes in California," *Water Resources Management* 21:315–329.

Rashedi, N. 1983. "Evapotranspiration Crop Coefficients for Alfalfa at Fallon, Nevada," M.S. Thesis presented to the University of Nevada, Reno, Nevada.

Reclamation (Bureau of Reclamation). 2008. "Sensitivity of Future CVP/SWP Operations to Potential Climate Change and Associated Sea Level Rise," Appendix R in Biological Assessment on the Continued Long-term Operations of the Central Valley Project and the State Water Project, prepared by the U.S. Department of the Interior, Bureau of Reclamation, Mid-Pacific Region, Central Valley Operations Office, Sacramento, California. August 2008. 134 p.

_____. 2010. Climate Change and Hydrology Scenarios for Oklahoma Yield Studies, prepared by the U.S. Department of the Interior, Bureau of Reclamation, Technical Service Center, Denver Colorado. April 2010. 71 p.

_____. 2011. West-wide Climate Risk Assessments: Bias-Corrected and Spatially Downscaled Surface Water Projections, Technical Service Center, Denver, Colorado, March 2011.

_____. 2012a. Colorado River Basin Water Supply and Demand Study. U.S. Department of the Interior, Bureau of Reclamation. Available at: http://www.usbr.gov/lc/region/programs/crbstudy/finalreport/studyrpt.html

_____. 2012b. Upper Colorado River Basin Consumptive Uses and Losses 2011–2015. Available at: http://www.usbr.gov/uc/library/envdocs/reports/crs/pdfs/cul2001-05.pdf

_____.2013a. Central Valley Project Integrated Resource Plan Technical Modeling Report prepared by the U.S. Department of the Interior, Bureau of Reclamation, Mid Pacific Region, Sacramento ,California

_____. 2013b. Downscaled CMIP3 and CMIP5 Climate Projections: Release of Downscaled CMIP5 Climate Projections, Comparison with Preceding Information, and Summary of User Needs. U.S. Department of the Interior, Bureau of Reclamation, Technical Service Center, Denver, Colorado, 116 p.

Also available at:
http://gdo-dcp.ucllnl.org/downscaled_cmip_projections/techmemo/downscaled_climate.pdf.

_____. 2013c. Upper Colorado River Basin Consumptive Uses and Losses Report 2006–2010. Available at: http://www.usbr.gov/uc/library/envdocs/reports/crs/pdfs/cul2006-2010prov.pdf

_____. 2014. West-Wide Climate Risk Assessment: Sacramento and San Joaquin Basins Climate Impact Assessment. Prepared for Reclamation by CH2M HILL under Contract No. R12PD80946. 54 p. Available at: http://www.usbr.gov/WaterSMART/wcra/docs/ssjbia/ssjbia.pdf

Reichler, T., and J. Kim. 2008. "How Well Do Coupled Models Simulate Today's Climate?" *Bulletin of the American Meteorological Society* 89(3):303–311.

Ritchie, J.T. 1972. "Model for predicting evaporation from a crop with incomplete cover," Water Resources Research, 8:1204–1213.

Rosenberg, N.J. 1981. The increasing CO_2 concentration in the atmosphere and its implication on agricultural productivity. I: Effects on photosynthesis, transpiration and water use efficiency. *Climatic Change* 3(3):265–279.

Rosenberg, N.J., D.J. Epstein, D. Wang, L. Vail, R. Srinivasan, and J.G. Arnold. 1999. "Possible Impacts of Global Warming on the Hydrology of the Ogallala Aquifer Region," *Climatic Change* 42:677–692.

Rush F.E. 1976. "Water Requirement and Efficiency of Sprinkler Irrigation of Alfalfa, Smith Valley, Nevada – A Case History," Nevada Department of Conservation and Natural Resources, Division of Water Resources, Water Resources Information Series Report 24, 10 p.

Sadek, M.F., M.M. Shahin, and C.J. Stigter. 1997. "Evaporation from the Reservoir of the High Aswan Dam, Egypt: A New Comparison of Relevant Methods with Limited Data," *Theory of Applied Climatology* 56:57–66.

Sakamotoa, C.M., and R.O. Gifford. 1970. Spring and Fall Low Temperature and Growing Season Probabilities in Nevada, University of Nevada, Reno, College of Agriculture, Bulletin B-26.

Salathé, E.P., P.W. Mote, and M.W. Wiley. 2007. "Review of scenario selection and downscaling methods for the assessment of climate change impacts on hydrology in the United States Pacific Northwest," *International Journal of Climatology* 27:1611–1621.

Sammis, T.W., E.G. Hanson, C.E. Barnes, H.D. Fuehring, E.J. Gregory, R.F. Hooks, T.A., Howell, and M.D., Finkner. 1979. Consumptive use and yields of crops in New Mexico, Las Cruces, New Mexico, Reports of the New Mexico Water Resources Research Institute, Report No. 115, pp. 1–107.

Sammis, T.W., C.L. Mapel, D.G. Lugg, R.R. Lansford, and J.T. McGuckin. 1985. "Evapotranspiration Crop Coefficients Predicted Using Growing Degree Days," *Transactions American Society of Agricultural Engineers* 28(3):773–780.

Santer, B.D., K.E. Taylor, P.J. Gleckler, C. Bonfils, T.P. Barnett, D.W. Pierce, T.M.L. Wigley, C. Mears, F.J. Wentz, W. Bruggemann, N.P. Gillett, S.A. Klein, S. Solomon, P.A. Stott, and M.F. Wehner. 2009. "Incorporating model quality

information in climate change detection and attribution studies," *Proceedings of the National Academy of Sciences* 106(35):14778–14783.

Shi, X., A.W. Wood, and D.P. Lettenmaier. 2008: "How Essential is Hydrologic Model Calibration to Seasonal Streamflow Forecasting?" *Journal of Hydrometeorology* 9:1350–1363.

Slack, J.R., A.M. Lumb, and J.M. Landwehr. 1993. "Hydroclimatic data network (HCDN): A U.S. Geological Survey streamflow data set for the United States for the study of climate variation, 1874–1988," U.S. Geological Survey Water Resource Investigations Report, 93-4076.

Slack, D.C., E.D. Martin, A.E. Sheta, F.A. Fox, Jr., L.J. Clark, and R.O. Ashley. 1996. "Crop Coefficients Normalized for Climatic Variability with Growing-degree-days," Proc., International Conf., Evapotranspiration and Irrigation Scheduling, San Antonio, Texas, C.R. Camp, E.J. Sadler, and R. E. Yoder (eds.). American Society of Agricultural Engineers, St. Joseph, Michigan, pp. 892–898.

Smith, R. 1991. Hatchery Trout Evaluations: American Falls Reservoir Fishery Evaluations, Idaho Fish and Game, Volume 086, Article 09.

Smith, J.A., G.N. Day, and M.D. Kane. 1992. "Nonparametric framework for long-range streamflow forecasting," *Journal of Water Resource Planning and Management* 118:82–92.

Snover A.K., A.F. Hamlet, and D.P. Lettenmaier. 2003. "Climate change scenarios for water planning studies: Pilot applications in the Pacific Northwest," *Bulletin of the American Meteorological Society* 84(11):1513–1518.

Snyder, R.L., D. Spano, C. Cesaraccio, and P. Duce. 1999. "Determining Degree-day Thresholds From Field Observations," *International Journal of Biometeorology* 42:177–182.

Stannard, D.I., M.W. Gannett, D.J. Polette, J.M. Cameron, M.S. Waibel, and J.M. Spears. 2013. Evapotranspiration from marsh and open-water sites at Upper Klamath Lake, Oregon, 2008–2010, U.S. Geological Survey Scientific Investigations Report 2013–5014, 66 p.

Stone, M.C., R.H. Hotchkiss, C.M. Hubbard, T.A. Fontaine, L.O. Mearns, and J.G. Arnold. 2001. "Impacts of Climate Change on Missouri River Basin Water Yield," *Journal of the American Water Resources Association* 37:1119–1129.

Tansey, M., C. Young, J. DeGeorge, and L. Shannon. 2011. Land Atmosphere Water Simulator (LAWS) Version 2.0, Bureau of Reclamation Report, Mid-Pacific Region, 168 p.

Taylor, K. E., R.J. Stouffer, and G.A. Meehl. 2012. A Summary of the CMIP5 Experiment Design. *Bulletin of the American Meteorological Society* 93:485–498.

Tebaldi, C., R.L. Smith, D. Nychka, and L.O. Mearns. 2005. "Quantifying Uncertainty in Projections of Regional Climate Change: A Bayesian Approach to the Analysis of Multi-model Ensembles," *Journal of Climate* 18:1524–1540.

Thornton, P.E., S.W. Running, and M.A. White. 1997. Generating surfaces of daily meteorological variables over large regions of complex terrain. *Journal of Hydrology* 190, Issues 3–4:214–251.

Thornton, P.E., and S.W. Running. 1999. "An improved algorithm for estimating incident daily solar radiation from measurements of temperature, humidity, and precipitation," *Agricultural and Forest Meteorology* 93:211–228.

Tootle, G.A., T.C. Piechota, and A.K. Singh. 2005. "Coupled Interdecadal and Interannual Oceanic/Atmospheric Variability and United States Streamflow," *Water Resources Research* 41(W12408).

Trask, J.C. 2007. Resolving Hydrologic Water Balances through Novel Error Analysis with Focus on Inter-annual and long-term Variability in the Tahoe Basin, University of California, Davis, Ph.D. Dissertation, 378 p.

USDA-NASS (United States Department of Agriculture, National Agricultural Statistics Service). 2010a. Cropland Data Layer [GIS Dataset]. Available at http://www.nass.usda.gov/research/Cropland/SARS1a.htm

_____. 2010b. Field Crops – Usual Planting and Harvesting Dates. October 2010, 50 p. Available at http://usda.mannlib.cornell.edu/MannUsda/viewDocumentInfo.do?documentID=1251

USDA-NRCS (United States Department of Agriculture, Natural Resources Conservation Service). 1991. "State Soil Geographic (STATSGO) Data Base Data use information," United States Department of Agriculture Natural Resources Conservation Service, National Soil Survey Center, Miscellaneous Publication number 1492.

USDA-SCS (United States Department of Agriculture, Soil Conservation Service). 1972. "National Engineering Handbook," Section 4, Table 10.1.

_____. 1974. Irrigation guide for Montana: Bozeman, Montana, U.S. Department of Agriculture (variously paged).

USGCRP (U.S. Global Change Research Program). 2009. Global Climate Change Impacts in the United States, T.R. Karl, J.M. Melillo, and T.C. Peterson (eds.). Cambridge University Press, 196 p.

Vallet-Coulomb, C., D. Legesse, F. Gasse, Y. Travi, and T. Chernet. 2001. "Lake evaporation estimates in tropical Africa," *Journal of Hydrology* 245(1-4):1–18.

Van Rheenen, N.T., A.W. Wood, R.N. Palmer, D.P. Lettenmaier. 2004. "Potential implications of PCM climate change scenarios for Sacramento-San Joaquin River Basin hydrology and water resources," *Climatic Change* 62:257–281.

Vano, J.A., N. Voisin, L. Cuo, A.F. Hamlet, M.M. Elsner, R.N. Palmer, A. Polebitski, and D.P. Lettenmaier. 2010. "Climate change impacts on water management in the Puget Sound region, Washington, USA." Climatic Change 102(1-2):261–286, DOI: 10.1007/s10584-010-9846-1.

Vicuna, S., and J.A. Dracup. 2007. "The evolution of climate change impact studies on hydrology and water resources in California," *Climatic Change* 82:327–350.

Wigley, T.M.L. 2004. "Input Needs for Downscaling of Climate Data." Discussion paper prepared for California Energy Commission Public Interest Energy Research Program, Rep 500-04-027.

Wigmosta, M.S., L.W. Vail, and D.P. Lettenmaier. 1994. "A distributed hydrology vegetation model for complex terrain," *Water Resources Research* 30:1665–1679.

Wilby, R.L., and T.M.L. Wigley. 1997. Downscaling general circulation model output: a review of methods and limitations. *Progress in Physical Geography* 21:530–548.

Wiley, M.W. 2004. "Analysis techniques to incorporate climate change information into Seattle's long range water supply planning," Master's Thesis, University of Washington, Seattle, Washington.

Wood, A.W., E.P. Maurer, A. Kumar, and D.P. Lettenmaier. 2002. "Long-range experimental hydrologic forecasting for the Eastern United States," *Journal of Geophysical Research-Atmospheres* 107(D20), 4429, DOI: 10.1029/ 2001JD000659.

Wood, A.W., L.R. Leung, V. Sridhar, and D.P. Lettenmaier. 2004. "Hydrologic implications of dynamical and statistical approaches to downscaling climate model outputs," *Climatic Change* 15:189–216.

Wood, A.W., A. Kumar, and D.P. Lettenmaier. 2005. "A retrospective assessment of climate model-based ensemble hydrologic forecasting in the western U.S.," *Journal of Geophysical Research* 110, D04105, DOI: 10.1029/ 2004JD004508.

_____. 2006. "A Test Bed for New Seasonal Hydrologic Forecasting Approaches in the Western United States," *Bulletin of the American Meteorological Society* 87:1699–1712.

Wright, J.L. 1981. "Crop Coefficients for Estimates of Daily Crop Evapotranspiration," Irrigation Scheduling for Water and Energy Conservation in the 80's, ASAE, St. Joseph, Michigan, pp. 18–26.

_____. 1982. "New evapotranspiration crop coefficients," *Journal of Irrigation and Drainage Engineering* 108(1):57–74.

_____. 1991. "Using weighing lysimeters to develop evapotranspiration crop coefficients," pages 191–199 in: R.G. Allen, T.A. Howell, W.O. Pruitt, I.A. Walter, and M.E. Jensen (eds.). Proc. of the International Symposium on Lysimetry, July 23–25, Honolulu, Hawaii, ASCE, 345 E. 47th St., New York, NY 10017-2398.

_____. 1993. "Nongrowing season ET from irrigated fields," pages 1005–1014 in: R.G. Allen and C.M.U. Neale (eds.). Management of Irrigation and Drainage Systems: Integrated perspectives. Proc. Workshop, ASCE Irrigation and Drainage Division, Park City, Utah, July 21–23, 1993.

_____. 2001. "Growing Degree Day Functions for Use With Evapotranspiration Crop Coefficients," CD-ROM, American Society of Agronomy, Agronomy Abstracts.

Yates, D., J. Sieber, D. Purkey, and A. Huber-Lee. 2005. "WEAP21 – A Demand-, Priority-, and Preference-Driven Water Planning Model. Part 1: Model Characteristics," *Water International*, 30(4):487–500.